EVALUATING THE COMPREHENSIVE MODEL ADOM WITH DATA FROM THREE SEASONS

JULY 1992

Ontario
Environment
Environnement

ISBN 0-7729-9987-2

EVALUATING THE COMPREHENSIVE MODEL ADOM WITH DATA FROM THREE SEASONS

JULY 1992

Cette publication technique
n'est disponible qu'en anglais.

PIBS 2064
Log 92-2206-108

EVALUATING THE COMPREHENSIVE MODEL ADOM WITH DATA FROM THREE SEASONS

Report prepared by:

Christopher Fung, Robert Bloxam, P.K. Misra,
Sonny Wong, and David Yap

Air Quality and Meteorology Section
Air Resources Branch
Ontario Ministry of the Environment
125 Resources Road, East Wing
Rexdale, Ontario M9W 5L1

PIBS 2064
Log 92-2206-108

TABLE OF CONTENTS

TABLE OF CONTENTS (cont'd.)

ACKNOWLEDGEMENTS

The development of ADOM was sponsored by the Ontario Ministry of the Environment, the Atmospheric Environment Service of Environment Canada and the Umweltbundesamt (UBA) of the Federal Republic of Germany. The Electric Power Research Institute (EPRI) of the U.S. funded work on developing an improved version of the cumulus cloud module for ADOM which is currently in use.

ENSR Consulting and Engineering (formerly ERT) developed the model and did the work reported in Sections 3.1, 3.2, 3.3, 4.1, 4.2, 4.5 and 4.6.

Support and contributions of the staff and management in Environmental Services Division and APIOS office of the Ontario Ministry of the Environment are gratefully acknowledged.

EXECUTIVE SUMMARY

This report summarises the findings of a comprehensive Eulerian atmospheric transport, transformation and deposition model ADOM (Acid Deposition and Oxidant Model) which was developed as part of the Ontario Ministry of the Environment's acid precipitation program. In 1982, following the Canada-U.S. Memorandum of Intent on Transboundary Pollution, it was argued that the simple linear acid deposition models being used at the time were inadequate to address the question of non-linearity. The question of non-linearity can be stated as: Will a change in the amount of acid precursors emitted bring about a proportionate change in the atmospheric acid loading. Thus, comprehensive numerical models, which attempt to represent the entire body of knowledge pertaining to the acidic precipitation processes within the practical limitations of current computers, were developed to address this question.

The development of ADOM was originally sponsored by the Ontario Ministry of the Environment, Environment Canada and the Umweltbundesamt (UBA) of the Federal Republic of Germany. Subsequently, the Electric Power Research Institute (EPRI) of the U.S. has funded work on improving the cumulus cloud module in ADOM and intercomparison of the model with a similar comprehensive model RADM (Regional Acid Deposition Model) developed by the U.S. Environmental Protection Agency. The first operational version ran in 1986. This report describes the components of ADOM as well as the evaluation and sensitivity runs completed to date to delineate model performance and to address the question of non-linearity.

The major evaluation studies that have been carried out are: Oxidant and Scavenging Characteristics of April Rain (OSCAR, April 1981) experiment, a Summer Oxidant Study (June 1983), a Winter

Study (January - February, 1985), Across North America Tracer Experiment (ANATEX, January - March, 1987) and the Eulerian Model Evaluation Field Study (EMEFS, July - September, 1988).

The earlier studies (OSCAR, Summer Oxidant, Winter Study and ANATEX) were limited in their scope and generated only a limited data set for some of the acidic species for model evaluation. The EMEFS was carried out with joint sponsorship by the Ontario Ministry of the Environment, Atmospheric Environment Service of Environment Canada, Environmental Protection Agency of the U.S. and Electric Power Research Institute of the U.S. during 1988 and 1990 with a view to obtaining a more comprehensive data base which includes both ground level and aircraft measurements of several acidic species, thereby allowing for a more complete evaluation of the model in three dimensions.

OSCAR was designed to provide information on the chemical constituents of spring precipitation as they relate to acid formation. Evaluation of the model with OSCAR wet deposition data showed that the model was able to reproduce 70-80 per cent of the sulphate concentrations in precipitation to within a factor of 2 and 60-80 per cent of the nitrate concentrations in precipitation to within a factor of 2 on an event (2 - 3 days) comparison.

The purpose of the winter study was to evaluate model performance and together with the results from OSCAR, determine the seasonal response of ADOM in regards to the nitrate to sulphate ratios in precipitation. Sulphate concentrations in precipitation were slightly overpredicted and nitrate concentrations in precipitation slightly underpredicted. More than 60 per cent of sulphate and 30 per cent of nitrate concentrations are predicted to be within a factor of two of the observations.

Further, the model simulated ratio of nitrate/sulphate was 2.4. vs. the observed value of 1.6 for this winter episode. During

the spring period, the modelled and observed ratios were 0.90 and 0.83, respectively. It was concluded from these evaluations that the high nitrate to sulphate ratios in winter can be partially explained by the slower oxidation of SO_2 to sulphate combined with less efficient precipitation scavenging of sulphate in winter time.

The ANATEX study was carried out to evaluate the transport module of the model. The large grid size (127 x 127 km) precludes a rigorous evaluation of the model for the episodic transport phenomena of ANATEX. However, when the data were averaged over the forty four day period, the modelled ground level concentration pattern was found to be in reasonable agreement with the corresponding observed pattern.

The Summer Oxidant Study was carried out to test the ability of the model to simulate the high ozone levels observed in the Windsor-Quebec Corridor. The modelled peak values of ozone were found to be in very good agreement with the corresponding observed values. This study corroborated the conclusions of previous Ontario studies where the episodic peak values of ozone in the Windsor-Quebec Corridor were attributed mostly to the long range transport of ozone and its precursors from the industrialized mid-western U.S.

The evaluation of the model with the EMEFS data was carried out using a common evaluation protocol developed by all the sponsors. The U.S. EPA model (RADM) was also evaluated using the same protocol. It was observed that both ADOM and RADM performed similarly when evaluated against the ground level data set. Further, the models were able to explain reasonably well the observed behaviour of the SO_2, SO_4, nitrate and NO_2 concentrations in air and nitrate and sulphate concentrations in precipitation.

One of the significant findings of this evaluation exercise is the importance of non-precipitating clouds in the formation of SO_4 in air. These clouds produce approximately 50 percent of the SO_4 in air. O_3 and H_2O_2 peak values are not reproduced well by these models, perhaps as a result of the large grid sizes employed.

ADOM was used to investigate the consequences of various emission control scenarios. These are summarized as follows:

When the SO_x emissions are reduced by 50 per cent across the domain, the reduction in sulphate in precipitation predicted by ADOM in the heavy emission areas was approximately 30-40 per cent during the spring (OSCAR) period and about 25 per cent during the winter period. The ground level SO_2 concentrations in air respond almost linearly to this 50 per cent change. Ground level sulphate concentrations decrease by 40 - 50 per cent over the heavy emission area. When both SO_x and NO_x are reduced by 50 per cent, the corresponding changes in sulphate in precipitation for each season are 25 to 35 per cent during OSCAR and 15 to 20 per cent during the winter episode. The reduction in nitrate concentrations in precipitation for these emission cuts is 50 to 60 per cent in heavy emission areas during OSCAR and approximately 10 per cent during the winter study.

It was also determined that aqueous oxidations account for more than half of the observed sulphate in precipitation and that the major aqueous pathway for production of sulphate in precipitation during spring is the oxidation of SO_2 by H_2O_2. For the winter period, the nighttime pathway for the formation of nitrate in precipitation is just as important as the daytime pathway.

Although model runs for the spring and winter periods indicate that wet deposition of sulphate responds non-linearly to emission

reductions, it must be pointed out that the response of total sulphur deposition (wet plus dry) is more linear because dry deposition responds linearly.

For the spring episode (OSCAR) the model predicted a 40 - 45 per cent reduction in total sulphur deposition (30 - 40 per cent for wet deposition and 50 per cent for dry deposition) in response to a 50 per cent reduction in SO_x emissions. Given the uncertainty in both model predictions and measurements, the model response for total sulphur deposition can be considered linear for practical applications. This implies that the emission reduction scenario results obtained to date using linear models cannot be negated on the basis of non-linearity arguments. It must be noted in this context that the models have not been evaluated against a data set where the emissions are substantially different from the present conditions. Validity of the model results for a very different emission configuration has to be interpreted with caution. It is believed that models such as ADOM, which include a comprehensive chemical mechanism, can be applied for different emission configurations since there are at present no basis to assume that the chemistry of the atmosphere would differ radically for other emission configurations from the present conditions.

List of Tables

LIST OF FIGURES

1. Introduction

As part of an effort to develop a reliable and cost-effective tool to address the scientific and policy aspects of the long-range transport of acidic precipitation, a comprehensive numerical model, the Acid Deposition and Oxidant Model (ADOM), has been developed. This model has been evaluated and some emission scenario runs have been performed. This report describes the model results obtained to date. After presenting the elements incorporated into ADOM, results obtained to date on model evaluation and sensitivity tests are given. The remaining work to validate the model and to produce a comprehensive set of emission scenario runs is also described.

The concept of comprehensive modelling of the long-range transport of acidic precipitation evolved from the parameterized linear models used in the 1970's. The usual assumptions and practices of these first generation numerical models are:

1) transport takes place within the planetary boundary layer and is approximated by two-dimensional advection;

2) pollutants can be tracked from the source to the receptor by following trajectory paths without considering chemical interactions with other sources or pollutants;

3) the conversion of acidic precursors to the final acidic species is linear;

4) precipitation scavenging can be parameterized knowing only the air concentrations of the species in the boundary layer and the precipitation rate or amount; and

5) dry deposition can be represented by a dry deposition velocity where often a single value is prescribed per species.

As scientists gained more understanding of the processes, the above assumptions were being increasingly challenged. First, transport in the atmosphere is three-dimensional, especially in the vicinity of the ever-present disturbances, like fronts and clouds. Because of these disturbances, any pollutant released will be subject to severe distortion and the continuous plume or circular puff assumption breaks down after the first few hours of travel. Material mixed or advected to higher levels in the atmosphere would then be subject to different winds and scavenging characteristics. Consequently, the basic framework of modelling has to be changed from a two-dimensional parcel (Lagrangian plume or puff) method to a three-dimensional approach. An Eulerian (grid based) approach has been selected since it offers greater flexibility and cost effectiveness in interacting-puff situations. Second, research in atmospheric chemistry suggested that nitrogen species together with oxidants are important determinants in the atmospheric acid loading and that in-cloud chemistry rivals the contribution of gas-phase chemistry to the overall loading. Below cloud scavenging is only a small part of wet removal in the atmosphere. This understanding has significant bearing on abatement policy and raises a question which is usually referred to as the issue of non-linearity: given the complex chemistry involved in the formation of acid species in the atmosphere, would a change in the emissions of acid precursors bring about a proportionate change in the resulting acidic deposition? Thus, a major purpose in comprehensive modelling is to shed light on the above question and to quantify the atmospheric response if it is not linear.

The need for comprehensive modelling was recognized by the scientists involved in writing the U.S. - Canada Memorandum of Intent on Transboundary Air Pollution (1982). These scientists made eleven recommendations to improve model performance and to gain confidence that the models were adequately simulating the acid precipitation system. A number of these recommendations dealt with

improving the emission and meteorological input data as well as providing more extensive and reliable evaluation data against which to make comparisons. Two specific recommendations involved the question of non-linearity and its possible impact on emission cuts and the importance of NO_x transport and deposition. Shortly afterwards, two parallel efforts in comprehensive modelling were initiated. The Regional Acid Deposition Model (RADM) was sponsored by the U.S. Environmental Protection Agency and developed by a group currently at the State University of New York. The Acidic Deposition and Oxidant Model (ADOM) was co-sponsored by the Ontario Ministry of the Environment, Environment Canada and UBA of the Federal Republic of Germany and developed by the ENSR Company in California. The formulation of the model as well as the testing and evaluation of ADOM are described in this report.

2. Comprehensive Modelling and Description of ADOM

Comprehensive modelling is an ambitious undertaking. If all that is currently known about the processes involved in the long-range-transport of acidic precipitation were incorporated into a numerical scheme, the computer resource requirements would exceed any practical limit. Not only will the execution of the code not be able to catch up with real time on the state-of-the-technology computer, the input requirements and the quantity of output data of such a model will tax any environmental agency's resources to the limit. Thus, scientific judgement is necessary to determine what is to be optionally included in the modelling framework to adequately address the questions at hand.

The basic unit of ADOM is a grid volume and each of these has to satisfy the mass conservation equation:

$$\underset{}{\frac{\partial C}{\partial t}} = \underset{I}{\vec{U} \cdot \vec{\nabla} C} + \underset{II}{\vec{\nabla} \cdot (K \vec{\nabla} \cdot C)} + \underset{III}{E} + \underset{IV}{C} + \underset{V}{D} \qquad (1)$$

This equation states that the change of concentration (C) in a control volume is given by the sum of the advection (I), diffusion (II), and the source and sink terms (emissions (III), chemical conversion (IV) and deposition (V)). For ADOM, the meteorological information needed for this equation comes from the output of the Canadian Meteorological Centre (CMC) weather forecasting spectral model which assimilates observations every six hours. To obtain data for the one hour time step used in the model, the "errors" in the forecast fields at the six hour point are determined by subtracting the forecast fields from the new data initialized fields for this hour. These errors are assumed to increase linearly from hour 0 to hour 6 in the model runs. In this sense, the model is used as a dynamic interpolator in space and time for the observations. This provides wind, pressure, temperature, humidity, cloud and precipitation data. Further processings of all these data were made for three reasons: 1. to grid these data to the finer spatial resolution ADOM needs, 2. to further refine the precipitation and cloud data through incorporation of observed data where these are available, and 3. to increase the vertical resolution of all these parameters within the boundary layer by running a one-dimensional boundary layer model between ground level and 2 km at each grid cell.

The equations for transport and diffusion are solved by various numerical schemes. For advection in the horizontal, a sophisticated cell-centre flux scheme based on the Blackman spline technique is used. Horizontal diffusion is solved by Crank-Nicolson time differencing and three-point finite difference expressions. Vertical diffusion, advection, dry deposition and emissions injection are accomplished through a low-order mass conserving algorithm that operates in either Crank-Nicolson or fully implicit modes depending on stability criteria and the maximum number of iterations allowed.

Emissions include area and point source releases of sulphur, nitrogen, ammonia, dust and hydrocarbon species. A list of all the emitted species considered in the model or steady state species for the latest version of ADOM is given in Table 1. Plume rise calculations based on Weil and Brower (1984) are made for each point source.

Two chemistry modules are incorporated in the model. The gas-phase chemistry module is condensed from a comprehensive chemistry scheme. This latest reaction scheme consists of 114 reactions among 47 species (Table 2) with reactive hydrocarbons grouped according to reactivity. Photo-chemistry is a function of solar elevation and cloud cover. Gas-phase chemistry is performed for every grid cell in the modelling domain at each time step.

Aqueous phase chemistry is performed whenever a cloud module is activated. For stratiform clouds the module is activated when a finite precipitation amount is given for that grid location. In the case of convective clouds calculations are performed for both precipitating and non-precipitating clouds. The aqueous-phase chemistry scheme has 25 reactions (Table 3) which includes transfer between the gas and aqueous phases. Since the nitrogen precursors to acidity (NO and NO_2) are very insoluble in water, nitrogen chemistry is not considered in the aqueous phase. The three major oxidation reactions for SO_2 are: oxidation by H_2O_2, O_3 and catalytic oxidation by O_2 in the presence of Fe and Mn. Mass transfer from gas to aqueous-phase makes use of forward and backward mass fluxes dependent on a sticking coefficient and the Henry's Law constant for the gas.

Two cloud physics modules try to simulate the stratus and the cumulus situations. The stratus module calculates the vapour condensation rate based on the vertical temperature profile of the grid column and the vertical velocity, and then divides the column

into a maximum of four homogeneous zones depending on the relative positions of the cloud base, cloud top, freezing and -20°C levels, as depicted in Figure 1. The cloud microphysical considerations are based on Kessler's (1969) bulk approach.

The cumulus module has evolved from a highly parameterized version to a more detailed treatment of mixing processes. The earlier version averages the vertically well-mixed concentration profile and the environmental concentration profile to obtain the in-cloud chemical concentration profiles, while the cloud water content is determined as a fraction of the adiabatic liquid water content of ascending parcels. This simplistic version is now replaced by a scheme (Raymond and Blyth, 1986) that allows sub-parcels in each parcel of ascending cloud air to mix in different proportion with the environmental air and eventually to settle at its level of neutral buoyancy. A schematic of this process is given in Figure 2.

The present version of ADOM allows for the co-existence of stratus and cumulus clouds. The cumulus module is first called to determine if the Raymond and Blyth's scheme can successfully form a cloud based on parcel mixing. If this is unsuccessful, the small scale precipitation (if any) which has been allocated to cumulus clouds is put into the total precipitation for the stratus cloud module which is called only when a finite precipitation is present. Both modules consider in-cloud and below-cloud scavenging of sulphur, nitrogen and oxidant species.

Dry deposition proceeds according to a deposition velocity which is inversely proportional to the sum of the area weighted aerodynamic, surface and canopy resistances. The aerodynamic resistance is determined from the meteorological input such as stability and applies to all species. The surface resistance is calculated from the land-use type and the physical and chemical

properties of the species. The canopy resistance responds to the incoming solar radiation and meteorology.

Land-use data are obtained from the gridding produced by Sirois and Voldner (1984). The anthropogenic emissions data are based on the U.S. National Acid Precipitation Assessment Program (NAPAP) emissions inventory. They are further gridded and the reactive hydrocarbons are lumped according to ADOM's requirements. These emissions include the sulphur, nitrogen, ammonia and hydrocarbon species. In the latest evaluations for the summer oxidant study (see Sections 3.2 and 4.5) and EMEFS (see Section 3.5), biogenic emissions are included. For EMEFS, the data came from the U.S. EPA and a canopy model which reacts to meteorology was used to adjust the biogenic emissions to the current conditions. The initial and boundary conditions used in the current version (ADOM II B) for the EMEFS simulation are given in Table 4.

The five major modules discussed above:

1. Advection (transport and diffusion)
2. Gas-phase chemistry
3. Aqueous-phase chemistry and scavenging
4. Cloud mixing and
5. Dry deposition

are integrated together within an Eulerian framework using the split operator approach as:

$$C^{n+1} = A_x \; A_y \; A_z \; A_c \; A_c \; A_z \; A_y \; A_x \; C^n$$

where C^n is the concentration of a species at time = n,

A_x, A_y are the horizontal transport and diffusion operators;

A_z is the vertical transport, diffusion, source injection and physical depletion operator, and
A_c is the central operator containing cloud mixing, dry deposition and all chemical conversion terms.

The decomposition of each operator into two parts and its application in opposite order during each time step causes the errors of order Δt which build up during the first half of the cycle to be cancelled out as the reverse operator application completes the time-marching cycle (MarChuk, 1975). The overall modelling system with all the input and output files is represented in Figure 3.

In all but one (ANATEX) case, ADOM is applied to a 33 x 33 horizontal grid domain (Figure 4) on a polar stereographic CMC projection true at 60°N. The grid resolution on this projection is 127 x 127 km which means that the distance between two adjacent nodes on the domain is less than 127 km as one goes south away from the 60°N latitude. The model allows for this by adjusting the wind vectors. In this way, the curvature of the earth is taken into consideration. The vertical dimension of the domain covers the first 10 km above ground and is partitioned into 12 logarithmically distributed levels with 8 levels located below 2 km.

3. Evaluation Studies

Five major evaluation studies have been made using ADOM. All but one (ANATEX) are made with the full ADOM model. These cover three of the four seasons (winter, spring and summer) of the year. These studies are described below in the order they were made.

3.1 The Oxidant and Scavenging Characteristics of April Rain (OSCAR) Experiments

This field experiment was carried out over several states in the northeastern U.S. during April 1981. Two surface networks (one of intermediate and the other high density) were set up across the experimental area and were activated when the forecast indicated an approaching precipitation system. Only data from the intermediate density network (Figure 4) which has 37 stations measuring sulphate, nitrate and the pH of precipitation were used for this evaluation. During that period, three episodes referred to as OSCAR II, III and IV were sampled. Only OSCAR II (April 11-15, 1981) and IV (April 21-24, 1981) provided data of reliable quality to evaluate model results.

During the OSCAR period, low pressure systems tracked from southern Canada or the U.S. mid-west to the OSCAR network area and then off the Atlantic coast. The western part of the intermediate density network experienced mostly showers and thunderstorms while the eastern portion had a mix of showers and steady precipitation. During OSCAR II most of the precipitation occurred on April 13 and 14. For OSCAR IV, a more organized and widespread precipitation pattern with greater persistence was observed. Most of the precipitation fell on the 22nd and 23rd of April. A total of 5 days of precipitation chemistry data (April 13 and 14 from OSCAR II and April 22-24 from OSCAR IV) are used for model evaluation.

OSCAR II and IV data have been used to evaluate the two versions of ADOM (an earlier version 15D and the most current version IIB). The model results were comparable for sulphate and nitrate in precipitation. Since the new (ADOM IIB) version has more realistic cloud processes built into it which may produce more realistic vertical profiles of the chemical species, only results from this new version are presented. Figure 5 gives the predicted

vs. observed sulphate concentration in precipitation at the 37 sites for OSCAR II and IV on a log-log scale. It is seen that about 70 per cent and 80 per cent of the predictions for OSCAR II and IV, respectively, are within a factor of two of the observed data. The plots also show that for OSCAR II, all points outside of the factor of 2 lines are underpredicted. For OSCAR IV, there is little systematic bias. The results for nitrate concentration in precipitation are given in Figure 6. About 60 per cent and 80 per cent of the nitrate predictions are within a factor of two of the observed values for OSCAR II and IV, respectively. Like the sulphate concentrations, nitrate in precipitation shows a slight underprediction and more scatter during OSCAR II than OSCAR IV. During OSCAR II there was more convective precipitation and the spatial variability was larger than during OSCAR IV. Thus, this performance is largely caused by the use of grid-cell averaged (127 x 127 km^2) precipitation as input to the model with the site specific observation for comparison. A plot of the input precipitation to the model vs. the observed (Figure 7) confirms the above contention. For OSCAR II, the input precipitation values are in general higher than the observed precipitation, thus leading to a lower than observed concentration in precipitation for both nitrate and sulphate. On the other hand, OSCAR IV input precipitation shows little bias and the concentrations in precipitation likewise show little bias.

An indirect comparison has been made between model predictions and observations by employing the washout ratio concept. This was performed with the version of the model using the simple cumulus cloud formulation. Nevertheless, the results should not be significantly different. The washout ratio has been employed in many simple models to estimate how much of the sulphur in air has been removed by precipitation. It is the ratio between the sulphur (or sulphate) concentration in precipitation to that in ground level air. Misra et al. (1985) and Chan and Chung (1986) have

reported washout ratio using several different definitions, some of which are:

$$W_{so4} = \frac{SO_4^{2-} \text{ in precipitation associated with sulphate in air}}{\text{sulphate in air}}$$

$$W_{so2} = \frac{SO_2 + SO_4^{2-} \text{ in precipitation associated with } SO_2 \text{ in air}}{SO_2 \text{ in air}}$$

$$W_1 = \frac{SO_2 + SO_4^{2-} \text{ in precipitation}}{\text{sulfate in air}}$$

$$W_2 = \frac{SO_2 + SO_4^{2-} \text{ in precipitation}}{SO_2 \text{ in air}}$$

$$W_3 = \frac{SO_2 + SO_4^{2-} \text{ in precipitation}}{SO_2 + \text{sulfate in air}}$$

$$W_{no3} = \frac{\text{nitrate in precipitation}}{\text{nitrate in air}}$$

The concentration in air is usually measured at 10 m above ground. Note that W_{so2} and W_{so4} cannot be measured directly. Chan and Chung (1986) have attempted to estimate these by regressing the sulphur in precipitation on concentrations of SO_2 and sulphate in air. These are used in the comparison with prediction which can be directly calculated from model output.

The washout ratio is not a complete representation of the scavenging ability of precipitation since the important physical parameters like precipitation rates and amounts are not considered. Rather, they represent a comparison between the two products (concentrations in air and precipitation) of all the processes considered in the long-range-transport of acidic precipitation. As such, it is simply viewed as a characteristic indicator of the process.

A comparison between the observed and model predicted washout ratios is given in Table 5. The observations are based on the long term averages of a few stations and consequently are not strictly

compatible with the model predicted washout ratios which are spatial averages over event data. Nevertheless, the general agreement between the observed and predicted washout ratios of sulphur and nitrogen species still serves to indicate that the model predictions are reasonable.

3.2 Evaluating ADOM's Ozone Prediction During a Summer Period

During June 9 to 17, 1983, southern Ontario experienced a major ozone episode when the one-hour ground level ozone concentrations frequently exceeded the Ontario criterion of 80 ppb. ADOM was used to simulate this oxidant episode with three objectives in mind: 1. to determine ADOM's performance in reproducing the O_3 trends and 2. to understand the contribution to southern Ontario ozone from transboundary transport of ozone and its precursors and 3. to determine the impact of biogenic hydrocarbons on peak ozone levels.

During this period, southern Ontario was dominated by a high pressure system which gradually moved northeastward. Winds were generally light, with directions changing from northeasterly to southerly as the high pressure moved toward the northeast.

For this simulation, a biogenic component of the hydrocarbon emissions are included in the model. This consisted of isoprene emissions along with α-pinene emissions and 25 per cent of 'other biogenic' hydrocarbon emissions which are lumped with the anthropogenic emissions, of higher alkenes. The remaining 75 per cent of other biogenic hydrocarbons are assumed to be non-reactive.

Figure 8 shows the time series plots for two grid cells (Southern Ontario and Northern Ohio). The values at all the available monitoring sites in each grid cell were averaged. The diurnal fluctuations of the ozone concentrations at both locations

are well captured by the model. Figure 9 shows the daily maximum ozone concentrations at all the sites for each day compared against model predictions for the period of the simulation. More than 95 per cent of the predicted peaks are within a factor of two of the observations and 70 per cent of the predicted peaks within a factor of 1.5 of the observations. These peak concentrations show only a slight bias with more points showing an underprediction than overprediction.

Table 6 shows the comparison of predicted and observed daily ground level air sulphate concentrations for a limited number of sites for June 11 and 17, 1983. These are the only data available during this period. From these very limited comparisons (with 2 co-located sites at Geo. St. Troop and Scra and Allentown WAEB Radio), ADOM performs better on June 11 than on June 17, 1983.

3.3 A Winter Simulation

This simulation was intended to delineate ADOM's performance for a winter period and to test the model response to emissions reductions for this season. The model response to emission reductions is reported in Section 4.2.

The period of simulation chosen for the winter period is from January 28 to February 7, 1985. The version of ADOM with the Raymond and Blyth (1986) cumulus cloud parcel mixing scheme was used for the model simulations. The data for comparison were obtained from the Acid Deposition System (ADS) data base which is an integrated, centralized data repository for atmospheric deposition monitoring networks data in North America. This includes daily precipitation data from the APIOS-D (Acidic Precipitation in Ontario Study - Daily), APN(Air and Precipitation Network), CAPMON (Canadian Air and Precipitation Monitoring Network), MAP3S (Multi-State Atmospheric Pollution Power Production

Study) and UAPSP (Utility Acid Precipitation Study Program) networks. For the period of this simulation, the number of monitoring stations within the ADOM domain for each day ranges between 10 and 21. Throughout the period, these represent monitoring stations in 51 ADOM grid cells which are given in Figure 10.

Figures 11 and 12 show the comparison of the predicted and observed sulphate and nitrate concentration in precipitation on a daily basis. Both of these plots show observed and modelled data ranging over two to three orders of magnitude. In the OSCAR study the data were confined to about one cycle of the log scale. The sulphate concentrations in precipitation have a tendency to be overpredicted while the nitrate concentrations in precipitation are underpredicted. Both plots show large scatter. In fact, less than 50 per cent of the model results for both plots are within a factor of 2 of the observed values. The mismatch between precipitation amounts input to the model and measured values at the precipitation gauge partially explains this scatter.

Figure 13 presents the scatter graph for the daily observed station and model grid averaged precipitation. Like the previous two plots, both the observed and model data range over more than two orders of magnitude. There is also very little correlation between the grid-cell averaged precipitation as calculated by the meteorological preprocessor and the amount measured at rain gauges. Only 25 per cent of the precipitation values are within a factor of two of the observed.

To pursue the hypothesis that the precipitation mismatch is largely responsible for the differences of sulphate and nitrate in precipitation, the ratio of model to observed sulphate and nitrate precipitation concentrations are plotted against the ratios of model precipitation to observed precipitation. Figures 14 and 15

show a definite negative correlation between the above mentioned ratios. When the ratio of the model concentration to observed concentration is much higher than 1 (i.e. model overpredicts), the ratio of model precipitation to observed precipitation is much lower than 1, i.e. the precipitation gauge is measuring higher precipitation than the grid average input to the model and vice versa. Linear regression analysis gives an R^2 correlation coefficient of 0.25 for sulphate in precipitation and an R^2 of 0.46 for nitrate in precipitation. Thus, 25 per cent and 46 per cent of the discrepancies between predicted and observed concentrations in precipitation can be explained by the mismatch between model and observed precipitation for sulphate and nitrate, respectively.

The precipitation event scatter plots of observed and predicted concentrations in precipitation (averaged over individual events) for sulphate and nitrate are given in Figures 16 and 17, respectively. The scatter relative to the previous plots for the daily performance is significantly reduced. The data points representing only one day of available data in the event average are indicated by asterisks and these have a greater tendency for model-observed discrepancies than the rest of the points. The trend for overprediction in the case of sulphate observed in the daily plot (Figure 11) is also apparent here in the event averaged plot.

The above discussion underlines the importance of precipitation input to the "performance" of any scavenging model. To gain an appreciation of how the model predictions compare to observations spatially, the monitoring stations were grouped into 5 regions and the regional averages of the observed are plotted together with the corresponding model averages on a map (Figures 18 and 19). It is seen that for sulphate in precipitation, the observed to predicted ratio is 0.95 in the region covering the heavy emissions area. The ratio decreases to the north and increases to the south.

A limited number of daily ground level air SO_2, sulphate and nitrate measurements is available from the ADS. These data are plotted against model predictions in Figures 20-22. Like the plots for the concentrations in precipitation, these comparisons show a large amount of scatter. SO_2 in air is overpredicted, while sulphate and nitrate in air are significantly underpredicted. In each case, less than 50 per cent of the predictions are within a factor of two of observations.

As nitrate to sulphate ratio in precipitation changes with the season of the year due to the decrease of sulphate formation in the winter, one would expect the ratio to peak in the winter. The range and geometric mean of the nitrate to sulphate ratio in precipitation for the model and from observations are presented for three cases (OSCAR II, OSCAR IV and the present winter study) in Table 7. From these numbers, it is seen that the model reproduces the trends of the observed seasonal variation well. The fact that the NO_x input to the model is too large (see Section 3.5) in the two runs should not alter this conclusion because preliminary indications suggest that sulphate in precipitation is not affected significantly while nitrate in precipitation decreases rather uniformly.

3.4 The ANATEX Study

The Across North America Tracer Experiment (ANATEX) was carried out between January and March 1987 to study atmospheric dispersion behaviour over North America (see Draxler and Heffter, 1989). Three inert perfluorocarbon tracers (PDCH, PMCH and PTCH) were released at ground level at regular 2½-day intervals from two locations in the U.S.: St. Cloud, Minnesota and Glasgow, Montana. The 2½-day intervals between individual releases throughout the entire duration of the experiment allowed the puffs to experience different meteorological conditions while keeping individual

releases separate. This arrangement also alternated releases between day and night. Seventy-seven ground monitoring stations were set up along arcs at approximately equal distance downwind of the Montana site. These stations (Figure 23) cover most of eastern North America and extend as far as Brownsville, Texas and as far north as Goose Bay, Labrador. The basic sampling time for the ground level measurements was 24 hours.

The data collected for ANATEX were used for evaluating long-range-transport models. Since the tracers being simulated are not affected by dry deposition, wet scavenging, chemical and photolytic activities, ADOM was adapted for this application by removing the corresponding chemistry and deposition modules and modifying the emissions to simulate releases at the specified intervals for the duration of the actual release (3 hours). The domain was also extended to the west and north to cover releases from both points. The resulting 38 x 36 domain is given in Figure 24.

The "stripped down" version of ADOM was run for the first 45 days of the three month period and the average pattern for the tracer PDCH released from St. Cloud for this period is plotted in Figure 24. The modelled pattern approximates concentric circles with the centre at the grid of tracer release (11,20). The observed pattern shows more irregularity and the maximum is shifted northeastward to lie over (12,21). Since the releases were made at ground level, the highest concentrations are expected to be measured at the "home" grid regardless of the wind direction. The observed pattern is limited by the density (or arrangement) of the monitoring stations close to the release points and in this case, the maximum concentration is measured at the station closest to the release which is located to the northeast of St. Cloud. This plot also shows that the observed maximum is much smaller than the predicted maximum. Detailed analyses of each release reveal that

the actual plumes frequently pass between monitoring stations without any portion being detected by the measuring instruments.

The PDCH daytime release made on January 5, 1987 (17-19Z) from St. Cloud, Minnesota produced daily concentration patterns (observed and predicted) as shown in Figure 25. The St. Cloud atmospheric sounding at 12Z shows a slightly stable boundary layer with the possibility of low level fog and stratiform clouds up to 800 m. The wind was from the south at the surface and southwest at the upper levels at 10 to 15 knots. St. Cloud is between two low pressure centres, one located to the north in northwest Ontario and the other to the west-south-west in South Dakota. A new low is forming in northeast Colorado. The warm front associated with the S. Dakota low moves from approximately 800 km southwest of St. Cloud to pass over St. Cloud by January 6th, 00Z. By this time the low pressure centre has moved to southeast N. Dakota. The surface wind is still from the southeast at 10 knots and the upper winds are more southerly.

Comparison of level 1 input winds for January 5 1987, 18Z, i.e. one hour into the three hour release from St. Cloud against the weather map for the corresponding period reveals that the locations of the lows in South Dakota and northwestern Ontario as well as the high in southern Ontario are well predicted. The wind speed and direction of about 10-12 knots from the south near the release point also correspond to that recorded on the surface maps. Level 5 (~ 600 m above ground) winds of about 15-16 knots from the southwest also represent the sounding information well near the release location. Six hours later, at 00Z January 6th, the level 1 wind pattern indicates that a new low has developed in Colorado which matches the weather map well. However, the low which was in South Dakota has now moved to northern Minnesota, and according to the input wind to the model, has practically disappeared with a very disorganized wind pattern and low wind speeds in this area.

On the weather map, however, this low still has considerable strength.

When the model predictions of this PDCH release are compared against the contours of observed data for the first three days after release (Figure 25), it is seen that the model contours are more widely spread in the east-west direction than the observed contours. This is due to stretching of the puff under the influence of the two lows (Colorado and James Bay) in the case of model predictions, whereas, in reality the puff first moves north and then south under the influence of the South Dakota low which rapidly passes by the location of the puff. The model input indicates incorrectly that this low has disappeared by the time it has caught up with the puff and hence, in the model, the two more distant lows take over. Due to the strength and closer proximity of the Colorado low, the puff travels further west in the predictions than in the observations, and by the time it starts travelling southwest under the influence of the approaching new Wyoming high it has practically moved out of the model domain.

These findings about model behaviour indicate the importance of correct resolution of pressure fields in determining the input transport velocities, which in turn determine the general movement of pollutant puffs in the atmosphere. In this case, even though the location of most of the significant low pressure points have been predicted remarkably well, the disappearance in the model input of a relatively weak low has resulted in model predictions which indicate predicted puff locations of about two thousand kilometers away from those observed, after two days of travel time. However, this model behaviour for a single puff at a single release point should average out when either many releases are considered or releases are made from many locations.

For the other analyses, the following observations are made:

1. The model reproduces the higher ground level concentrations usually observed when the puff is under the influence of a high pressure system.

2. The modelled concentrations during the first two days after release are usually higher than observations due to the frequent missing of the monitoring stations by the actual plume.

3. Subsequent to the first two days, the modelled concentrations are generally lower than what the observations show. This might be caused by enhanced dispersion due to the numerical scheme in the Eulerian model.

4. The initial spread of the emitted material throughout the grid box of 127 x 127 km in the horizontal can cause deviations in the trajectories of the advected puff even in the absence of complicating small-scale features.

5. The inability of the model wind field to capture small-scale features such as a weak front can cause significant deviations of a single puff trajectory.

6 The present ADOM transport scheme and the accompanying meteorological data are suitable for studying a single source over a period of about a month or for multiple source studies (over 200-300 sources for the present domain) over a shorter period of a few days.

3.5 Eulerian Model Evaluation Field Study

ADOM was evaluated using data from the Eulerian Model Evaluation Field Study (EMEFS). During this field study in the summer of 1988, an intensive effort was made to collect both surface and aircraft data.

A "Model-Evaluation Protocol" (Barchet, 1989) has been developed to provide guidance on the types of tests to be carried out. This protocol has been reviewed by an External Review Panel consisting of 10 experts. It outlines tests to stress the ADOM and RADM models to determine their strengths and applicability. At this stage of the evaluation, only simple statistical techniques have been employed. Comparisons have so far been limited to ground level air and precipitation concentrations. The measured concentrations of most species are available as 24-hr averages while measured ozone concentrations are available hourly. The following sections describe the findings of the evaluation of ADOM with data from the July - September 1988 period.

The data from the monitoring networks are stratified and averaged for comparison with model output. The EMEFS measurement sites are classified into nine regions (Figure 26) based on emissions and meteorological characteristics. Four sites, which were determined to be too close to urban areas were not classified into the nine regions and designated as "U". A site in Massachusetts did not fit into any region and was left as a site by itself designated by "M". Sites outside of these classifications are designated as "0".

The following sections present results of comparison of model outputs with surface observations for the periods, July 19 - August 5, 1988 and August 25 - September 27, 1988. The division is made on the basis of meteorology, Period 1 (July 19 - August 5)

being drier than the Period 2 (August 25 - September 27). It is to be noted in interpreting these results that the dry deposition formulation for the period, July 19 - August 5, 1988 is somewhat different from the other period. The dry deposition module used for the period July 29 - August 5 is expected to give slightly lower deposition velocities for SO_2 and O_3 than the dry deposition module used for the second period.

Figure 27 shows the comparison of modelled vs observed ground level concentration for SO_2 for the second period. The model appears to slightly overpredict the SO_2 concentrations. The correlation between modelled and observed SO_2 concentrations is good. Similar results are obtained when modelled and observed ground level SO_2 concentrations are compared for the first period as shown in Figure 27A.

Figures 28A and 28B give the SO_2 time series plots for the second period for Regions 3 and 5. The trends for the first period for the same regions are shown in Figures 28C and 28D. The temporal trends can, to a first approximation, be attributed to the SO_2 response to precipitation. For Region 5 which covers the heavy emissions area of Ohio, an increasing SO_2 concentration can be related to build up during a dry period, while a decreasing concentration can be attributed to scavenging and rapid in-cloud conversion. The behaviour of Region 3 can also be explained by the above factors, together with transport into and out of the region. Region 5 during Period 1 experienced fog and haze. For Period 2, both Regions 3 and 5 experienced three well-defined precipitation events: 25-26 August and 4-5 September as well as 28-29 August for Region 5 and 29-30 August for Region 3.

Figures 29A and 29 show the comparison of the ground level concentrations of SO_4^{2-} for Period 1 and Period 2 respectively. The model slightly overpredicts the SO_4^{2-} concentrations during Period

1 and underpredicts these concentrations during Period 2. It is noted that non-precipitating clouds are responsible for a significant amount of production of SO_4^{2-} (Ref. Venkatram and Karamchandani, 1991). In an earlier model simulation where non-precipitating clouds were not included, it was observed that the modelled SO_4^{2-} concentrations were severely underpredicted. Including the contributions from non-precipitating clouds to the SO_4^{2-} formation improves the model results as shown in Figures 29A and 29. However, more work remains to be done on the mixing formulations within these clouds.

The sulphate time series plots for Periods 1 and 2 for Regions 3 and 5 are shown in Figure 30 and 30A respectively. The periodicity of the observed data is accurately reproduced by the model. The observed peaks are sometimes underpredicted. For both regions, the fluctuations are caused by a combination of washout by precipitation and transport into and out of the region.

Figure 31 shows the comparison of modelled vs observed total sulphur (SO_2 and SO_4^{2-}) concentrations for Period 2. There is a slight overprediction of total sulphur by the model consistent with the earlier results for SO_2 and SO_{42-} separately. Total sulphur results for Period 1 are not shown here, although from the comparison with SO_2 and SO_4^{2-} individually for this period one would expect the total sulphur comparison to be similar in nature to Period 1.

Figures 32 and 32A show the modelled vs. observed sulphate concentration in precipitation for Period 2 and Period 1 respectively. For both periods, two characteristics are immediately apparent: there is little systematic bias and the scatter is large. The first observation is supported by the mean of the observed and modelled values. For Period 2, the mean observed value is 2.33 mg/l and the mean modelled value is 2.68 mg/l. The two agree to within 15 per cent of each other.

The large scatter can be attributed to the fact that the comparison shown in Figures 32 and 32A is between point (for observed) and area-averaged (for modelled) values. Subgrid scale variability in precipitation can cause considerable mismatch in the comparison if the observed precipitation amount deviates from the grid average. The highly sporadic nature of precipitation will also introduce significant mismatch.

Figures 33 and 33A give the modelled vs observed NO_2 ground level concentrations for Period 2 and Period 1 respectively. There were only a few observations of NO_2 during Period 1 making it difficult for a meaningful interpretation of the comparison results. For Period 2 the comparison between modelled and observed NO_2 concentrations shows little bias with the predicted mean being 6.25 $\mu g/m^3$ compared to the observed mean of 5.54 $\mu g/m^3$.

The averaged NO_2 time series plots for Regions 3 and 6 for Period 2 are given in Figures 34 and 34A. (Region 5 shows many missing days, therefore, the results for Region 6 were presented instead). NO_2 is overpredicted in Region 3. The model appears to predict the magnitudes of NO_2 concentrations in Region 6 well, although the observed periodicity is not reproduced by the model predictions for about half of the period.

Since NO_2 is mainly formed through gas-phase reactions and is not very soluble in water, the fluctuations in the time series are a result of gas-phase chemical conversion and transport. The lack of correlation between the time trends in some regions may be attributed to the dominance of local sources (because of the rapid NO to NO_2 conversion) coupled with local air flow patterns.

The modelled vs. observed comparison of ground level total nitrate (nitric acid vapour plus particulate nitrate) concentrations for Periods 1 and 2 is given in Figures 35A and 35.

Total nitrate is overpredicted by the model for both the Periods. The correlation between modelled and observed values is good. The overprediction may be partially attributed to the fact that HNO_3 is readily deposited to the surface. This is expected to establish strong gradients in HNO_3 concentrations in the vertical. The modelled values for total NO_3^- is an average over a depth of approximately 56m whereas measurements are carried out typically at a height of 3-10 m.

The averaged nitrate concentration time series plots for Regions 3 and 5 during Periods 1 and 2 are given in Figures 36A and 36.

The modelled time series match the observed time series remarkably well, with little phase shift. In the model all nitrates are produced in the gas phase and absorbed into the clouds. Thus precipitation scavenging is expected to predominately influence the time series of modelled nitrates. The close match between the modelled and observed time series for total NO_3^- suggests that the model formulation of wet scavenging of NO_3^- is reasonable.

Figures 37A and 37 show the comparison of modelled vs observed concentrations of NO_3^- in precipitation. There is considerable scatter in this comparison although there is little apparent bias between the modelled and observed values. The intermittency in precipitation fields can explain some of this scatter as in the case of SO_4^{2-} concentrations in precipitation. Also, the formulation of particulate NO_3^- in the model is approximate. This, coupled with the fact that NH_3 emissions are very uncertain, can introduce some uncertainty in the production and spatial distribution of particulate nitrates. Further, in-cloud formation of NO_3^- is assumed to be negligible in the model. These factors may also be responsible for part of the observed scatter.

The modelled ground level ozone concentration time series are compared with the corresponding observed time series for ozone at several regions as shown in Figures 38A to 38F for Period 1 and Period 2. Several points are noteworthy in these comparisons. First, the diurnal trends in ozone are well reproduced by the model. Second, the model simulates the peak ozone concentrations reasonably well when they do not exceed 50 to 60 ppb. However, the peak concentrations exceeding 50 to 60 ppb are not reproduced by the model well.

Several sensitivity studies with emissions of VOC's, boundary conditions of NO_x and VOC concentrations, dry deposition velocity of ozone and the mixing formulation in the atmospheric boundary layer have been made to understand the cause of the underprediction. None has produced the desired effect of only increasing the magnitude of the ozone peak concentrations. It has been suggested that peak ozone concentrations in excess of 50 to 60 ppb are dominated by sub-grid scale distribution of NO_x and VOC sources and the sub-grid scale chemistry. It is noted that ADOM employs a horizontal grid of approximately 127 km x 127 km. This grid size may be too large to enable proper simulation of the peak ozone concentrations. Subgrid scale effect, in combination with some effects that have been investigated, may be the key to improving ADOM's prediction of diurnal ozone peak.

3.6 Preliminary Comparison of Linear and Comprehensive Models

The Ontario Ministry of the Environment's (OME) linear Lagrangian model was run using the wind, precipitation and total emissions data that served as input to ADOM for the EMEFS period. The SO_2 ground level concentrations, the sulphate ground level

concentrations and the sulphate concentrations in precipitation predicted by the linear Lagrangian model are given in Figures 39-41. Concentrations of SO_2 in air are overpredicted by approximately 110 per cent (best fit line forced through the origin has a slope of 2.1) while the sulphate concentrations in air are scattered about the 1:1 line. The best fit line forced through the origin for the sulphate in precipitation has a slope of about 0.87, indicating a 10-15 per cent underprediction.

Linear Lagrangian models are usually simple enough that some parametric values can be adjusted to alter performance. For the OME Lagrangian model, the parameters that will most significantly affect model performance are: mixing height, conversion rate of SO_2 to sulphate, wet scavenging coefficients and dry deposition velocities.

Adjusting the mixing height in the OME Lagrangian model will affect all the species by changing the volume over which the species spread. For this run, a daily average mixing height of 800 m corresponding to fall conditions was used.

The conversion rate of SO_2 to sulphate will change the ratio of SO_2 to sulphate with distance away from the source. A higher conversion rate would result in greater decrease in the ratio of SO_2/sulphate with distance away from the source. The spatial pattern of both species will be affected.

The scavenging coefficient used in this model for sulphate (3×10^{-4}/s) is one order of magnitude higher than that for SO_2. The coefficient for each species can be adjusted independently. If the SO_2 scavenging coefficient is adjusted, it will affect the amount of SO_2 available for conversion to sulphate and the SO_2 spatial distribution. Though it appears from the relative magnitude of the scavenging coefficients of SO_2 and sulphate that

the same percentage change to the two coefficients would affect sulphate more, the actual pattern is more complicated than that. During heavy precipitation, SO_2 and sulphate can be scavenged out rapidly leaving insignificant amounts for subsequent scavenging. In this case, the amount scavenged is relatively insensitive to the values of the scavenging coefficients.

The dry deposition velocity used in this model is 5 mm/s for SO_2 and 0.5 mm/s for sulphate. Consequently, a change in the SO_2 dry deposition velocity would affect SO_2 directly. However, sulphate would also be affected by a change in SO_2 through SO_2 to sulphate conversion.

Given the biases seen in the Lagrangian model concentrations, the following parameter adjustments could be considered:

(1) Increase the mixed layer height and thus lower the SO_2 and sulphate air concentrations.

(2) Increase the conversion rate of SO_2 to sulphate to reduce the positive bias of SO_2 in air and any negative bias of sulphate in air produced by increasing the mixed layer height.

(3) Adjust the dry deposition velocities and wet scavenging rates to tune the model to match the data further.

Since the Lagrangian model results can only be compared for 3 species (SO_2 and sulphate in air and sulphate in wet deposition), it is possible to produce good results at the expense of poor performance in dry deposition or in the vertical distribution of the species. For example, increasing the boundary layer height required to reduce SO_2 air concentrations will result in more SO_2 at higher levels. Also, any set of tuned parameters would be

specific to the current distribution and magnitude of sources. Good model performance at ground level for the species examined could be limited to these specific conditions. Also, as can be seen by comparing the performance of the comprehensive and linear models (e.g. Figure 27 with Figure 39, Figure 29 with Figure 40), the comprehensive model shows less scatter than the linear model. It has been noted that the OME linear Lagrangian model produces a smoother field (Misra et al. (1989) and Section 4.1) than the comprehensive models. Thus, the comprehensive model has better spatial resolution than linear models.

In order to make the linear Lagrangian model perform better for the three species examined, the parametric values would be altered without any justification other than to make the results look good. This is difficult to defend scientifically. The other aspect of a good scientific model is its ability to address questions and to respond to different situations (i.e. different source mixes and locations). A model with limited physics and chemistry tuned to present conditions is not as useful for scientific purposes. Even if the system behaved linearly with an emission cut, the best parameter values for present conditions would not necessarily give good performance in different situations.

ADOM has been used successfully as a diagnostic tool in the case of the NO emissions. What allowed ADOM to be used in this way is the confidence that modellers have in the model, having included what is currently known about the processes in the long-range-transport of acidic precipitation. In the process of trying to explain the sulphate air concentration underprediction in both ADOM and RADM, some processes which so far have been neglected or are still unknown may be found to be important, thus enhancing our understanding. In this way, comprehensive models can actually make contributions to the science of acidic precipitation.

In summary, the performance and scientific utility of linear models are limited by their formulation and inherent assumptions. On the other hand, comprehensive models provide a framework for future improvements and can yield answers consistent with the science.

4. Scenario and Sensitivity Tests with ADOM

Perturbation runs have been made with ADOM to answer two types of questions:

1. If the model is an accurate representation of nature, then how would nature respond to different emission scenarios, especially to a scenario involving reduction in sulphur emissions. If the response is not linear, then the degree of non-linearity has to be quantified.
2. What are the major mechanisms responsible for the model's response?

The first issue is a policy consideration and the second one a scientific question. The major sensitivity runs using ADOM are discussed below, starting with the first issue.

4.1 Emission Reduction Tests during a Spring Period

The atmosphere has the potential to respond non-proportionately to emission reductions through oxidant limitation. Earlier linear models of the statistical or Lagrangian type cannot address these situations because detailed chemistry is not considered in their formulations. Comprehensive models like ADOM and RADM have been developed to address the question of non-proportionate response to emission changes, and to gain a better understanding of the science through detailed representation of the physical and chemical processes.

The first simulation of an emission reduction scenario with ADOM was performed for the OSCAR period. Comparison of model predictions with observations for this period has already been reported in Section 3.1. For this simulation, a base case run for a twenty day period (April 10 - 29, 1981) was first made. Then the results of an emission scenario over the same period are compared with the base case results to determine model response. The SO_2 emissions and precipitation input for this run are given in Figures 42 and 43. Figure 42 shows three grid squares having SO_2 emissions between 2000 and 5000 metric tonnes per day. The first one contains the Sudbury super-stack to the immediate north of Lake Huron. The other two grid squares straddle the Ohio and Pennsylvania border. Many other grid squares in the northeastern U.S. also have substantial SO_x emissions. As noted in Section 3.1, the weather patterns during OSCAR were such that low pressure disturbances tracked across southeastern Canada and northeastern U.S., with the heaviest precipitation to the south of the Great Lakes. Figure 43 shows a double peak in the precipitation contours with the higher peak just south of Lake Michigan and the other on the Ohio Pennsylvania border. Both of these peaks are above 110 mm over the twenty day period.

The major results of this base case simulation for the entire twenty days are given in Figures 44-48. The ground level concentration of SO_2 (Figure 44) shows a pattern that closely resembles the SO_2 emissions pattern. The highest contours are around the Ohio-Pennsylvania border where the highest emissions per ADOM grid square are also located. The concentration here is above 60 $\mu g\ m^{-3}$. The grid containing the INCO stack at Sudbury shows a local maximum. However, the maximum concentration here only reaches 40 $\mu g\ m^{-3}$. This is due to the height at which the emission is released. The physical height of this INCO stack is 381 m above ground which is the tallest stack in North America. The 5 $\mu g\ m^{-3}$ contour for SO_2 encloses the eastern half of the U.S. and includes

the southern one-third of Ontario and the southern tip of Quebec. It also follows the eastern coastline of the U.S. fairly well.

The pattern of sulphate concentration in air (Figure 45) shows a greater spatial extent than the SO_2 pattern. The extent of the sulphate, e.g. the 2 $\mu g\ m^{-3}$ contour, reaches far out into the ocean. Notably different from the SO_2 pattern is the position of the maximum which is now on the North Carolina-South Carolina border and the lack of fine details overall. This is to be expected as sulphate is formed from SO_2 at a rather slow (1-2 per cent per hour) rate. At the same time as sulphate is being formed, transport and diffusion work to spread out the concentration, thus producing a smoother pattern. Precipitation scavenging also affects the location of the maximum 20 day average air sulphate concentrations.

The pattern of nitrate concentration in air (Figure 46) shows a ridge of high values starting from Lake Erie extending southeast through Ohio to Kentucky. There is also another strong maximum in southern Louisiana. Except for the position of the maximum, the ground level concentration patterns of sulphate and nitrate resemble each other. These two species have the following in common: they both are secondary species formed from acidic precursors and they are both scavenged rapidly by precipitation. The location of the major emissions for the two are also similar. Power plants in the U.S. produce both SO_2 and NO_x. The major differences between the two are: gas-phase conversion of NO_x to nitrate is more rapid than the 1-2 per cent for SO_2 to sulphate, aqueous conversion of NO_x to nitrate in cloud is insignificant whereas it is believed that in-cloud processes are responsible for a significant part of ground level sulphate production and dry deposition of sulphate is insignificant whereas nitrate deposits readily to a water surface. The first two dissimilarities between sulphate and nitrate mentioned above may work to the net effect of

producing a similar overall conversion from acid precursor to the final acid for sulphur and nitrogen, thus producing a similar ground level pattern.

The sulphate concentrations in precipitation for this OSCAR scenario (Figure 47) show many fine scale features. Towards the southern end of the domain are some tight contours formed near the precipitation region boundary. Large sulphate concentrations are associated with small precipitation amounts, but the deposition of sulphate is not large. For our considerations, these can be ignored. In the area of heavy precipitation (Figure 43), the sulphate concentration in precipitation is around 30-40 μ mole l^{-1}. Considering the large amount of precipitation in this area, it is reasonable to conclude that the largest wet deposition of sulphate also occurs in the same vicinity which, in this case, happens to co-incide with the heavy emission region of the U.S. The pattern of nitrate concentration in precipitation (Figure 48) shows some tight contours near the precipitation boundary as in the case of the sulphate in precipitation. The area around Ohio and Pennsylvania shows 20-60 μ mole l^{-1} of nitrate.

In order to gain a better appreciation of ADOM's prediction, the Ontario Ministry of the Environment (OME) linear Lagrangian model was run for the first 16 days of this 20-day period with the same input data used for ADOM and the results compared with ADOM's wet sulphate deposition prediction for the same period. The reason for leaving out the last four days in the linear model run is because each initialization of a trajectory in the linear model requires 4 days of subsequent data and no data beyond April 29, 1981 are available. For the linear model, the wet flux of the sulphate (Figure 49) pattern is fairly smooth with quasi-concentric contours centred on western Pennsylvania. The maximum is about 800 $\mu g\ m^{-2}h^{-1}$ for this 16-day average. The corresponding pattern generated by ADOM (Figure 50) also shows a maximum which is

slightly larger than 600 $\mu g\ m^{-2}h^{-1}$ at the western side of Pennsylvania about 1 grid cell to the south of the maximum produced by the linear model. It is seen from this comparison that ADOM predicts that sulphate wet deposition will extend further east than predicted by the linear model, causing the peak value to be lower and a 200 $\mu g\ m^{-2}h^{-1}$ contour to appear to the east of Nova Scotia and another 200 $\mu g\ m^{-2}h^{-1}$ to extend down to the east of Rhode Island. ADOM shows more fine structure than the linear model. The smoothness of the Lagrangian model pattern is partially an artifact of its scavenging formulation which scavenges the entire puff when only the puff centre encounters precipitation. Also, since the modelled puffs expand as they travel downwind, smoother deposition field occurs.

Comparison of the 16-day average ground level air sulphate concentration pattern produced by the linear model (Figure 51) with the corresponding pattern by ADOM (similar to Figure 45 and consequently not shown) reveals that the extent of the 4 $\mu g\ m^{-3}$ contours for both models are similar and that local maxima within the model domain are in similar locations (western Pennsylvania and western Carolinas) except the relative magnitudes are reversed, i.e. the linear model shows a stronger maximum at Pennsylvania than in the Carolinas.

From the above comparisons of the two models, it can be concluded that both models produce similar gross features of wet sulphate deposition and ground level concentration. If both models are run for longer periods, e.g. up to 1 year, then the detail features observed for ADOM will have substantially disappeared because of the averaging effect. The predictions of both models will then be comparable.

It is noted that linear models have a proven record to simulate the present deposition pattern on a time scale of a year

or longer (e.g. Clark et al., 1987 on the ISDME project). This is a result of the calibration of parameters like the scavenging coefficients, dry deposition velocity, SO_2 oxidation rate and mixing height etc. to the present conditions. Therefore, in this sense, linear models can match the performance of comprehensive models for the present conditions. For emissions scenario projections, linear models assume that an emission reduction translates into a corresponding wet deposition reduction (except for a small background deposition term included in the model). Thus, if the OME linear Lagrangian model simulates a 50 per cent across-the-board reduction in SO_x emissions for the 16-day period, the patterns produced would be very similar to those in Figures 49 and 51 except that the labelled values are halved.

ADOM was run with 50 per cent of the SO_x (SO_2 + sulphate) in the base case emissions (boundary and initial conditions remaining the same) for the same 16-day period and the results were compared with the base case. Figure 52 shows the percentage change of the sulphate in precipitation in response to this emissions change. The entire domain shows a reduction of sulphate in precipitation. In the vicinity of the heavy emissions areas, the reduction is between 30 to 40 per cent of the base case. A 40 to 50 per cent reduction was found for the southern U.S. and over the Atlantic Ocean. Thus, by reducing SO_x emissions by 50 per cent across the domain, a 30-40 per cent reduction occurs in areas which include sensitive receptors.

The response of ground level air SO_2 concentrations to the 50 per cent SO_x emissions reduction is plotted on Figure 53. This shows that the response is approximately linear. More than half the area of the domain is found within the 50 per cent contour. The other areas outside are mainly affected by the boundary conditions.

Figure 54 shows the ground level air sulphate response to the 50 per cent across the domain reduction of SO_x emissions. Almost half of the domain is included in the -40 per cent contour and the remaining areas, like the results presented for SO_2, show dominance by the boundary conditions. Thus, the response of ground level air sulphate concentration is still non-linear and the degree of non-linearity is somewhere between the non-linearity of wet sulphate (30 - 40 per cent reduction in response to 50 per cent SO_x reduction) and the linear response of air SO_2.

Since dry deposition of sulphate is very ineffective and for all practical purposes can be ignored, and dry deposition of SO_2 is proportional to the ground level SO_2 air concentration which has been determined to respond linearly to an SO_x reduction, then dry deposition of SO_x can also be considered linear. It should be noted that total deposition (wet plus dry) is more linear in its response to a SO_x emission reduction than was found for wet deposition alone.

The surmise is that the fraction of the sulphur advected out of the domain must be less for the emission reduction scenario than in the base case model run. After examining the ground level air sulphate, the above contention seems to be contradicted because the modelled concentrations are more than 50 per cent of the base case values (Figure 54) and the wind speeds have not changed. The non-linear response of the model is however related to in-cloud processes and it would be at these heights that changes in the distribution of sulphur between air and cloud water would be expected. A reduction in the export of sulphur from the model domain at higher levels in the atmosphere would preserve the mass balance and account for the non-linear response in wet sulphate deposition.

One more emission reduction scenario was made with both SO_x and NO_x emissions cut by 50 per cent. Figure 55 shows the sulphate in precipitation response which indicates that it is even more non-linear than the previous case. In the vicinity of the heavy emission area, reductions of less than 30 per cent are sometimes seen. A reason for this may be the competition of oxidants between SO_x and NO_x. Since oxidants like OH and O_3 participate in the conversion of both SO_2 and NO_x and in the production of H_2O_2 which is needed for aqueous conversion, reducing NO_x emissions may free up more oxidants for converting more SO_2 to sulphate.

The response of nitrate in precipitation to the simultaneous reduction of SO_x and NO_x by 50 per cent is given in Figure 56. The pattern does not show a undirectional response as was found for sulphate wet deposition. In some locations, the response exceeded the initial reduction of 50 per cent. More than 60 per cent reduction in nitrate in precipitation over significant areas resulted. This phenomenon may be due to the manner in which gas-phase oxidants are being competed for by the sulphur and nitrogen species (since the nitrogen species do not react in the aqueous-phase).

4.2 Emissions Reduction Tests during a Winter Period

The two scenario runs (50 per cent reduction in SO_x emissions and 50 per cent reduction in both SO_x and NO_x emissions) performed for the OSCAR study are repeated for the winter study. The performance of ADOM for this period covering January 29 to February 7, 1985 was reported in Section 3.3. The average sulphate and nitrate concentrations in precipitation for this period are given in Figures 57 and 58, respectively.

Figure 59 shows the change in sulphate in precipitation in response to a 50 per cent reduction in SO_x emissions. Over the

heavy emissions area to the south of the Great Lakes, the average reduction in sulphate in precipitation is about 25 per cent. This is lower than the 30-40 per cent that was predicted for the OSCAR period. Over the ocean, the response to this 50 per cent reduction in SO_x seems to be less non-linear (-35 to -40 per cent). The total precipitation (Figure 60) during this period shows a complicated pattern with rather localized (on a spatial scale of 100-300 km) precipitation except out over the ocean. The details of the response pattern are likely to be affected by the structure in the total precipitation.

A major reason for a non-linear response in wet sulphate deposition has been thought to be oxidant limitations in clouds as in-cloud scavenging of SO_2 and subsequent oxidation to sulphate produces at least half of the sulphate in precipitation. The major aqueous chemical process involved is the SO_2-H_2O_2 reaction. Since one molecule of H_2O_2 is consumed in oxidizing one molecule of SO_2, the ratio of SO_2 to H_2O_2 in air would indicate how effective this process is. Figure 61 presents the ambient SO_2/H_2O_2 ratio averaged for the entire winter study period for the base case. Both the SO_2 and H_2O_2 values (moles) were integrated for the entire depth of the grid column. Since clouds tend to mix material vertically, the column integrated mass would be more representative of actual in-cloud concentration than the ratio for any one layer. The SO_2/ H_2O_2 ratio contour has a peak near the Ohio-Pennsylvania border where the highest SO_x emissions are normally found. Overall, as one moves away from this region the ratio decreases, yet the ratio of 5 contour covers most of the area of interest to us. This is still quite far from the ratio of 1 which is required for complete conversion of SO_2 to sulphate by this SO_2-H_2O_2 pathway. By reducing the SO_x emissions, which is over 95 per cent SO_2, by 50 per cent, the ratio is approximately halved. Yet, the oxidant-starved situation in the heavy emissions area is still not alleviated, thus explaining the non-linearity experienced.

When SO_x and NO_x are reduced simultaneously by 50 per cent, the sulphate in precipitation responded even more non-linearly (Figure 62), reducing only by 15 to 20 per cent in the heavy emissions area. This is the same as the trend predicted for OSCAR, i.e. cutting both NO_x and SO_x simultaneously, increases non-linearity, and is probably due to oxidant competition. The nitrate in precipitation response to this simultaneous 50 per cent reduction in SO_x and NO_x is plotted on Figure 63 which shows a less than 10 per cent change in the heavy emissions area. This is the largest non-linearity that we have encountered so far. The response of the ground level NO_2 concentration to the 50 per cent simultaneous reduction of SO_x and NO_x (Figure 64) shows only a 25 per cent or less reduction in the heavy emissions area. The further one goes away from this region, the smaller the non-linearity becomes until the reverse trend is experienced in Canada, the Atlantic Ocean, and in most areas to the west of Iowa and south of Tennessee. It should be noted that for these winter simulations, the model predicts low ground level ozone concentrations. Figure 65, shows that over most of the land area, the average ozone concentration for this period is no more than 9 ppb and in the heavy emissions area about 3 ppb. Individual comparisons of the prediction with observed values at specific times show that the model usually underpredicts ozone. The model predictions over land never exceed 30 ppb for this period while much higher values have been observed.

The underprediction of O_3 suggests that the production of other radicals like OH which are related to the ozone concentration is insufficient, causing the non-linearity in both the sulphate and nitrate in precipitation. Thus, until the reason for the ozone underprediction is identified, the model response to emission cuts for this winter season must be viewed with caution.

4.3 Suppression of Major Aqueous Oxidation Mechanisms

In Section 4.1, it was shown that ADOM's prediction of sulphate in precipitation responded non-linearly to a 50 per cent reduction in the SO_x emissions. Five mechanisms are responsible for the sulphate in precipitation. They are: in-cloud scavenging of sulphate, below cloud scavenging of sulphate and three aqueous oxidation mechanisms for converting SO_2 to sulphate in cloud water. The contribution of each of the three aqueous oxidation mechanisms to the overall sulphate in precipitation is investigated here. This will identify the dominant aqueous oxidation mechanism and is the first step in understanding what causes the model's non-linear response. The next section will investigate the response of individual chemical pathways to SO_x reduction. This will directly point out what causes non-linearity.

For the present simulations, the period from April 19 to 24, 1981 (which covers OSCAR IV) was chosen because of the consistent precipitation experienced over the heavy emissions area in Canada and the U.S. The daily precipitation amounts of the last three days are shown in Figure 66. During the last 3 days of this period, a large low pressure system tracked from southern Saskatchewan through Wisconsin and then to the New England states. Significant precipitation started on April 22, 1981 with showers and thundershowers dominating to the west of Lake Michigan while rain and drizzle fell over northwestern Ontario. As the disturbance moved eastward, more precipitation was experienced over northeastern U.S. and southeastern Canada until the disturbance moved out over the Atlantic on April 24, 1981. Only model results for the period from April 22 to 24, 1981 are used for the present analyses and only results of representative days are presented. The first 3 days of the run were made to "flush out" the initial conditions and allow the model to settle to an equilibrium with the emission fields.

The three major aqueous chemical processes studied here are: oxidation of SO_2 to sulphate by H_2O_2, by O_3 and the catalytic oxidation of SO_2 to sulphate by O_2 in the presence of Fe and Mn. Each of these pathways is turned off individually and the resulting sulphate concentrations in precipitation are compared with the base case for each of the last three days of simulations. Then all three of the above processes are turned off simultaneously to estimate the approximate contribution of aqueous oxidation to total sulphate concentration in precipitation. The word "approximate" is used here because with the suppression of one reaction, other reactions will partly compensate for the change. For example, if aqueous oxidation by H_2O_2 is suppressed, more SO_2 will be available for oxidation by O_3, resulting in more sulphate production through this pathway. The processes that can contribute to sulphate concentrations in precipitation, on top of the three studied here, are nucleation scavenging and below-cloud scavenging of sulphate. The amount of sulphate available for these two processes are in turn affected by the availability of SO_2. To determine the exact contribution of each oxidation reaction, the percentage of each of the species formed by a particular pathway must be tracked internally in the model. This is not done in this analysis. The model is in this sense treated as a "black box".

Each of the three aqueous chemical processes is turned off by setting the reaction rate constants to zero while all other mechanisms such as mass transfer into cloud water and gas phase chemical reactions are left unaltered. The base case concentrations of sulphate in precipitation for April 23-24, 1981 for the four oxidation suppression cases are given in Figure 67.

Suppression of Aqueous H_2O_2 Oxidation

Figure 68 shows the percentage change from base case runs in daily-averaged concentrations of sulphate in precipitation for

April 24 when aqueous H_2O_2 oxidation is suppressed. The trends of all three days are similar. Sulphate concentrations have generally decreased although there are isolated pockets of small increases. The increases could be due to larger SO_2 air concentrations being advected into the area and converted to sulphate by gas or aqueous phase processes. The general decrease in sulphate precipitation concentrations reflects the reduction in aqueous-phase oxidation of SO_2 to sulphate. Neglecting the changes in the northeast corner of the domain which result from a local flow pattern and are affected by the boundary conditions, the largest percentage decrease usually occurs at the leading edge (east side) of the precipitating region away from the heavy emission areas near Ohio and Pennsylvania. On this last day, significant changes are also seen at the rear of the precipitation region.

Suppression of SO_2 Oxidation by O_3

Figure 69 shows the percentage change of sulphate concentrations in precipitation for April 23 and 24, 1981 when aqueous O_3 oxidation is suppressed. Except for small isolated pockets, sulphate precipitation concentration has decreased overall. Outside of the heavy precipitation region (where heavy precipitation is defined as greater than 10 mm/day) the changes are small. Within or in the immediate vicinity of the heavy precipitation region the changes can be as high as 18 per cent on the 22nd, 29 per cent on the 23rd and 26 per cent on the 24th. This pattern is the opposite of that found for H_2O_2 suppression where the maximum changes occur away from the heavy precipitation region.

Suppression of the Catalytic Oxidation of SO_2 by O_2

The simulations with suppressed oxidation by O_2 in the presence of Fe and Mn reveals insignificant changes (much less than

1 percent) in all species involved and consequently are not shown here.

Total Suppression of Aqueous Reactions

The pattern of percentage change in sulphate precipitation concentrations for April 23, 1981 when all aqueous reactions are turned off is shown in Figure 70. The sulphate precipitation concentration decreased at all places except for a small patch near the northeast corner resulting from boundary condition effects during the first two days. Most of the changes in sulphate precipitation concentrations ranged from 30 to 70 percent. Unlike the patterns due to suppression of H_2O_2 or O_3 oxidation, this pattern shows little or no general gradient within the main precipitating region. This result was expected since the patterns resulting from suppressing H_2O_2 and suppressing O_3 were negatively correlated near the main precipitation region.

Discussion of the Results

Without the benefit of tracking the species discussed here through the source and sink mechanisms in the model code, some of the following discussions rely on our understanding of the mechanisms involved and are sometimes qualitative. When the H_2O_2 reaction is suppressed, significant changes in the sulphate precipitation concentration (Figure 68) usually occur in areas experiencing low precipitation amounts. Some exceptions to this are found in the last simulation day where significant changes (> 30 per cent) are found in some areas experiencing more than 10 mm of precipitation.

Because of H_2O_2's high solubility, its concentration in cloud/rain water will have an inverse relation to the liquid water content in clouds. On the other hand, the concentrations of other

less-soluble species in cloud/rain water will not be similarly affected by the cloud liquid water content. In the absence of cloud, the air concentrations of H_2O_2 and O_3 above the mixed layer do not vary substantially from one grid to another. Consequently, with the onset of a cloud in the model, higher H_2O_2 concentrations can be expected in cloud water over light precipitation regions while O_3 concentrations in cloud water remain fairly uniform for all precipitating regions. Thus, the conversion of SO_2 to sulphate through H_2O_2 oxidation has a larger contribution to sulphate precipitation concentrations in light precipitation areas.

The above argument is strengthened by the analysis of vertical concentration profiles generated by ADOM. An example of this is given in Figure 71 for grid (16,19) in central Ontario which shows that H_2O_2 in air is almost completely eliminated with the onset of precipitation at 0600 GMT on April 23, 1981, while the air concentrations of other species remain largely unchanged. This grid covers the Sudbury area where the largest single point source of SO_x (International Nickel Company) is located. This source is responsible for the significant peak in SO_2 concentration at around 0.6 km above the surface before the onset of precipitation. Though only the first 6 hours with precipitation are shown, this condition persists throughout the entire precipitation period. Even a small liquid water content in cloud is effective in removing most of the H_2O_2. After H_2O_2 is depleted, SO_2 can only be converted to sulphate in cloud through the oxidation by O_3 (the action of O_2 in the presence of Fe and Mn being relatively unimportant). Given enough time, as in persistent precipitation, significant amount of SO_2 would be converted through oxidation by O_3.

When the percentage changes for the suppression of individual processes are added together they amount to significantly less than the percentage changes experienced when all aqueous oxidation reactions are suppressed (see Figure 72). In the main

precipitation region, this figure shows that adding up the effects of suppressing the individual oxidation reaction can result in underestimating the combined effects by more than half. Compensation for one suppressed process by another is very substantial. This shows that even though H_2O_2 oxidation of SO_2 in the aqueous phase is very rapid, the persistence of O_3 during continuous precipitation can significantly affect the SO_2 oxidation when H_2O_2 is depleted. Thus caution must be exercised in interpreting the individual effects of each process in a complex model with more than one possible feedback mechanisms.

From the above considerations, it can be concluded that the contributions of all aqueous chemical processes to sulphate in precipitation may be larger than the range of 40 to 60 per cent indicated in Figure 70. Gas-phase conversion of SO_2 to sulphate will partially compensate for the suppressed aqueous oxidations. Thus, by extrapolation, it is possible that aqueous-phase oxidation actually accounts for 50 to 80 per cent of the sulphate in precipitation.

Table 8 gives the change in the total amount of sulphate that is deposited through precipitation over the entire model domain as a result of oxidants suppression. Although as shown previously (Figures 68 and 69) O_3 oxidation can be as significant as H_2O_2 oxidation in heavy precipitation regions, the overall contribution of O_3 oxidation to the production of sulphate is less than a third of the sulphate production due to H_2O_2 oxidation. On specific days, e.g. April 21, 1981, total O_3 oxidation over the entire domain can be as low as 5 per cent of the H_2O_2 oxidation. The daily contribution of all oxidants as seen by suppressing all aqueous oxidations to wet deposited sulphate within the model domain (last row in Table 8) is within the range of 40 to 50 per cent. This is between 1.4 and 1.7 times the sum of the two rows above (H_2O_2 and O_3 suppression individually).

4.4 Suppression of SO_2 Oxidation Pathways with SO_x Emissions Reductions

The sensitivity tests in the previous section have identified the aqueous oxidation of SO_2 by H_2O_2 as the most important pathway for the production of sulphate in precipitation. Yet, the contribution of the SO_2-O_3 reaction in the production of sulphate in precipitation can in certain situations (continuous precipitation and heavy emissions) rival that of the H_2O_2-SO_2 pathway. This section addresses the question of which of these two pathways would respond non-linearly to SO_x reduction by simultaneously suppressing a pathway and imposing a 50 per cent SO_x emission reduction.

Figure 73 shows the response of sulphate in precipitation to a 50 per cent reduction in SO_x emissions for April 23 and 24, 1981 when H_2O_2 is the only major aqueous phase oxidant. Departure from linearity is displayed here as (base case - 2 x 50 per cent emission cut case)/base case. The responses that lag behind the reduction percentage will be represented as a negative number and vice versa.

The base case for this run is the O_3 oxidation suppressed case shown in Figure 69. All three days (April 22-24) show significant non-linearity. Some areas experience non-linearity greater than -60 per cent while the majority of the grids show non-linearity of -40 to -60 percent. On the 24th, a sizeable strip bordering the eastern edge of the precipitation region shows close-to-linear behaviour. Apart from this trend, no other spatial pattern is obvious.

Figure 74 shows the model's response to a 50 per cent reduction in SO_x emissions on April 24, 1981 when H_2O_2 oxidation is suppressed. The base case for this run is the H_2O_2 oxidation

suppressed case in Figure 68. This is plotted in the same manner as in the last figure. Significant non-linearity is experienced for all three days though only the last day is shown. The degree of non-linearity is slightly less than the previous case. Away from the boundaries only a small fraction of the grids show more than a -40 per cent departure from linearity. Most other grids show between -10 to -30 per cent departure from linearity.

Figure 73b shows that the only region indicating close-to-linear response to an SO_x emission cut is in remote areas. Over the Atlantic where the SO_2 concentration is low and H_2O_2 is in relatively abundant supply, a linear relationship occurs between sulphate in precipitation and SO_x emissions. Closer to the emission sources, non-linearity is experienced through H_2O_2 limitations.

For the case where the only major oxidant is O_3, the situation is different. Since O_3 concentration in air is usually one to two orders of magnitude higher than H_2O_2 and O_3 is not very soluble in water, oxidant limitation through rapid depletion cannot cause non-linearity. With less SO_2 in the air due to the 50 per cent reduction, less sulphate is formed in the aqueous-phase leading to higher pH values in cloud water which in turn increases the solubility of SO_2 in water with a net effect of producing more sulphate than a linear response would give. Higher pH values also increase the reaction rate for O_3 oxidation. The same is not true for the H_2O_2 - SO_2 reaction. In this case, the slower H_2O_2 - SO_2 reaction at higher pH values has offset the change in SO_2 solubility to bring about a pH independent conversion rate of SO_2 to sulphate - via H_2O_2 oxidation (Seinfeld (1980) and Schwartz (1982)). Thus, the aqueous O_3 - SO_2 reaction is inherently non-linear as opposed to the oxidant limited non-linear behaviour of the H_2O_2 -SO_2 reaction. Further, the slow rate of SO_2 - O_3 aqueous

phase reaction introduces non-linearity if the cloud life-time is short.

A key to the importance of O_3 in converting SO_2 to sulphate is the residence time of the cloud liquid water. A short residence time would not allow the slow O_3-SO_2 reaction to proceed very far. Thus an accurate parameterization of the cloud microphysics in the model is critical. This will have to be investigated further.

4.5 Sensitivity of Ozone in Ontario to NO_x and RHC

The summer oxidant study reported in Section 3.2 has established the performance of ADOM in predicting the temporal trends and magnitudes of ground level concentrations of ozone. This study assesses the impact of emission scenarios on the ground level ozone concentration in Ontario by performing five runs, each representing a different emission scenario. The base case for this comparison is the ground level ozone concentration generated in the run described in Section 3.2.

The period of interest is June 9 - 17, 1983. During this period, southern Ontario experienced a major ozone episode with frequent exceedance of the Ontario air quality criterion for ozone (80 ppb). This study tries to determine whether controlling the emissions of NO_x and/or RHC in Ontario alone can help to reduce the number of exceedances of the provincial air quality criterion. The five scenario runs are:

A. Eliminate emissions of NO_x completely in Ontario
B. Eliminate emissions of anthropogenic RHC completely in Ontario
C. Eliminate emissions of both NO_x and anthropogenic RHC completely in Ontario
D. Reduce emissions of NO_x in the U.S. by half, and

E. Reduce emissions of anthropogenic RHC in the U.S. by half.

Ontario is divided into three zones for analysis. They are (Figure 75): southern, central and northern Ontario. It is realized that southern Ontario has most of the NO_x and anthropogenic RHC emissions of Ontario whereas emissions in central and northern Ontario are mainly biogenics which have not been changed in these scenario runs.

In order to assess the probability of an exceedance for a certain emission scenario, the model prediction which is a unique number, must be translated into a probability of exceedance. Karamchandani et al. (1989) assumed that the observed data would form a log-normal distribution about each model prediction. The point on this log-normal distribution associated with the Ontario criterion can be calculated and the area under the curve beyond this point represents the probability of exceedance. As the model prediction changes, the distribution and consequently the area under each segment of the distribution also changes. From this, the probability of exceedance is estimated for each scenario. The mathematics of this approach is given in Karamchandani et al. (1989). The results of this analysis and other comparisons are given for the first emission reduction scenario and the results of other scenarios are highlighted.

The base case maximum ground level ozone concentration in Ontario (Figure 76) for June 14, 1983 shows that the two grid cells on the north shore of Lake Ontario experience the highest ozone concentration of between 160 and 185 ppb. The grid cell on the left covers metro Toronto. All of southern Ontario is predicted to experience more than 60 ppb. Central and northern Ontario experienced much less ozone. From Figure 77, almost 70 per cent of southern Ontario has a 90 to 100 per cent chance of exceeding the

Ontario ozone criterion. When the NO_x emissions in Ontario are eliminated (Figure 78), southern Ontario experiences the greatest drop in peak ozone concentration. This ranges from no change to as much as -33 per cent. The changes in the highest value of each region for each of the days in this period are given in Table 9. By comparing this with Figure 76 for southern Ontario, the maximum percentage decrease in O_3 concentration happens also to the grid where the highest O_3 peak occurs. The same is true for central Ontario. Yet for northern Ontario, the peak ozone concentrations at the grid cell where the maximum occurs are not affected.

On June 11, 1983, the value of the 1-hour ozone maximum in southern Ontario has actually increased by 3 per cent when NO_x emissions in Ontario are eliminated. Since ozone concentrations depend on the balance and absolute magnitude of NO and NO_2, eliminating the local emission of NO_x (which is mostly NO) would shift the balance of NO and NO_2 with the ratio (lower NO/NO_2) favouring higher O_3 values. An increase in O_3 values when Ontario NO_x emissions were eliminated was only seen on June 11, 1983 because the NO_x concentrations were too low on the other days of the episode. June 11, 1983 has the highest NO_x concentration of the period in southern Ontario during the episode.

Table 10 shows changes in the average (over all the grid cells) base case 1-hour maximum ozone concentrations in Ontario when NO_x emissions were eliminated in Ontario. These reductions range from 8 to 16 per cent in southern Ontario, 3 to 17 per cent in central Ontario and 0 to 3 per cent in northern Ontario. The probability of ozone exceeding the Ontario criterion of 80 ppb when NO_x emissions are eliminated from Ontario is given in Figure 79. Comparing this with the base case shows that the probability of exceeding has decreased in some grid squares. Nevertheless, eight grid squares out of the original eleven still show 90-100 per cent chance of exceeding the Ontario standard. The daily range of

probabilities of exceeding the Ontario ozone standard for each of the three regions is given in Table 11 for all the five scenarios. For southern Ontario, the effect of eliminating NO_x emissions from Ontario has slightly decreased the upper range of probabilities for most of the days. June 11, 1983 shows that the highest value in the range of probabilities has increased. This is consistent with the observation of increased ozone on this day.

The percentage changes in NO_x concentration relative to the average base case concentration for the three cases which involve NO_x reduction are given in Table 12 for the three regions. For the two cases of NO_x being eliminated from Ontario, southern Ontario experienced upward of 80 per cent reduction in NO_x everyday. Central and northern Ontario experienced a smaller percentage of NO_x reduction.

Eliminating anthropogenic emissions of reactive hydrocarbon in Ontario produces minor changes in both the peaks of the maximum (less than 10 per cent in southern Ontario and close to 0 per cent elsewhere) and the probability of exceeding the ozone criterion. The effect on the daily average RHC concentration in Ontario is largest in southern Ontario (31-44 per cent) and diminishes to no more than 15 per cent in central Ontario and 1 per cent in northern Ontario. This is to be expected from the distribution of anthropogenic and biogenic sources in Ontario. Central and northern Ontario have mostly biogenic emissions of RHC.

Eliminating both NO_x and anthropogenic RHC emissions from Ontario produces an effect on ozone which is very similar to Scenario A when only NO_x is eliminated from Ontario. For southern Ontario, the percentage change of the maximum ozone concentration as a result of this emission scenario is smaller than and within 2 per cent of the corresponding Scenario A values in Table 9 for each day. This is reflected in the probability of exceedance of the

Ontario ozone criterion (Table 11). The range of probabilities for Scenario C are rarely different from that of Scenario A for all three regions. The NO_x concentrations are no different from that of Scenario A. The above suggests that ozone production over southern Ontario during this episode is NO_x limited. Reducing NO_x emissions reduces ozone concentration. Further control of RHC produces a small effect on ozone concentrations.

When the NO_x emissions in the U.S. are reduced by 50 per cent and the Ontario emissions left intact, the daily maximum ozone peak concentration decreased by up to 15 per cent over Ontario on a daily basis (Table 13). On June 14, 1983 which has the highest ozone peak during that episode, the decrease was only 6 per cent. Average ozone concentration decreased by 1 to 17 per cent in southern and central Ontario and decreased less than 2 per cent in northern Ontario (Table 14). By comparing this scenario with the case where NO_x emissions in Ontario is eliminated, it is noticed that ozone in central and northern Ontario has decreased more in the present case.

A possible explanation may be found in the wind pattern which on June 12, 1983 shows a high pressure centre over Ohio. To the west of this high, air was pumped from the U.S. midwest into southwestern Ontario. The wind then turned east transporting effluents from west to east across the province. In this way, central and northern Ontario are being more directly affected by U.S. emissions than southern Ontario. The above contention is indirectly supported by the data in Table 12 which show that the percentage decrease in NO_x for this Scenario D is higher in central and northern Ontario than in southern Ontario. Nevertheless, these higher percentage decreases should be taken in perspective since the absolute NO_x concentrations in these areas were very small to start with.

Table 11 shows that the probability of exceeding the Ontario ozone criterion is slightly reduced from the base case during the present scenario. Except for the first two days, the present scenario of cutting U.S. NO_x emissions by 50 per cent seems to be more effective than eliminating NO_x from Ontario in controlling ozone exceedances.

Reducing anthropogenic RHC emissions in the U.S. by 50 per cent has insignificant impact on the average ozone and ozone peaks in all regions of Ontario. Thus the probability of exceeding the Ontario ozone criterion is also marginally affected as shown in Table 11.

From the above results, it can be concluded that none of the emissions cut scenarios considered in this study has a very significant impact (e.g. reduce the probability of exceedance by more than half) on the ozone levels of southern Ontario. Of the two species considered, reducing or eliminating anthropogenic RHC is the least effective means of controlling ground level ozone concentrations in the summer. Cutting NO_x is relatively more effective. However, cutting NO_x emitted in the U.S. by 50 per cent proves more effective in reducing ozone in southern Ontario than completely eliminating NO_x in Ontario. Thus, any emission reduction strategy to control ozone in the summer would be inadequate without U.S. participation.

4.6 Sensitivity Study on the Sulphate and Nitrate Pathways in the Winter

Two sensitivity studies were made to determine the relative importance of different pathways during a winter period (January 28 - February 7, 1985). The base case of this study has been described in Section 3.3.

For the sulphur system, all the aqueous pathways for the production of sulphate are switched off: oxidation of SO_2 by H_2O_2, by O_3 and the catalytic oxidation of SO_2 to sulphate in the presence of Fe and Mn. This leaves the gas phase oxidation of SO_2 by OH as the major pathway for the production of sulphate. Figure 80 shows the percentage change in wet deposition of sulphate as a result of suppressing all the aqueous pathways. The changes are about -50 per cent. It has been demonstrated in Section 4.3 for the OSCAR period that compensating effects will work to mitigate the effect of suppressing one of a number of pathways with the same end points. Thus, the reductions shown in Figure 80 would represent the lower limit of the contribution of the aqueous pathways. It can be concluded that even for this winter period in which a lot of clouds consist of ice, aqueous reactions still account for more than 50 per cent of the total sulphate in precipitation.

For the nitrogen system, one of the major pathways for the production of nitric acid from NO_2 is through

$$NO_2 + O_3 \rightarrow NO_3 + O_2 \qquad (2)$$
$$NO_3 + NO_2 \rightarrow N_2O_5 \qquad (3)$$
$$N_2O_5 + H_2O \rightarrow 2HNO_3 \qquad (4)$$

However, this pathway is not as effective during daytime as during nighttime since the NO_3 formed is quickly photolysed:

$$NO_3 \xrightarrow{h\nu} NO_2 + O \qquad (5)$$

During the night, reactions (3) and (4) can proceed to its final stage of producing nitrate.

During the winter, the above reaction is thought to be just as important as the NO_2 + OH route because of the lower OH concentration and the increased number of night hours during

winter. The strength of this pathway equations (2-4) is tested by switching the reactions off.

Figure 81 shows the percentage change in nitrate wet deposition over the ten-day period in response to the NO_3/N_2O_5 pathway being shut off. Over most of the domain, the change is a reduction of between 40 to 60 per cent. In northern Quebec, the change is a reduction of more than 80 per cent because of the low concentration of OH in this area. However, it is noted that the wet deposition in northern Quebec is also small. Given the compensating effect as pointed out for the sulphate sensitivity study which should also be at work here, it can be concluded that the nighttime pathway of NO_3/N_2O_5 is at least comparable to , if not more important than, the NO_2 + OH pathway for this winter period.

5. Summary and Conclusions

A comprehensive model of long-range transport of acidic deposition has been developed and tested for various scenarios and conditions. With this model, ADOM, we attempt to achieve two goals:

1. to quantify accurately the source-receptor relationship on acidic emissions and deposition that currently exists in eastern North America, and

2. to assess the atmospheric response to projected emission scenarios (e.g. reductions) over eastern North America.

The first goal aims to establish model credibility through comparison with present acidic deposition and air quality patterns. This is a prerequisite to the second goal of making meaningful projections of various emission scenarios.

In the past, linear models of long-range-transport have been shown to be able to reproduce the wet deposition pattern of sulphate over an extended duration (1 year and longer) with good accuracy (e.g. Clark et al., 1987). However, this success has also pointed to an inherent weakness of this type of model: their simplicity has allowed parameters within the model to be adjusted so that overall model prediction of wet deposition of sulphate matches observations well. In so doing, their agreement with observations is fortuitous, having given the correct answer for a combination of possibly wrong reasons. This has actually been demonstrated for one model in the evaluation effort of the International Sulphur Deposition Model Evaluation.

Apart from the wet deposition of sulphate patterns that have been evaluated for linear models so far, other fields like SO_2 and sulphate in air have not been widely used for evaluating linear models because these data have been scarce until recently. Runs made with the OME's linear Lagrangian model have shown that it becomes progressively more difficult for a simple model like this to predict well on parameters other than wet sulphate. To obtain a reasonable match, model parameters would have to be adjusted just for the sake of gaining in performance.

It has long been known that chemical reactions in the atmosphere are non-linear (i.e. a proportionate change in chemical products will not result when an acidic precursor emission is altered) through different processes (e.g. oxidant limitation). The uncertainty is whether the atmospheric system as a whole responds linearly or not because of the intricate interactions of the physico-chemical processes. The inherent simplifications and weaknesses of linear models disqualify them for this task of providing an answer to whether the atmosphere would respond linearly or not to emission changes.

Comprehensive models, on the other hand, utilizes a different approach. Information on the detailed physical and chemical processes which affect source-receptor relationships are integrated into a modular framework within the constraints of reasonably available computer resources and input data. Once the credibility of a model is established, projections for future scenarios can be made which address the question of linearity.

Over the last three years, (1987-1990), the comprehensive model ADOM has been run for data sets covering three seasons of the year with the following results:

1. **The OSCAR (Oxidant and Scavenging Characteristics of April Rain) Study.**

   This model was run for a 20-day period with sulphate and nitrate concentrations in precipitation available on 5 of those days. Scatter graphs of model versus observed results show 70-80 per cent of the predicted sulphate and 60-80 per cent of the predicted nitrate concentrations in precipitation were within a factor of two of the observed values. Systematic biases were small (slight underprediction during OSCAR II). Comparison of the modelled with observed scavenging ratios reveals that the two are in general agreement.

2. **A Summer Oxidant Study**

   Intended to establish the credibility of ADOM with regards to ozone prediction and eventually to assess control strategies and the relative (U.S. vs. Canada) contributions to ambient ozone in southern Ontario, this 10 day study for June 1983 indicates that the diurnal trends of ozone are reproduced by the model and that over 95 per cent of the predicted daily

ozone maxima are within a factor of two of the observed daily maxima. In addition to the importance of oxidants in their own right (i.e. ambient ozone concentrations), they are critical in the conversion of SO_2 and NO_x to sulphate and nitrate for acid precipitation studies, hence this study was done.

3. A Winter Simulation

Since oxidation processes can proceed very differently in the winter, a 10 day run for the winter of 1985 was performed. Sulphate concentrations in precipitation are slightly over-predicted while nitrate concentrations are underpredicted. The daily average data show large scatter compared with observations. Further analysis shows that the observed station precipitation values are often 1 or 2 orders of magnitude different from grid average model precipitation data. This mismatch in precipitation accounts for much of the scatter between model and observed precipitation concentrations.

4. The ANATEX (Across North America Tracer Experiment) Study

The advection module of ADOM was evaluated against tracer's data in a 45 day simulation during which perfluorocarbons were released at 2½ day intervals. This study shows that the model resolution cannot capture some small scale meteorological features like the detailed flow near a front or a weak low. This leads to discrepancies between the predicted and observed puff patterns for individual releases but such differences are less important for either continuous releases from many point sources or releases from one source averaged over a period of time.

5. The EMEFS (Eulerian Model Evaluation Field Study)

During this field study, an intensive effort was made to monitor species in the air and in precipitation at 77 sites across eastern North America. Comparisons to date have been limited to ground level data. The ground level air concentrations of sulphur and nitrate species are well reproduced by the model on average. The average sulphate and nitrate concentrations in precipitation are predicted well though there is a lot of scatter. As in earlier studies, the scatter in the precipitation concentration data can be related to differences between observed station and modelled grid average precipitation. Further evaluations and sensitivity runs with this data set are currently underway.

The major emission scenario and sensitivity studies made with ADOM are:

1. A 50 per cent reduction in SO_x emissions during a 20 day spring period (OSCAR). This resulted in a 30-40 per cent reduction in wet sulphate deposition in the heavy emissions area and is the first indication from a comprehensive numerical model of the degree of non-linearity in the atmospheric precipitation system. However, for total deposition (wet plus dry) the result was a 40-45 per cent reduction. This is not far from a linear response.

2. A 50 per cent reduction in SO_x emissions during a 10-day winter period. Between 20-35 per cent reduction in wet sulphate deposition resulted. This is more non-linear than during the spring (OSCAR) period but the precipitation pattern shows large spatial variability. A scenario run for a more prolonged period is needed to

quantify the degree of non-linearity in wet sulphate deposition during the winter.

3. Suppression of major aqueous SO_2 to sulphate conversion pathways. This reveals that aqueous conversion of SO_2 by H_2O_2 is the dominant process. However, the pathway through oxidation with ozone can rival that of H_2O_2 in heavy emission areas.

4. Suppressing a major aqueous SO_2 to sulphate conversion pathway together with a 50 per cent reduction in SO_x emissions during a spring period shows that both SO_x oxidations by H_2O_2 and O_3 can lead to non-linearity.

5. Reducing RHC and/or NO_x in the U.S. and Canada by various percentages. This series of runs suggests that the ozone experienced in southern Ontario cannot be reduced to the acceptable criteria (80 ppb) without the U.S. cutting back on its ozone precursors. On a regional basis NO_x cutbacks were found to be slightly more effective than RHC reductions but very large cutbacks are needed to have a significant impact on ozone levels.

6. Suppressing the gas phase $NO_2 + O_3$ reaction in the winter. This reveals that nighttime chemistry of NO_3 and N_2O_5 contributes about 50 per cent to the wet nitrate deposition in winter.

From the above, it is clear that every task of model evaluation and sensitivity study is a major undertaking which includes establishing a series of data files for model input and evaluation. In addition, interpretation of the model results would often require checking the original formulation and model code and extracting and processing large amounts of data and in some cases performing further model runs. Efforts to gather data for model

evaluation (e.g. OSCAR and EMEFS) often require other resources like ground level monitoring and aircraft measurements. An effort of this nature must be seen as an iterative and ongoing process and interactions between the groups working on different aspects are necessary. In this process the model has also made significant contributions to other areas. For example, during the EMEFS evaluation, the model results have been used to diagnose a major error in the emission inventory which had not been detected for at least five years and which also affects other comprehensive models.

ADOM has been partially tested and some discrepancies between predictions and observations have been noted. The process of model validation will have to continue along two directions:

1. To explain and, if necessary, to improve model formulations to enhance performance on species that have been evaluated so far, and

2. To evaluate ADOM on other parameters that are made available through the two phases of EMEFS. This includes aircraft data and other chemical species that are related to acid deposition.

The above processes will lead to new understandings of the various mechanisms and their interactions in the atmosphere. Also, it will constrain the model to predict the correct answer based on the best of our incomplete but growing knowledge.

Although model runs for the spring and winter periods indicate that wet deposition of sulphate responds non-linearly to emission cuts, it must be pointed out that the response of total sulphur deposition (wet plus dry) is more linear because dry deposition responds linearly. Since the winter simulation was over a short episode with large spatial variability in precipitation and

possible model problems with average oxidant levels, the modelled response to emission cuts during the winter is not conclusive.

For the spring episode (OSCAR) the model predicted a 40 - 45 per cent reduction in total sulphur deposition (30 - 40 per cent for wet deposition and 50 per cent for dry deposition) in response to a 50 per cent reduction in SO_x emissions. Given the uncertainty in both model predictions and measurements, the model response for total sulphate deposition can be considered linear for practical applications. This implies that the emission reduction scenario results obtained to date using linear models cannot be negated on the basis of non-linearity arguments. It must be noted in this context that the models have not been evaluated against a data set where the emissions are substantially different from the present conditions. Validity of the model results for a very different emission configuration has to be taken with caution. It is believed that, models such as ADOM, which include a comprehensive chemical mechanism, can be applied for different emission configurations since there are at present no basis to assume that the chemistry of the atmosphere would differ radically for other emission configurations from the present conditions.

REFERENCES

Brachet W.R. and Dennis R.L. (1989) NAPAP Model Evaluation, Volume I: Protocol. Prepared for U.S. EPA.

Chan W.H. and Chung D.H.S. (1986) Regional Scale Precipitation Scavenging of SO_2, SO_4, NO_3 and HNO_3. Atmos. Environ. 20, 1397-1402.

Clark T.L., Dennis R.L., Voldner E.C., Olson M.P., Seilkop S.K. and Alvo M. (1987) International Sulphur Deposition Model Evaluation. U.S. EPA Publication No. EPA/600/3-87/008. AES Publication No. ARD-87-1.

Draxler R.R. and Heffter J.L. (1989) Across North America Tracer Experiment (ANATEX) Volume I: Description, Ground-level Sampling at Primary Sites and Meteorology. NOAA Technical Memorandum ERL ARL-167.

Karamchandani P.K., Venkatram A. and Kunstal G. (1989) Application of ADOM to an Oxidant Episode. Volume I: Model Evaluation, Volume II, ERT Document No. 2518-001-102.

Kessler E. (1969) On the Distribution and Continuity of Water Substance in Atmospheric Circulation. Met. Monograph 10. American Met. Soc., Boston, Mass.

Marchuk G.I. (1975) Methods of Numerical Mathematics. New York: Springler - Verlog. 316 pp.

Misra P.K., Chan W.H., Chung D. and Tang A.J.S. (1985) Scavenging Ratios of Acidic Pollutants and their use in Long-Range Transport Models. Atmos. Environ. 19, 1471-1475.

MOI (1982) Atmospheric Science and Analysis. Report prepared under the Memorandum of Intent on Transboundary Air Pollution signed by Canada and the United States on August 5, 1980.

Raymond D.J. and Blyth A.M. (1986) A Stochastic Mixing Model for Nonprecipitating Cumulus Clouds. J. Atmos. Sc., 43, 2708-2718.

Schwartz S.E. (1988) Mass-Transport Limitation to the Rate of In-cloud Oxidation of SO_2: Re-examination in the Light of New Data, Draft paper submitted to Atmos. Environ.

Seinfeld J.H. (1980) Lectures in Atmospheric Chemistry, American Institute of Chemical Engineering, Monograph Series 12, Volume 76, 1980. 98 pp.

Sirois A. and Voldner E.C. (1984) Estimates of Dry Deposition Velocity in North America, Part I. Land Use Data Bank. Canadian Meteorological Research Report 1-84. Environment Canada.

Venkatram A., Karamchandani P.K., Misra P.K. (1988) Testing a Comprehensive Acid Deposition Model. Atmos. Environ. 22, 737-747.

Venkatram A., Karamchandani, P.K. (1991) The Role of Cloud Processes in Non-Precipitating Clouds in Producing Ambient Sulfate: Sensitivity Studies with a Comprehensive Model. Presented at the 19th International Technical Meeting on Air Pollution Modelling and its Applications, Ierapetra, Crete, Greece, September 29 - October 4.

Weil J. and Brower R.P. (1984) An Updated Gaussian Plume Model for Tall Stack, J. Air Poll. Control Ass. 34, 818-827.

TABLE 1. LIST OF ALL SPECIES AND HOW THEY ARE HANDLED IN ADOM (Version II B)

	SPECIES NAME	SPECIES		MODELLED	ADVECTED	EMITTED	WET DEPOSITED	DRY DEPOSITED
				(YES = 1, NO = 0)				
01	SULFUR DIOXIDE	SO2	=	1	1	1	1	1
02	SULFATE	SO4	=	1	1	1	1	1
03	NITRIC OXIDE	NO	=	1	1	1	0	0
04	NITROGEN DIOXIDE	NO2	=	1	1	1	1	0
05	OZONE	O3	=	1	1	0	1	0
06	HYDROGEN PEROXIDE	H2O2	=	1	1	0	1	1
07	NITRIC ACID	HNO3	=	1	1	0	1	1
08	PAN	PAN	=	1	1	0	1	0
09	PROPANE	C3H8	=	1	1	1	0	0
10	>C3 ALKANES	ALKA	=	1	1	1	0	0
11	ETHENE	ETHE	=	1	1	1	0	0
12	>C2 ALKENES	ALKE	=	1	1	1	0	0
13	TOLUENE	TOLU	=	1	1	1	0	0
14	HIGHER AROMATICS	AROM	=	1	1	1	0	0
15	FORMALDEHYDE	HCHO	=	1	1	1	1	0
16	ACETALDEHYDE	ALD2	=	1	1	1	1	0
17	METHYL ETHYL KETONE	MEK	=	1	1	1	1	0
18	METHYL GLYOXAL	MGLY	=	1	1	0	0	0
19	GENERAL DICARBONYL	DIAL	=	1	1	0	0	0
20	ORGANIC PEROXIDE	ROOH	=	1	1	0	1	0
21	O-CRESOL	CRES	=	1	1	1	0	0
22	NITROUS ACID	HONO	=	1	1	1	0	0
23	ALKYL NITRATE	RNO3	=	1	1	0	1	0
24	ISOPRENE	ISOP	=	1	1	1	0	0
25	HYDROPEROXY RADICAL	HO2	=	1	1	0	0	0
26	TOTAL RO2 RADICALS	RO2	=	1	1	0	0	0
27	CH3CO3 RADICAL	MCO3	=	1	1	0	0	0
28	AMMONIA	NH3	=	1	1	1	1	1
29	SOIL DUST	DUST	=	1	1	1	1	1
30	OXYGEN- SINGLET D	O*SD	=	1	0	0	0	0
31	ATOMIC OXYGEN	O	=	1	0	0	0	0
32	NITROGEN TRIOXIDE	NO3	=	1	0	0	0	0
33	NITROGEN PENTOXIDE	N2O5	=	1	0	0	0	0
34	PERNITRIC ACID	HNO4	=	1	0	0	0	0
35	HYDROXYL RADICAL	OH	=	1	0	0	0	0
36	GENERAL RO2	RO2R	=	1	0	0	0	0
37	GENERAL RO2 #2	R2O2	=	1	0	0	0	0
38	ALKYL NO3 RO2	RO2N	=	1	0	0	0	0
39	PHENOXY RADICAL	BZO	=	1	0	0	0	0
40	CRIGEE BIRADICAL	CRG1	=	1	0	0	0	0
41	CRIGEE BIRADICAL	CRG2	=	1	0	0	0	0
42	METHANE	CH4	=	1	0	0	0	0
43	ETHANE	C2H6	=	1	0	0	0	0
44	CARBON MONOXIDE	CO	=	1	0	0	0	0
45	WATER VAPOR	H2O	=	1	0	0	0	0
46	OXYGEN	O2	=	1	0	0	0	0
47	AIR	M	=	1	0	0	0	0

TABLE 2. LIST OF ALL GAS PHASE REACTIONS IN ADOM (Version II B)
Reactions that show no product (eg. 46) indicate that the products are outside the species considered in the present version.

1.	1.NO2	+	1.HV	-->	1.NO	+	1.O			
2.	1.O	+	1.O2 + M	-->	1.O3					
3.	1.O	+	1.NO2	-->	1.NO					
4.	1.O	+	1.NO2	-->	1.NO3					
5.	1.NO	+	1.O3	-->	1.NO2					
6.	1.NO2	+	1.O3	-->	1.NO3					
7.	1.NO	+	1.NO3	-->	2.NO2					
8.	2.NO	+	1.O2	-->	2.NO2					
9.	1.NO2	+	1.NO3	-->	1.N2O5					
10.	1.N2O5			-->	1.NO2	+	1.NO3			
11.	1.N2O5	+	1.H2O	-->	2.HNO3					
12.	1.NO2	+	1.NO3	-->	1.NO	+	1.NO2			
13.	1.NO3	+	1.HV	-->	1.NO					
14.	1.NO3	+	1.HV	-->	1.NO2	+	1.O			
15.	1.O3	+	1.HV	-->	1.O					
16.	1.O3	+	1.HV	-->	1.O*SD					
17.	1.O*SD	+	1.H2O	-->	2.OH					
18.	1.O*SD	+	1.M	-->	1.O					
19.	1.NO	+	1.OH	-->	1.HONO					
20.	1.HONO	+	1.HV	-->	1.NO	+	1.OH			
21.	1.NO2	+	1.H2O	-->	1.HONO	+	-1.NO2	+	1.HNO3	
22.	1.NO2	+	1.OH	-->	1.HNO3					
23.	1.HNO3	+	HV	-->	1.NO2	+	1.OH			
24.	1.HNO3	+	1.OH	-->	1.NO3					
25.	1.CO	+	1.OH	-->	1.HO2					
26.	1.O3	+	1.OH	-->	1.HO2					
27.	1.NO	+	1.HO2	-->	1.NO2	+	1.OH			
28.	1.NO2	+	1.HO2	-->	1.HNO4					
29.	1.HNO4			-->	1.NO2	+	1.HO2			
30.	1.HNO4	+	HV	-->	1.NO2	+	1.HO2			
31.	1.HNO4	+	1.OH	-->	1.NO2					
32.	1.O3	+	1.HO2	-->	1.OH					
33.	2.HO2			-->	1.H2O2					
34.	2.HO2	+	1.M	-->	1.H2O2					
35.	2.HO2	+	1.H2O	-->	1.H2O2					
36.	2.HO2	+	1.H2O	-->	1.H2O2					
37.	1.H2O2	+	HV	-->	2.OH					
38.	1.H2O2	+	1.OH	-->	1.HO2					
39.	1.NO3	+	1.HO2	-->	1.HNO3					
40.	1.NO3	+	1.HO2 +M	-->	1.HNO3					
41.	1.NO3	+	1.HO2 +H2O	-->	1.HNO3					
42.	1.NO3	+	1.HO2 +H2O	-->	1.HNO3					
43.	1.SO2	+	1.OH	-->	1.SO4	+	1.HO2			
44.	1.RO2	+	1.NO	-->	1.NO					
45.	1.RO2	+	1.HO2	-->	1.HO2					
46.	2.RO2			-->						
47.	1.RO2	+	1.MCO3	-->	1.MCO3					
48.	1.ROOH	+	1.HV	-->	1.HO2	+	1.OH			
49.	1.HCHO	+	1.HV	-->	2.HO2	+	1.CO			
50.	1.HCHO	+	1.HV	-->	1.CO					

```
51.   1.HCHO +  1.OH     -->  1.HO2  +  1.CO
52.   1.HCHO +  1.NO3    -->  1.HNO3 +  1.HO2  +  1.CO
53.   1.HCHO +  1.HO2    -->  1.RO2R +  1.RO2
54.   1.ALD2 +  1.OH     -->  1.MCO3
55.   1.ALD2 +  1.HV     -->  1.CO   +  1.HCHO +  1.HO2  +  1.RO2R
                             +  1.RO2
56.   1.ALD2 +  1.NO3    -->  1.HNO3 +  1.MCO3
57.   1.MCO3 +  1.NO     -->  1.NO2  +  1.HCHO +  1.RO2R +  1.RO2
58.   1.MCO3 +  1.NO2    -->  1.PAN
59.   1.MCO3 +  1.HO2    -->  1.ROOH +  1.HCHO
60.   2.MCO3             -->  2.HO2  +  2.HCHO
61.   1.PAN              -->  1.MCO3 +  1.NO2
62.   1.MEK  +  1.HV     -->  1.ALD2 +  1.MCO3 +  1.RO2R +  1.RO2
63.   1.MEK  +  1.OH     -->  .5ALD2 +  .5HCHO +  1.MCO3 + 1.5RO2R
                           + 1.5RO2
64.   1.MGLY +  1.HV     -->  1.MCO3 +  1.HO2  +  1.CO
65.   1.MGLY +  1.OH     -->  1.MCO3 +  1.CO
66.   1.MGLY +  1.NO3    -->  1.HNO3 +  1.MCO3 +  1.CO
67.   1.CH4  +  1.OH     -->  1.HCHO +  1.RO2R +  1.RO2
68.   1.C2H6 +  1.OH     -->  1.ALD2 +  1.RO2R +  1.RO2
69.   1.C3H8 +  1.OH     -->  .3ALD2 +  .5MEK  +  1.RO2R +  1.RO2
70.   1.ALKA +  1.OH     -->B01*HCHO +B02*ALD2 +B03*MEK  +B04*RO2N
                           +B05*RO2R +B06*R2O2 +B07*RO2
71.   1.RNO3 +  1.OH     -->  1.NO2  + .15MEK  +1.53ALD2 + .16HCHO
                           +1.39R2O2 +1.39RO2
72.   1.RO2N +  1.NO     -->  1.RNO3
73.   1.RO2N +  1.HO2    -->  1.ROOH +  1.MEK
74.   1.RO2N +  1.RO2    -->  1.RO2  +  .5HO2  +  1.MEK
75.   1.RO2N +  1.MCO3   -->  1.HCHO +  1.HO2  +  1.MEK
76.   1.R2O2 +  1.NO     -->  1.NO2
77.   1.R2O2 +  1.HO2    -->  1.ROOH
78.   1.R2O2 +  1.RO2    -->  1.RO2
79.   1.R2O2 +  1.MCO3   -->  1.HCHO +  1.HO2
80.   1.RO2R +  1.NO     -->  1.NO2  +  1.HO2
81.   1.RO2R +  1.HO2    -->  1.ROOH
82.   1.RO2R +  1.RO2    -->  .5HO2  +  1.RO2
83.   1.RO2R +  1.MCO3   -->  1.HCHO +  1.HO2
84.   1.ETHE +  1.OH     -->1.56HCHO + .22ALD2 +  1.RO2R +  1.RO2
85.   1.ETHE +  1.O3     -->  1.HCHO + .12HO2  + .42CO   +  .4CRG1
86.   1.ETHE +  1.O      -->  1.HCHO +  1.HO2  +  1.CO   +  1.RO2R
                           +  1.RO2
87.   1.ETHE +  1.NO3    -->  1.NO2  +  2.HCHO +  1.R2O2 +  1.RO2
88.   1.ALKE +  1.OH     -->B08*HCHO +B09*ALD2 +  1.RO2R +  1.RO2
89.   1.ALKE +  1.O3     -->B10*HCHO +B11*ALD2 +B12*RO2R +B12*RO2
                           +B13*HO2  +B14*OH   +B15*CO   +B25*CRG1
                           +B26*CRG2
90.   1.ALKE +  1.O      -->B16*CO   +B17*MEK  +B18*HCHO +B19*ALD2
                           +B20*HO2  +B21*RO2R +B21*RO2
91.   1.ALKE +  1.NO3    -->  1.NO2  +B08*HCHO +B09*ALD2 +  1.R2O2
                           +  1.RO2
92.   1.SO2  +  1.CRG1   -->  1.SO4  +  1.HCHO
93.   1.SO2  +  1.CRG2   -->  1.SO4  +  1.ALD2
94.   1.CRG1 +  1.H2O    -->
95.   1.CRG2 +  1.H2O    -->
```

```
 96.   1.CRG1 +  1.HCHO   -->
 97.   1.CRG2 +  1.HCHO   -->
 98.   1.CRG1 +  1.ALD2   -->
 99.   1.CRG2 +  1.ALD2   -->
100.   1.TOLU +  1.OH     --> .16CRES + .16HO2  + .84RO2R +  .4DIAL
                             + .84RO2  + .14MGLY + .11HCHO + .11CO
101.   1.AROM +  1.OH     --> .17CRES + .17HO2  + .83RO2R + .83RO2
                            +B22*DIAL +B23*MGLY +B24*HCHO +B24*CO
102.   1.DIAL +  1.OH     -->  1.MCO3
103.   1.DIAL +  1.HV     -->  1.HO2  +  1.CO   +  1.MCO3
104.   1.CRES +  1.OH     -->  .2MGLY + .15RO2N + .85RO2R +  1.RO2
                             + .08CRES
105.   1.CRES +  1.NO3    -->  1.HNO3 +  1.BZO  + .50CRES
106.   1.BZO  +  1.NO2    -->  1.RNO3
107.   1.BZO  +  1.HO2    -->
108.   1.BZO              -->
109.   1.ISOP +  1.OH     -->  1.HCHO +  1.ETHE + .20ALD2 + .27MGLY
                             + .70HO2  + .90R2O2 + .10RO2N +  1.RO2
                             + .20MCO3
110.   1.ISOP +  1.O3     -->  1.HCHO + .50ETHE + .40ALD2 + .20MGLY
                             + .40HO2  + .10OH   + .20CRG2
111.   1.ISOP +  1.O      -->  1.ETHE +  1.ALD2 + .60HO2  + .50R2O2
                             + .50RO2
112.   1.ISOP +  1.NO3    -->  1.NO2  +  1.HCHO +  1.ALD2 +  1.R2O2
                             +  1.RO2
113.   1.OH   +  1.HO2    -->
114.   1.ROOH +  1.OH     --> .50RO2R + .50OH   + .50RO2
```

TABLE 3. LIST OF ALL AQUEOUS PHASE REACTIONS IN ADOM (Version II B)

1.	1.SO4P1	-->	B1*SO4= +	B3*H+
2.	1.SO2G	-->	B1*HSO3 +	B1*H+
3.	1.HSO3 + 1.H+	-->	B2*SO2G	
4.	1.O3G	-->	B1*O3	
5.	1.O3	-->	B2*O3G	
6.	1.HPXG	-->	B1*H2O2	
7.	1.H2O2	-->	B2*HPXG	
8.	1.HNO3	-->	B1*NO3- +	B1*H+
9.	1.NO3- + 1.H+	-->	B2*HNO3	
10.	1.RPXG	-->	B1*ROOH	
11.	1.ROOH	-->	B2*RPXG	
12.	1.NH3G	-->	B1*NH4+ +	B1*OH-
13.	1.NH4+ + 1.OH-	-->	B2*NH3G	
14.	1.DUST	-->	B5*FEMN +	B4*HCO3 + B4*CAT1+
15.	1.CO2G	-->	B1*HCO3 +	B1*H+
16.	1.HCO3 + 1.H+	-->	B2*CO2G	
17.	1.H+ + 1.OH-	-->	1.00H2OA	
18.	1.H2OA	-->	1.00H+ +	1.00OH-
19.	1.HSO3 + 1.O3	-->	1.00SO4= +	1.00H+
20.	1.HSO3 + 1.H2O2	-->	1.00SO4= +	1.00H+
21.	1.HSO3 + 1.ROOH	-->	1.00SO4= +	1.00H+
22.	1.HSO3 (FEMN)	-->	1.00SO4= +	1.00H+
23.	1.SO4P2	-->	B1*SO4= +	B1*H+ + B1*NH4+
24.	1.SO4P3	-->	B1*SO4= +	B3*NH4+
25.	1.NNO3P	-->	B1*NO3- +	B1*NH4+

TABLE 4. INITIAL AND BOUNDARY CONDITIONS FOR ADOM (VERSION IIB) FOR THE EMEFS RUN

SPECIES	INITIAL CONCENTRATION FILE (SCON) CONCENTRATION (UG/M**3) FOR LAYERS 1-12				BOUNDARY CONDITION FILE (BCON) BOUNDARY CONDITIONS (UG/M**3) FOR LAYERS 1-12				
					INFLOW				OUTFLOW
	LEVELS 1 - 4	LEVELS 5 - 7	LEVELS 8 - 10	LEVELS 11, 12	LEVELS 1 - 4	LEVELS 5 - 7	LEVELS 8 - 10	LEVELS 11, 12	LEVELS 1 - 12
SO2 =	.377E 00	.239E 00	.979E-01	.241E-01	.377E 00	.239E 00	.979E-01	.241E-01	.241E-01
SO4 =	.188E 01	.143E 01	.587E 00	.181E 00	.188E 01	.143E 01	.587E 00	.181E 00	.181E 00
NO =	.177E-01	.112E-01	.459E-02	.113E-02	.177E-01	.112E-01	.459E-02	.113E-02	.113E-02
NO2 =	.271E 00	.171E 00	.703E-01	.173E-01	.271E 00	.171E 00	.703E-01	.173E-01	.173E-01
O3 =	.848E 02	.116E 03	.117E 03	.632E 02	.848E 02	.116E 03	.117E 03	.632E 02	.632E 02
H2O2=	.234E 01	.253E 01	.260E 01	.144E 01	.234E 01	.253E 01	.260E 01	.144E 01	.144E 01
HNO3=	.371E 00	.235E 00	.482E-01	.296E-01	.371E 00	.235E 00	.482E-01	.296E-01	.296E-01
PAN =	.475E 00	.451E 00	.370E 00	.228E 00	.475E 00	.451E 00	.370E 00	.228E 00	.228E 00
C3H8=	.259E 01	.197E 01	.135E 01	.579E 00	.259E 01	.197E 01	.135E 01	.579E 00	.579E 00
ALKA=	.334E 02	.190E 02	.104E 02	.240E 01	.334E 02	.190E 02	.104E 02	.240E 01	.240E 01
ETHE=	.165E 01	.835E 00	.428E 00	.105E 00	.165E 01	.835E 00	.428E 00	.105E 00	.105E 00
ALKE=	.942E 00	.179E 00	.147E-01	.903E-03	.942E 00	.179E 00	.147E-01	.903E-03	.903E-03
TOLU=	.144E 01	.686E 00	.141E 00	.346E-01	.144E 01	.686E 00	.141E 00	.346E-01	.346E-01
AROM=	.132E 01	.418E 00	.685E-01	.105E-01	.132E 01	.418E 00	.685E-01	.105E-01	.105E-01
HCHO=	.118E 01	.895E 00	.459E 00	.113E 00	.118E 01	.895E 00	.459E 00	.113E 00	.113E 00
ALD2=	.518E 00	.328E 00	.135E 00	.414E-01	.518E 00	.328E 00	.135E 00	.414E-01	.414E-01
MEK =	.424E 00	.215E 00	.132E 00	.406E-01	.424E 00	.215E 00	.132E 00	.406E-01	.406E-01
MGLY=	.424E-03	.215E-03	.220E-04	.135E-04	.424E-03	.215E-03	.220E-04	.135E-04	.135E-04
DIAL=	.495E-03	.251E-03	.257E-04	.158E-04	.495E-03	.251E-03	.257E-04	.158E-04	.158E-04
ROOH=	.365E-03	.185E-03	.190E-04	.117E-04	.365E-03	.185E-03	.190E-04	.117E-04	.117E-04
CRES=	.636E-03	.322E-03	.330E-04	.203E-04	.636E-03	.322E-03	.330E-04	.203E-04	.203E-04
HONO=	.277E-03	.140E-03	.144E-04	.884E-05	.277E-03	.140E-03	.144E-04	.884E-05	.884E-05
RNO3=	.713E-03	.361E-03	.370E-04	.228E-04	.713E-03	.361E-03	.370E-04	.228E-04	.228E-04
ISOP=	.267E 00	.253E-01	.208E-02	.128E-02	.267E 00	.253E-01	.208E-02	.128E-02	.128E-02
HO2 =	.194E-03	.984E-04	.101E-04	.621E-05	.194E-03	.984E-04	.101E-04	.621E-05	.621E-05
RO2 =	.359E-03	.182E-03	.187E-04	.115E-04	.359E-03	.182E-03	.187E-04	.115E-04	.115E-04
MCO3=	.442E-03	.224E-03	.229E-04	.141E-04	.442E-03	.224E-03	.229E-04	.141E-04	.141E-04
NH3 =	.334E 00	.127E 00	.260E-01	.639E-02	.334E 00	.127E 00	.260E-01	.639E-02	.639E-02
DUST=	.196E 01	.746E 00	.153E 00	.376E 00	.196E 01	.746E 00	.153E 00	.376E 00	.376E 00

Table 5: Geometric means and standard deviations of predicted and observed washout ratios

	W_{so2}		W_{so4}		W_{no3}		W_1		W_2		W_3	
	Mean	S.D.	Mean	S.D.	Mean	S.D.	Mean	S.D.	Mean	S.D.	Mean	S.D.
Model values (OSCAR II)	0.11×10^6	6.57	0.74×10^6	2.17	1.23×10^6	5.62	1.13×10^6	1.95	0.41×10^6	8.88	0.29×10^6	4.88
Model values (OSCAR IV)	0.13×10^6	3.38	0.68×10^6	2.40	1.13×10^6	4.58	1.05×10^6	2.24	0.43×10^6	7.56	0.27×10^6	3.93
Observations Chan and Chung 1986	0.11×10^6 to 0.29×10^6		0.26×10^6 to 0.44×10^6									
Misra et al., 1985					0.74×10^6 to 2.09×10^6	2.55 3.42	0.70×10^6 to 0.88×10^6	2.86 2.24	0.34×10^6 to 0.76×10^6	3.91 4.80	0.22×10^6 to 0.37×10^6	3.19 3.71
Barrie and Neustadter							0.98×10^6 to 1.35×10^6	2.20 to 3.00				

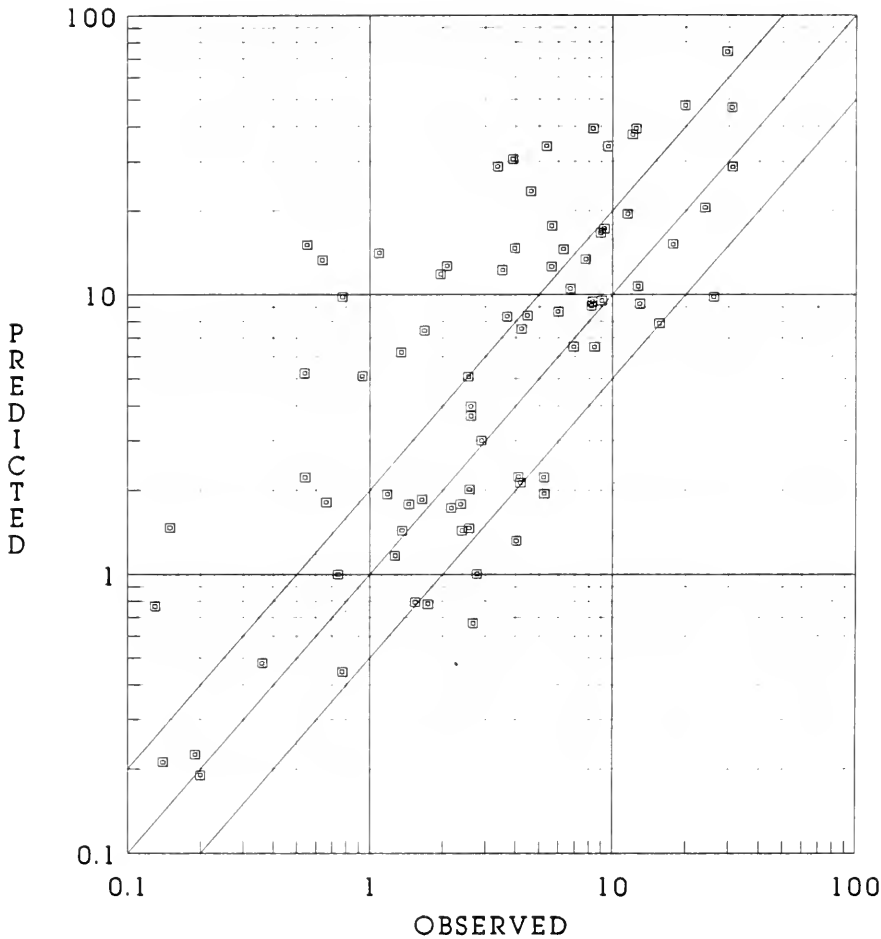

Figure 20. Predicted vs. observed daily ground level air SO_2 concentrations ($\mu g/m^3$) for the winter study period. The diagonal is the 1:1 line and the line on each side is the factor of 2 line.

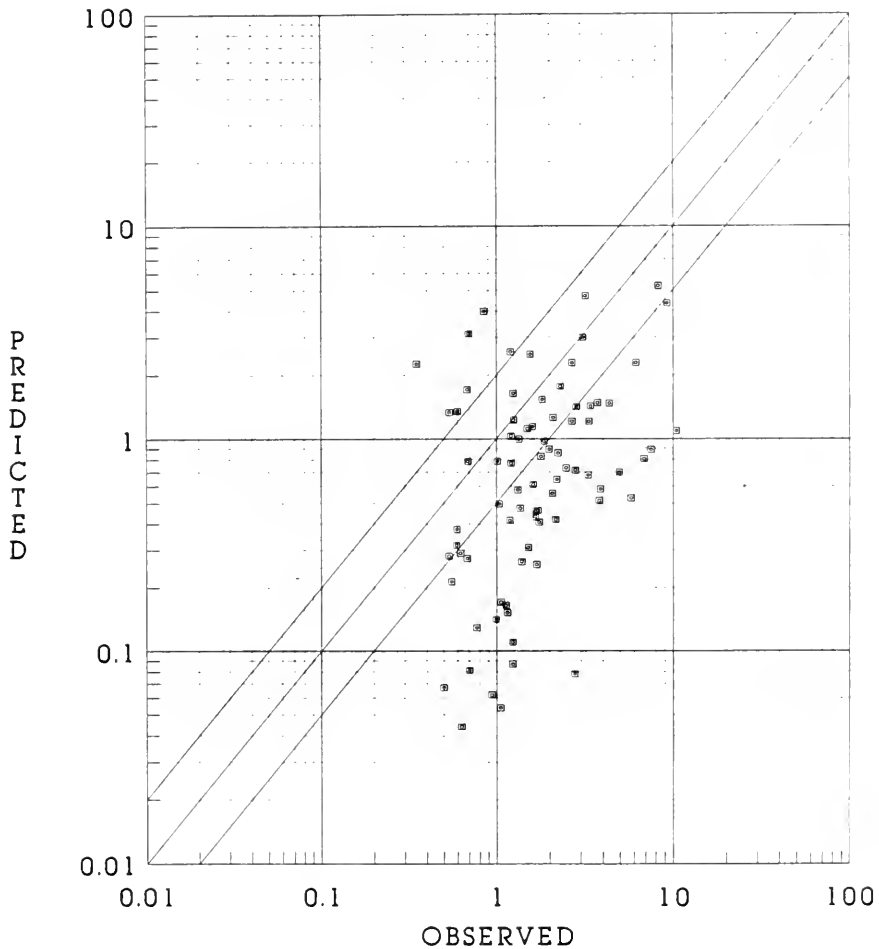

Figure 21. Predicted vs. observed daily ground level air sulphate concentrations ($\mu g/m^3$) for the winter study period. The diagonal is the 1:1 line and the line on each side is the factor of 2 line.

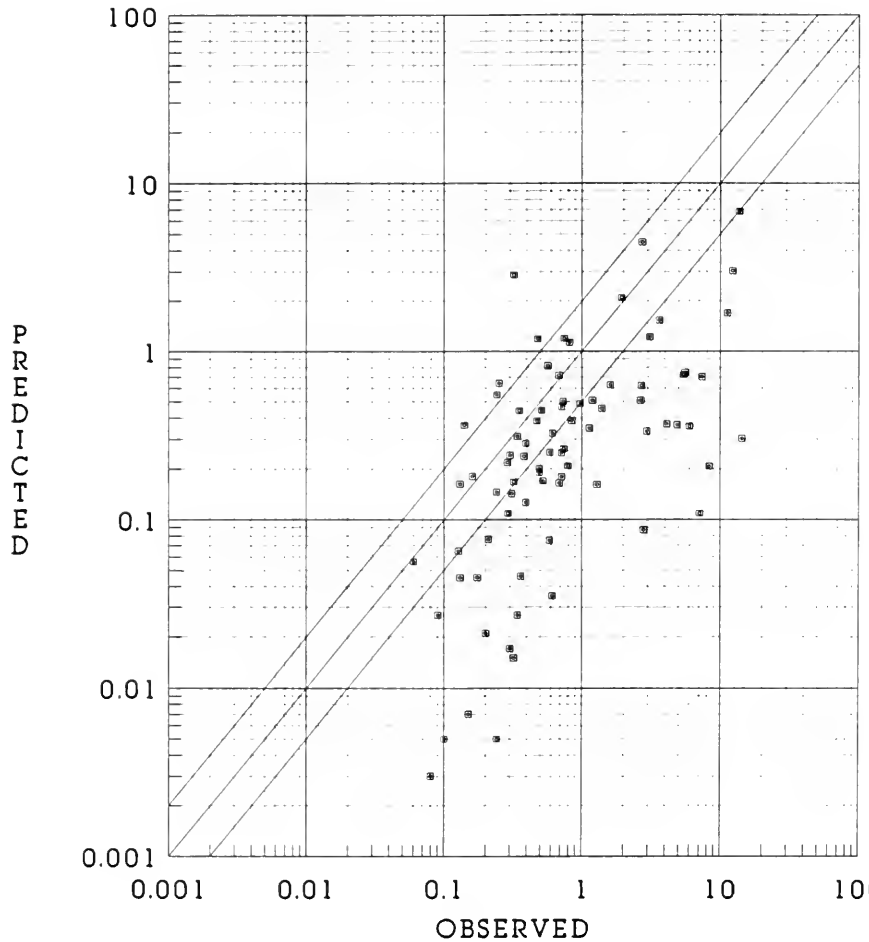

Figure 22. Predicted vs. observed daily ground level air nitrate concentrations ($\mu g/m^3$) for the winter study period. The diagonal is the 1:1 line and the line on each side is the factor of 2 line.

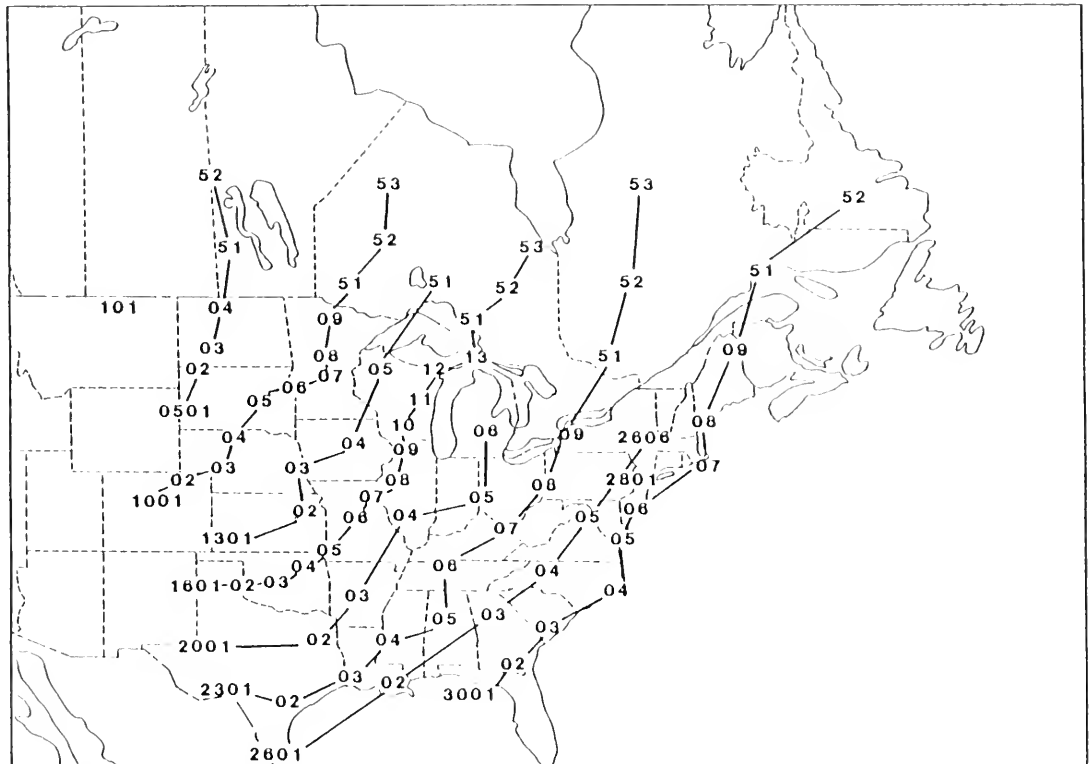

Figure 23. The ANATEX monitoring and release sites. The exact station location is at the centre of each site number. The lines joining the numbers are approximate equidistant arcs away from 101 (Glasgow, Montana). The number at the southern end of the arc indicates the approximate distance away from Glasgow e.g. 1001 is about 1000 km away.

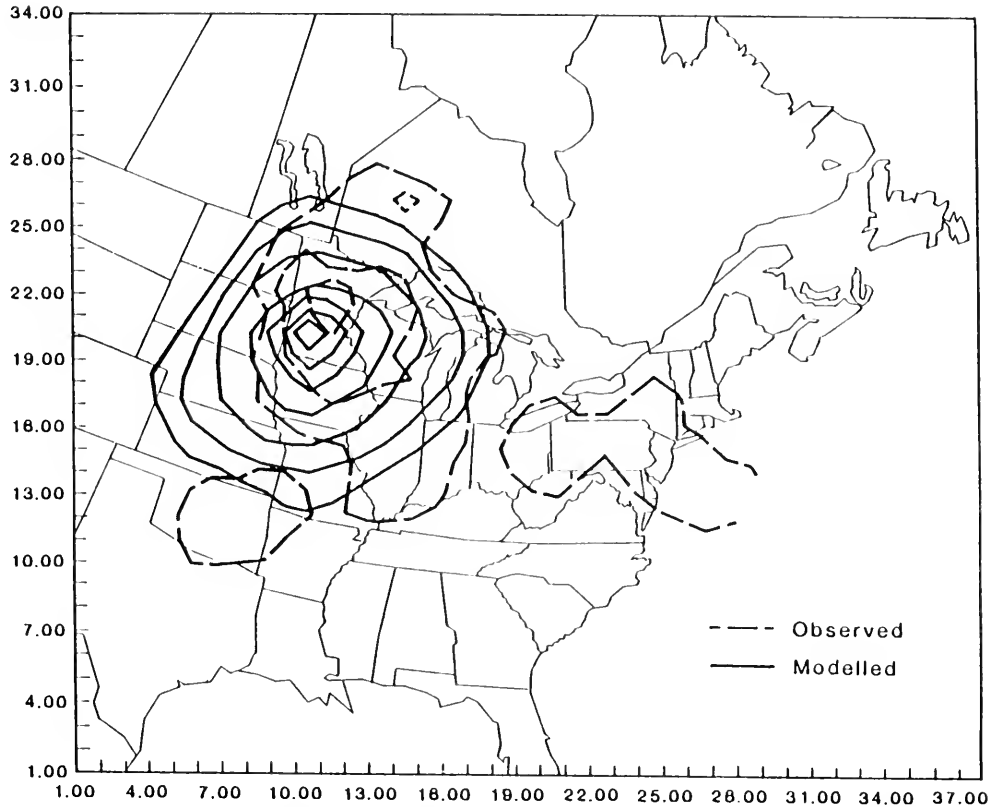

Figure 24. The observed and predicted PDCH pattern for the first 44 days of the ANATEX run. The contours are 0.5, 1, 2, 5, 10, 20, 50, 100, fl/l with the outermost contour being 0.5.

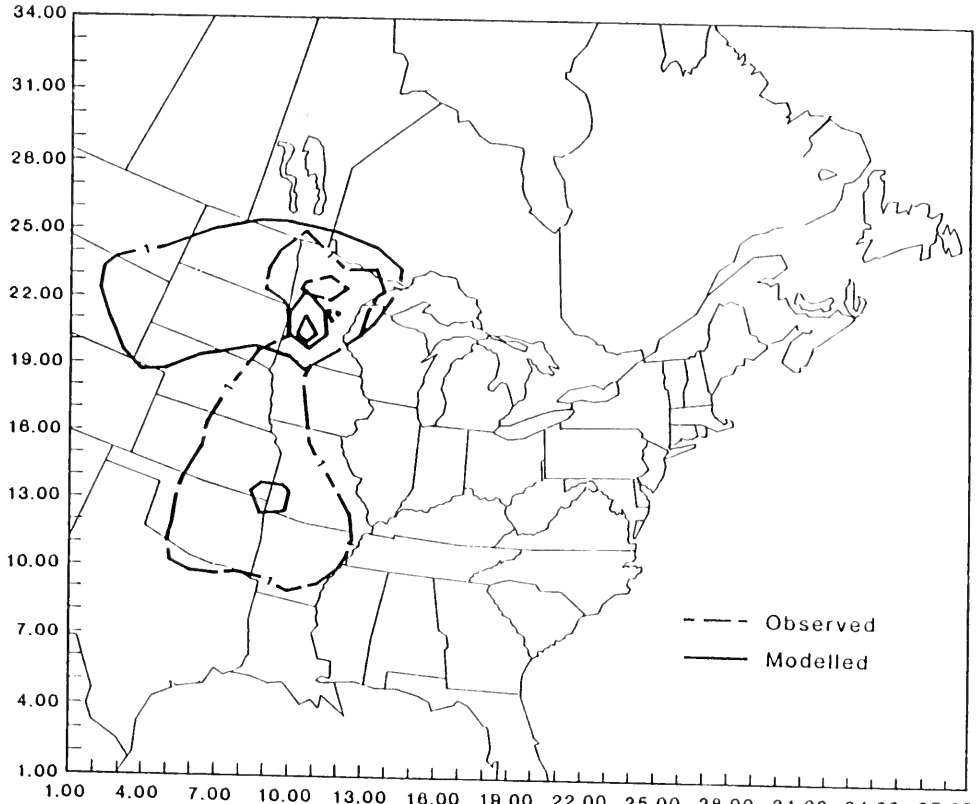

Figure 25. The observed and predicted PDCH pattern for the first three days of the first release of the ANATEX run. The observed contours start at 1 fl/l on the outside and increase in steps of 4 fl/l. The predicted contours start at 1 fl/l on the outside and increase in steps of 10 fl/l.

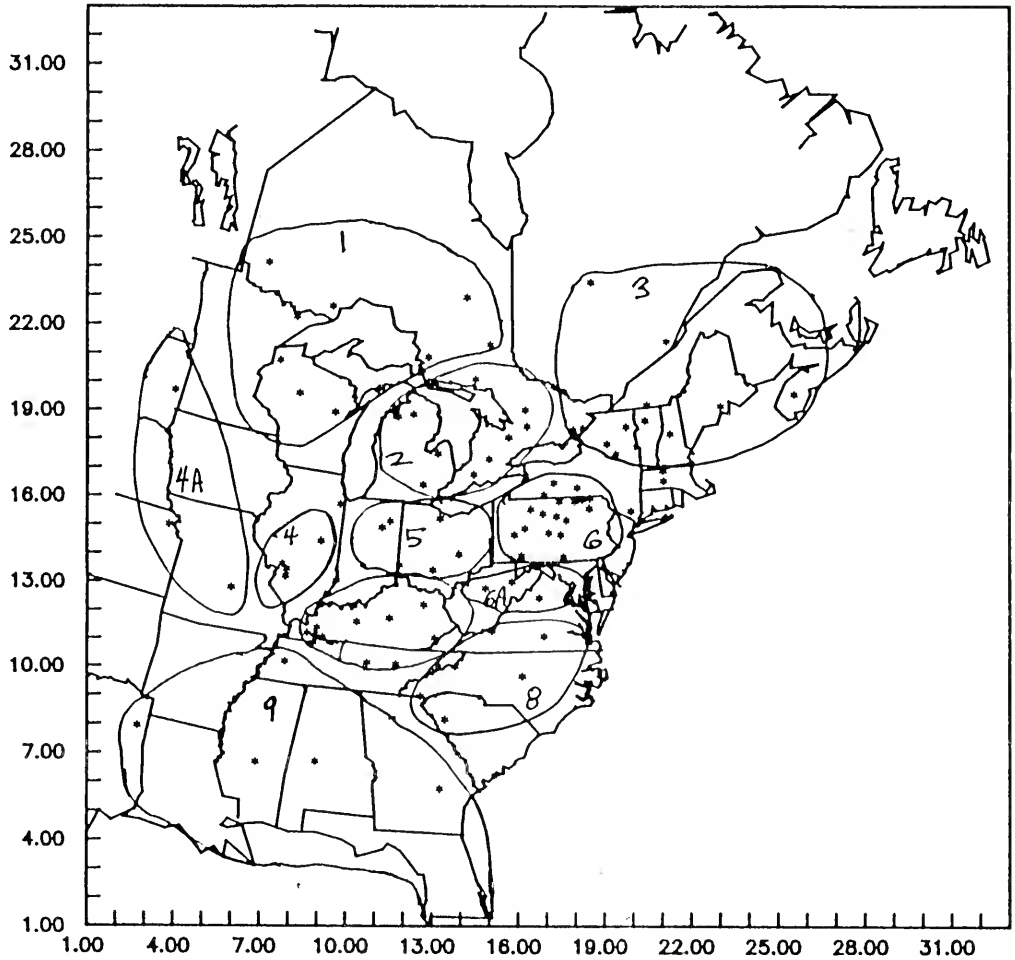

Figure 26. The ground based monitors of the EMEFS with the outline of the nine regions for our evaluations.

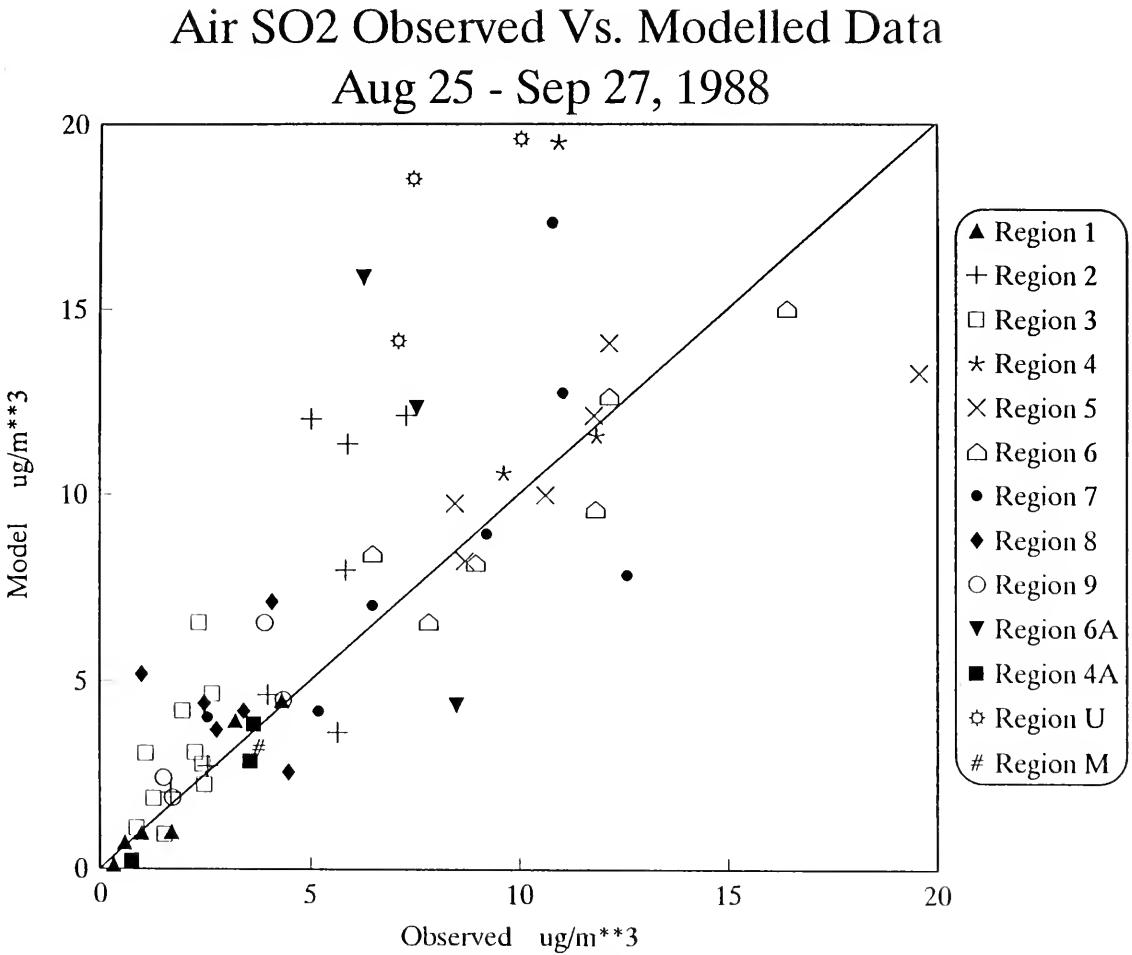

Figure 27. Modelled vs. observed ground level concentrations for SO2 for August 25 - September 27, 1988 for EMEFS.

TABLE 6

Comparison of Observations and Model Predictions of Daily Average Sulfate Concentrations ($\mu g/m^3$) for the Summer Oxidant Study

Site Name	Date	Grid	Observed	Predicted
Perry County	6/11/83	18,14	17.50	21.00
Bristol Fdr School	6/11/83	19,14	16.10	17.20
Geo. St. Troop & Scra	6/11/83	19,15	13.80	12.50
Allentown WAEB Radio	6/11/83	19,15	9.50	12.50
Perry County	6/17/83	18,14	8.10	8.88
Bristol Fdr School	6/17/83	19,14	28.40	10.00
Geo. St. Troop & Scra	6/17/83	19,15	9.20	12.70
Allentown WAEB Radio	6/17/83	19,15	24.2	12.70
Mt. Pleasant HS	6/17/83	20,17	18.4	8.91

Table 7. Observed and Predicted Nitrate/Sulfate Ratios in Precipitation

Study	Observed		Modelled	
	Range	Geometric Mean	Range	Geometric Mean
OSCAR II	0.21 - 2.53	0.89	0.55 - 1.19	0.82
OSCAR IV	0.53 - 1.49	0.91	0.52 - 1.47	0.83
Winter	0.23 - 14.8	2.40	0.20 - 4.53	1.62

Table 8: Total SO_4^{2-} deposited through precipitation over the entire model domain

Day (April, 1981)	19	20	21	22	23	24
Base case total wet deposition(1000 tons)	23.5	27.4	22.1	35.5	66.3	65.6
Change in total mass (%) with suppression of H_2O_2 oxidation	-19.1	-22.9	-30.4	-30.3	-25.1	-23.3
Of O_3 oxidation	- 5.8	- 7.5	- 1.6	- 5.0	- 8.0	- 6.8
Of all aqueous oxidations	-38.3	-50.8	-51.9	-50.9	-47.5	-50.6

Date	SOUTHERN ONTARIO		CENTRAL ONTARIO		NORTHERN ONTARIO	
	1hr. Max. O3	Change	1hr. Max. O3	Change	1hr. Max. O3	Change
6/09/83	96	-13%	59	-20%	52	0%
6/10/83	82	-15%	67	-3%	66	0%
6/11/83	67	3%	87	0%	95	0%
6/12/83	106	-3%	72	0%	41	0%
6/13/83	160	-3%	112	-20%	57	0%
6/14/83	185	-33%	127	-19%	56	0%
6/15/83	159	-16%	116	-4%	109	0%
6/16/83	128	-3%	71	0%	95	0%
6/17/83	69	-5%	40	-49%	60	0%

Table 9. Highest base case 1-hr maximum ozone concentrations (ppb) in Ontario and changes in concentrations when Ontario NO_x emissions are reduced by 100% during the summer oxidant study.

Date	SOUTHERN ONTARIO		CENTRAL ONTARIO		NORTHERN ONTARIO	
	Ave. 1hr. O3	Change	Ave. 1hr. O3	Change	Ave. 1hr. O3	Change
6/09/83	78	-9%	41	-5%	39	-1%
6/10/83	60	-9%	40	-7%	42	-1%
6/11/83	52	-12%	50	-4%	44	-1%
6/12/83	70	-10%	40	-6%	24	-2%
6/13/83	109	-11%	56	-5%	30	0%
6/14/83	137	-15%	59	-5%	24	-1%
6/15/83	125	-16%	62	-3%	24	-1%
6/16/83	75	-8%	28	-5%	22	-1%
6/17/83	49	-13%	19	-17%	24	-3%

Table 10. Average base case 1-hour maximum ozone concentrations (ppb) in Ontario and changes in concentrations when Ontario NO_x emissions are reduced by 100% during the summer oxidant study.

SOUTHERN ONTARIO						
Date	Base Case	Scenario A	Scenario B	Scenario C	Scenario D	Scenario E
6/09/83	11-71	6-62	9-69	7-64	10-71	11-71
6/10/83	1-53	0-41	0-47	0-40	0-48	0-50
6/11/83	1-29	0-32	0-26	0-30	0-26	1-19
6/12/83	1-81	0-79	1-81	1-78	0-68	0-77
6/13/83	6-100	0-100	6-100	0-100	4-95	5-100
6/14/83	34-100	7-100	33-100	7-100	25-100	32-100
6/15/83	72-100	45-99	58-100	45-99	60-97	69-100
6/16/83	13-93	8-92	13-93	8-92	7-82	11-91
6/17/83	0-31	0-26	0-30	0-26	0-22	0-26

CENTRAL ONTARIO						
Date	Base Case	Scenario A	Scenario B	Scenario C	Scenario D	Scenario E
6/09/83	0-17	0-13	0-17	0-13	0-15	0-17
6/10/83	0-28	0-25	0-28	0-25	0-26	0-28
6/11/83	0-61	0-61	0-61	0-61	0-58	0-61
6/12/83	0-37	0-36	0-37	0-36	0-22	0-37
6/13/83	1-86	1-68	1-86	1-69	0-74	0-84
6/14/83	0-93	0-84	0-93	0-84	0-84	0-92
6/15/83	0-88	0-84	0-88	0-84	0-74	0-85
6/16/83	0-35	0-34	0-35	0-34	0-19	0-32
6/17/83	0-2	0-0	0-1	0-0	0-1	0-2

NORTHERN ONTARIO						
Date	Base Case	Scenario A	Scenario B	Scenario C	Scenario D	Scenario E
6/09/83	0-9	0-9	0-9	0-9	0-8	0-9
6/10/83	0-26	0-25	0-26	0-25	0-25	0-26
6/11/83	0-71	0-72	0-71	0-72	0-69	0-71
6/12/83	0-2	0-2	0-2	0-2	0-1	0-2
6/13/83	0-14	0-14	0-14	0-14	0-8	0-14
6/14/83	0-13	0-13	0-13	0-13	0-9	0-13
6/15/83	0-84	0-84	0-89	0-84	0-71	0-82
6/16/83	0-71	0-71	0-71	0-71	0-55	0-69
6/17/83	0-18	0-18	0-18	0-18	0-18	0-18

Scenario A: Ontario NOx emissions reduced by 100%.
Scenario B: Ontario anthropogenic RHC emissions reduced by 100%.
Scenario C: Ontario NOx and anthropogenic RHC emissions reduced by 100%.
Scenario D: U.S. NOx emissions reduced by 50%.
Scenario E: U.S. anthropogenic RHC emissions reduced by 50%.

Table 11. Range of probabilities (%) of maximum 1-hour ozone concentrations exceeding the Ontario ozone criterion of 80 ppb in southern, central and northern Ontario during the summer oxidant study.

SOUTHERN ONTARIO				
Date	Base Case NOx	Scenario A	Scenario C	Scenario D
6/09/83	5.3	-85%	-84%	-9%
6/10/83	5.2	-80%	-80%	-11%
6/11/83	7.3	-86%	-86%	-8%
6/12/83	3.7	-82%	-82%	-5%
6/13/83	4.6	-82%	-83%	-3%
6/14/83	6.0	-86%	-87%	-1%
6/15/83	5.2	-82%	-82%	-3%
6/16/83	6.1	-80%	-80%	-7%
6/17/83	6.4	-85%	-85%	-6%

CENTRAL ONTARIO				
Date	Base Case NOx	Scenario A	Scenario C	Scenario D
6/09/83	0.4	-84%	-84%	-7%
6/10/83	0.4	-77%	-77%	-8%
6/11/83	0.8	-70%	-70%	-12%
6/12/83	0.6	-43%	-44%	-20%
6/13/83	0.8	-47%	-47%	-18%
6/14/83	0.9	-52%	-52%	-15%
6/15/83	0.8	-46%	-47%	-14%
6/16/83	0.7	-62%	-62%	-12%
6/17/83	0.5	-78%	-78%	-6%

NORTHERN ONTARIO				
Date	Base Case NOx	Scenario A	Scenario C	Scenario D
6/09/83	0.05	-47%	-47%	-2%
6/10/83	0.08	-35%	-34%	-8%
6/11/83	0.12	-20%	-20%	-14%
6/12/83	0.12	-17%	-17%	-23%
6/13/83	0.15	-12%	-12%	-26%
6/14/83	0.12	-23%	-23%	-16%
6/15/83	0.12	-17%	-17%	-22%
6/16/83	0.07	-20%	-20%	-19%
6/17/83	0.05	-29%	-29%	-6%

Scenario A: Ontario NOx emissions reduced by 100%.
Scenario C: Ontario NOx and anthropogenic RHC emissions reduced by 100%.
Scenario D: U.S. NOx emissions reduced by 50%.

Table 12. Percent changes in NO_x concentrations relative to the average base case concentrations (ppb) during the summer oxidant study.

Date	SOUTHERN ONTARIO		CENTRAL ONTARIO		NORTHERN ONTARIO	
	1hr. Max. O3	Change	1hr. Max. O3	Change	1hr. Max. O3	Change
6/09/83	96	0%	59	-2%	52	0%
6/10/83	82	-3%	67	-2%	66	0%
6/11/83	67	-1%	87	-1%	95	-1%
6/12/83	106	-12%	72	-12%	41	-2%
6/13/83	160	-15%	112	-12%	57	-9%
6/14/83	185	-6%	127	-13%	56	-7%
6/15/83	159	-11%	116	-15%	109	-12%
6/16/83	128	-15%	71	-13%	95	-12%
6/17/83	69	-12%	40	-3%	60	0%

Table 13. Highest base case 1-hour maximum ozone concentrations (ppb) in Ontario and changes in concentrations when the U.S. NO_x emissions are reduced by 50% during the summer oxidant study.

Date	SOUTHERN ONTARIO		CENTRAL ONTARIO		NORTHERN ONTARIO	
	Ave. 1hr. O3	Change	Ave. 1hr. O3	Change	Ave. 1hr. O3	Change
6/09/83	78	-3%	41	-1%	39	0%
6/10/83	60	-6%	40	-3%	42	-1%
6/11/83	52	-6%	50	-7%	44	-2%
6/12/83	70	-12%	40	-13%	24	-5%
6/13/83	109	-13%	56	-12%	30	-4%
6/14/83	137	-12%	59	-14%	24	-2%
6/15/83	125	-12%	62	-17%	24	-6%
6/16/83	75	-10%	28	-12%	22	-5%
6/17/83	49	-7%	19	-7%	24	-1%

Table 14. Average base case 1-hour maximum ozone concentrations (ppb) in Ontario and changes in concentrations when the U.S. NO_x emissions are reduced by 50% during the summer oxidant study.

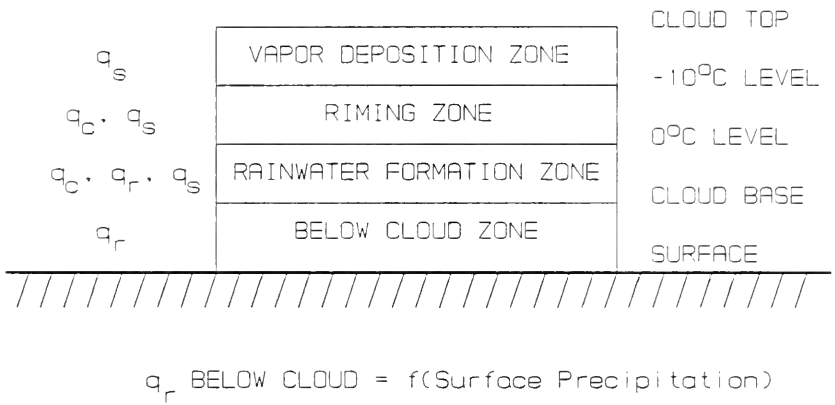

Figure 1. Schematic representation of the stratus cloud module. qc, qr, and qs represent the processes of cloud water, rain water and snow, respectively, at each zone.

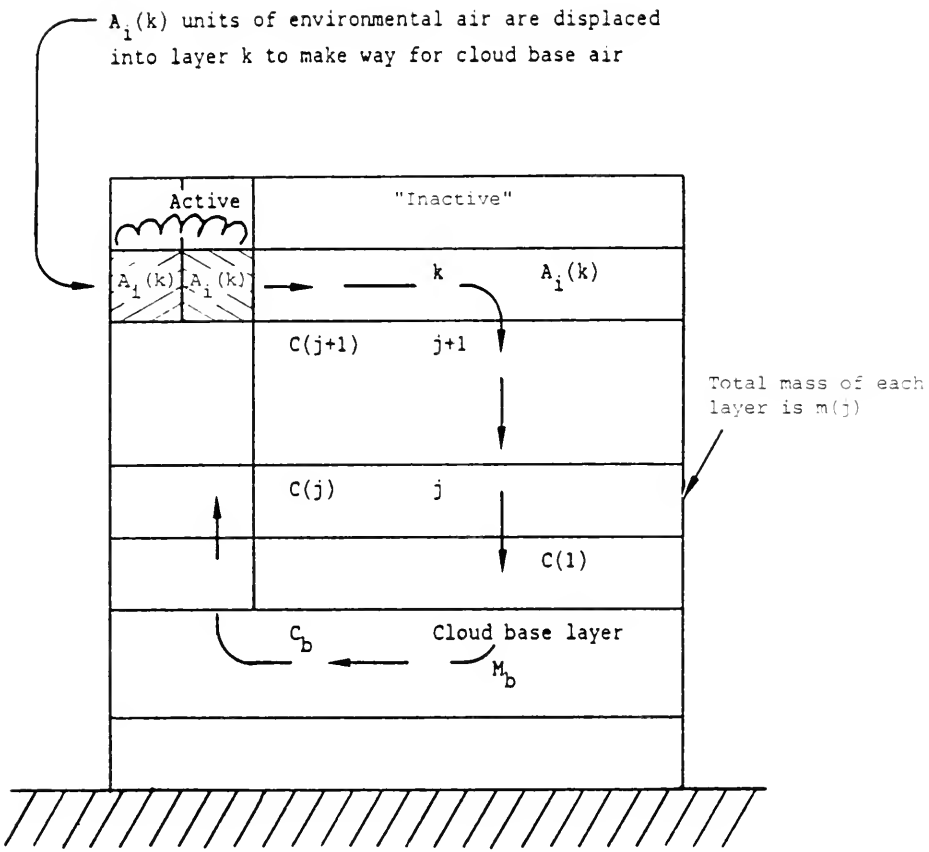

Figure 2. Schematic representation of the cumulus cloud module: Redistribution of pollutants during the life cycle of a cloud C(j) and C_b are the concentrations of layer j and the cloud base layer. M_b is the mass of air below cloud.

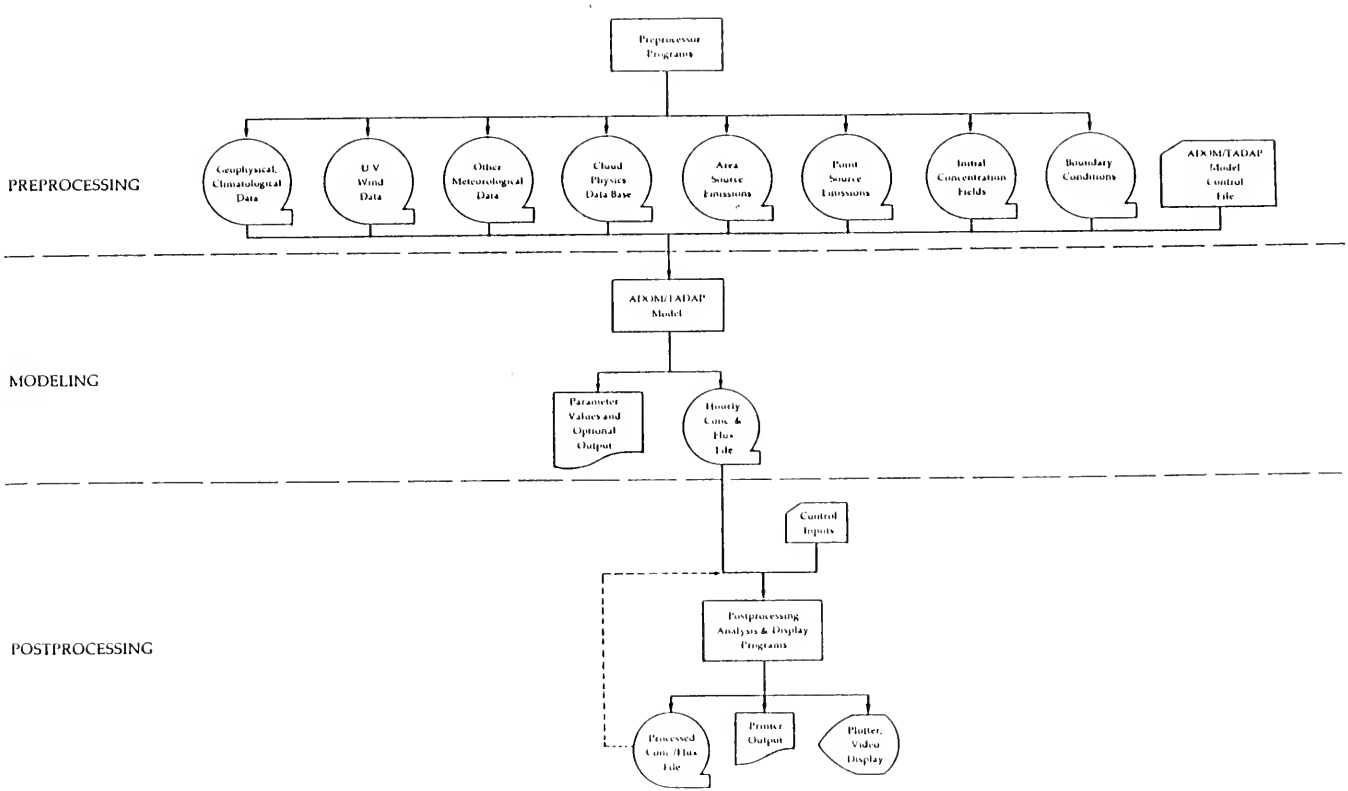

Figure 3. Schematic representation of the ADOM modelling system.

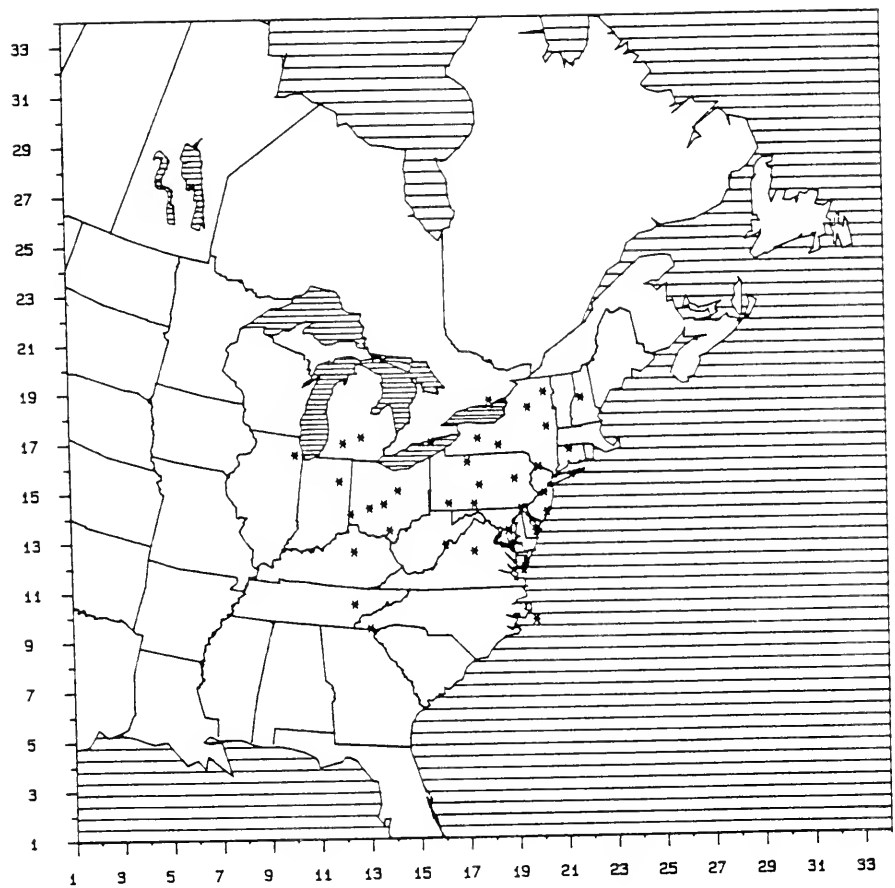

Figure 4. ADOM modelling domain with OSCAR intermediate density sites.

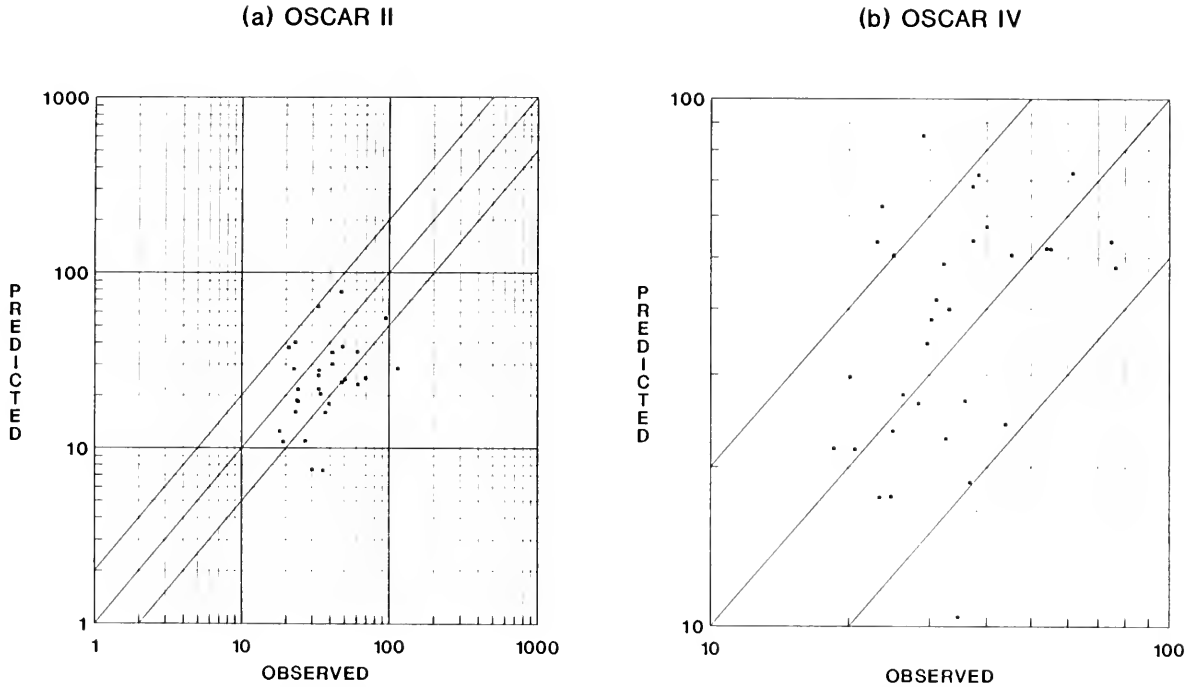

Figure 5. ADOM's predicted vs observed sulphate concentration in precipitation (μM) during OSCAR II (a) and OSCAR IV (b). The diagonal is the 1:1 line and the line on each side is the factor of 2 line.

(a) OSCAR II

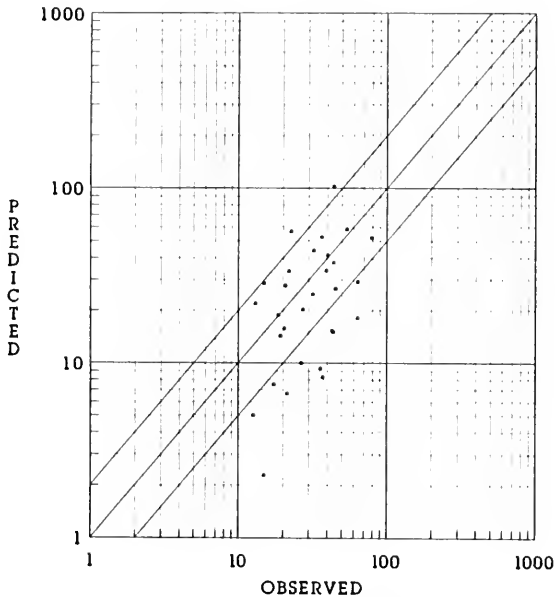

(b) OSCAR IV

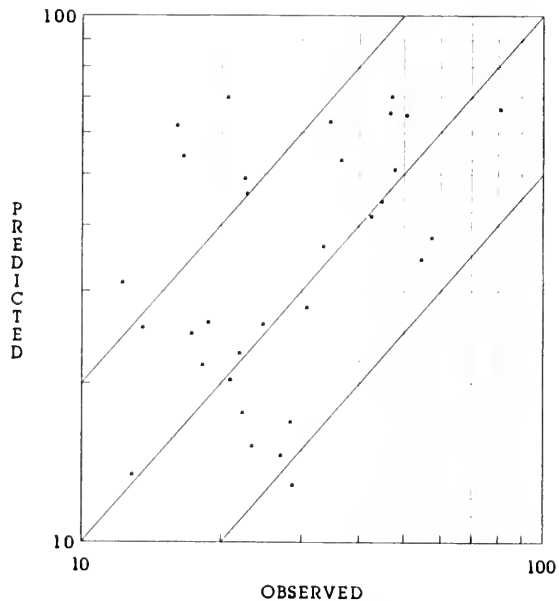

Figure 6. ADOM's predicted vs observed nitrate concentration in precipitation (μM) during OSCAR II (a) & IV (b). The diagonal is the 1:1 line and the line on each side is the factor of 2 line.

(a) OSCAR II

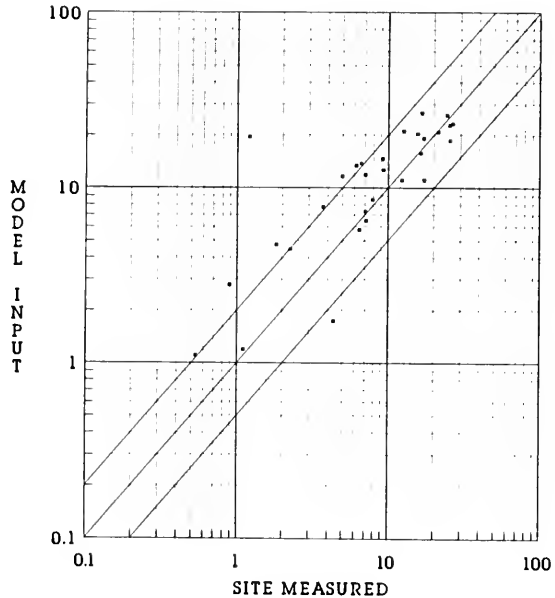

(b) OSCAR IV

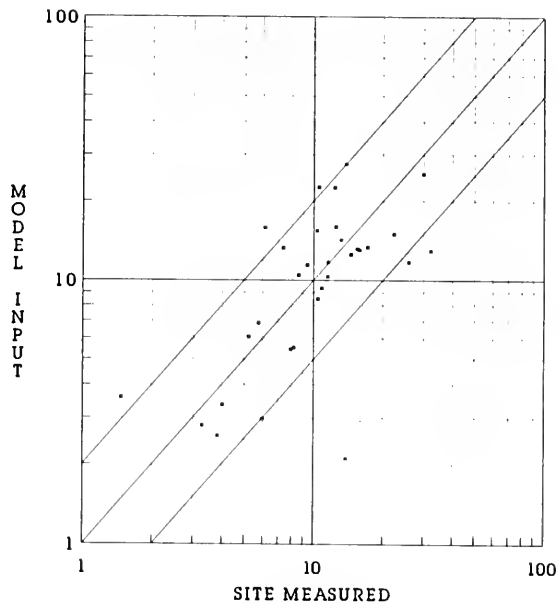

Figure 7. ADOM input precipitation vs. site measured precipitation for OSCAR II (a) & IV (b). The diagonal is the 1:1 line and the line on each side is the factor of 2 line. The unit is mm.

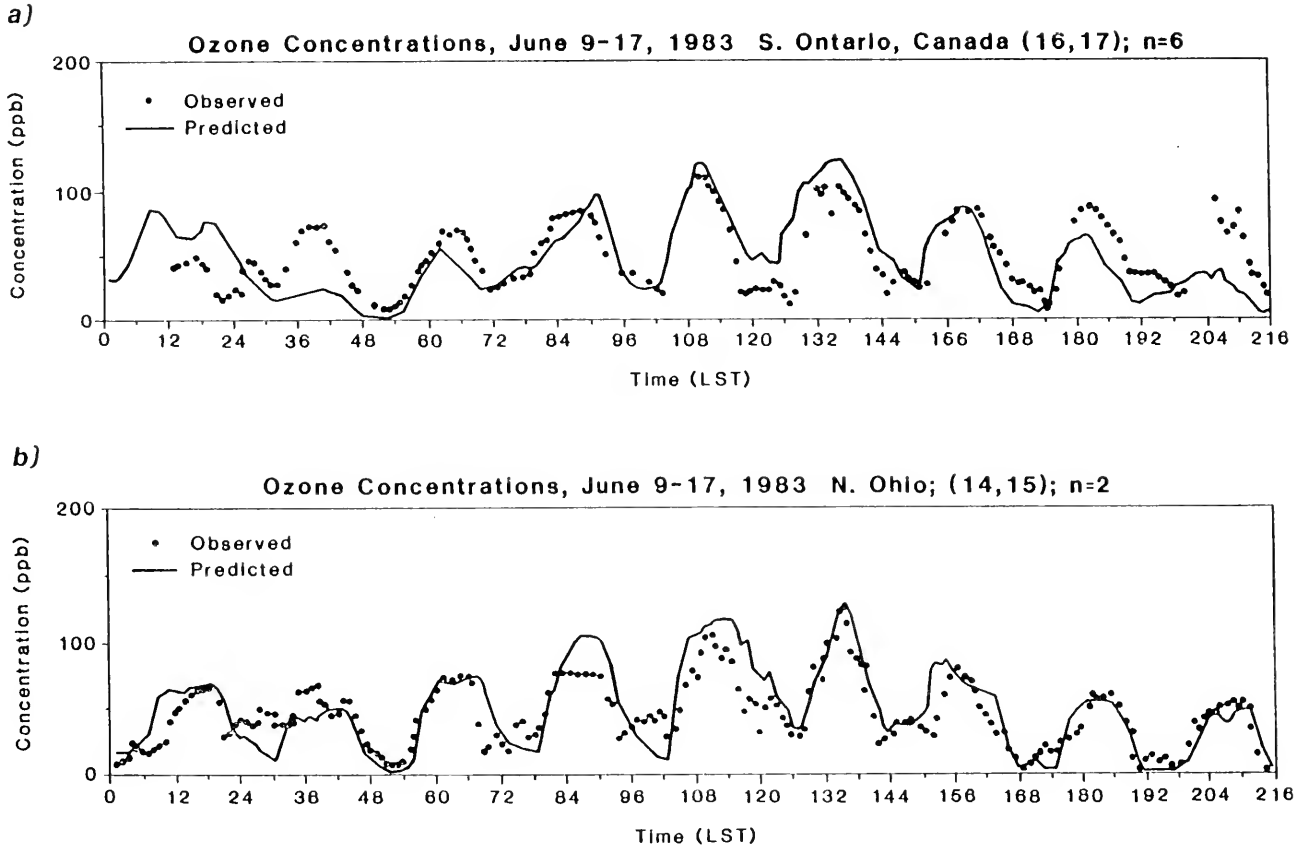

Figure 8. Time series plot of ozone for two sites during the summer oxidant study.

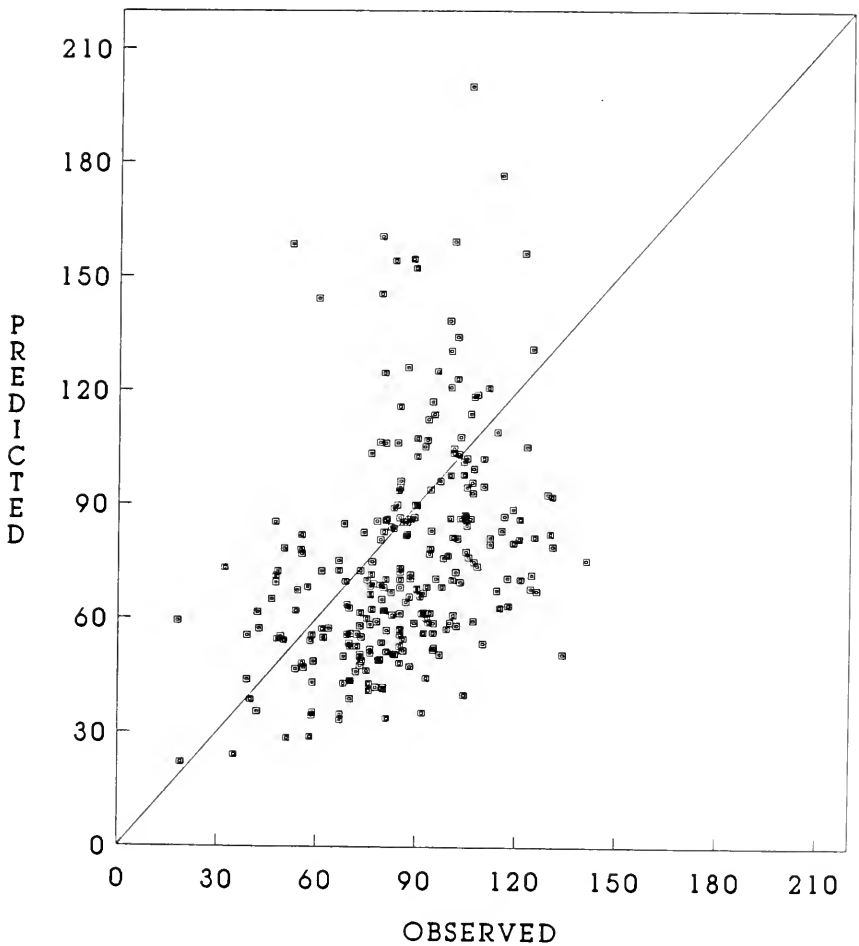

Figure 9. Comparison of model predicted and observed dialy ozone maximum for all the sites for each day of the summer oxidant study in ppb. The diagonal is the 1:1 line and on each side are the factor of 1.5 and 2 lines.

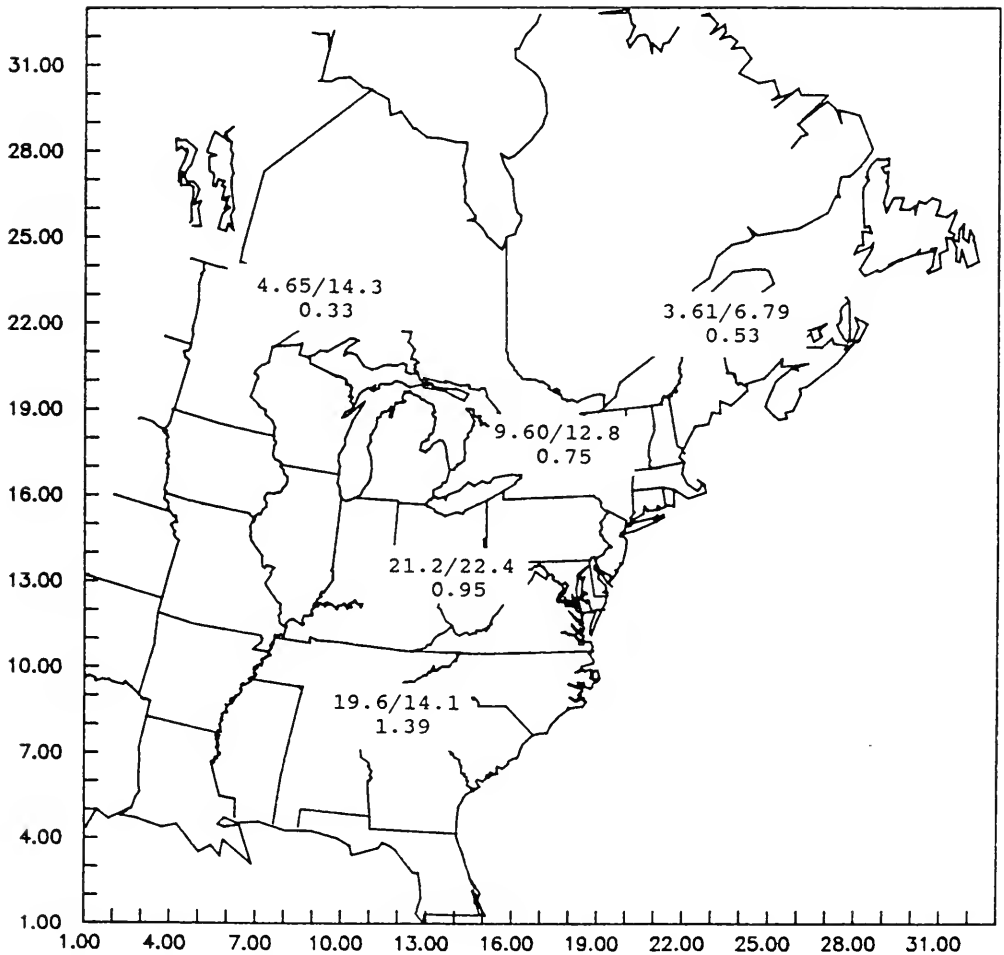

Figure 18. Regionally averaged observed and predicted sulphate concentrations (μM) in precipitation for the winter study. The ratio of observed to predicted concentration is shown below each observation/ prediction pair.

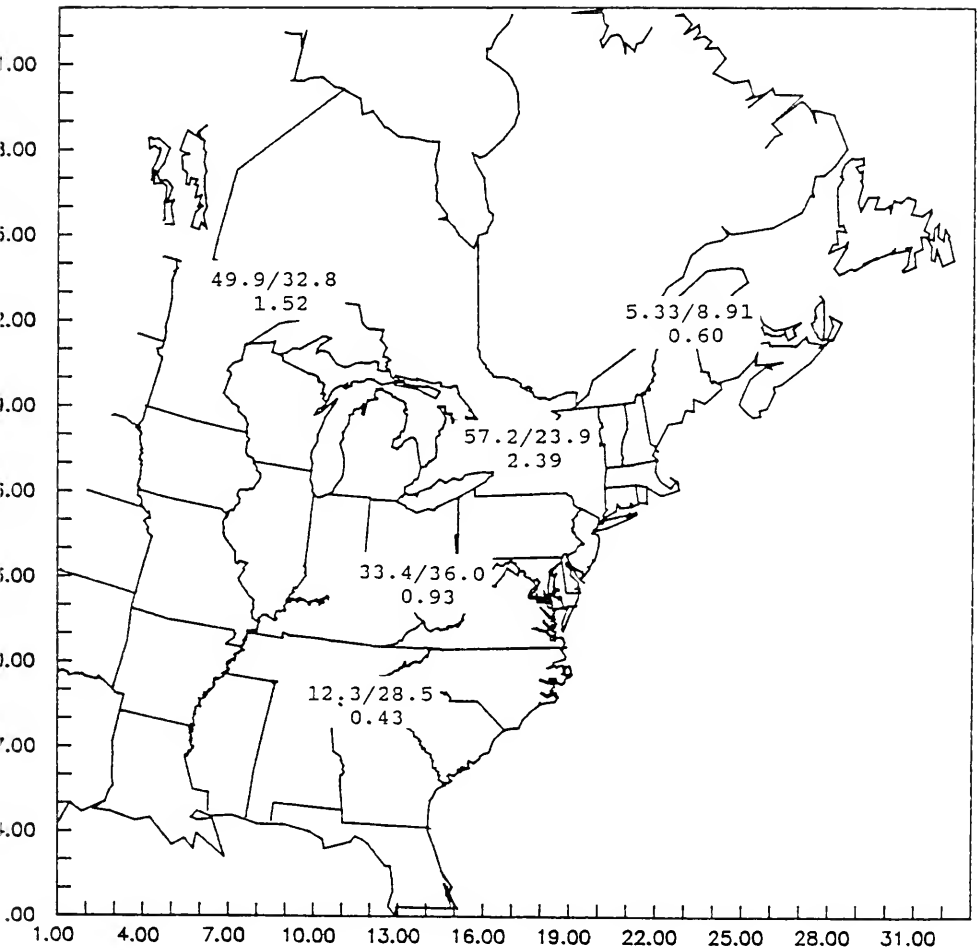

Figure 19. Regionally averaged observed and predicted nitrate concentrations (μM) in precipitation for the winter study. The ratio of observed to predicted concentration is shown below each observation/ prediction pair.

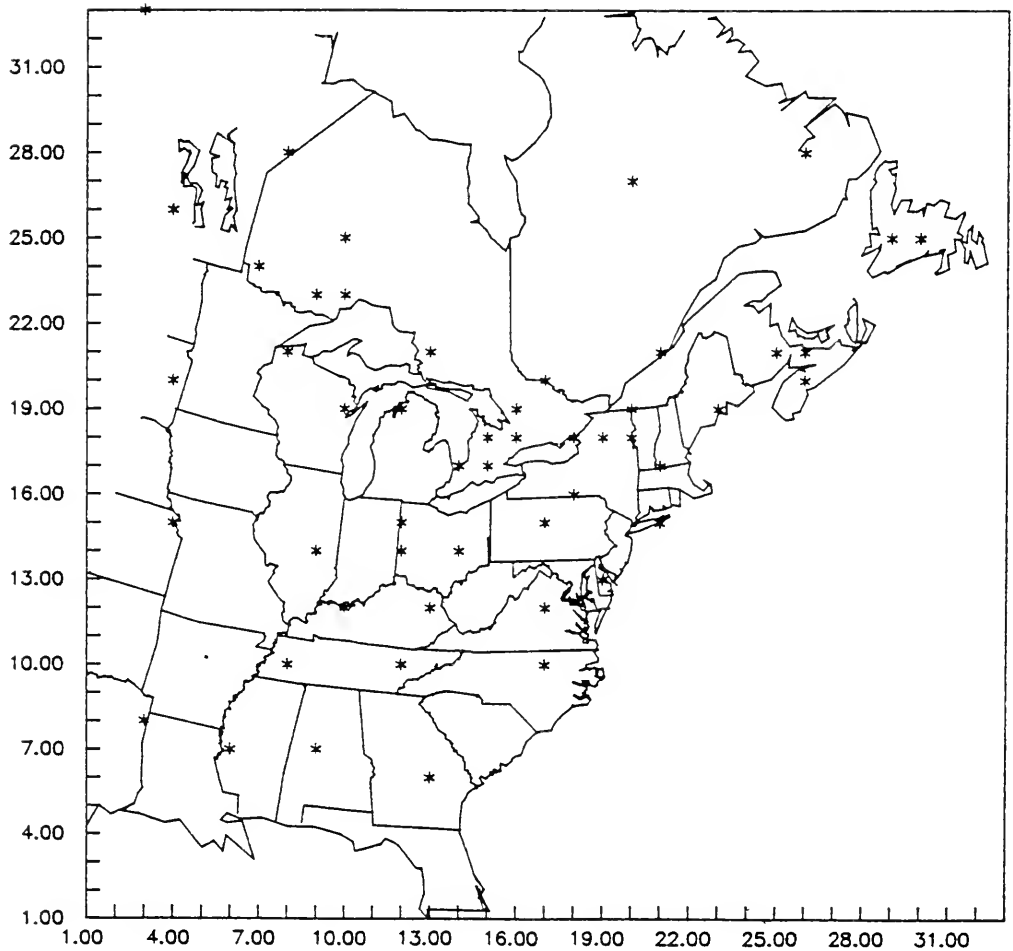

Figure 10. Location of stations from which monitoring data are available for the winter simulation.

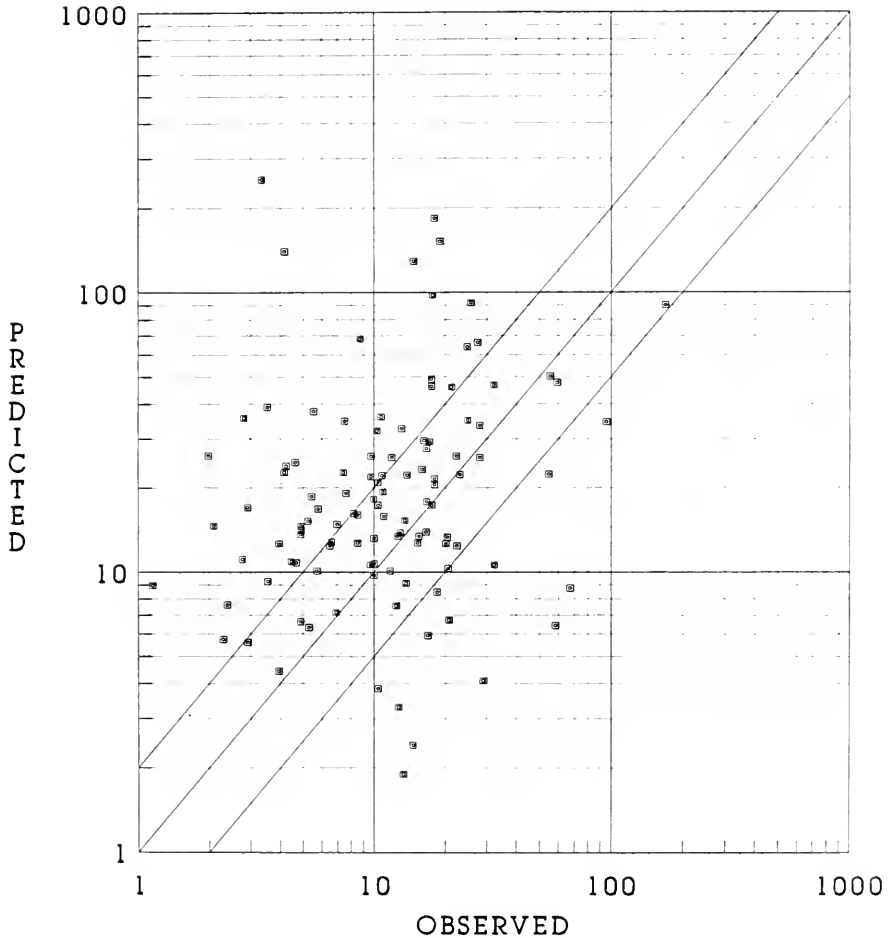

Figure 11. Comparison of daily ADOM predicted and observed sulphate concentration (μM) in precipitation during the winter study. The diagonal is the 1:1 line and the line on each side is the factor of 2 line.

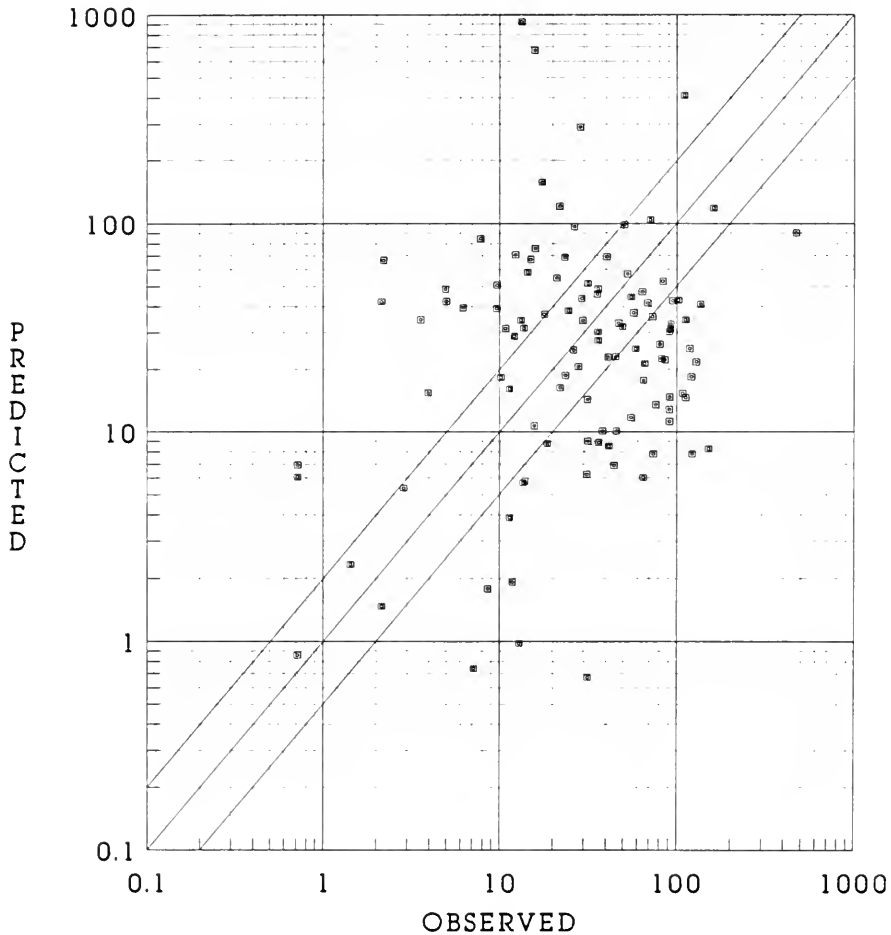

Figure 12. Comparison of daily ADOM predicted and observed nitrate concentration (μM) in precipitation during the winter study. The diagonal is the 1:1 line and the line on each side is the factor of 2 line.

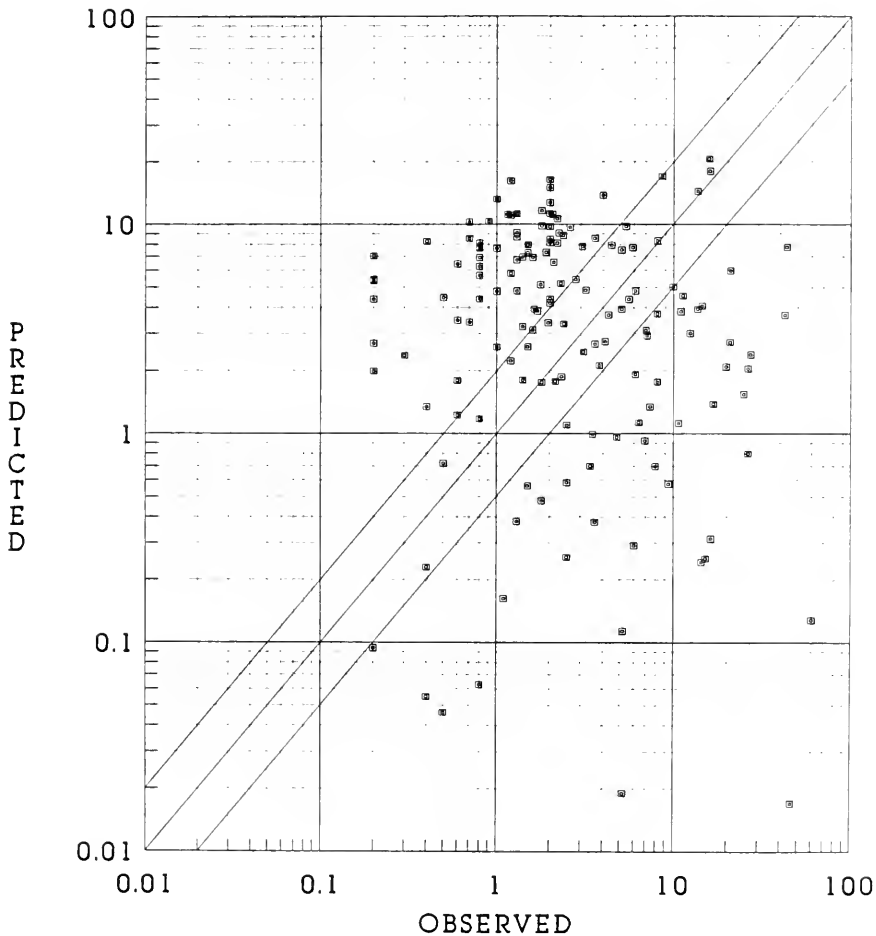

Figure 13. Comparison of daily total observed and model input precipitation (mm) during the winter study. The diagonal is the 1:1 line and the line on each side is the factor of 2 line.

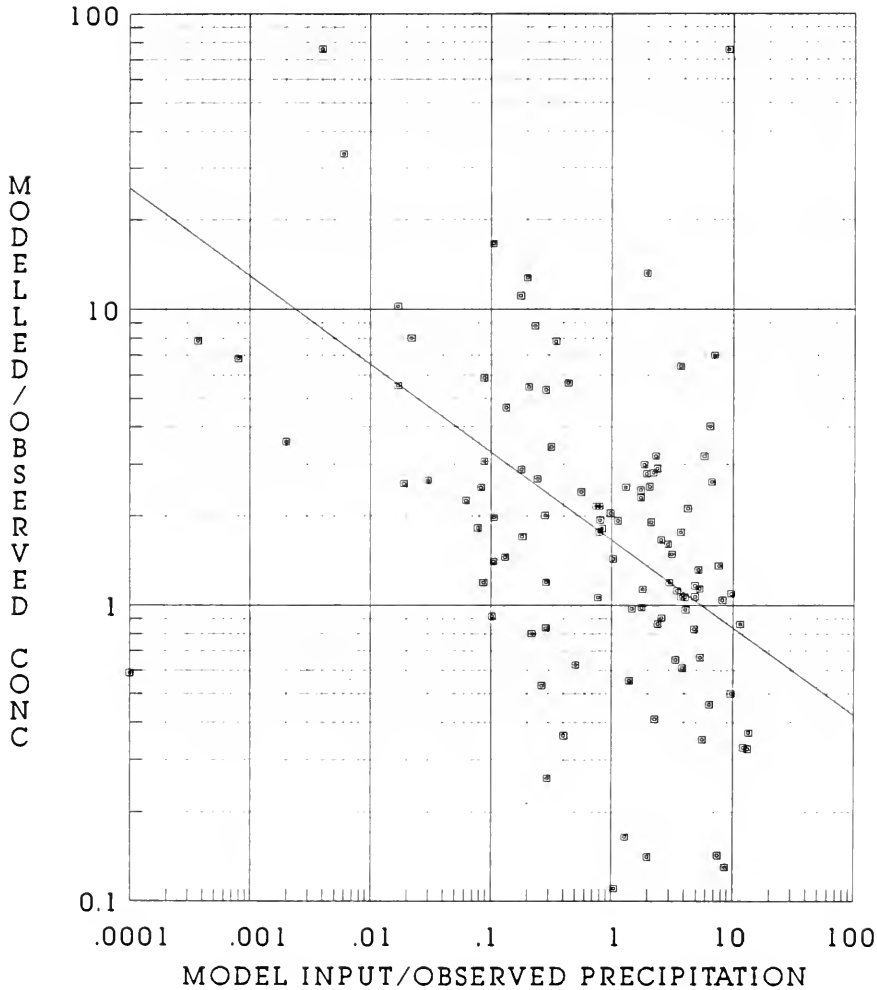

Figure 14. Ratio of model to observed sulphate concentration in precipitation vs. ratio of model input precipitation to observed precipitation for the winter study. The solid line is the best fit line from linear regression analysis.

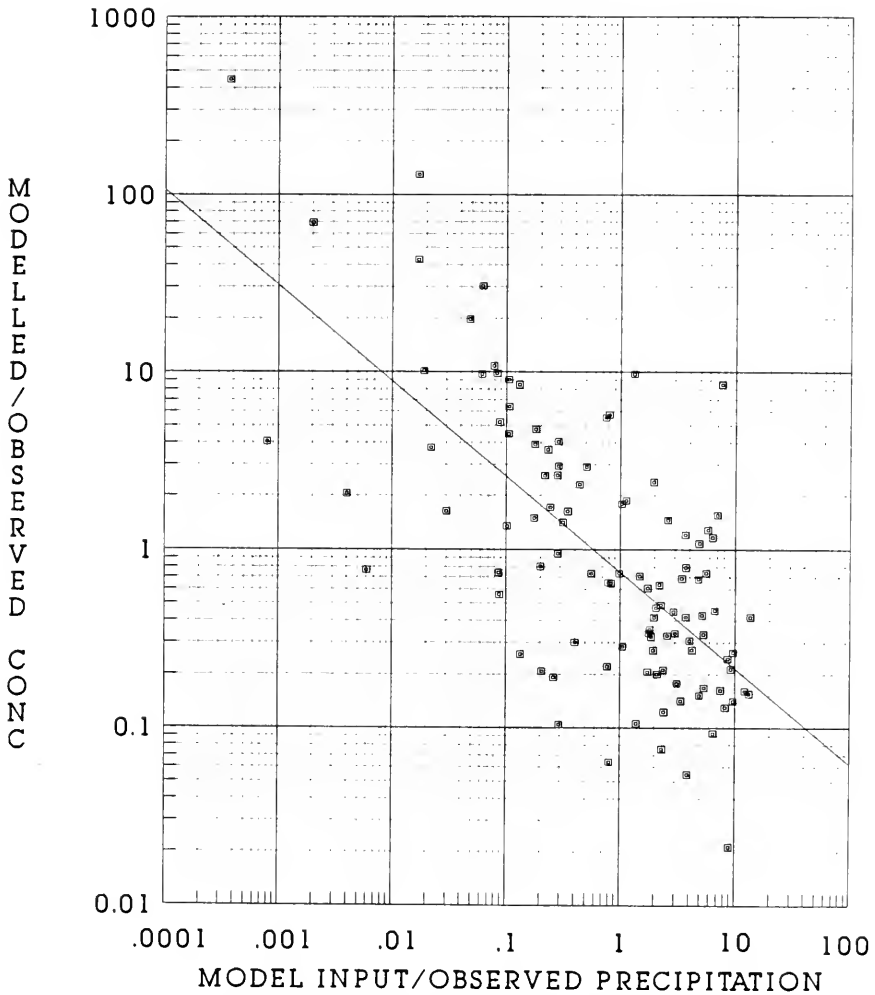

Figure 15. Ratio of model to observed nitrate concentration in precipitation vs. ratio of model input precipitation to observed precipitation for the winter study. The solid line is the best fit line from linear regression analysis.

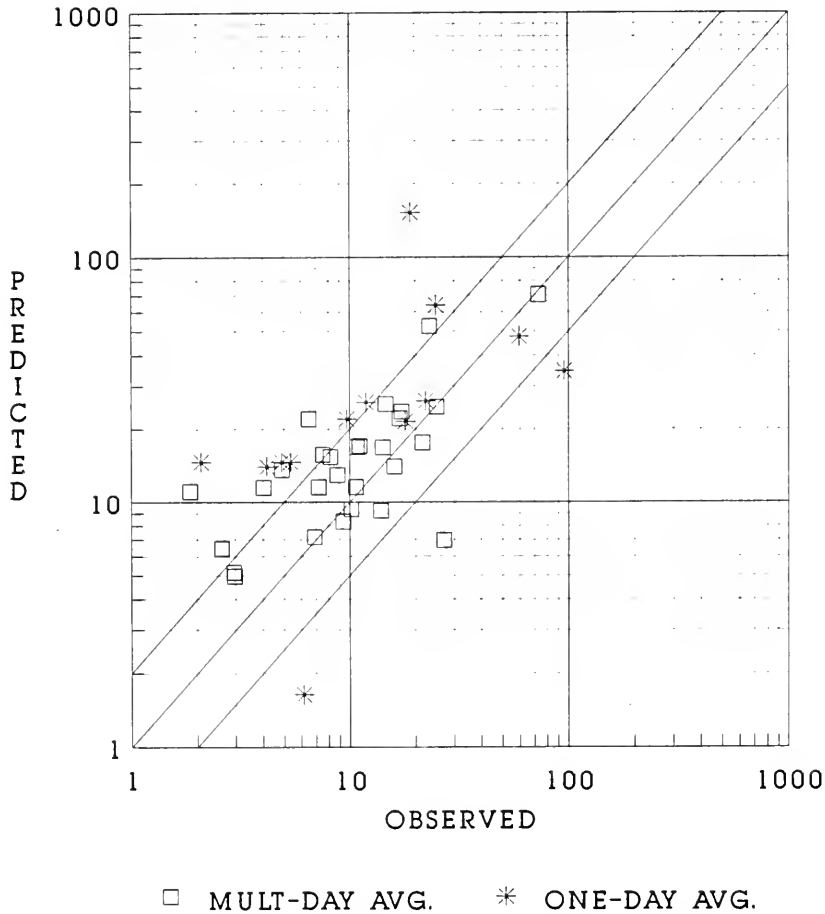

Figure 16. Comparison of event averaged observed and modelled sulphate concentration (μM) in precipitation for the winter study. The diagonal is the 1:1 line and the line on each side is the factor of 2 line.

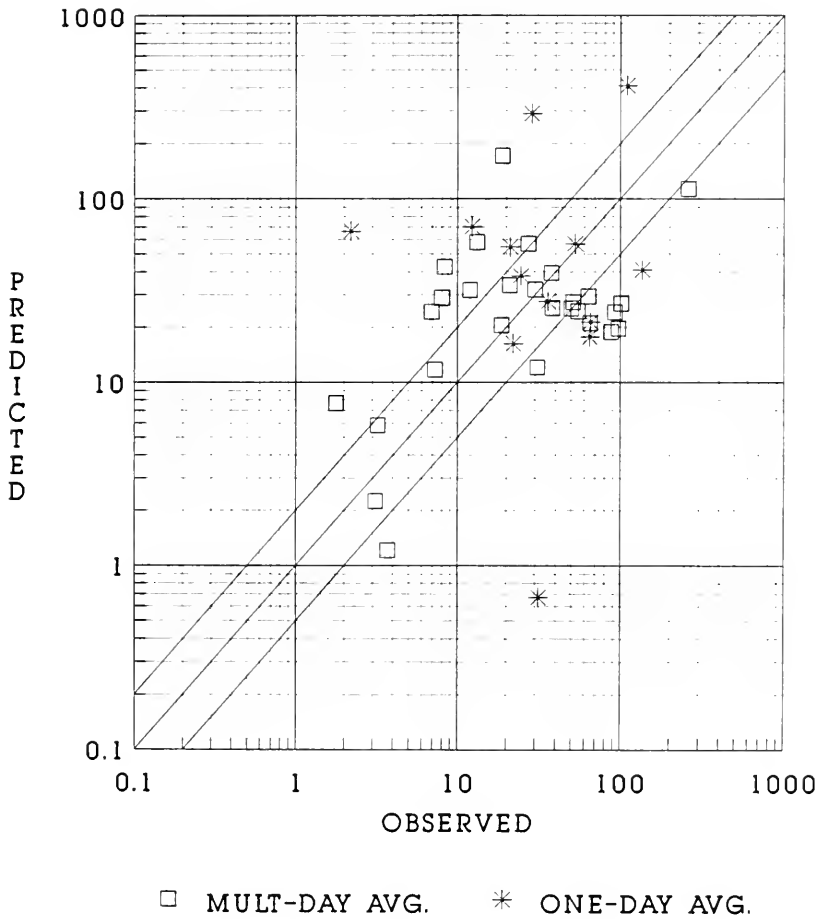

Figure 17. Comparison of event averaged observed and modelled nitrate concentration (μM) in precipitation for the winter study. The diagonal is the 1:1 line and the line on each side is the factor of 2 line.

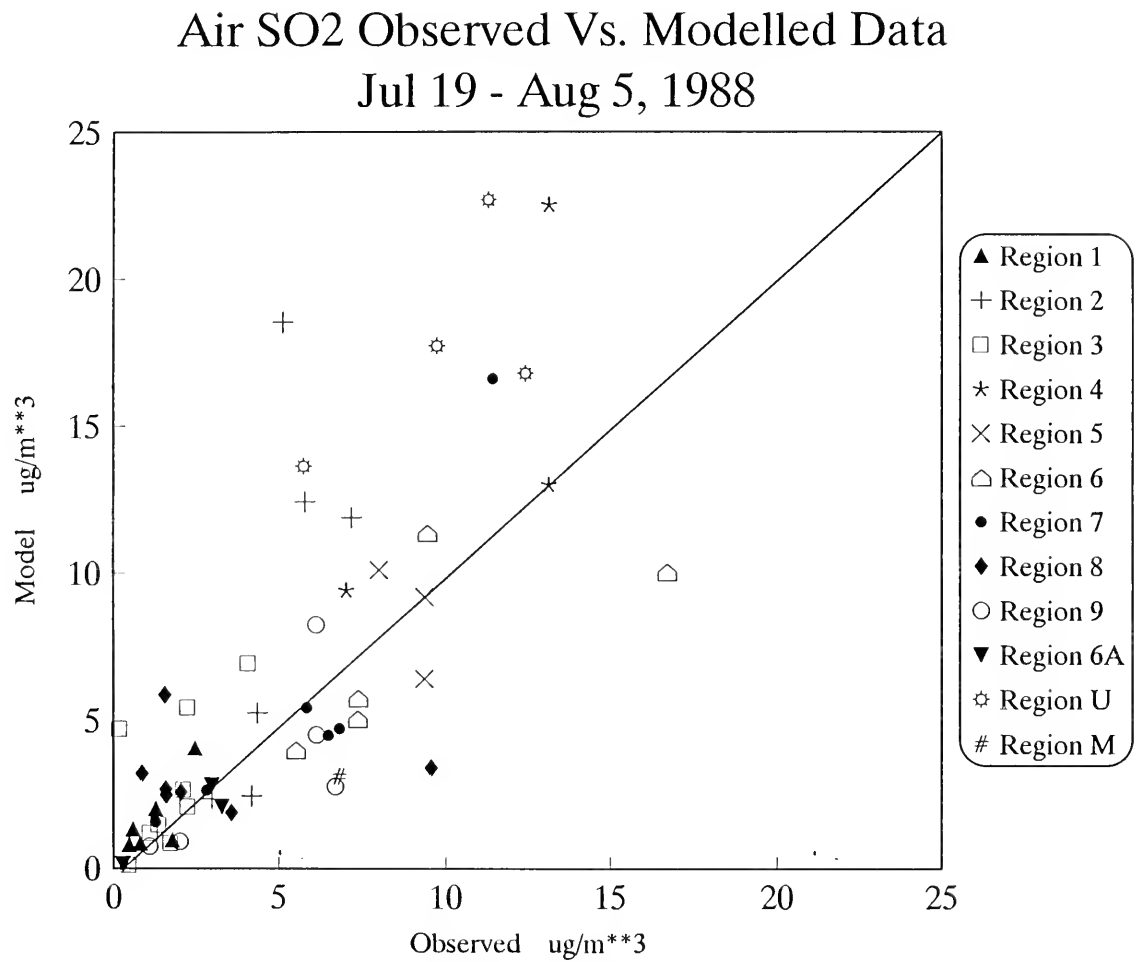

Figure 27 a. Modelled vs. observed ground level concentrations for SO2 for July 19 - August 5, 1988 for EMEFS.

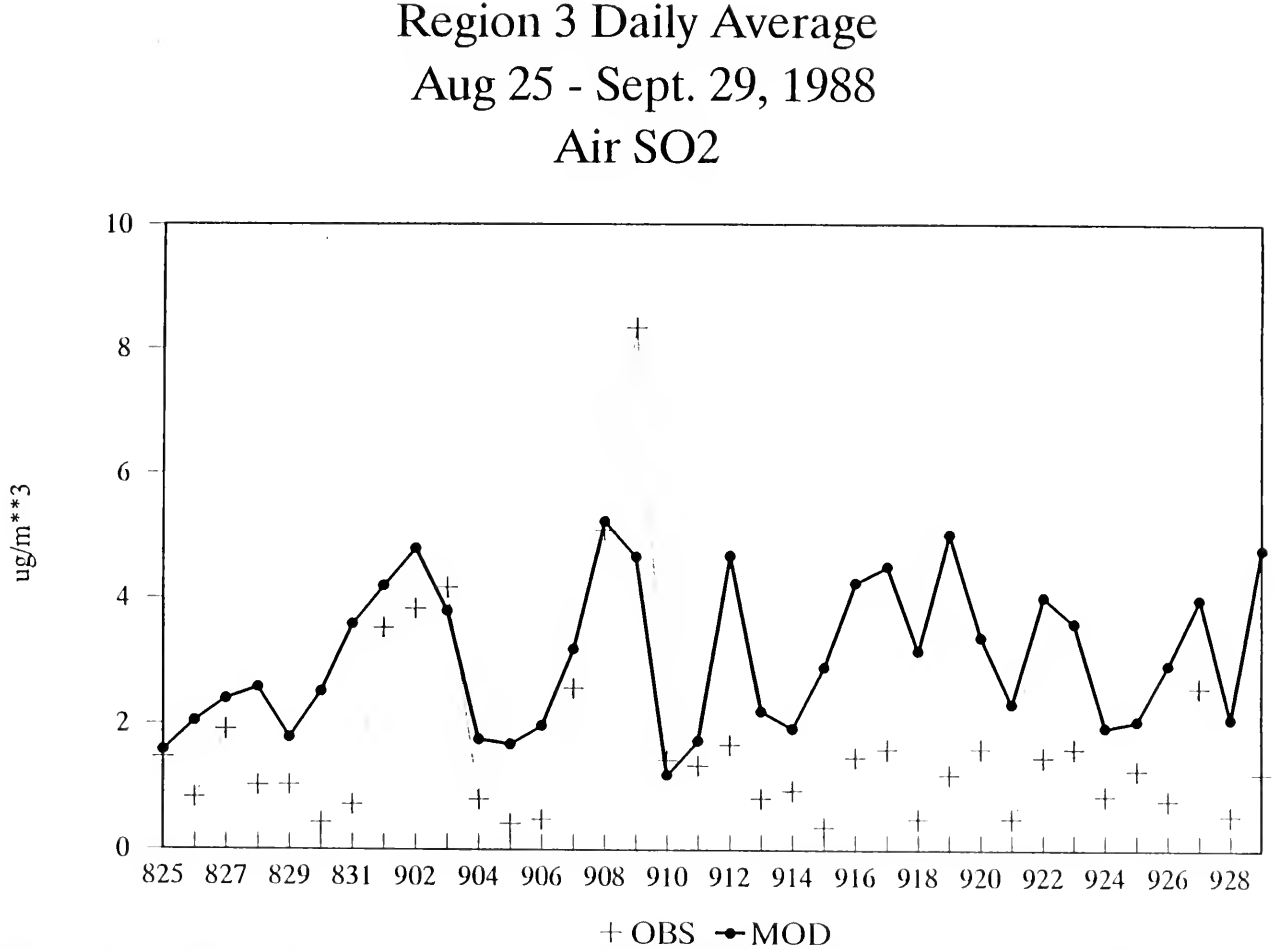

Figure 28 a. Time series plots of regional average predicted and observed concentrations of SO2 for August 25 - September 29, 1988.

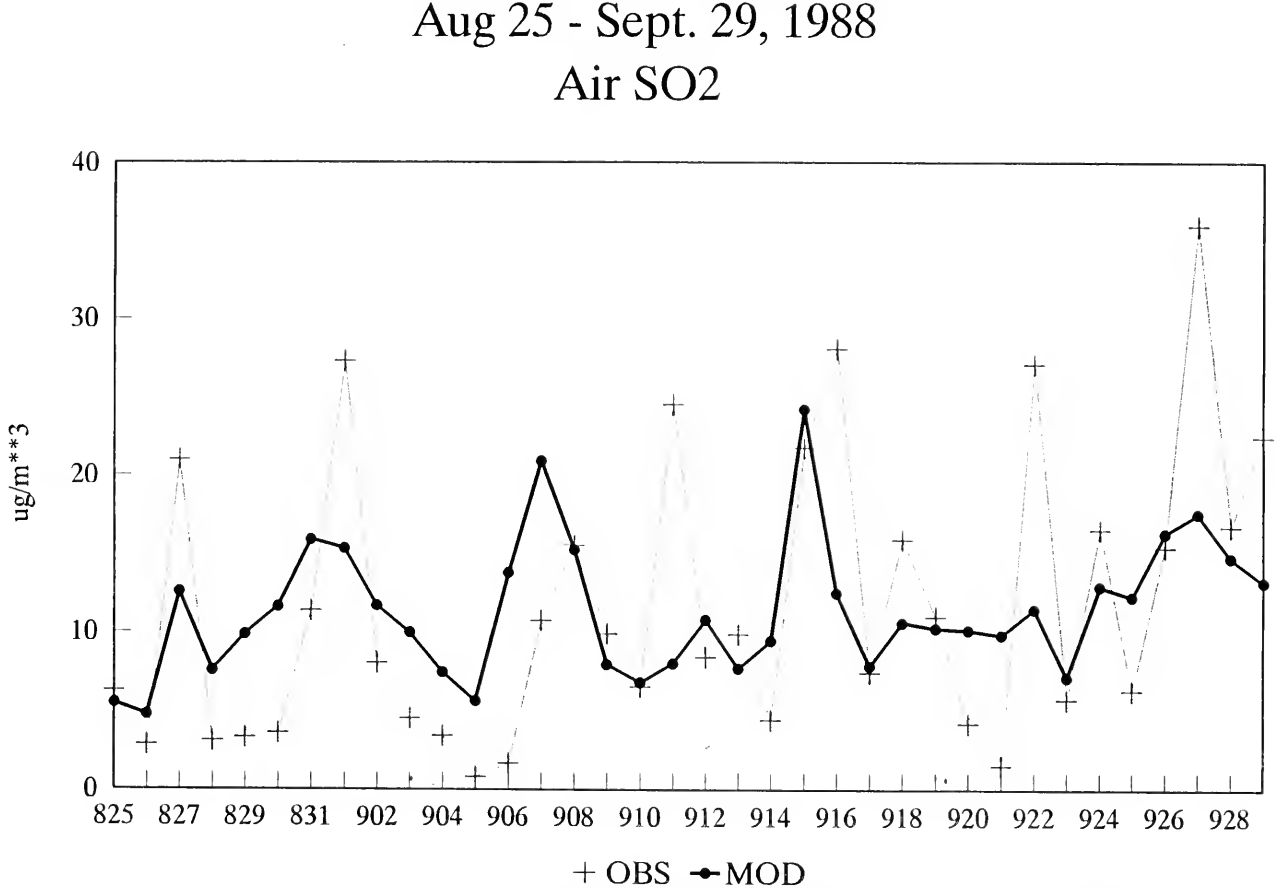

Figure 28 b. Time series plots of regional average predicted and observed concentrations of SO2 for August 25 - September 29, 1988 for EMEFS.

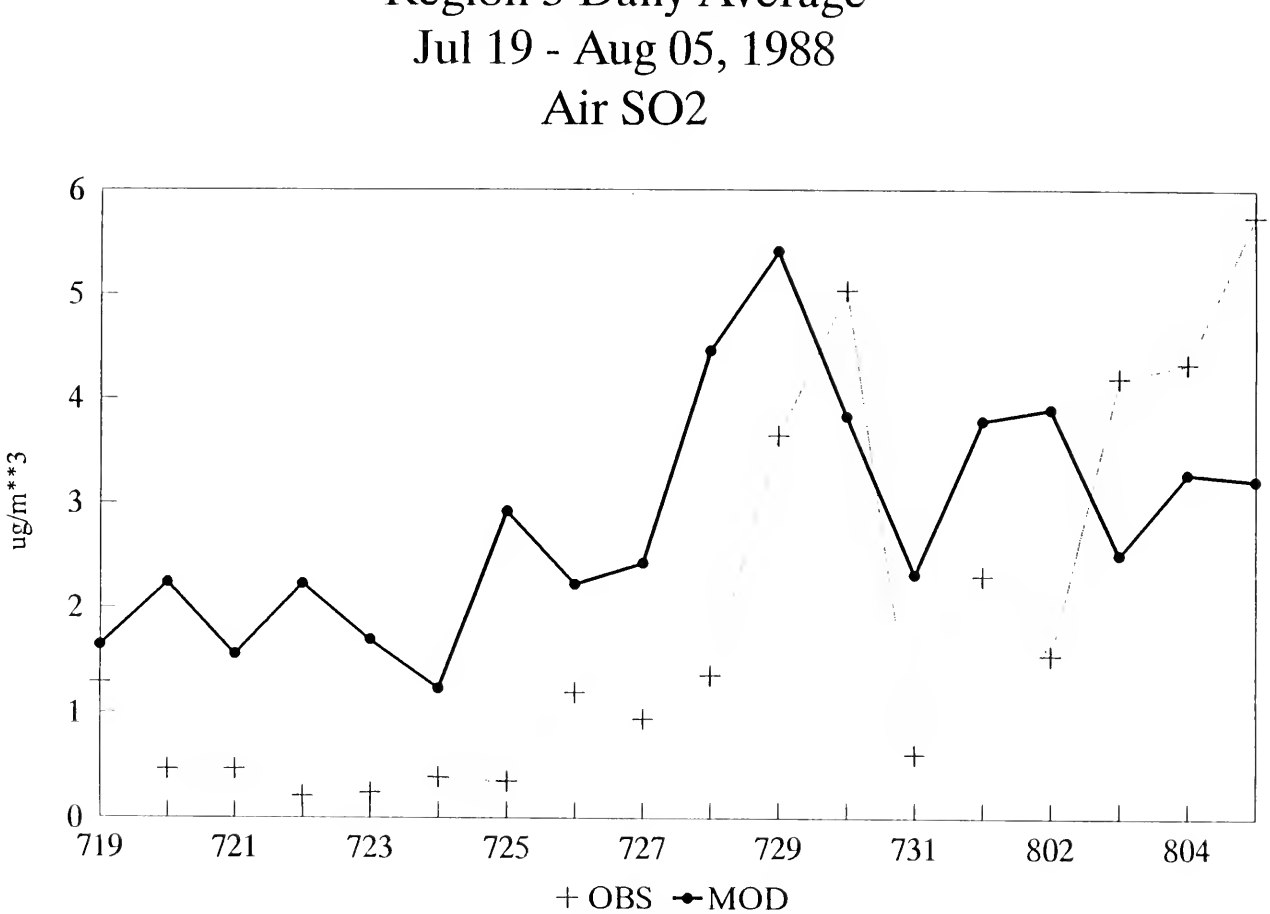

Figure 28 c. Time series plots of regional average predicted and observed concentrations of SO2 for July 19 - August 5, 1988 for EMEFS.

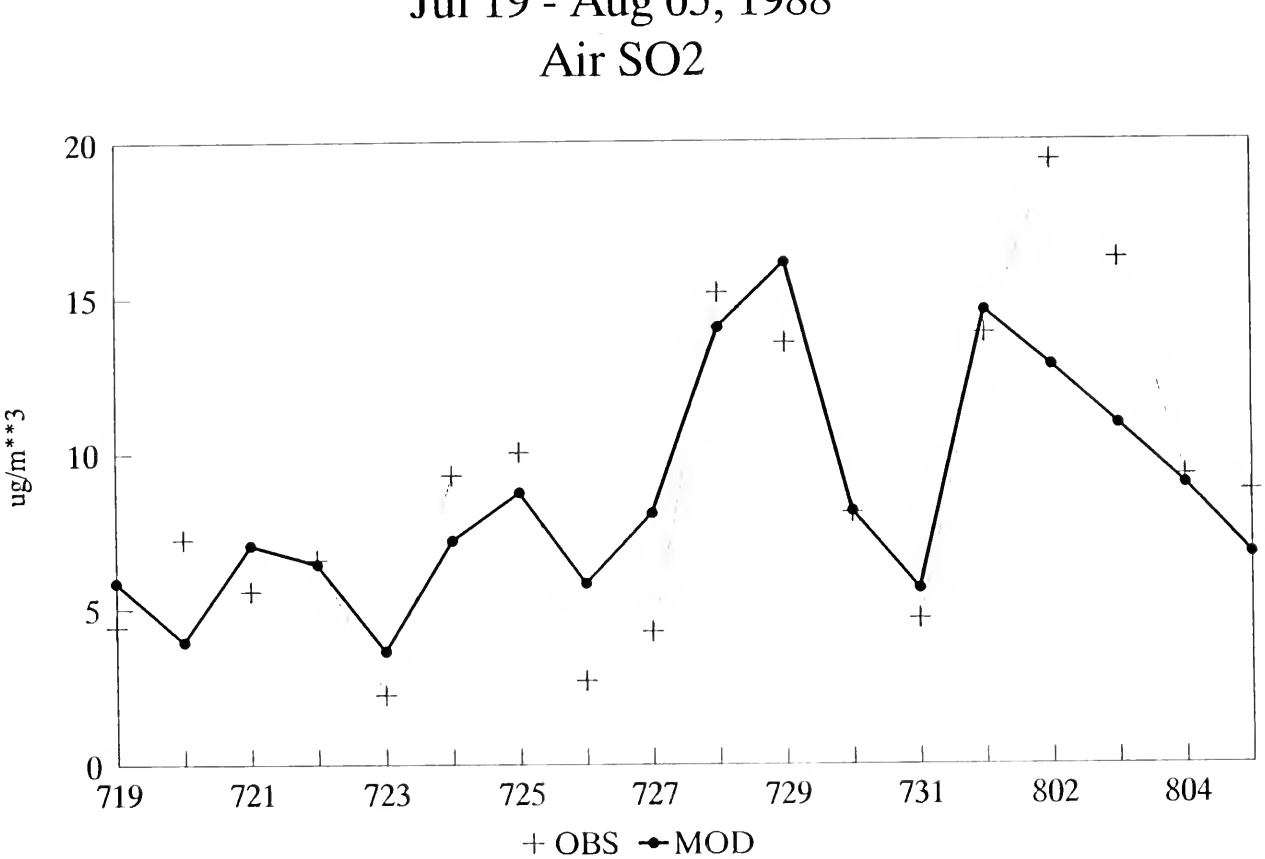

Figure 28 d. Time series plots of regional average predicted and observed concentrations of SO2 for July 19 - August 5, 1988 for EMEFS.

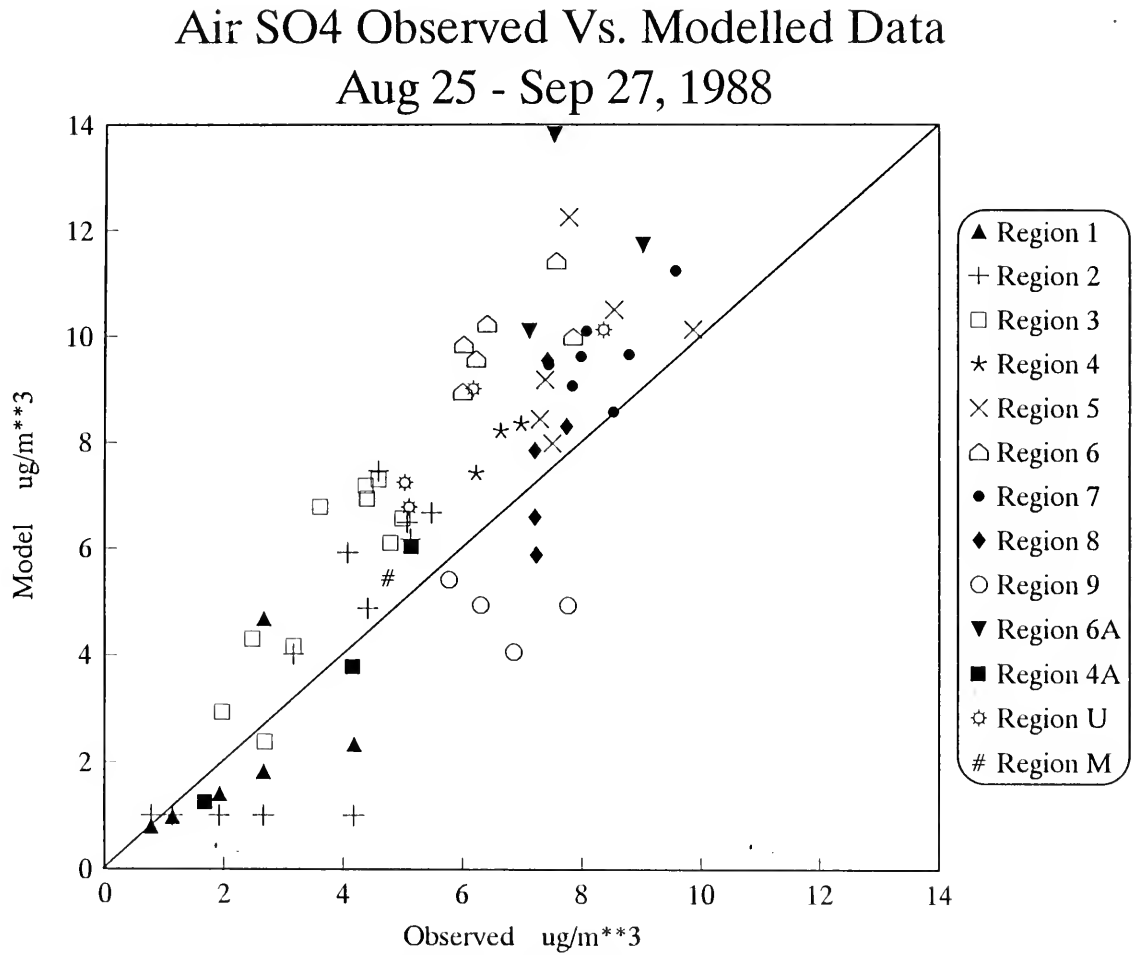

Figure 29. Modelled vs. observed ground level concentrations for sulphate for August 25 - September 27, 1988 for EMEFS.

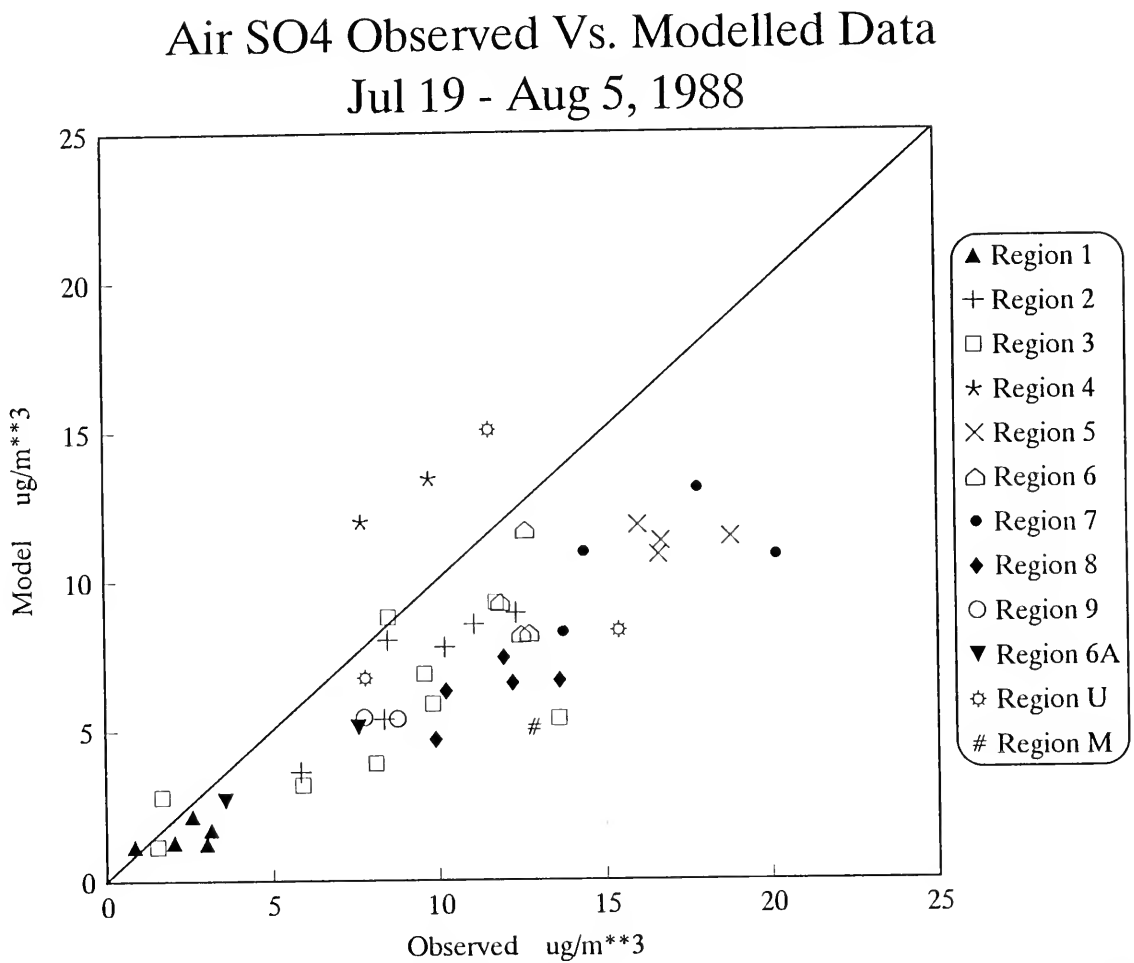

Figure 29 a. Modelled vs. observed ground level concentrations for sulphate for July 19 - August 5, 1988 for EMEFS.

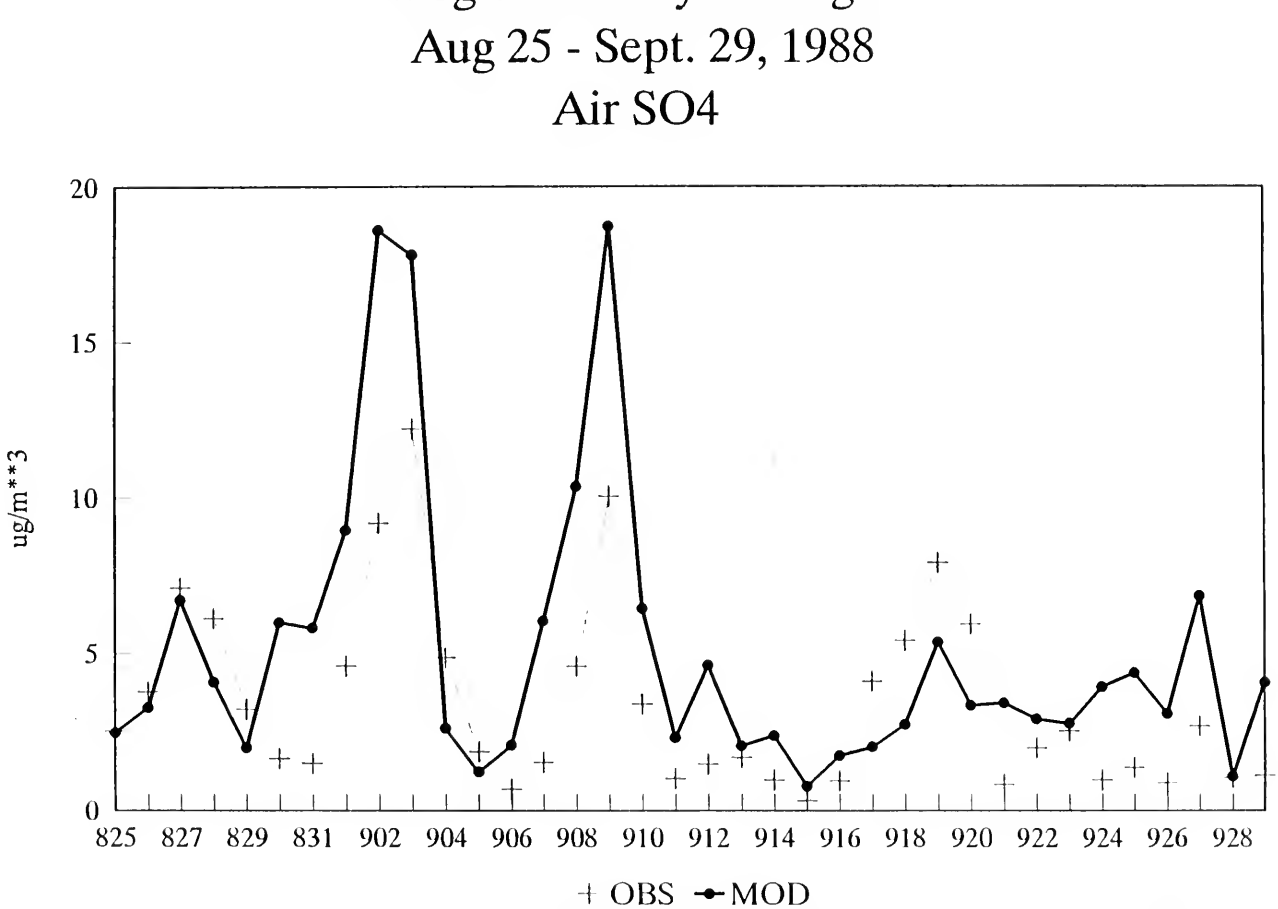

Figure 30 a. Time series plots of regional average predicted and observed concentrations of sulphate for August 25 - September 29, 1988.

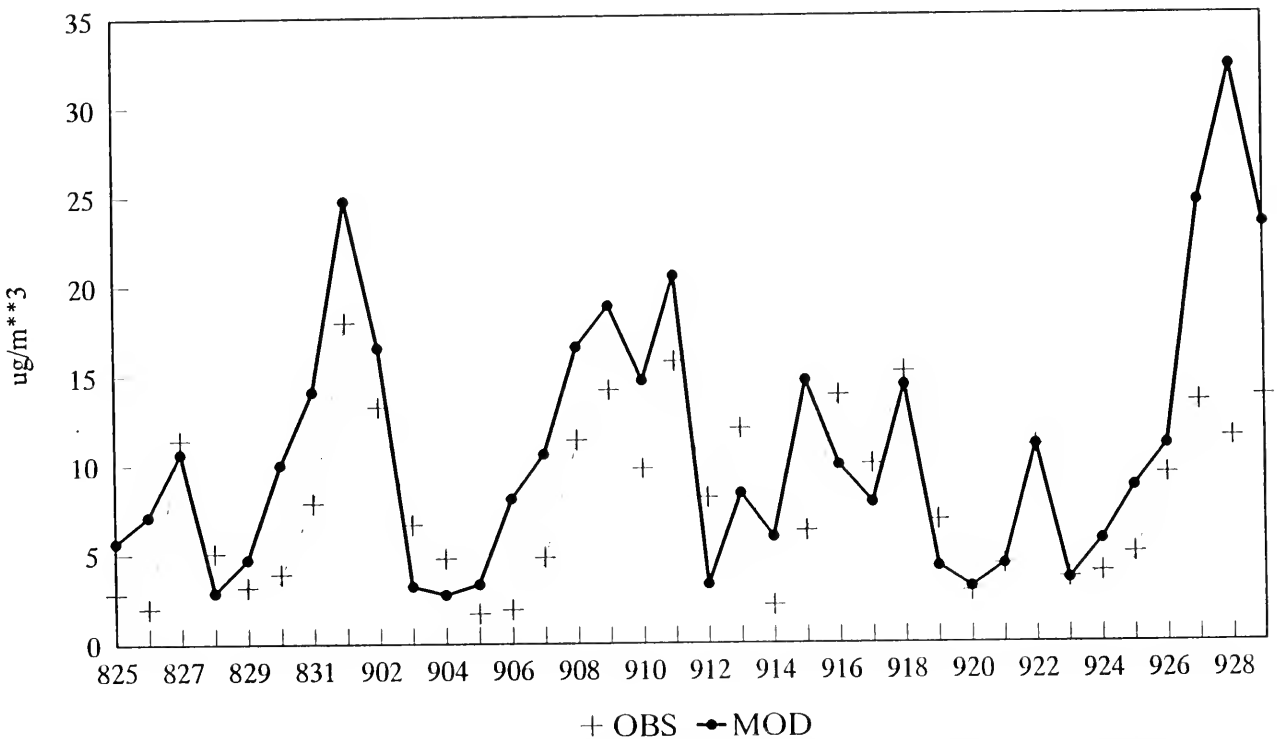

Figure 30 b. Time series plots of regional average predicted and observed concentrations of sulphate for August 25 - September 29, 1988.

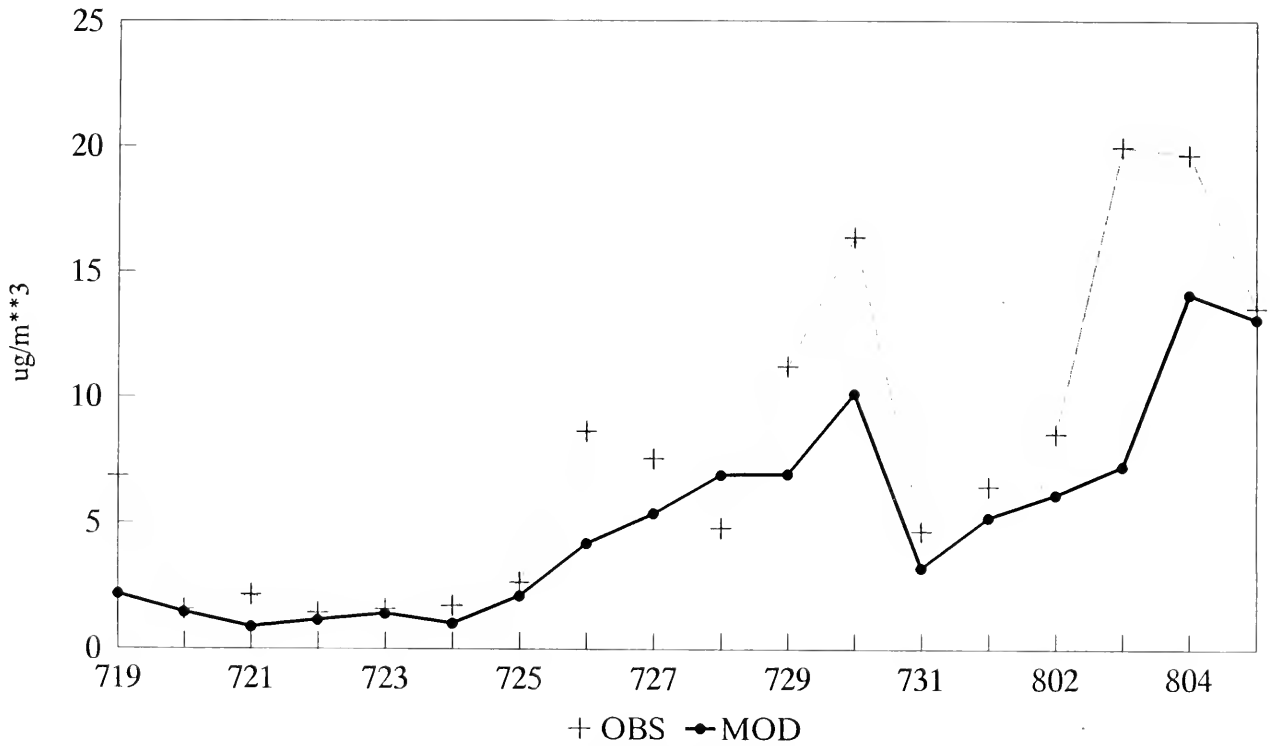

Figure 30 c. Time series plots of regional average predicted and observed concentrations of sulphate for July 19 - August 5, 1988 for EMEFS.

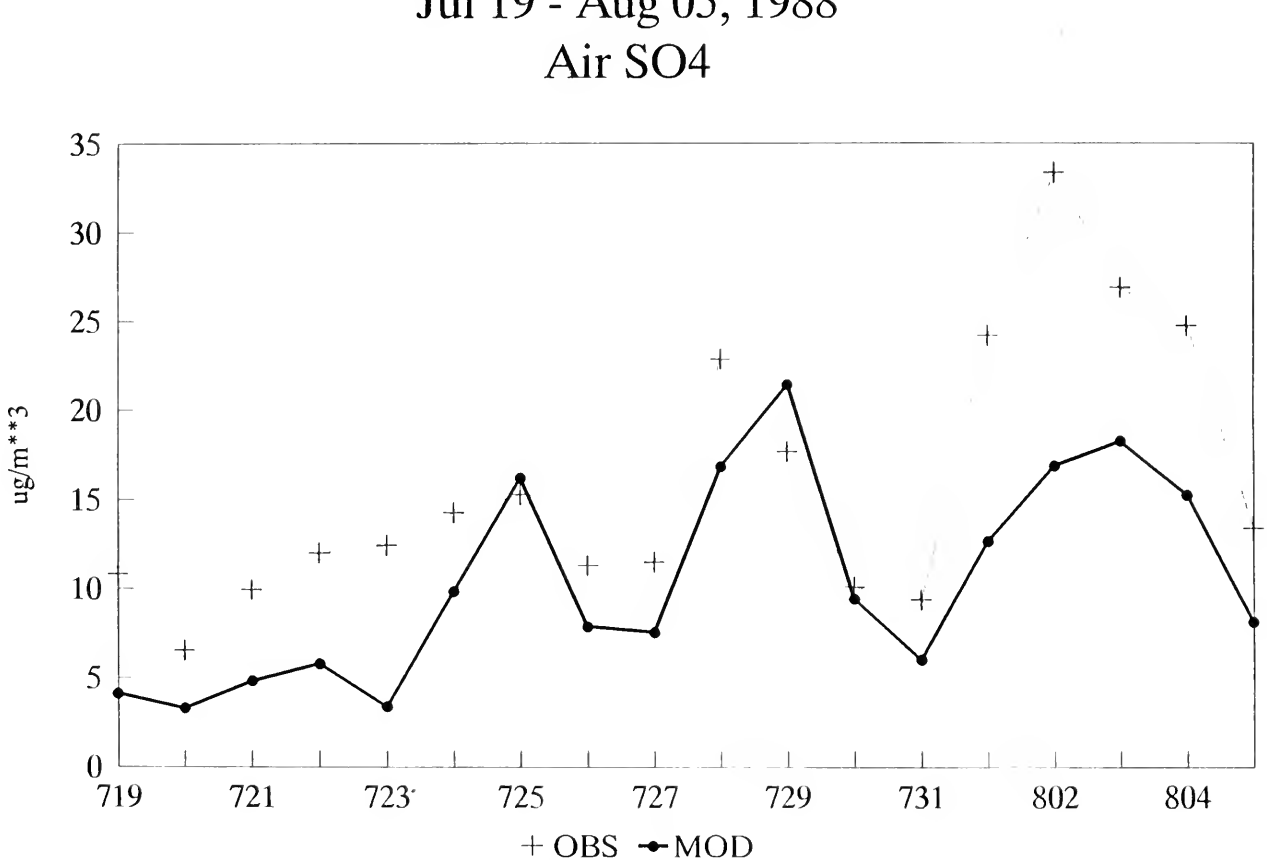

Figure 30 d. Time series plots of regional average predicted and observed concentrations of sulphate for July 19 - August 5, 1988 for EMEFS.

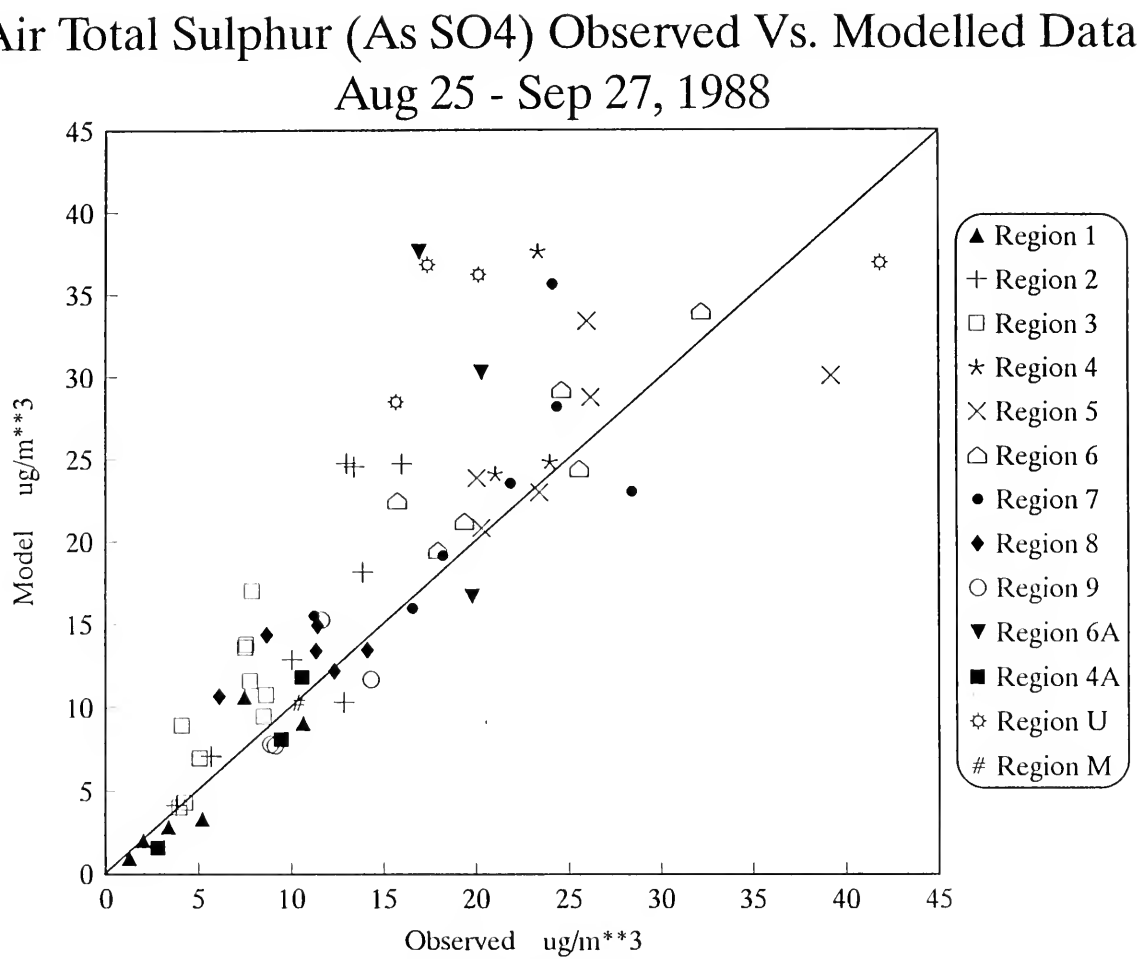

Figure 31. Modelled vs. observed ground level concentrations for total sulphur for August 25 - September 27, 1988 for EMEFS.

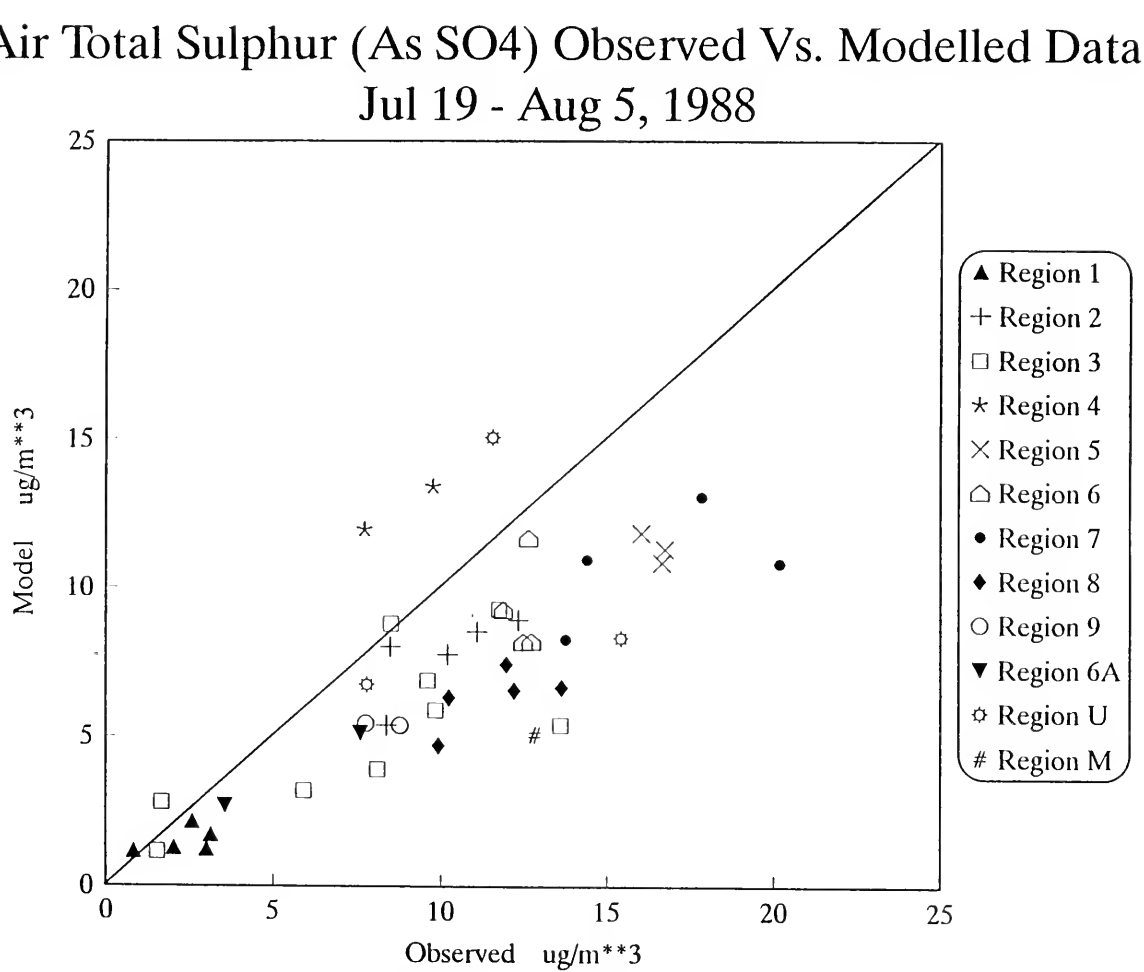

Figure 31 a. Modelled vs. observed ground level concentrations for total sulphur for July 19 - August 5, 1988 for EMEFS.

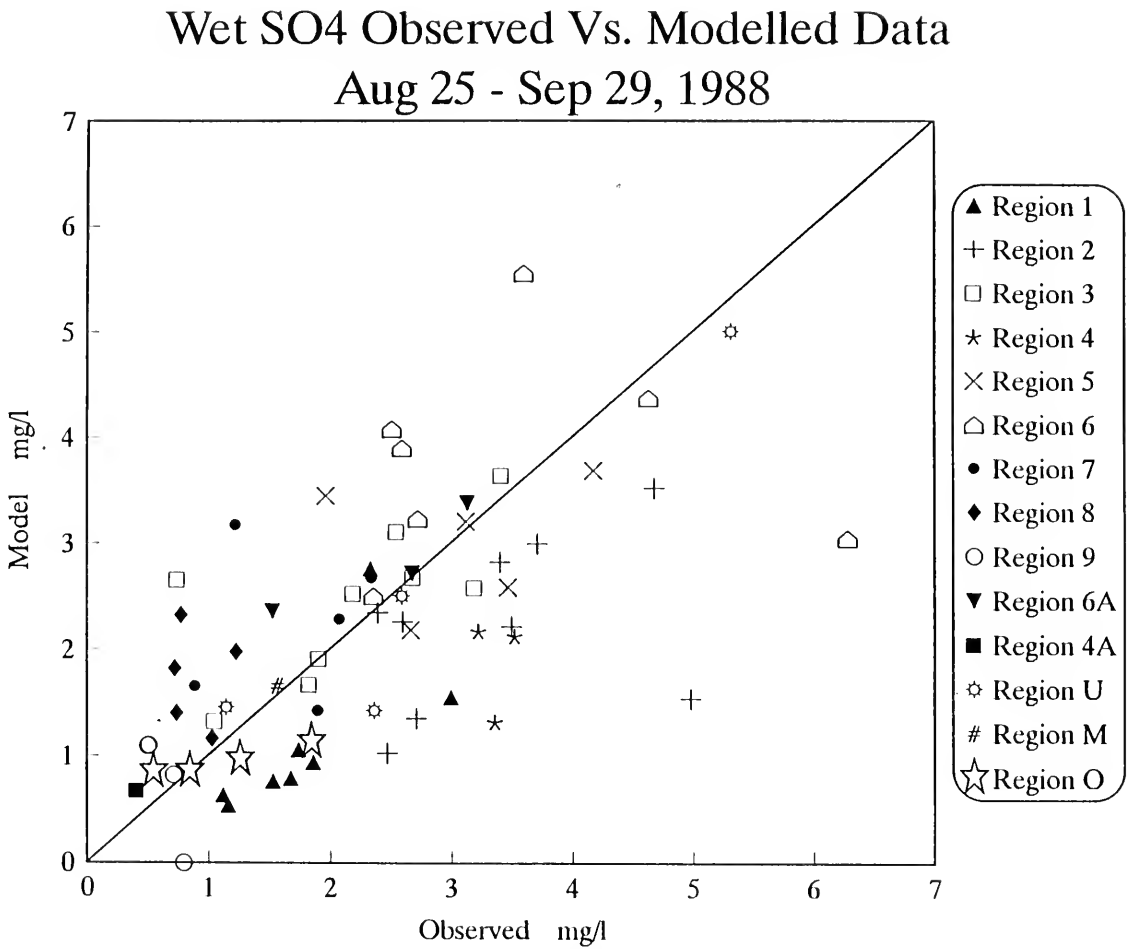

Figure 32. Modelled vs. observed sulphate concentrations in precipitation for August 25 - September 29, 1988 for EMEFS.

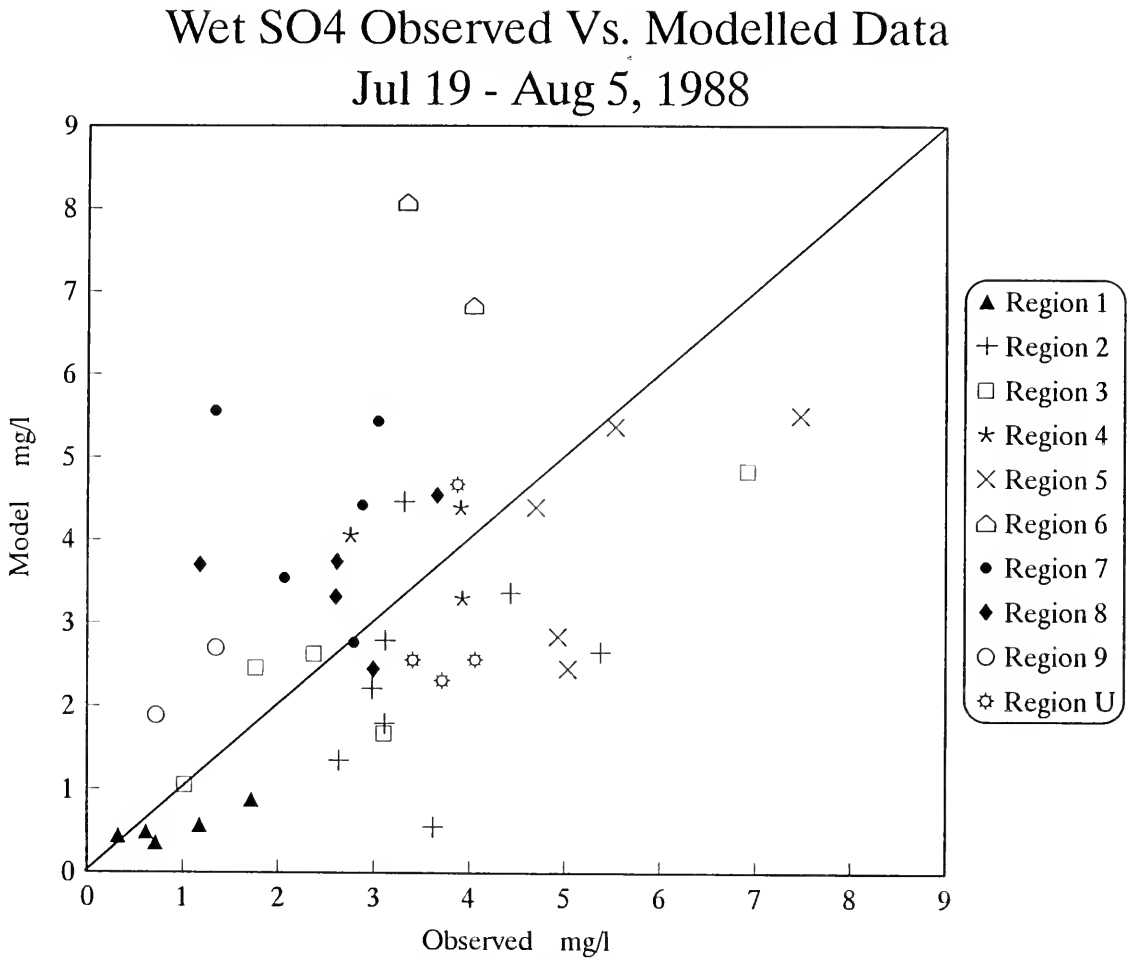

Figure 32 a. Modelled vs. observed sulphate concentrations in precipitation for July 19 - August 5, 1988 for EMEFS.

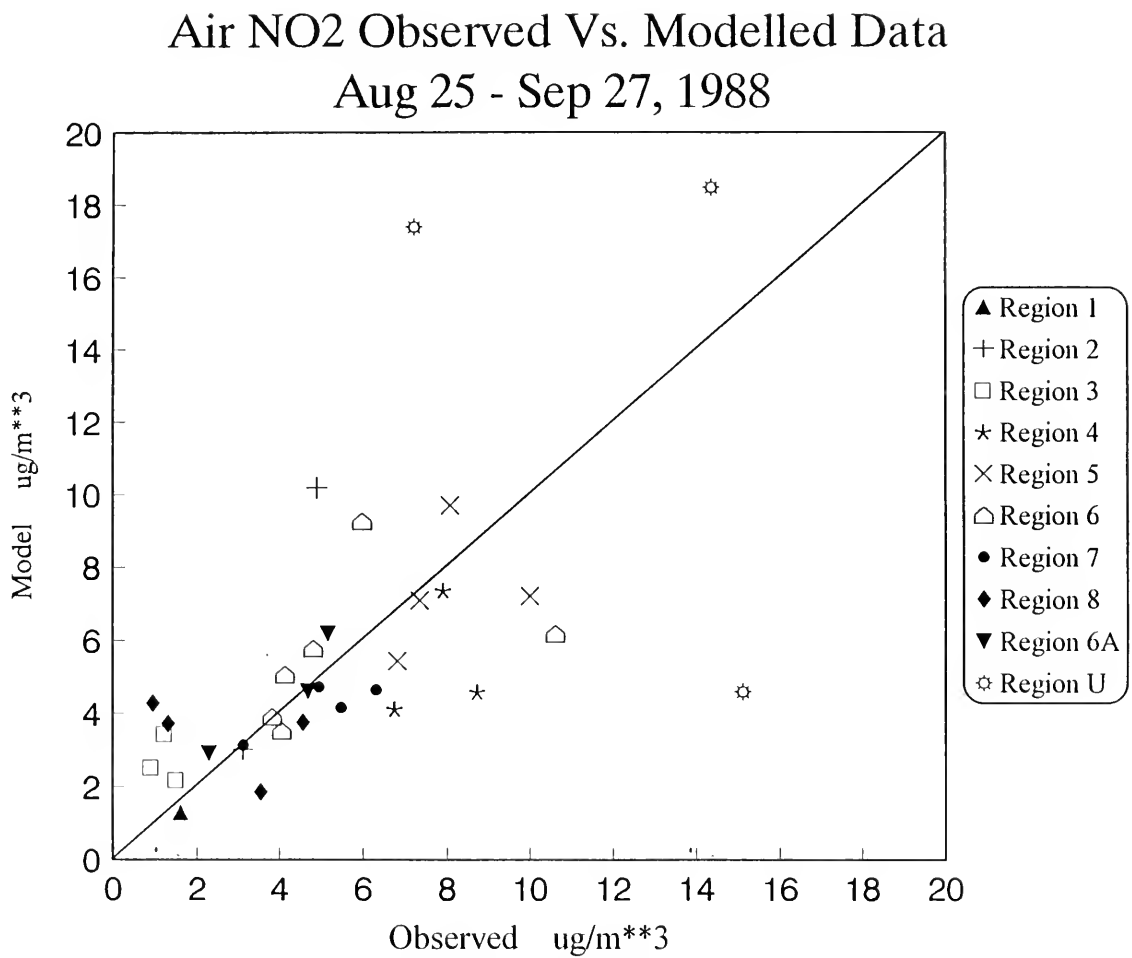

Figure 33. Modelled vs. observed ground level concentrations for NO2 for August 25 - September 27, 1988 for EMEFS.

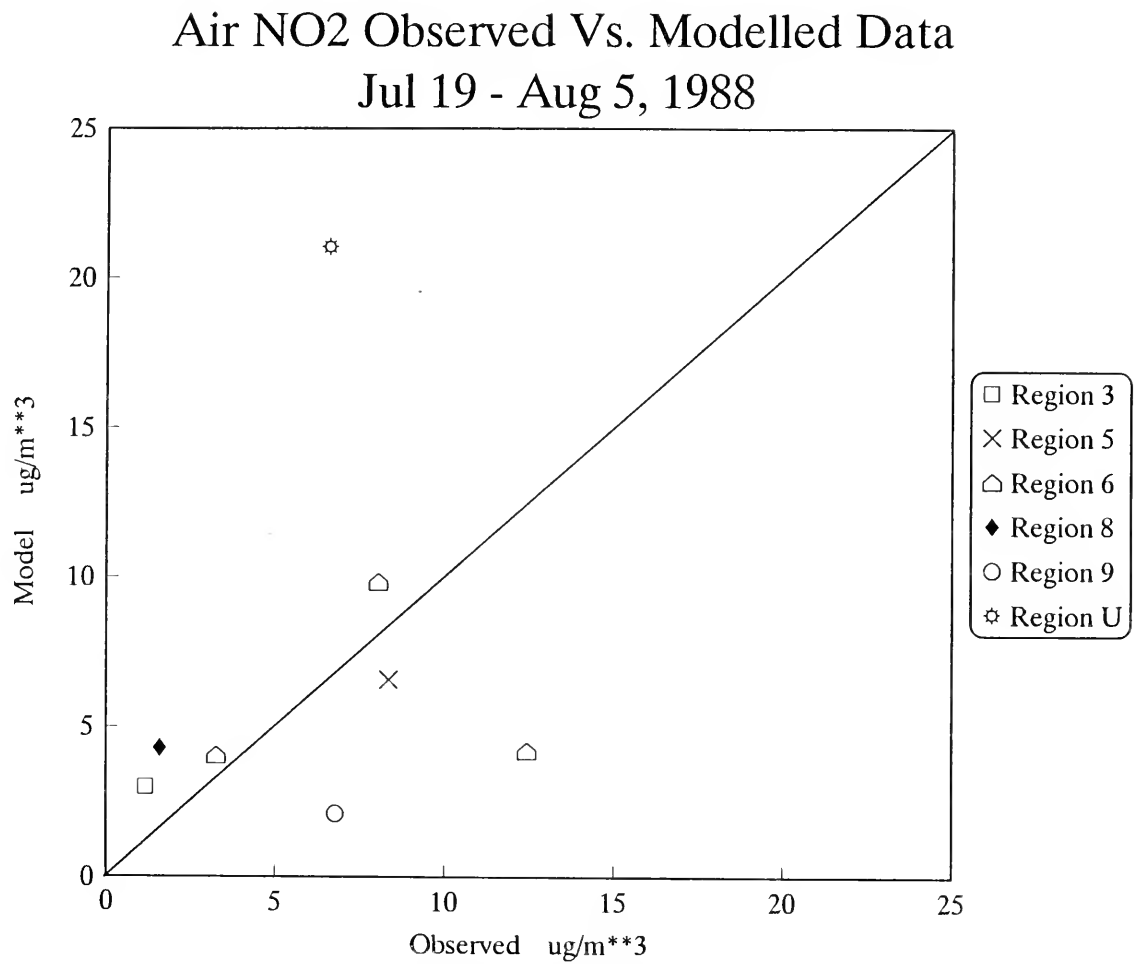

Figure 33 a. Modelled vs. observed ground level concentrations for NO2 for July 19 - August 5, 1988 for EMEFS.

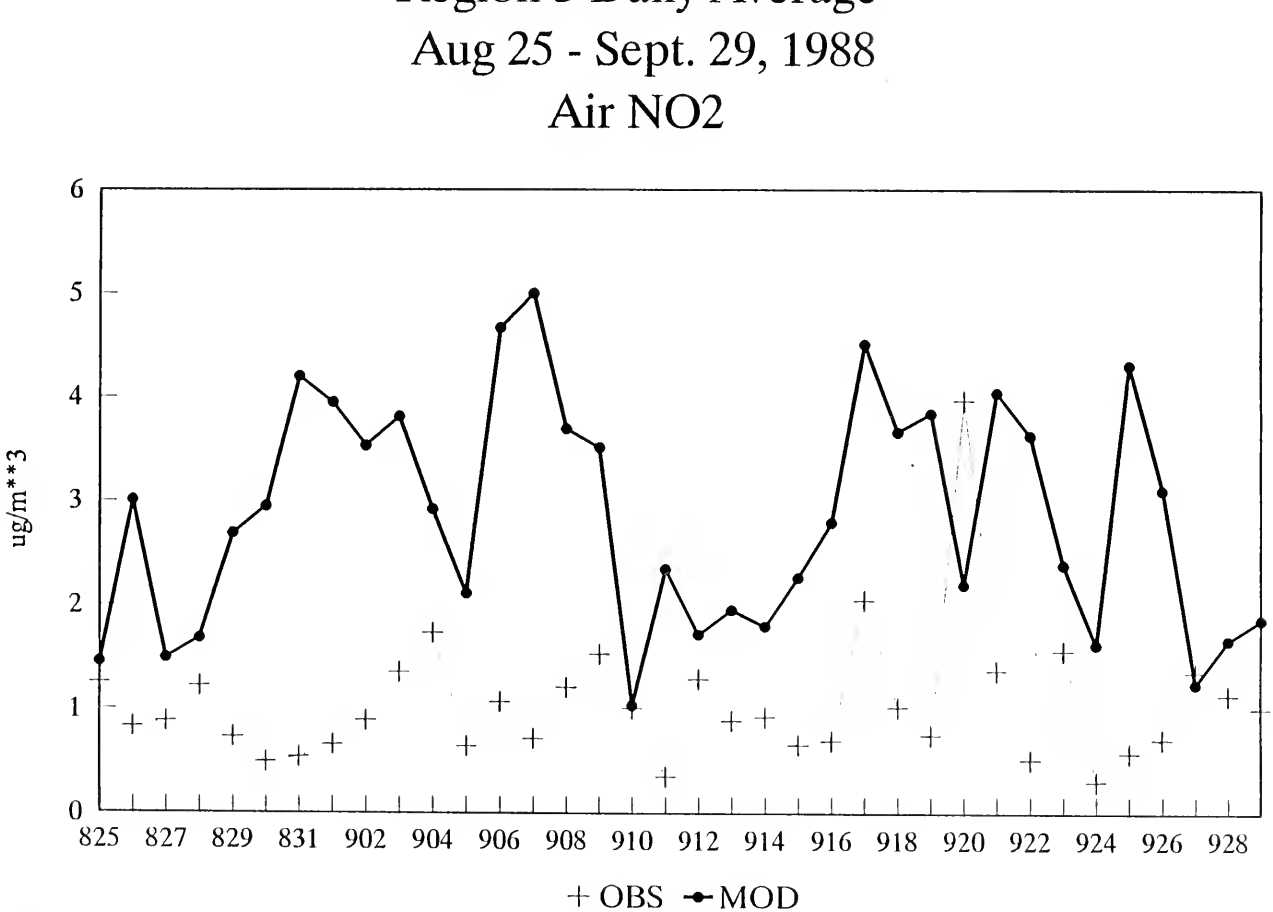

Figure 34. Time series plots of regional average predicted and observed concentrations of NO2 for August 25 - September 29, 1988.

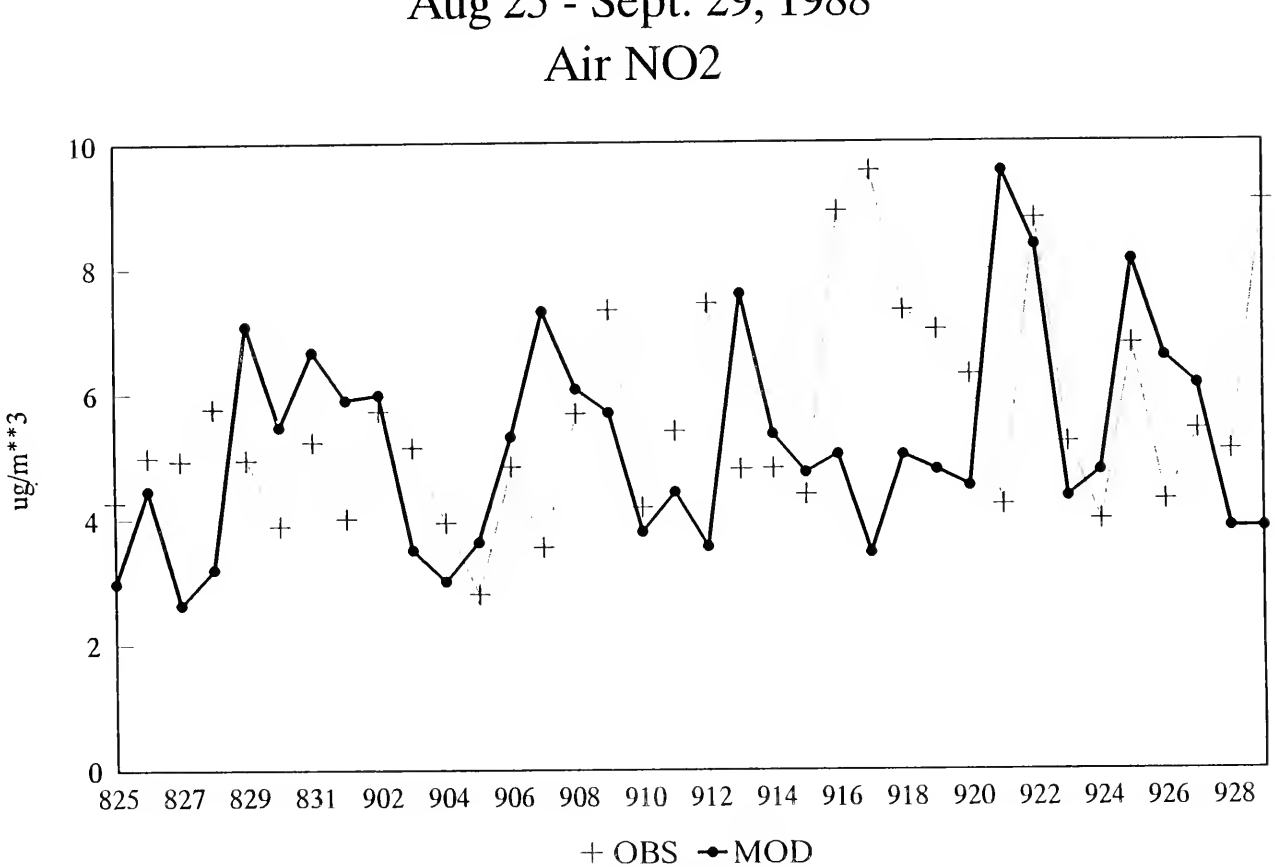

Figure 34 a. Time series plots of regional average predicted and observed concentrations of NO2 for August 25 - September 29, 1988.

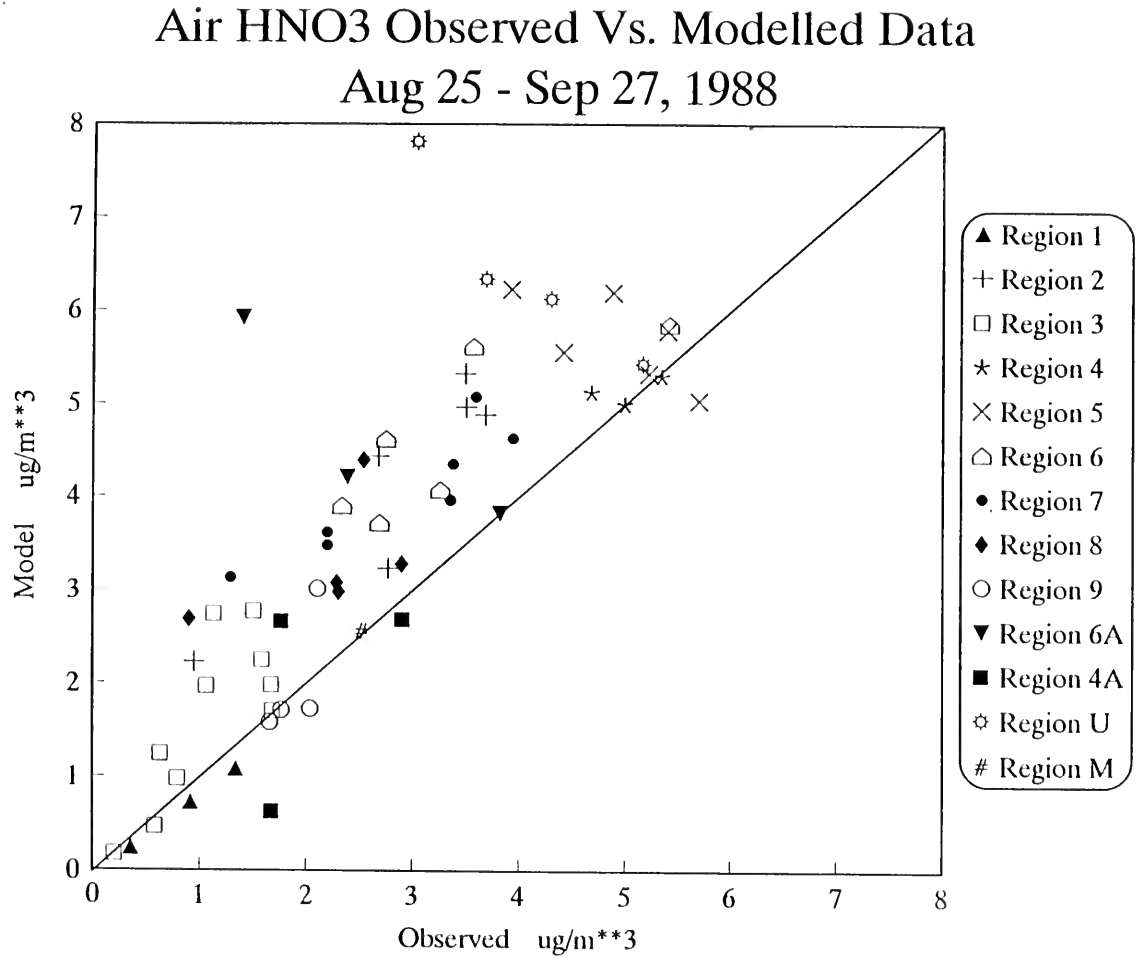

Figure 35. Modelled vs. observed ground level concentrations for nitrate for August 25 - September 27, 1988 for EMEFS.

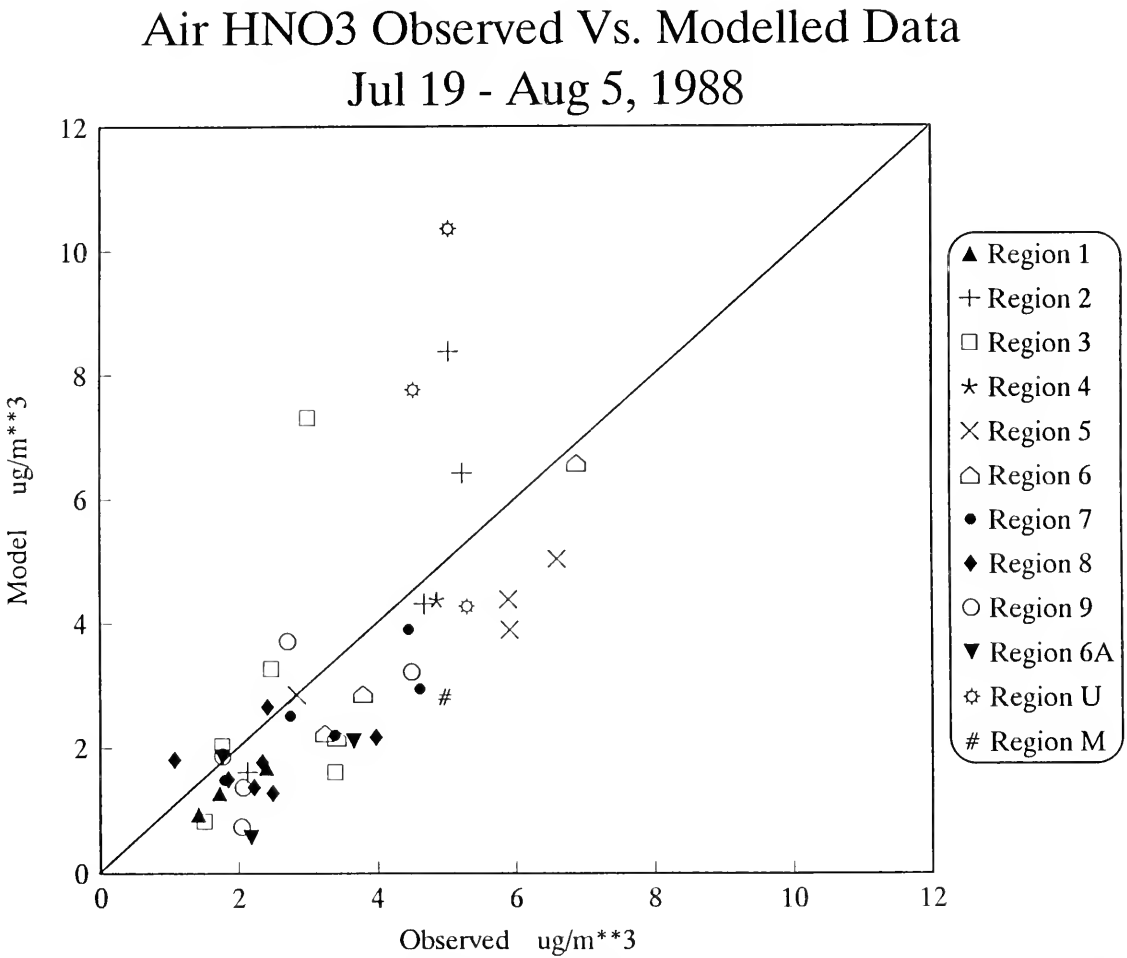

Figure 35 a. Modelled vs. observed ground level concentrations for nitrate for July 19 - August 5, 1988 for EMEFS.

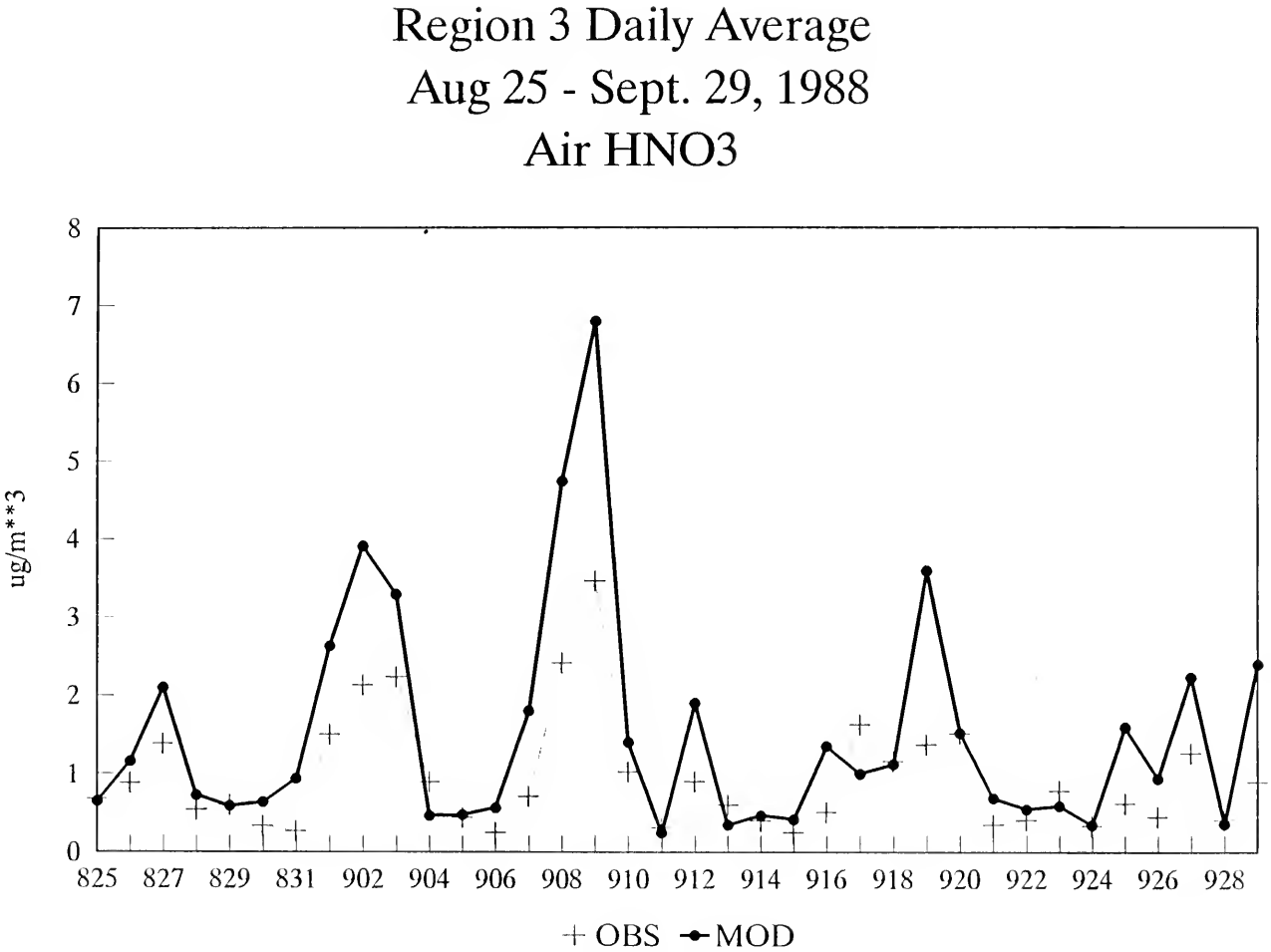

Figure 36 a. Time series plots of regional average predicted and observed concentrations of nitrate for August 25 - September 29, 1988.

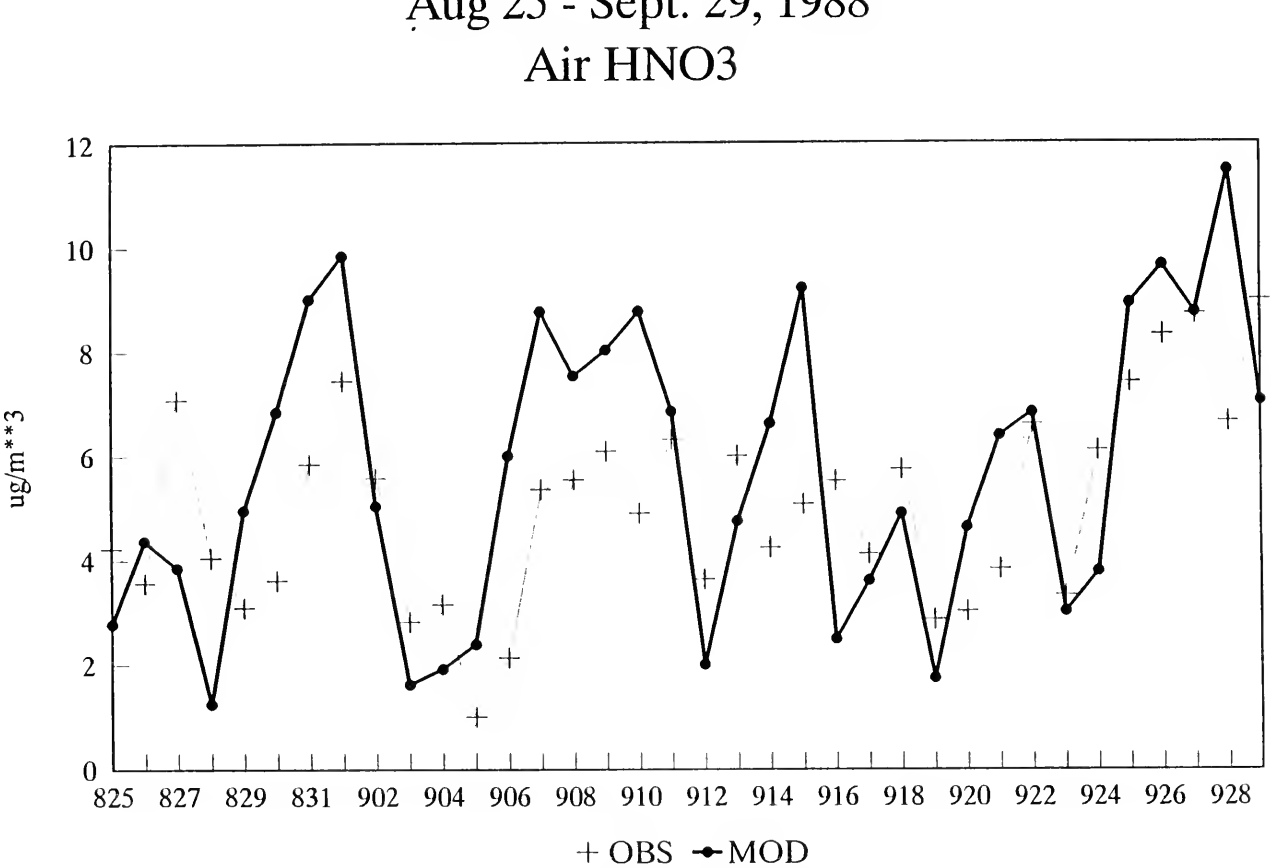

Figure 36 b. Time series plots of regional average predicted and observed concentrations of nitrate for August 25 - September 29, 1988.

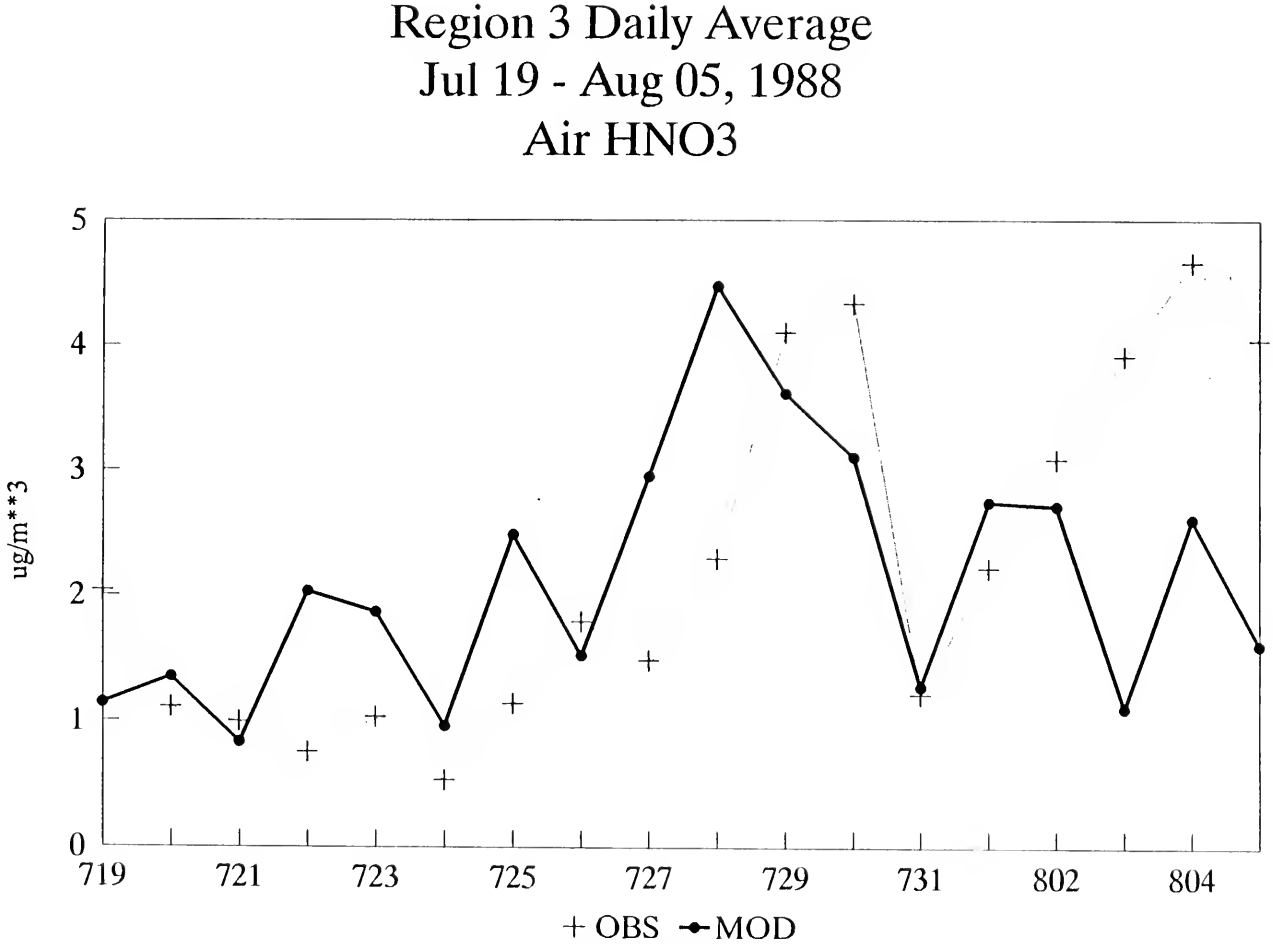

Figure 36 c. Time series plots of regional average predicted and observed concentrations of nitrate for July 19 - August 5, 1988 for EMEFS.

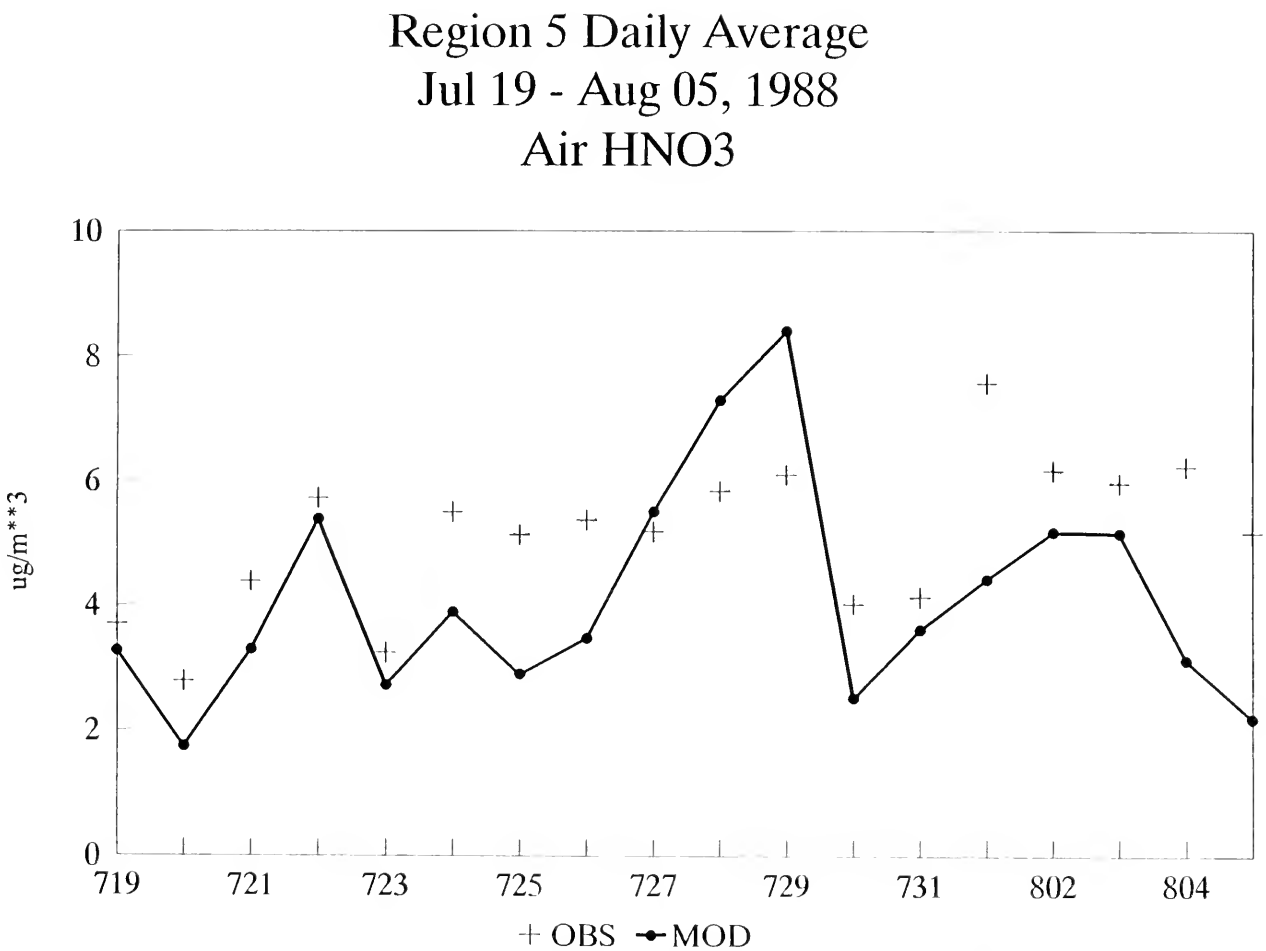

Figure 36 d. Time series plots of regional average predicted and observed concentrations of nitrate for July 19 - August 5, 1988 for EMEFS.

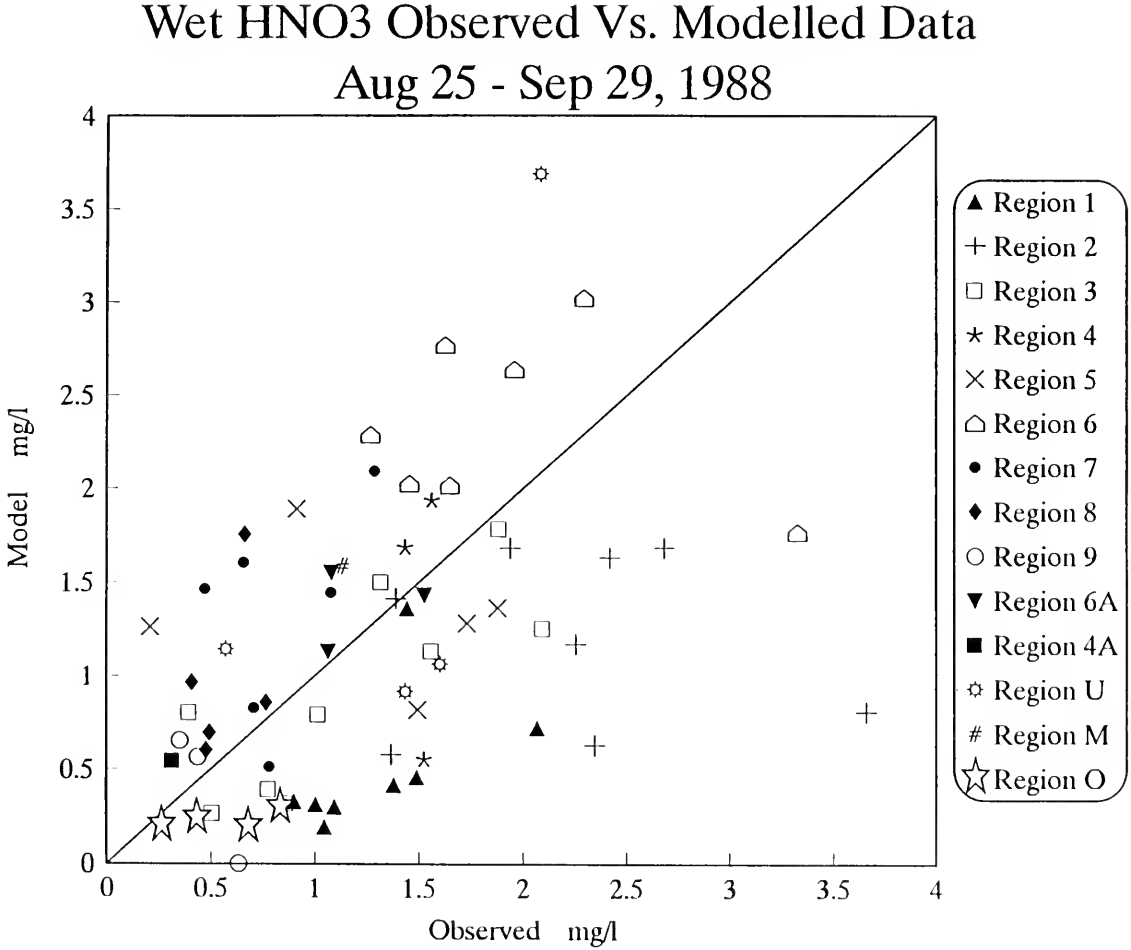

Figure 37. Modelled vs. observed nitrate concentrations in precipitation for August 25 - September 29, 1988 for EMEFS.

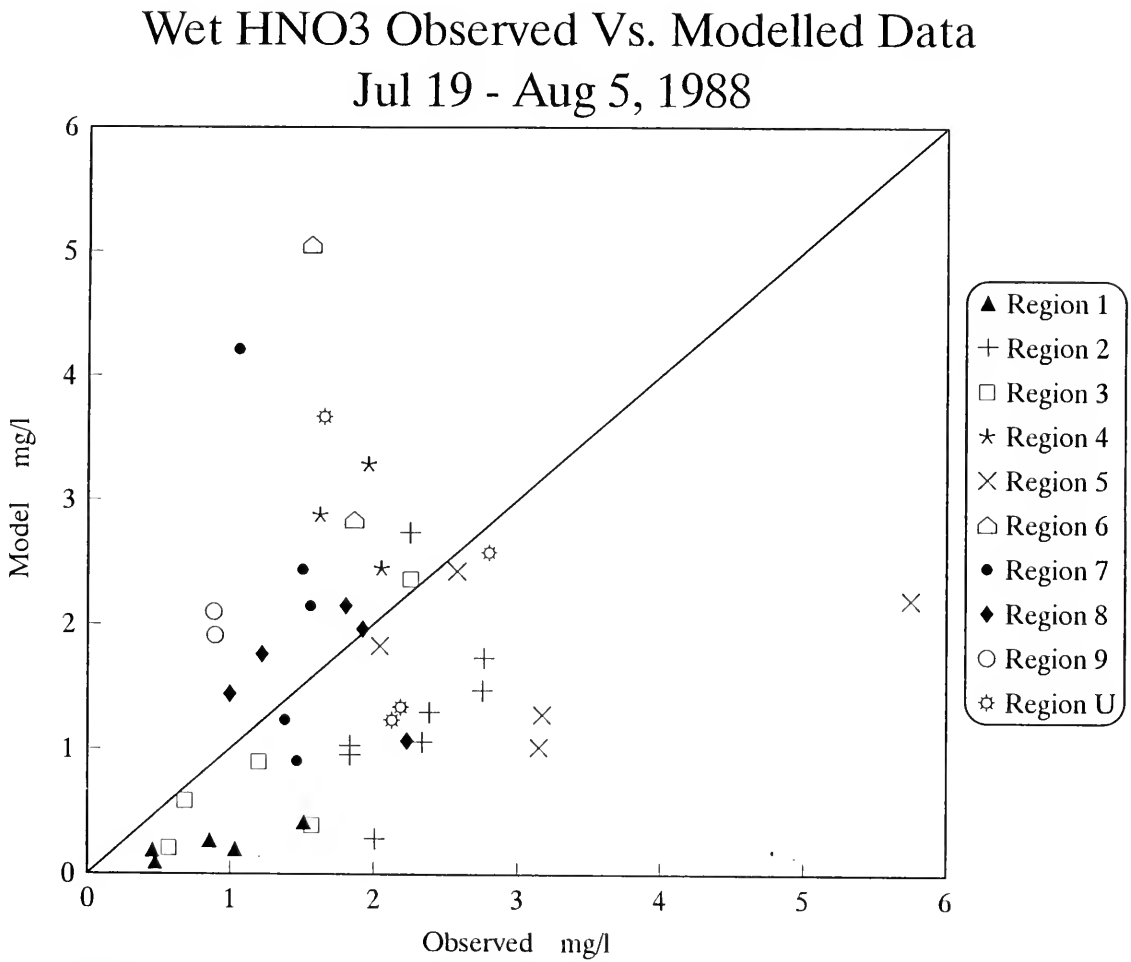

Figure 37 a. Modelled vs. observed nitrate concentrations in precipitation for July 19 - August 5, 1988 for EMEFS.

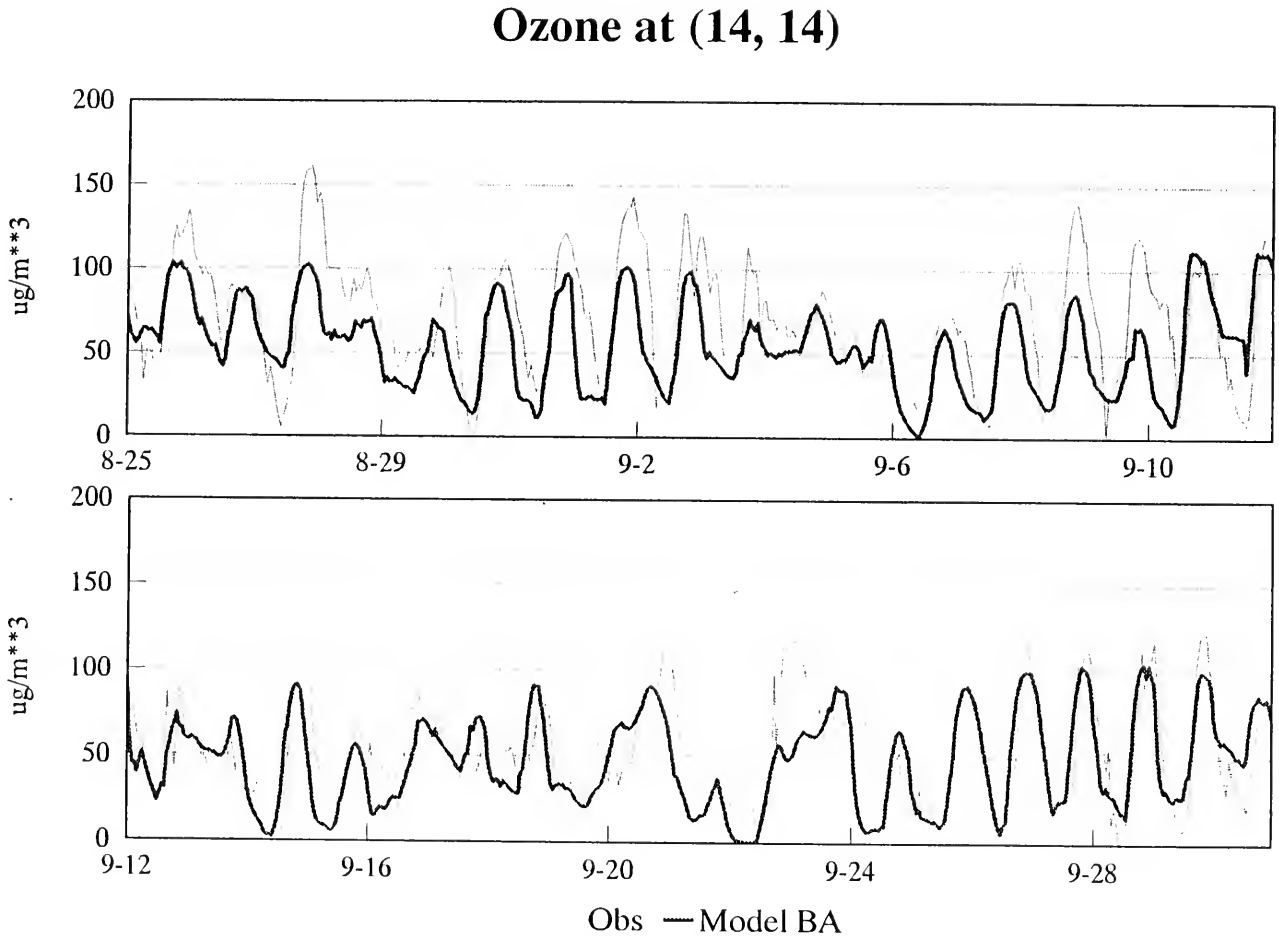

Figure 38 a. Hourly concentrations of predicted and observed ozone at grid (14, 14) for August 25 - September 29, 1988.

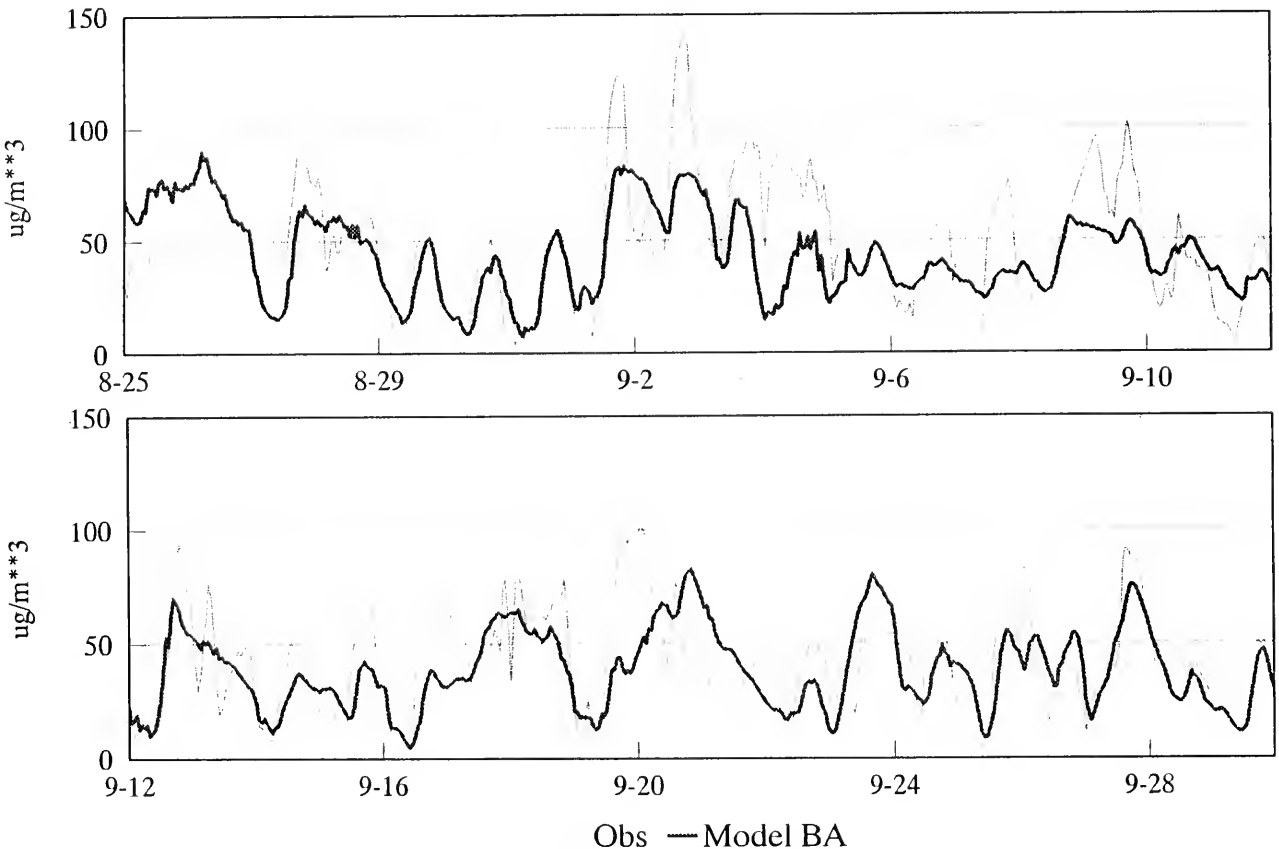

Figure 38 b. Hourly concentrations of predicted and observed ozone at grid (16, 19) for August 25 - September 29, 1988.

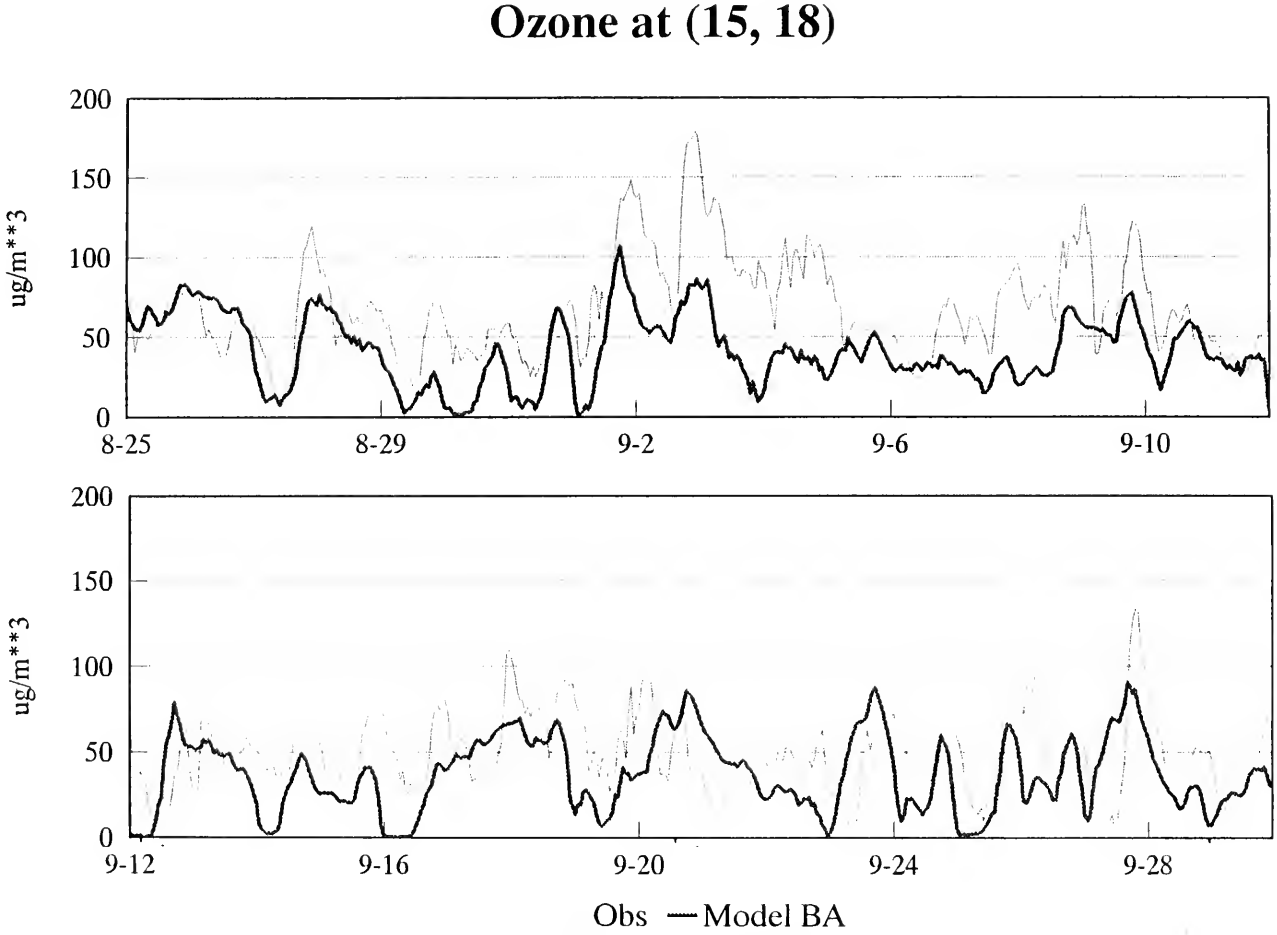

Figure 38 c. Hourly concentrations of predicted and observed ozone at grid (15, 18) for August 25 - September 30, 1988.

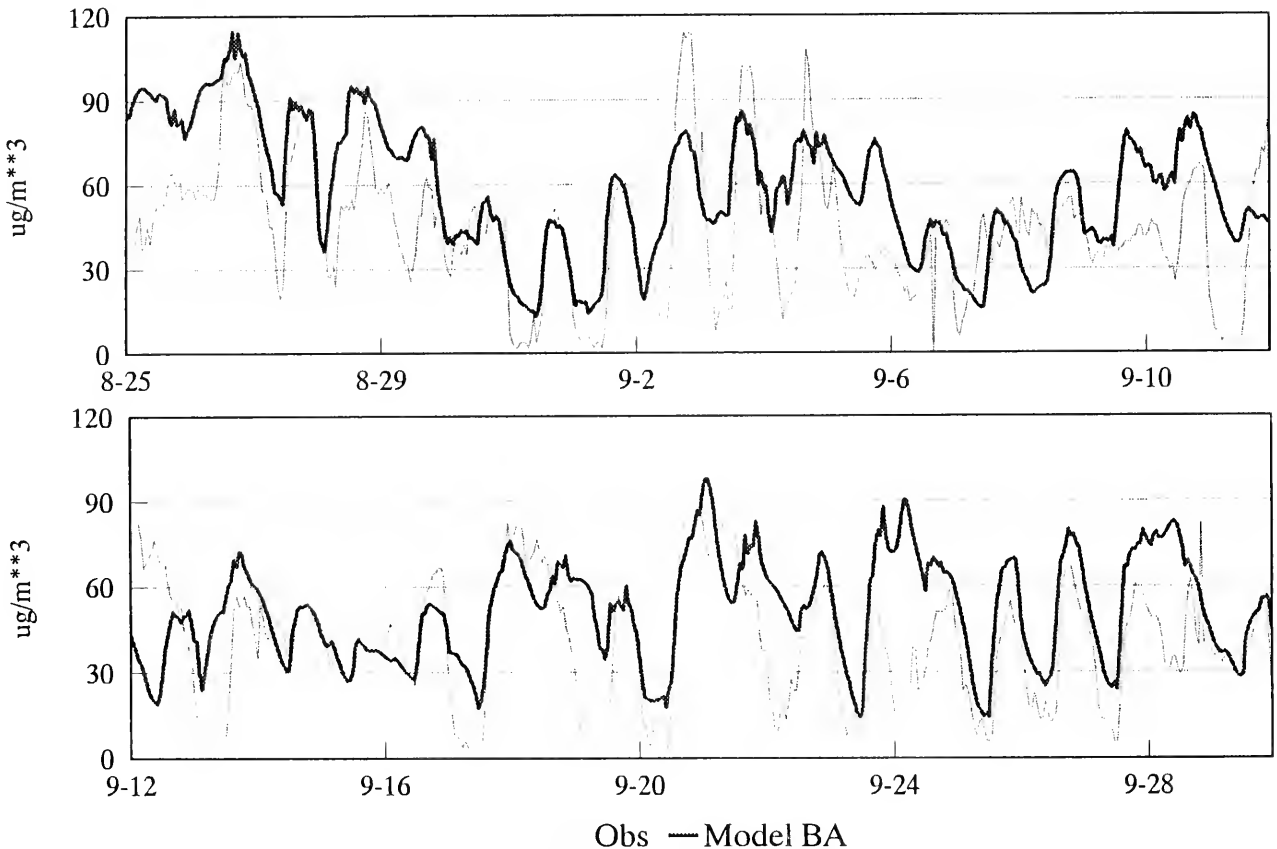

Figure 38 d. Hourly concentrations of predicted and observed ozone at grid (23, 19) for August 25 - September 29, 1988.

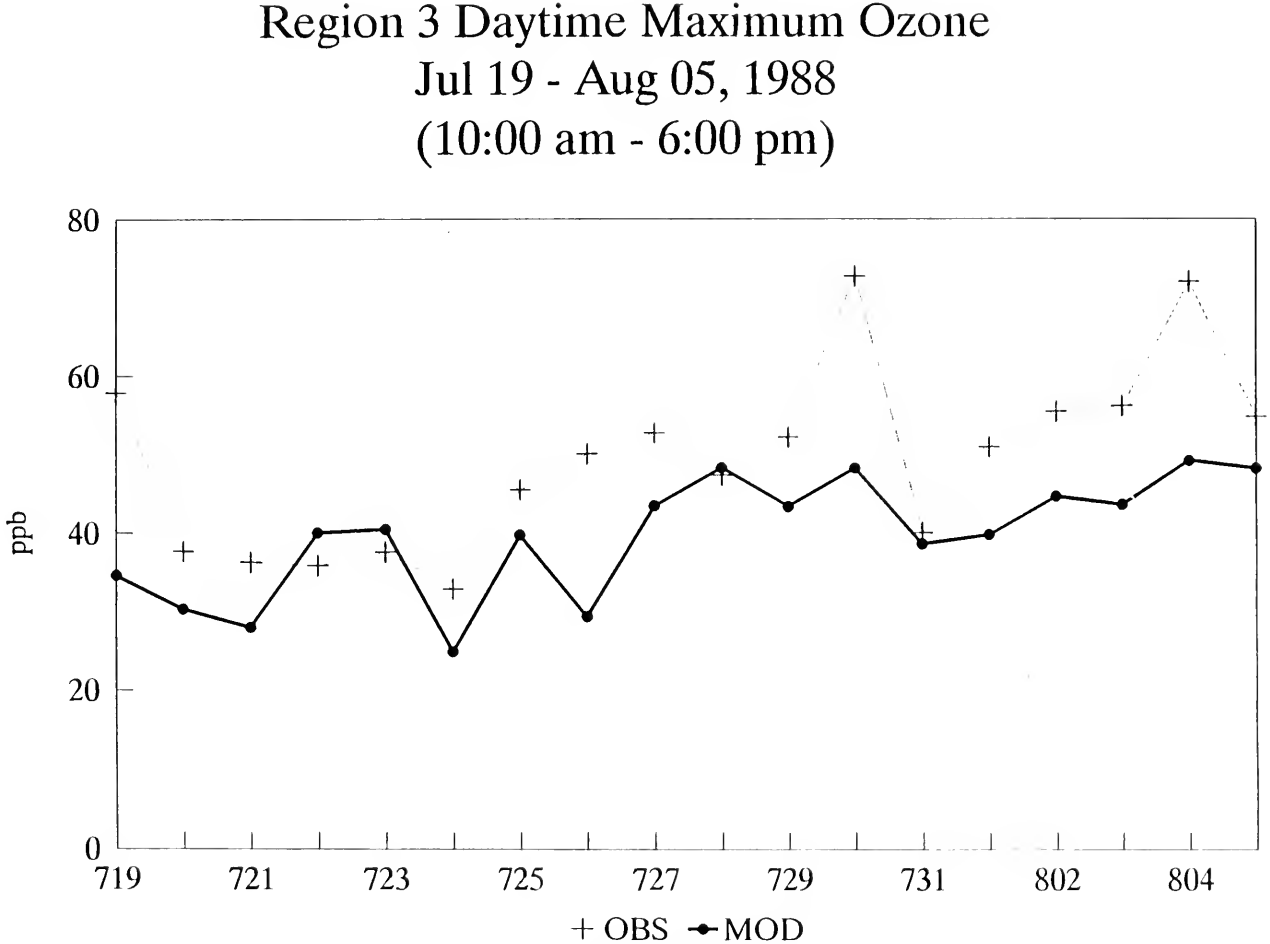

Figure 38 e. Daytime predicted and observed maximum ozone concentration (between 10:00 a.m. and 6:00 p.m. local time) for Region 3 for July 19 - August 5, 1988.

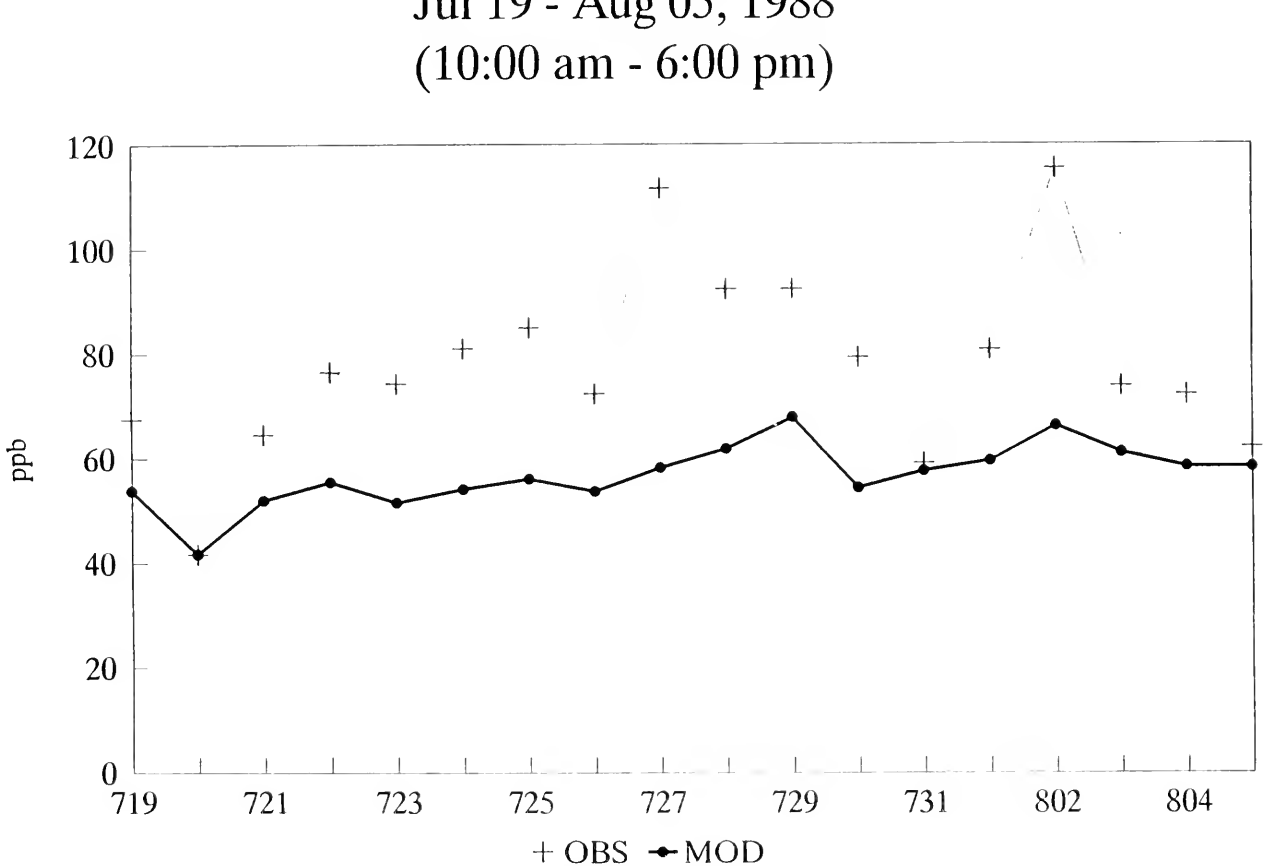

Figure 38 f. Daytime predicted and observed maximum ozone concentration (between 10:00 a.m. and 6:00 p.m. local time) for Region 5 for July 19 - August 5, 1988.

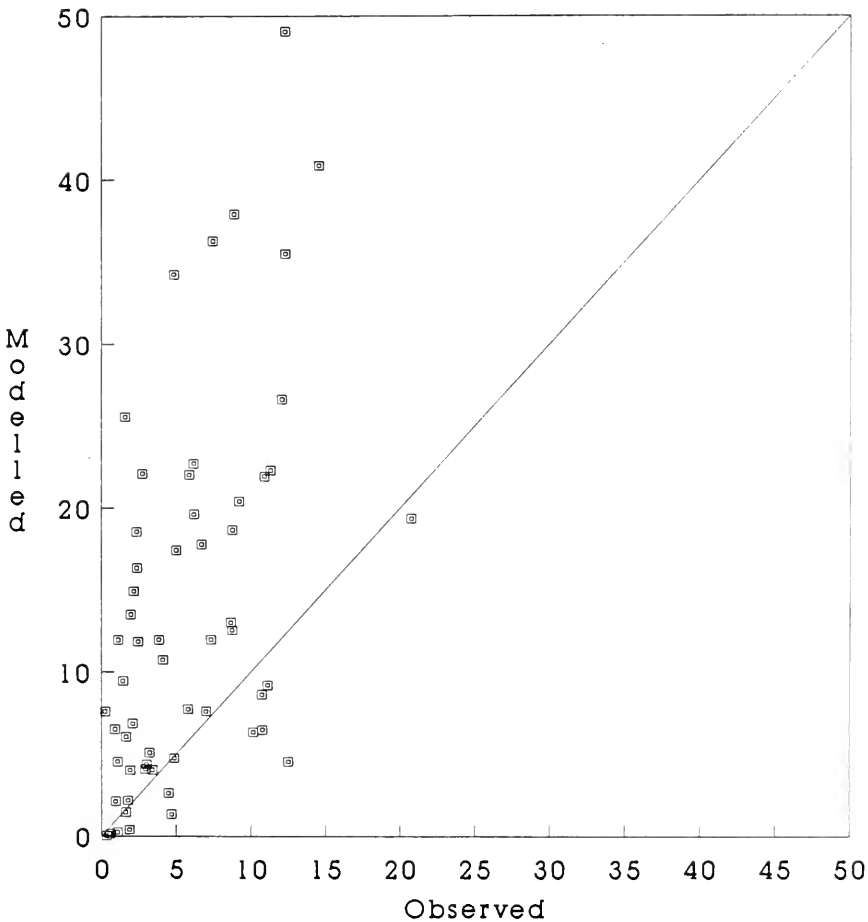

Figure 39. OME Lagrangian model predicted SO_2 ground level concentration vs. observations ($\mu g/m^3$) for August 25 - September 29, 1988.

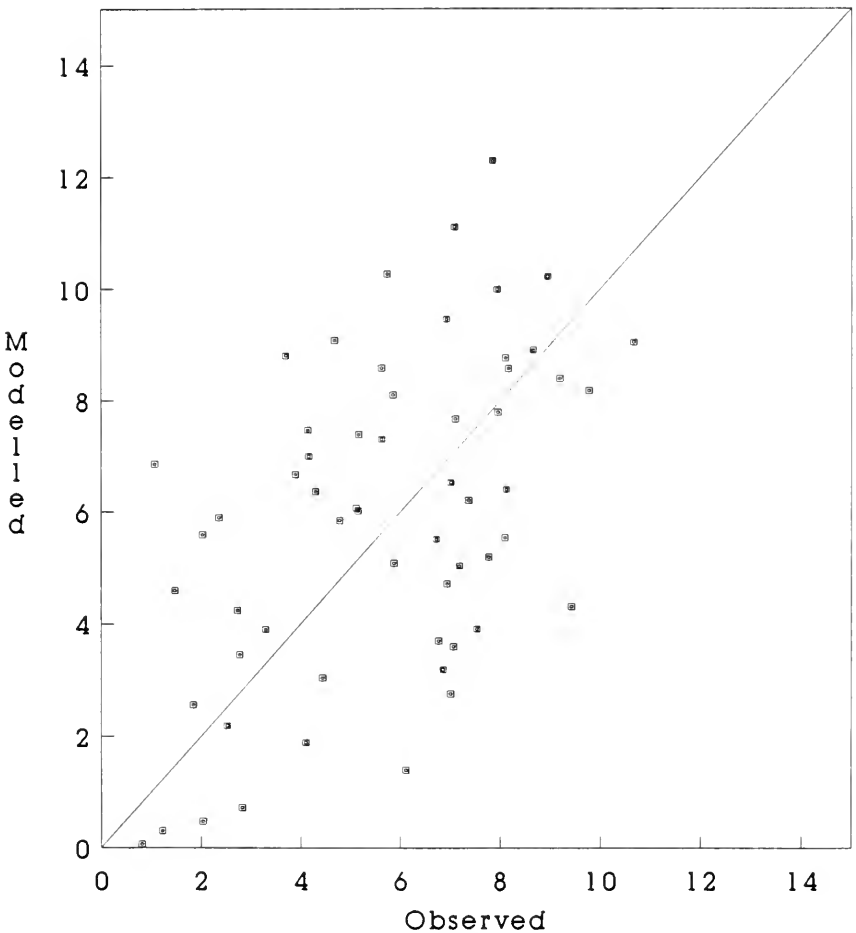

Figure 40. OME Lagrangian model predicted sulphate ground level concentration vs. observations ($\mu g/m^3$) for August 25 - September 29, 1988.

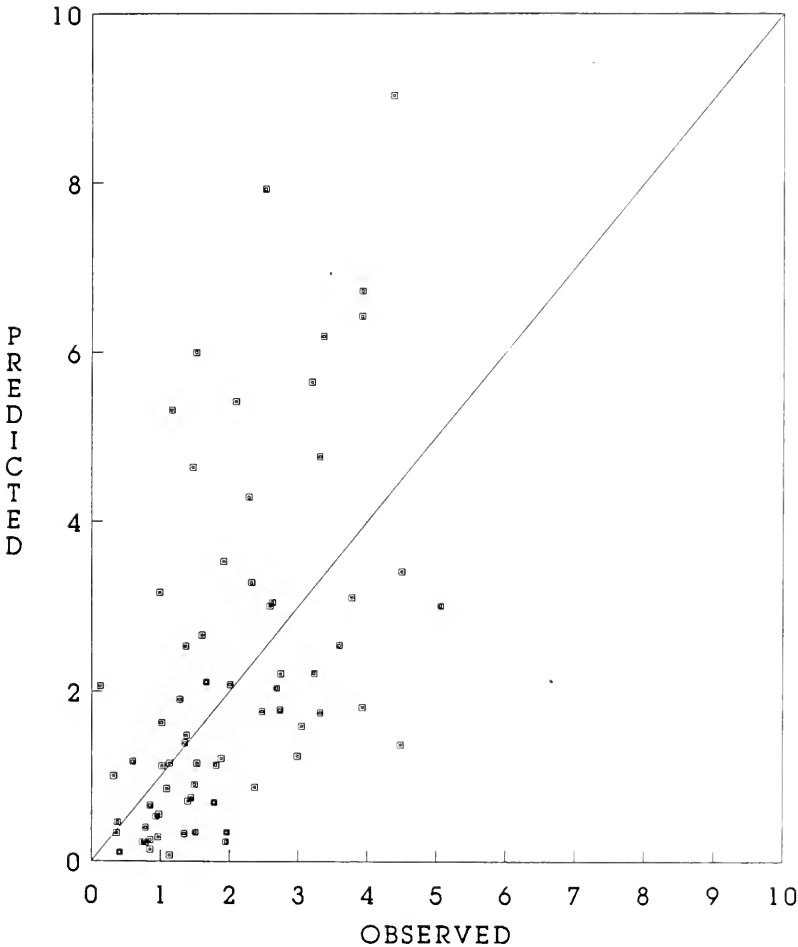

Figure 41. OME Lagrangian model predicted sulphate concentration in precipitation vs. observations (mg/l) for August 25 - September 29, 1988.

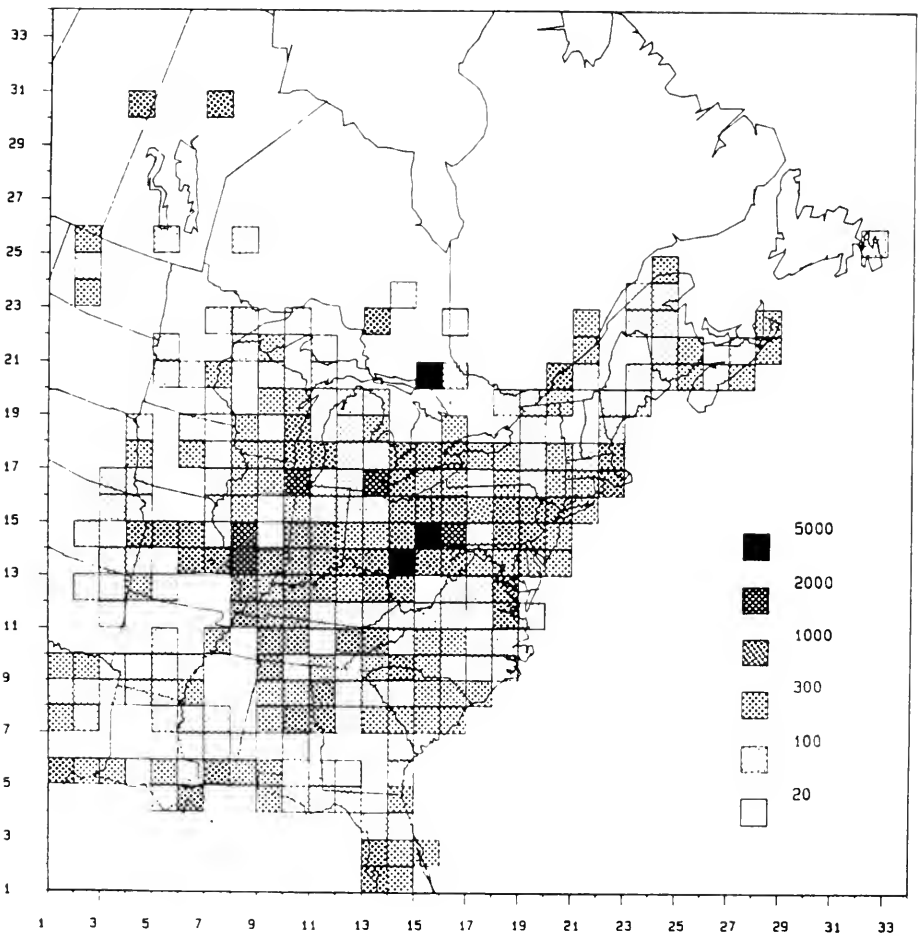

Figure 42. Total SO_2 emission rate (tonnes per day) within each ADOM grid cell. The solid boxes are between 2000 and 5000 tonnes per day while the empty boxes are below 20 tonnes per day.

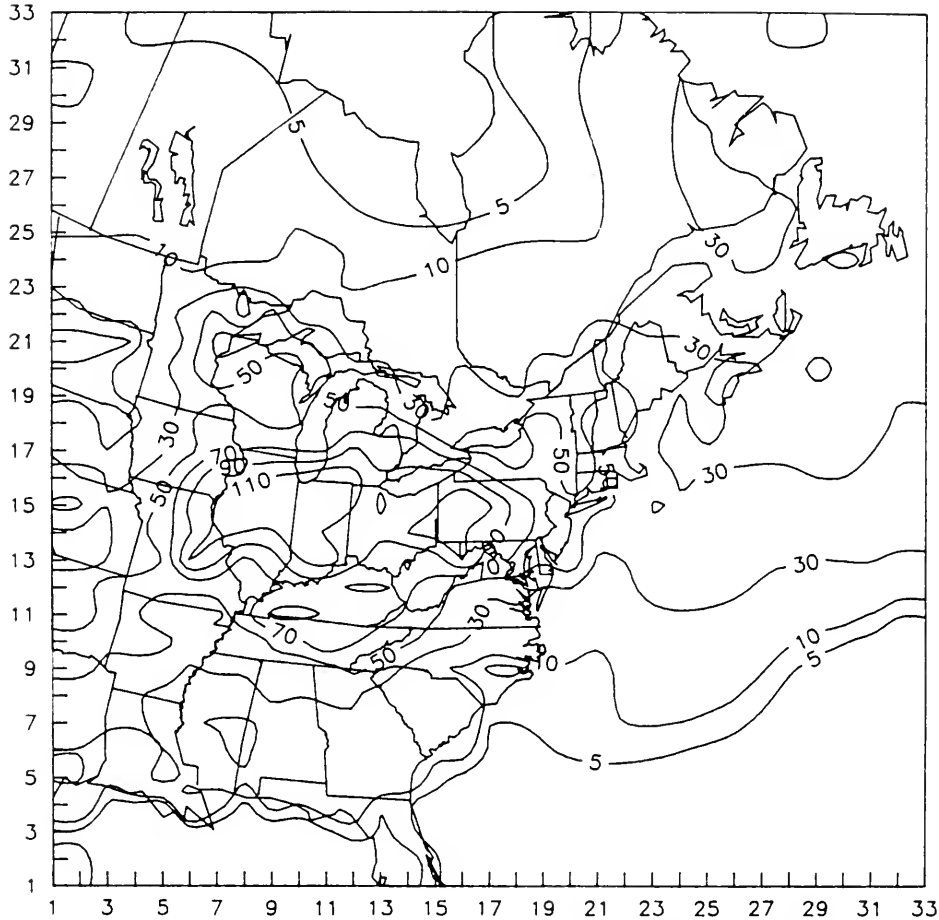

Figure 43. Total precipitation amount (mm) from April 10 to April 29, 1981.

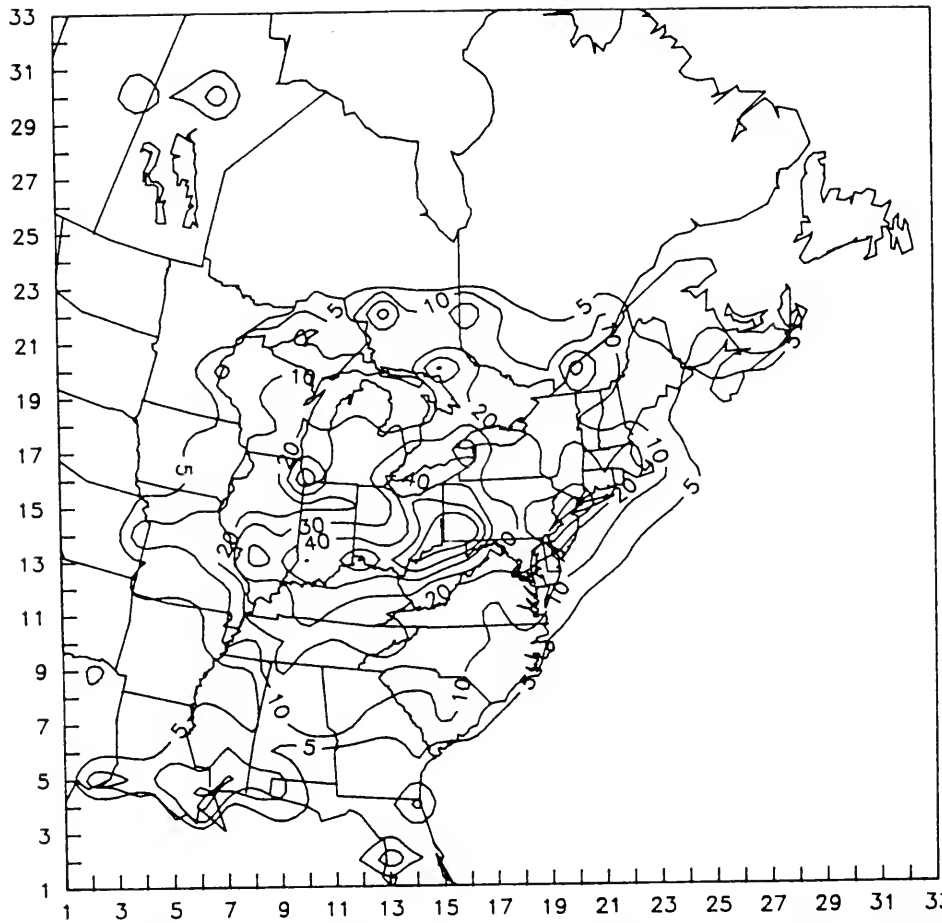

Figure 44. ADOM's prediction of ground level SO_2 concentrations ($\mu g/m^3$) in air for April 10 to April 29, 1981.

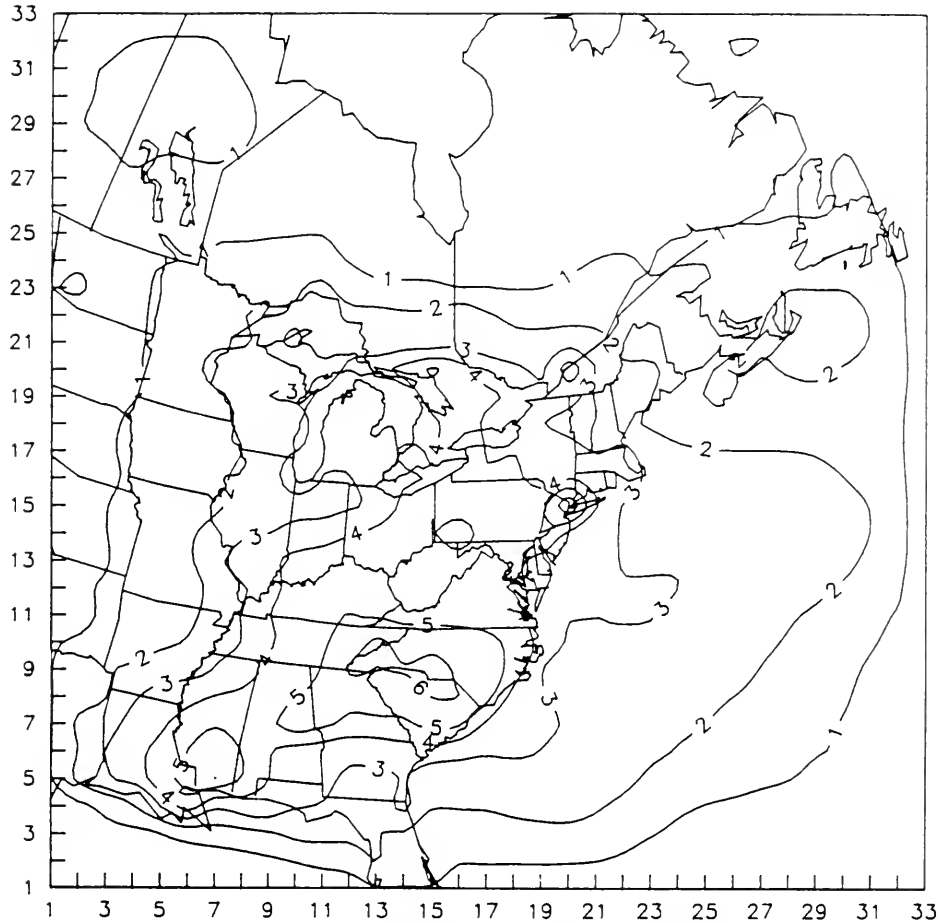

Figure 45. ADOM's prediction of ground level SO_4^{2-} concentration ($\mu g/m^3$) in air for April 10 to April 29, 1981.

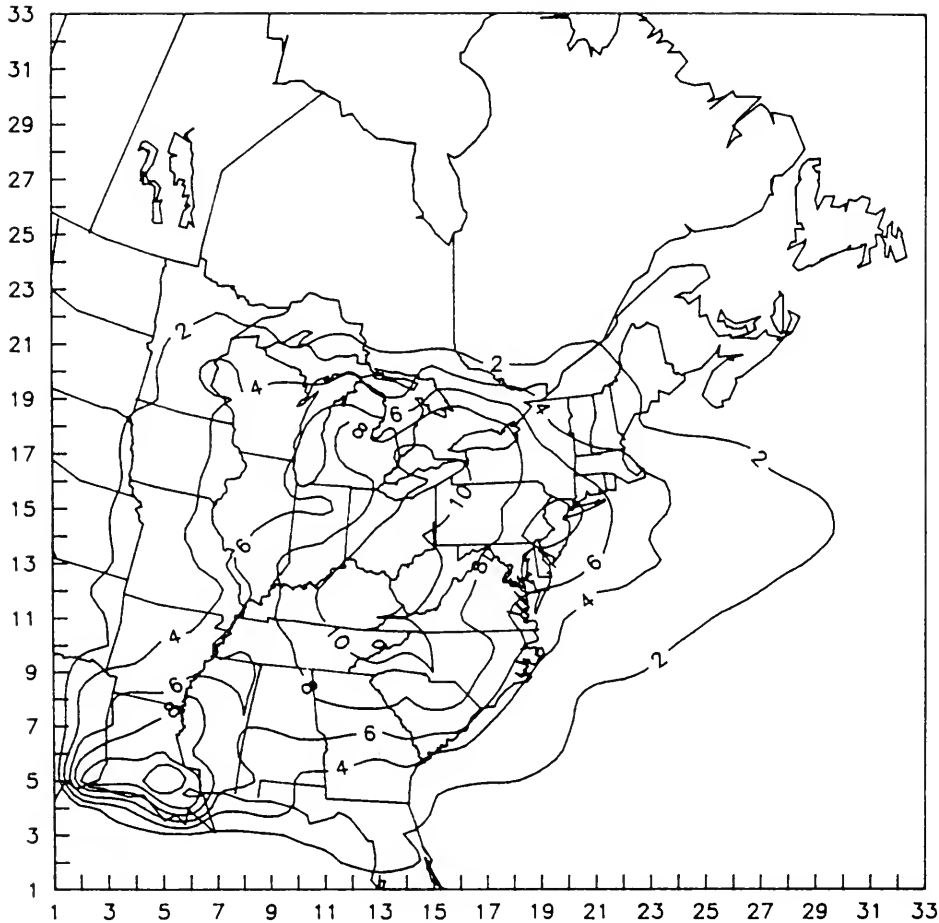

Figure 46. ADOM's prediction of ground level nitrate concentration ($\mu g/m^3$) in air for April 10 to April 29, 1981.

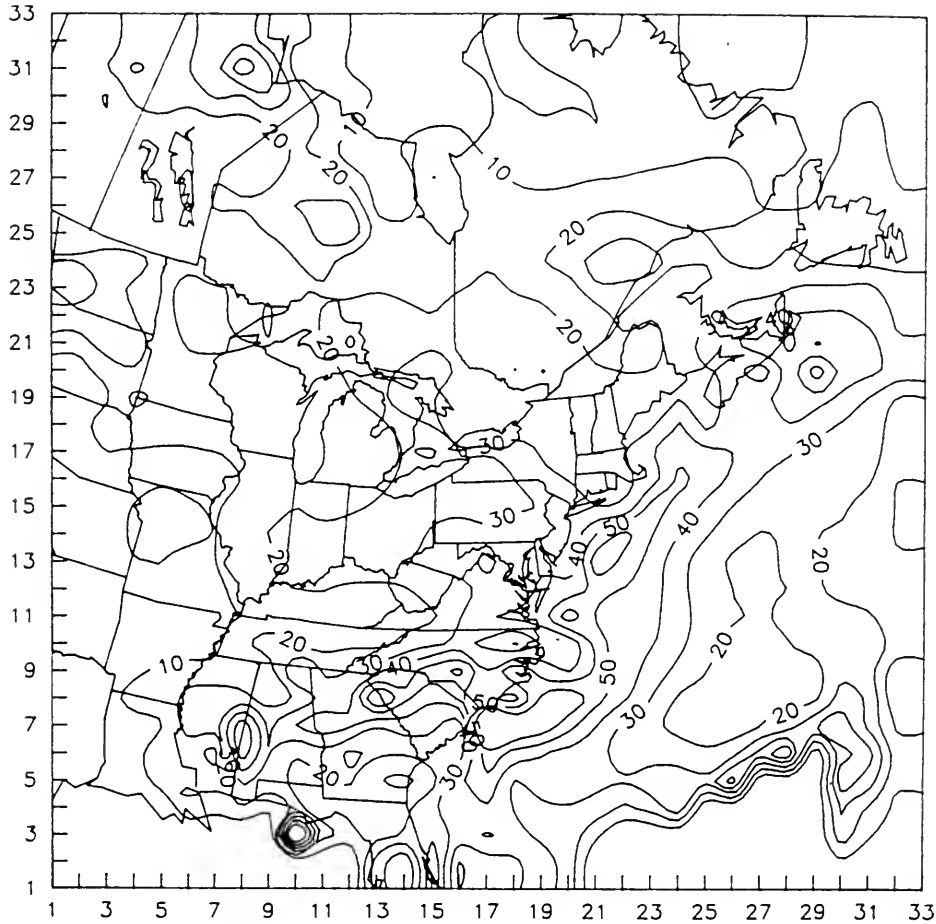

Figure 47. ADOM's prediction of ground level SO_4^{2-} concentrations (μ moles l^{-1}) in precipitation for April 10 to April 29, 1981.

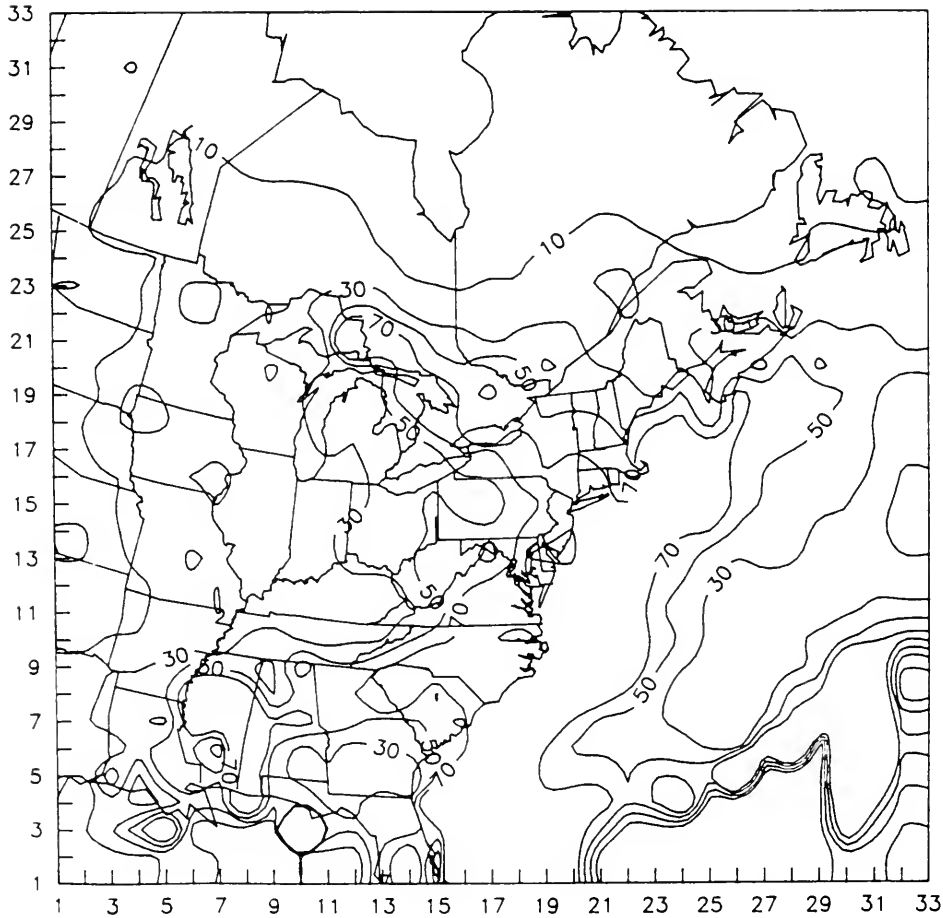

Figure 48. ADOM's prediction of ground level nitrate concentrations (μ moles l^{-1}) in precipitation for April 10 to April 29, 1981.

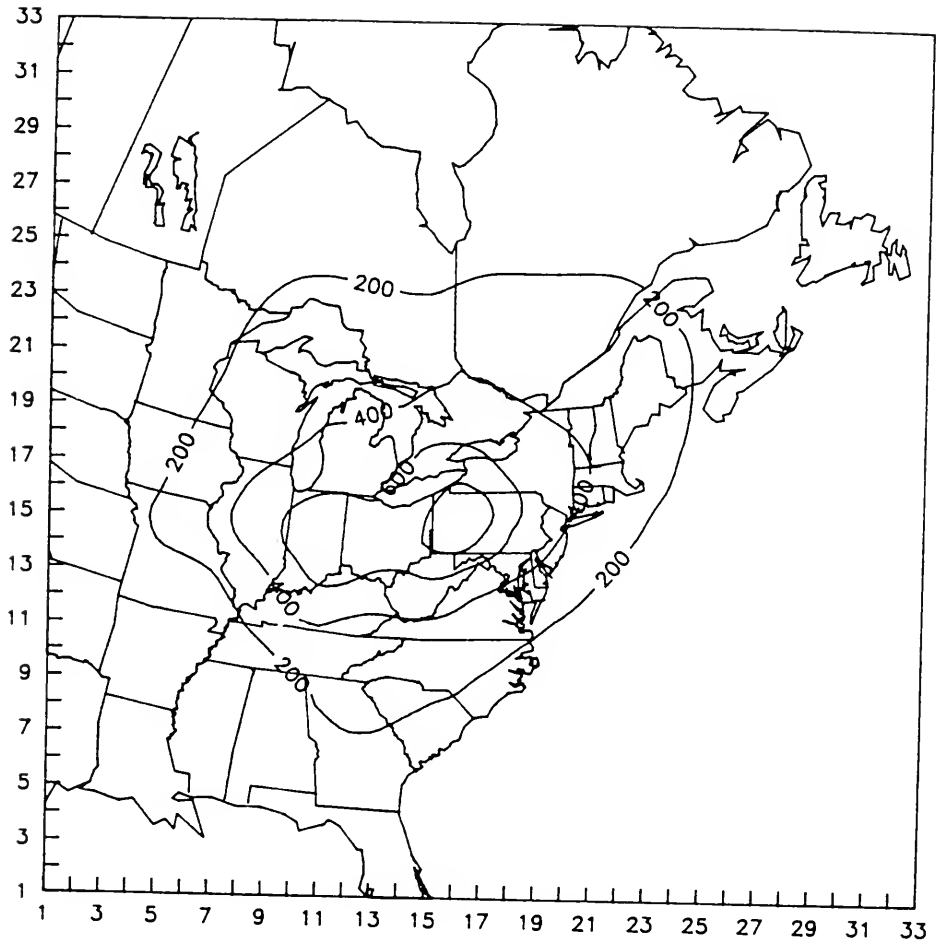

Figure 49. OME's Lagrangian model's prediction of wet flux ($\mu g\ m^{-2}\ h^{-1}$) of SO_4^{2-} for April 10 to April 25, 1981.

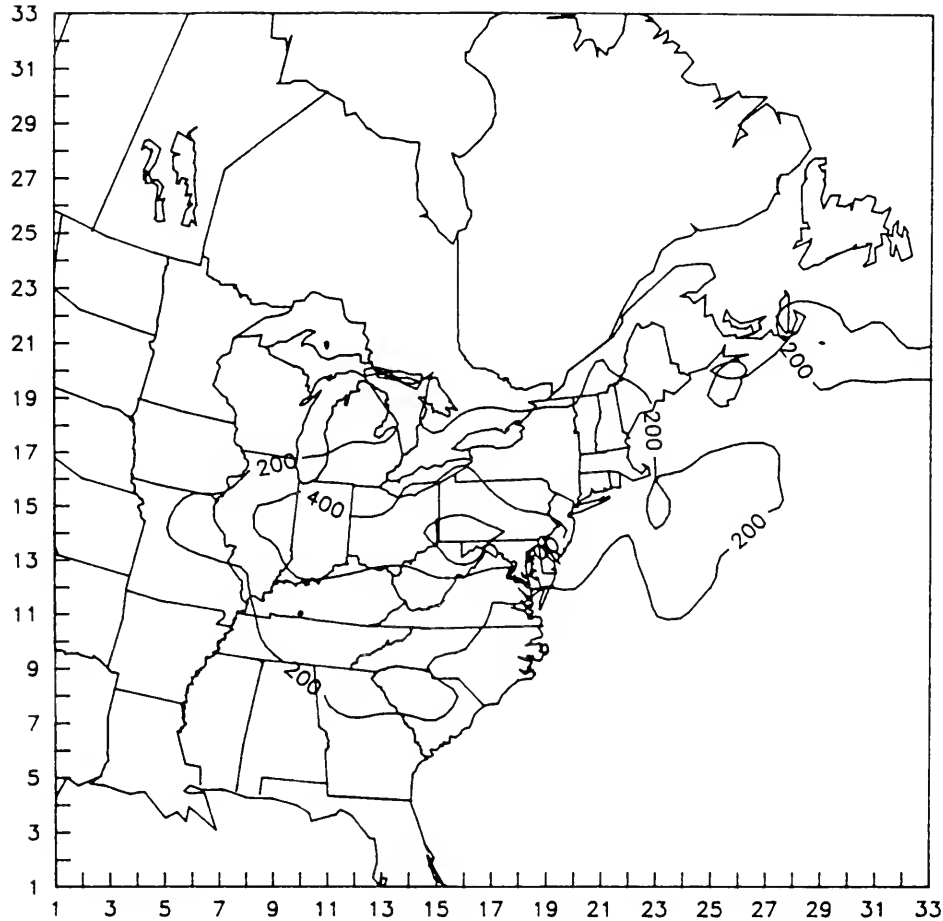

Figure 50. ADOM's prediction of wet flux ($\mu g\ m^{-2}\ h^{-1}$) of SO_4^{2-} for April 10 to April 25, 1981.

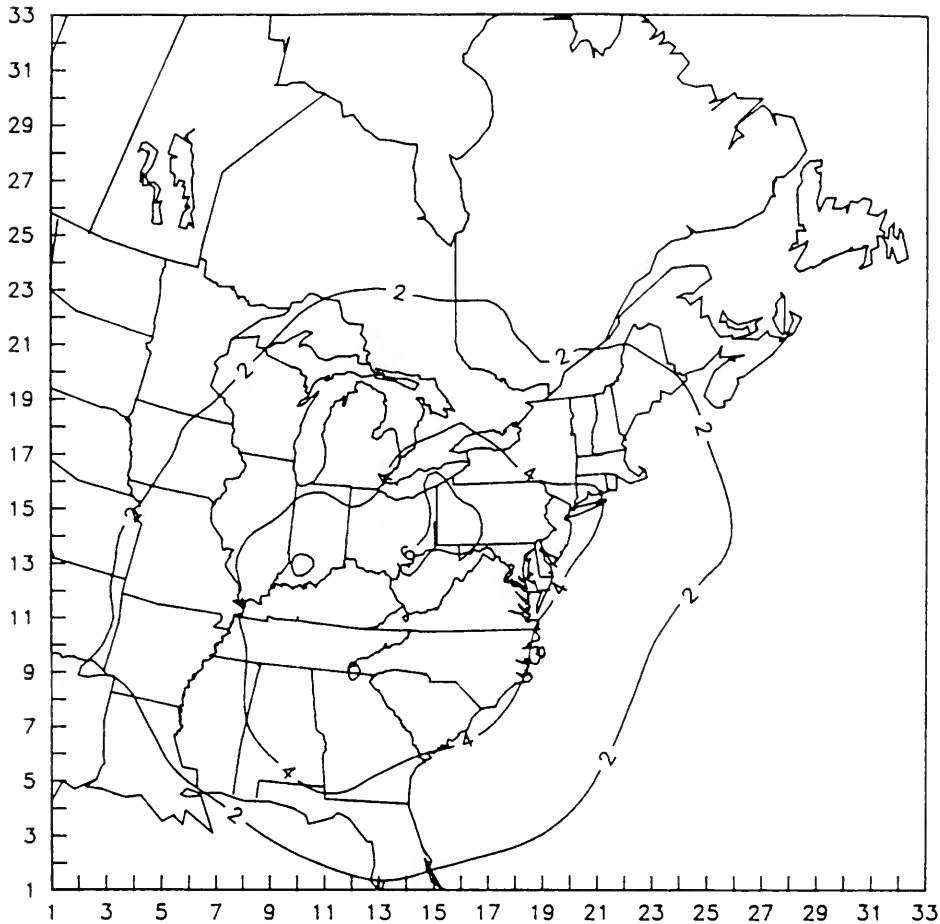

Figure 51. OME's Lagrangian model's prediction of SO_4^{2-} ground level concentration ($\mu g/m^3$) for April 10 to April 25, 1981.

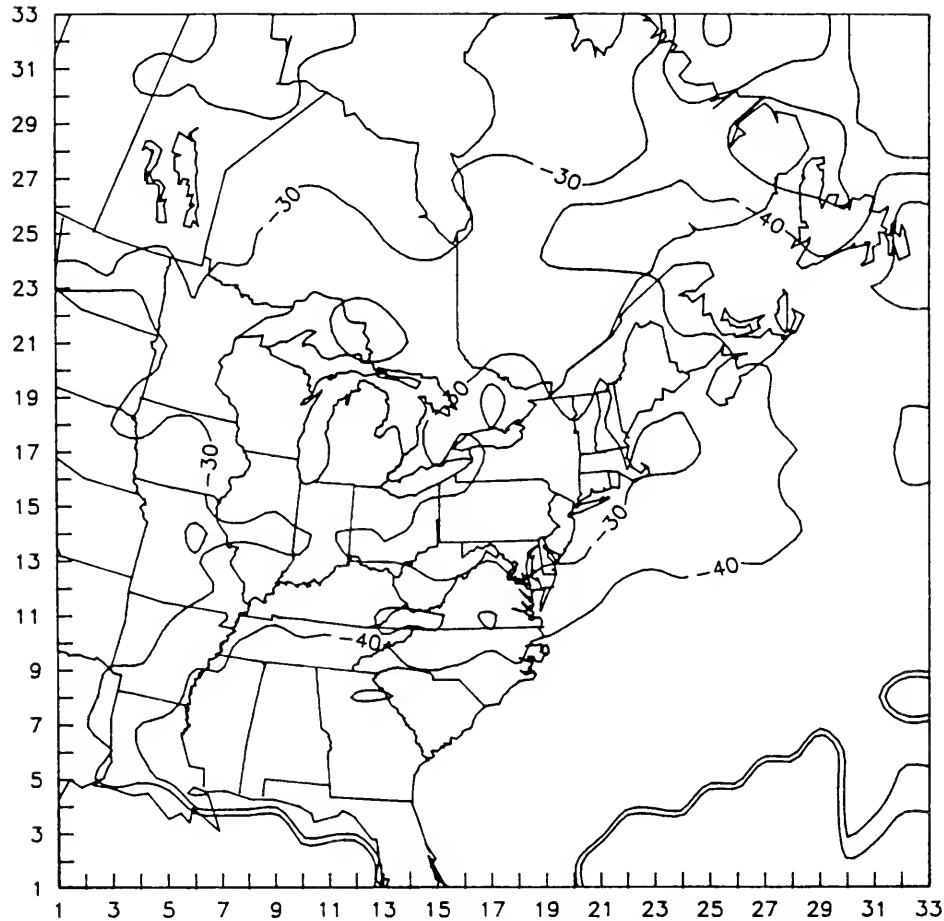

Figure 52. Change (%) in ADOM's predicted SO_4^{2-} in precipitation in response to a 50% reduction of SO_x emissions during OSCAR.

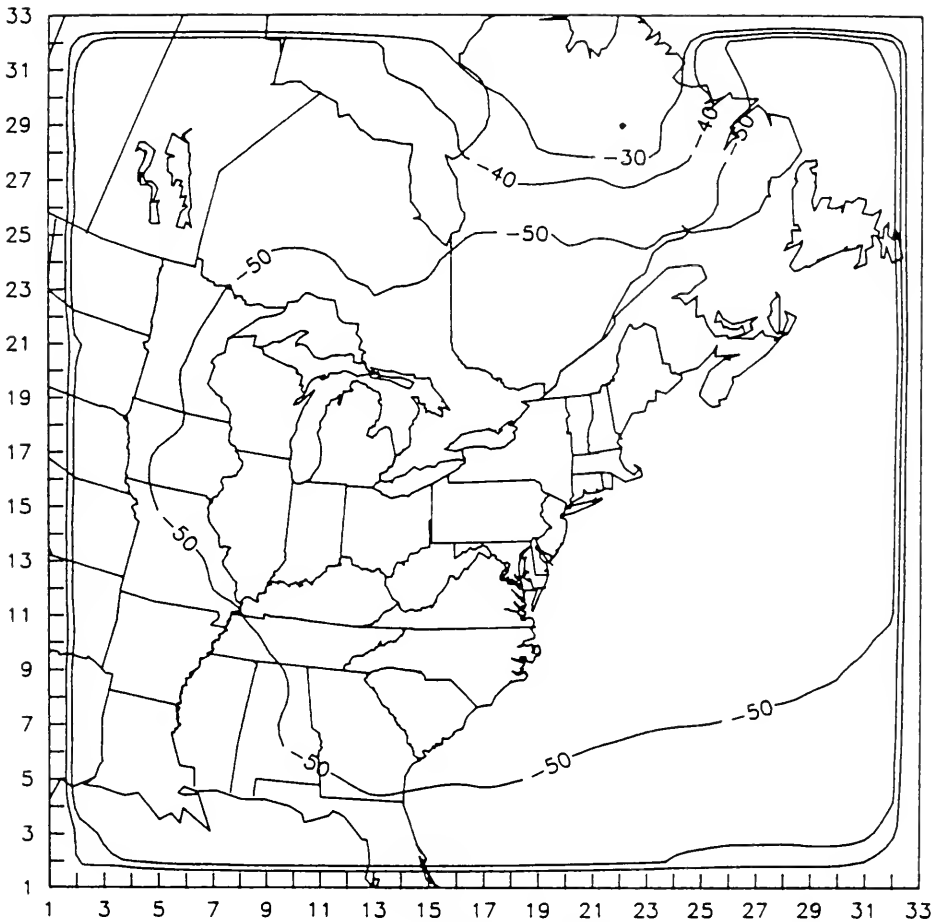

Figure 53. Change (%) in ADOM's predicted SO_2 ground level concentration in response to a 50% reduction of SO_x emissions during OSCAR.

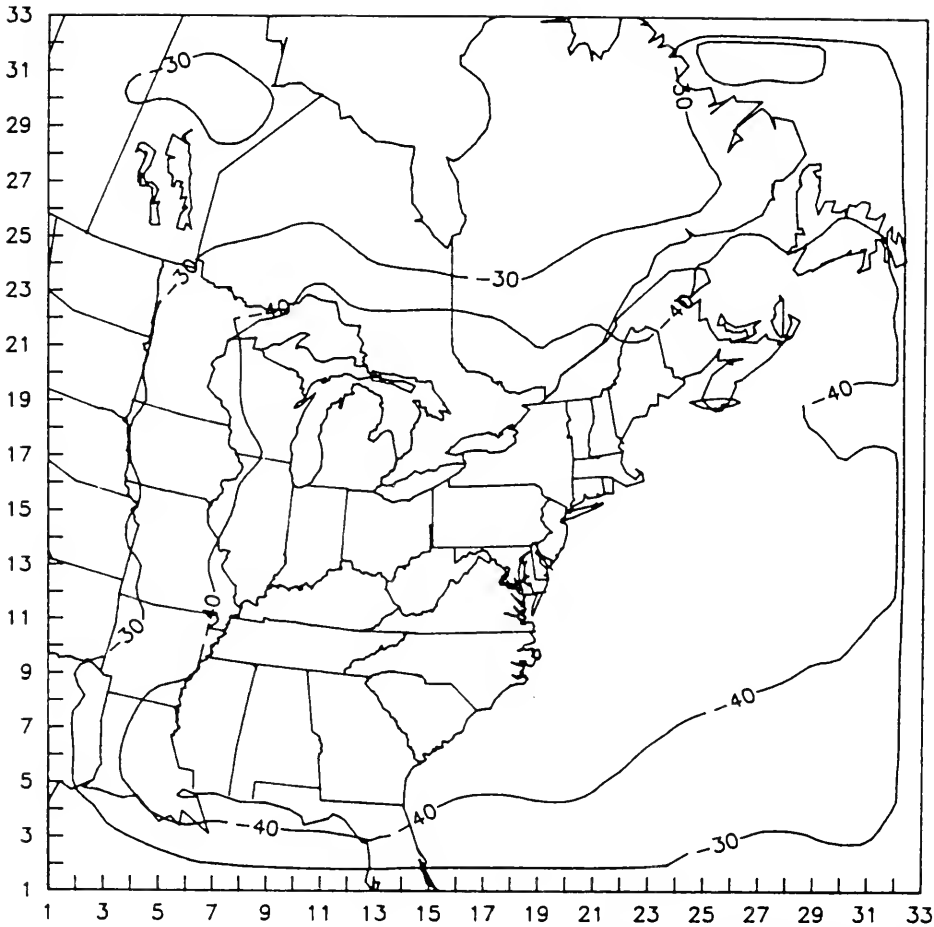

Figure 54. Change (%) in ADOM's predicted SO_4^{2-} ground level concentration in response to a 50% reduction of SO_x emissions during OSCAR.

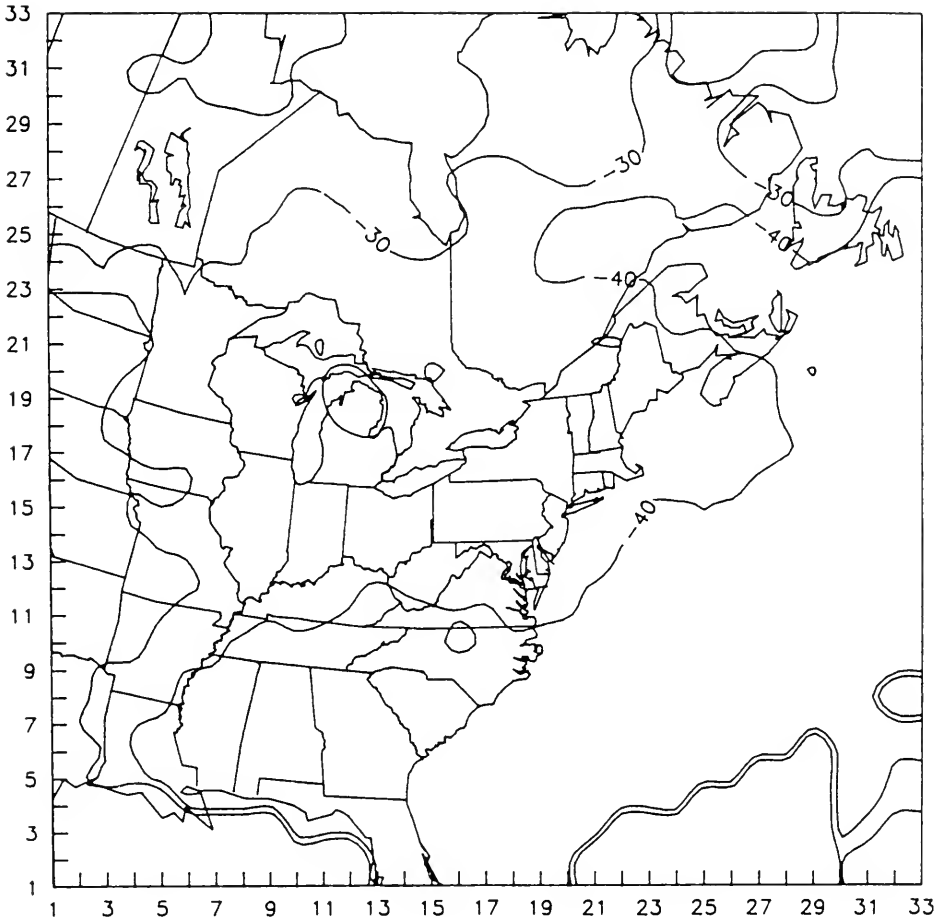

Figure 55. Change (%) in ADOM's predicted SO_4^{2-} in precipitation in response to a 50% reduction of both SO_x and NO_x emissions during OSCAR.

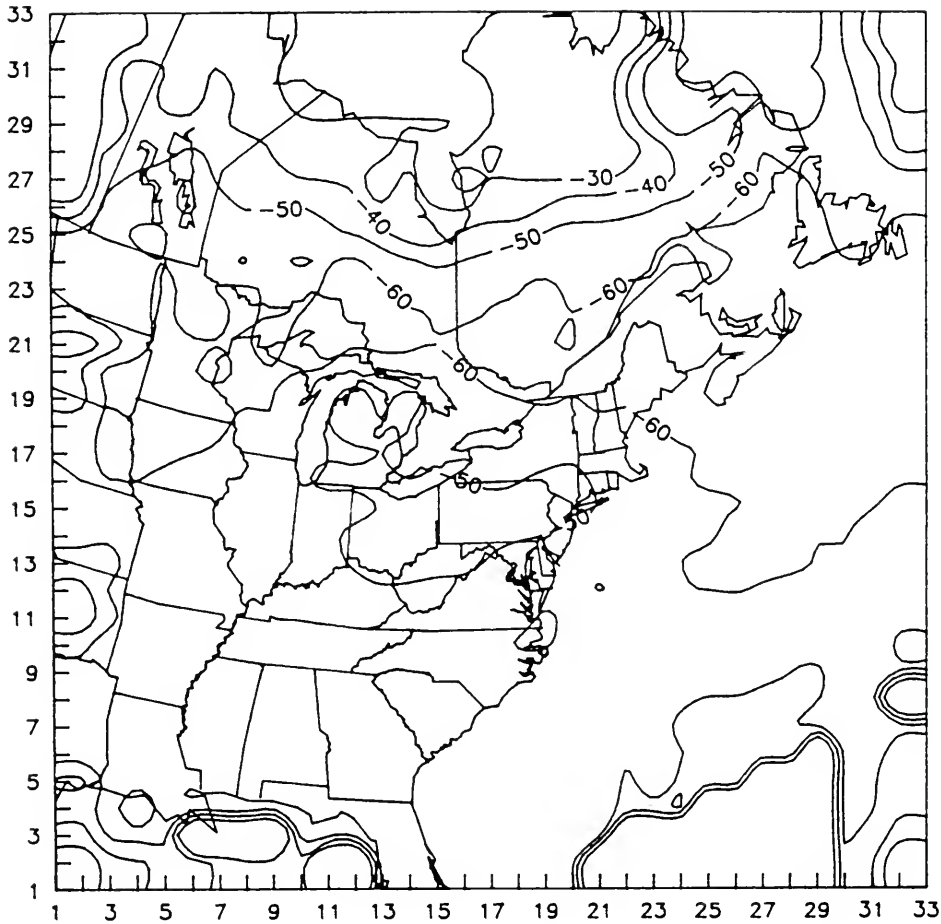

Figure 56. Change (%) in ADOM's predicted nitrate in precipitation in response to a 50% reduction of both SO_x and NO_x emissions during OSCAR.

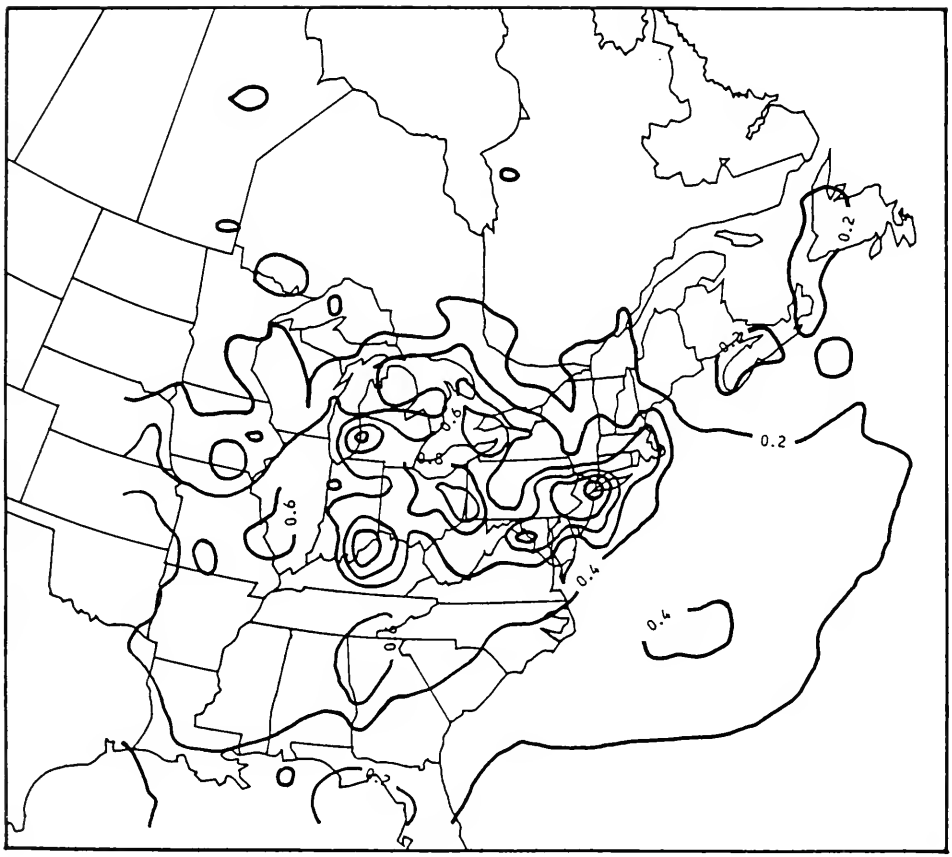

Figure 57. Predicted wet sulphate deposition (kg/ha) during the winter study (January 28 - February 7, 1985).

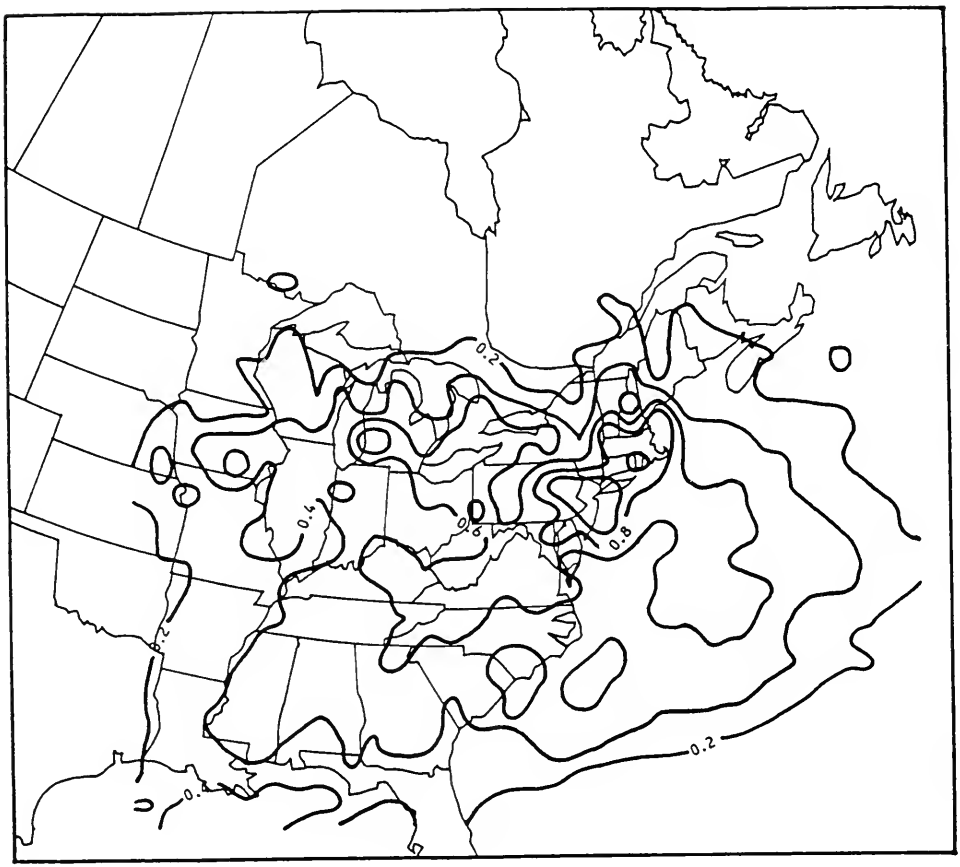

Figure 58. Predicted wet nitrate deposition (kg/ha) during the winter study (January 28 - February 7, 1985).

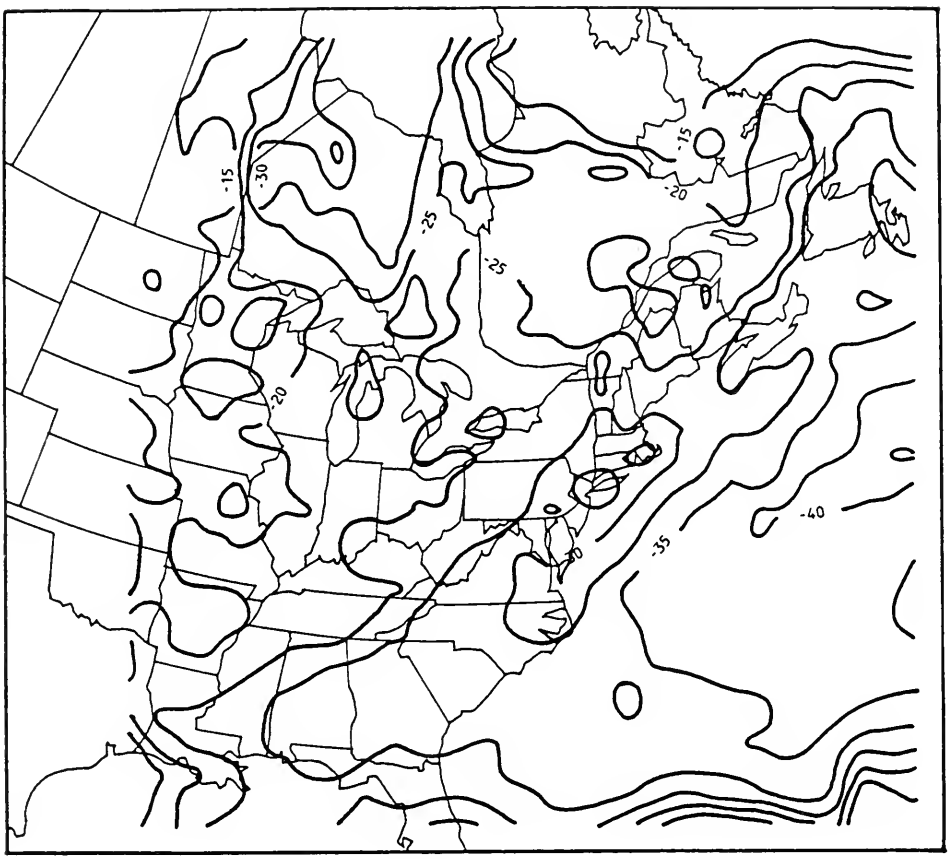

Figure 59. Change (%) in ADOM's predicted SO_4^{2-} in precipitation in response to a 50% reduction of SO_x emissions during the winter study (January 28 to February 7, 1985).

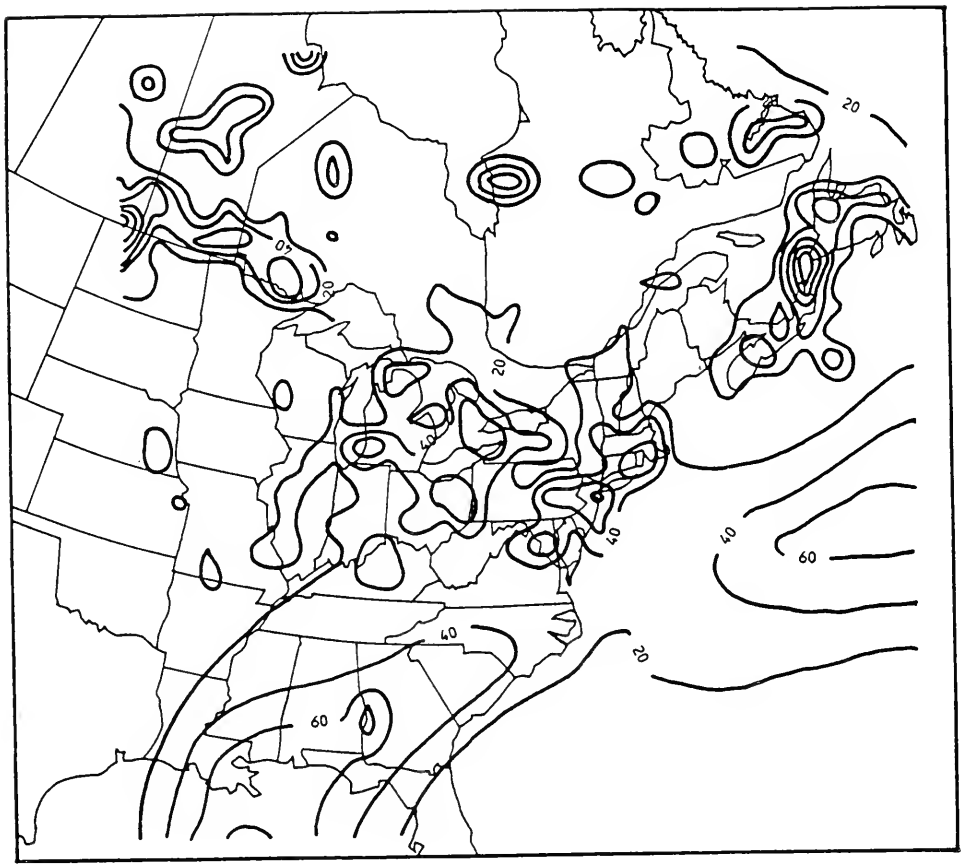

Figure 60. Total precipitation amount (mm) input to ADOM for the winter study period (January 28 to February 7, 1985).

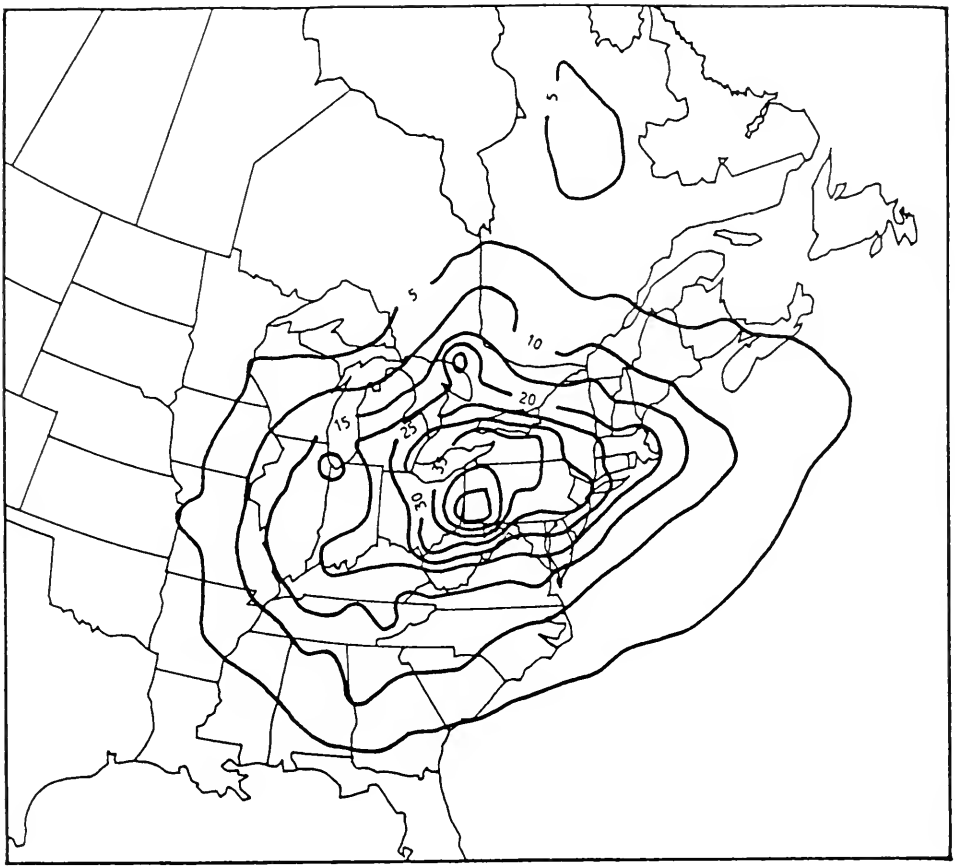

Figure 61. Ratio of the column integrated SO_2 to H_2O_2 for the winter study (January 28 to February 7, 1985).

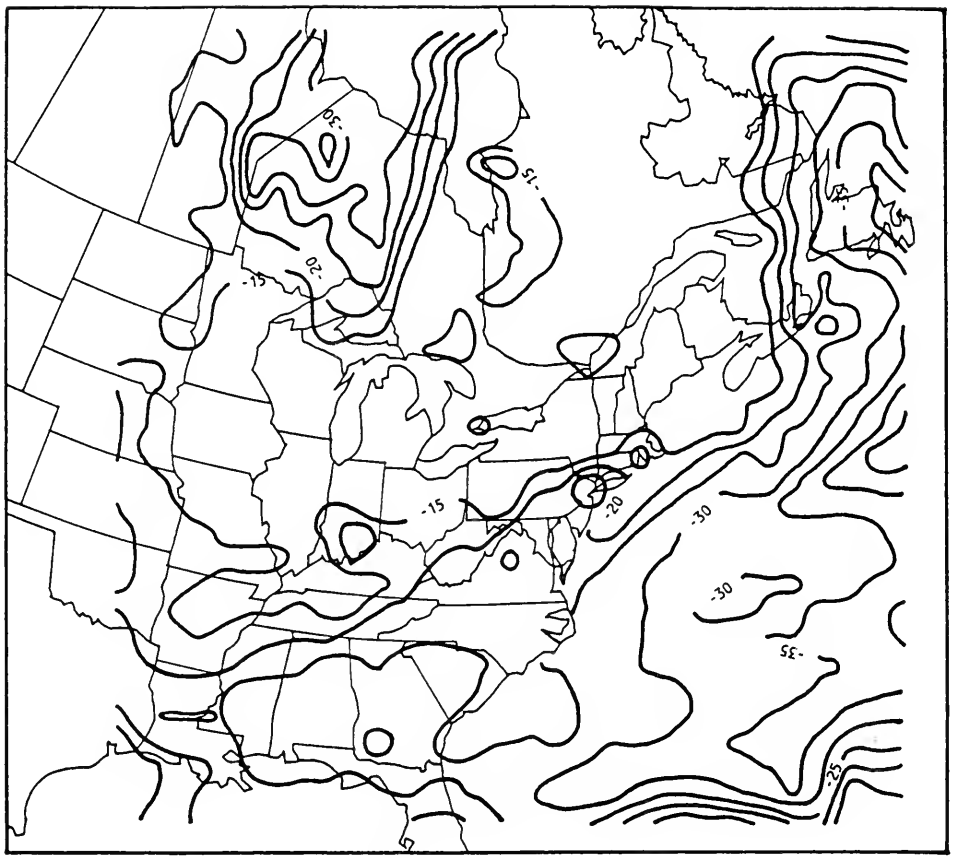

Figure 62. Change (%) in ADOM's predicted SO_4^{2-} in precipitation in response to a 50% reduction of both SO_x and NO_x emissions during the winter study (January 28 to February 7, 1985).

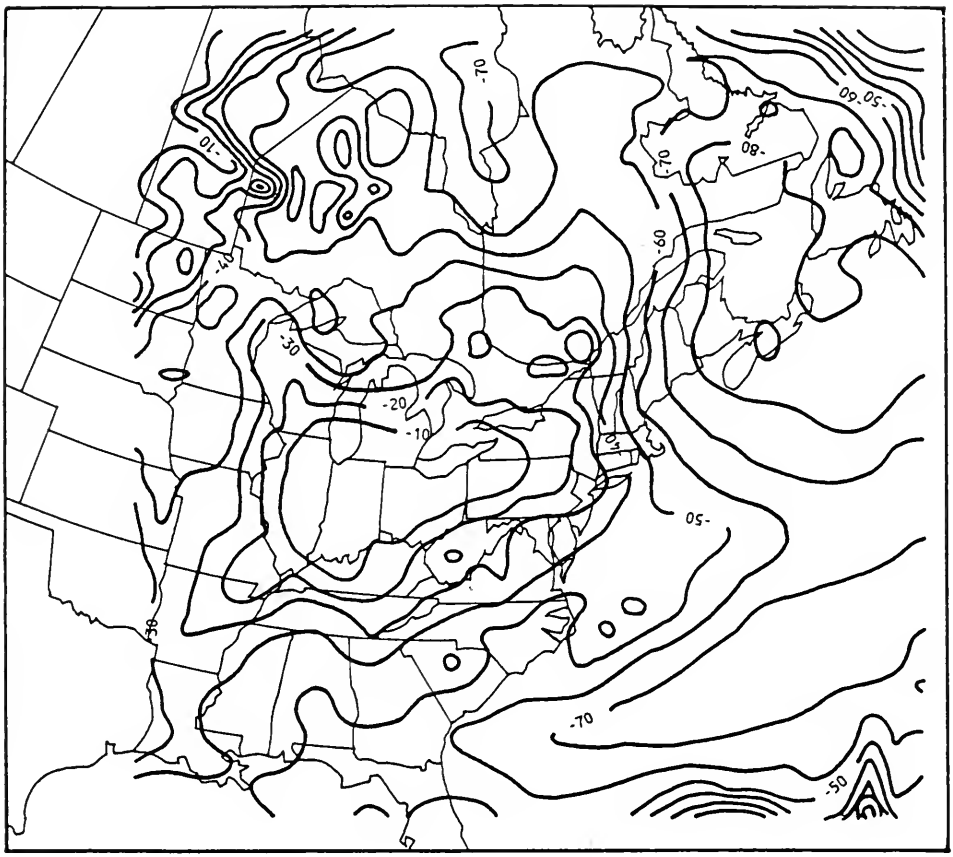

Figure 63. Change (%) in ADOM's predicted nitrate in precipitation in response to a 50% reduction of both SO_x and NO_x emissions during the winter study (January 28 to February 7, 1985).

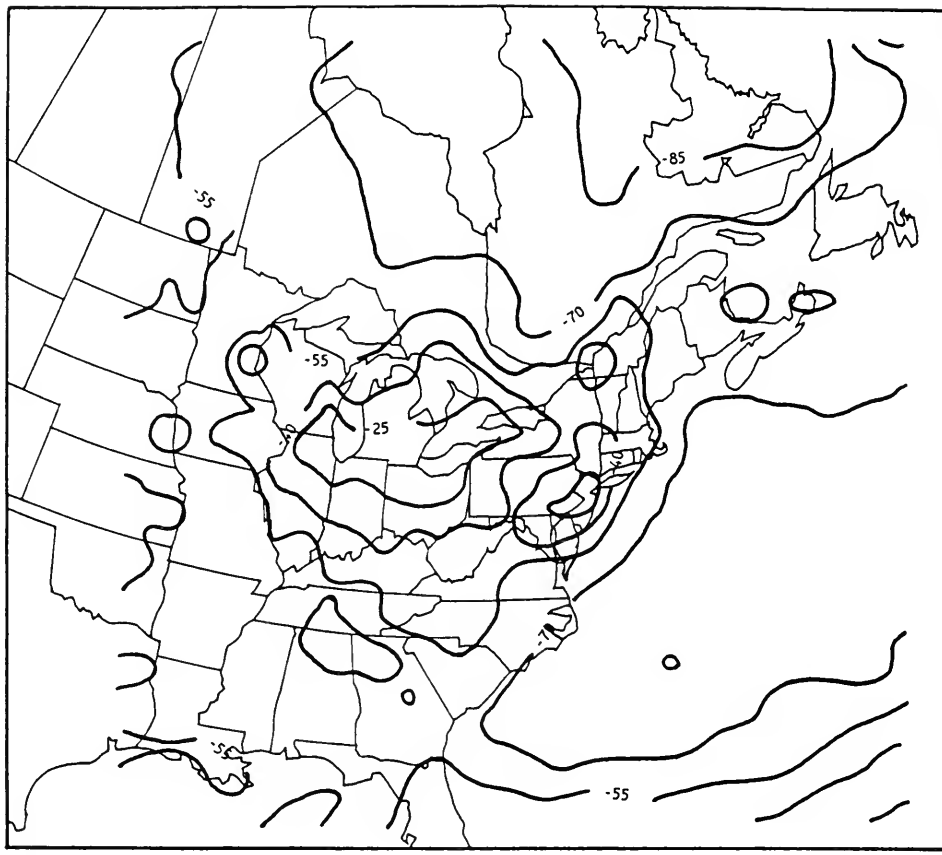

Figure 64. Change (%) in ADOM's predicted ground level NO_2 concentrations in precipitation in response to a 50% reduction of both SO_x and NO_x emissions during the winter study (January 28 to February 7, 1985).

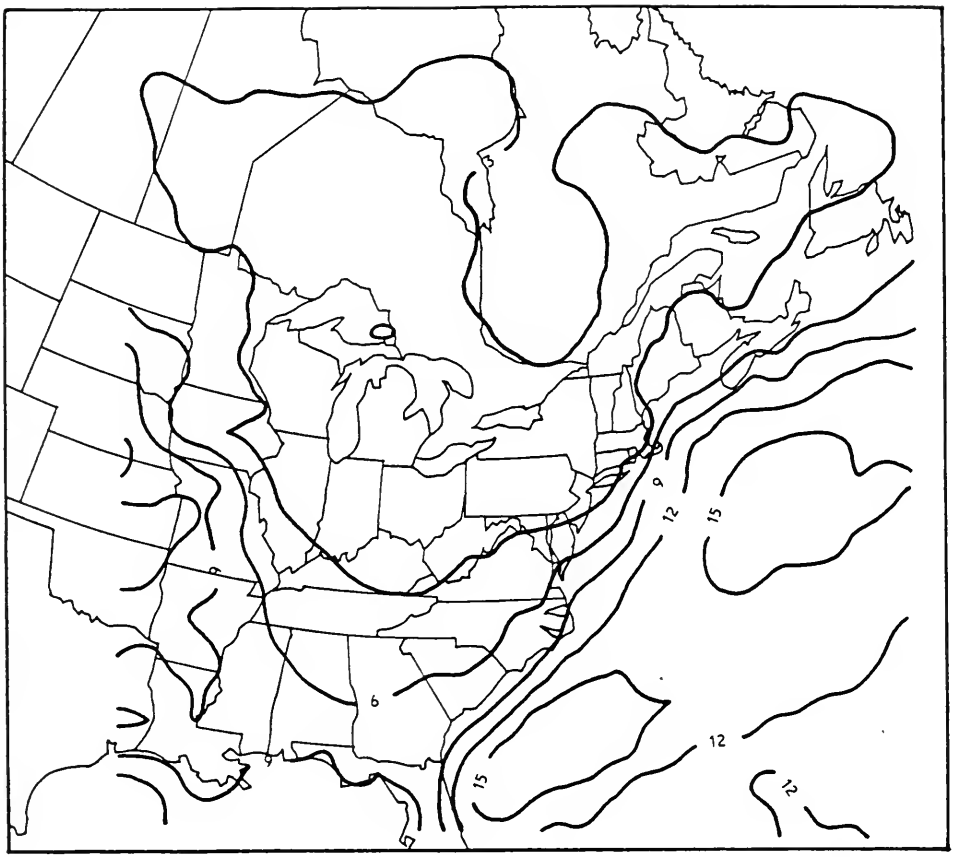

Figure 65. Contour of the event-averaged ozone concentration (ppb) for the winter study (January 28 to February 7, 1985).

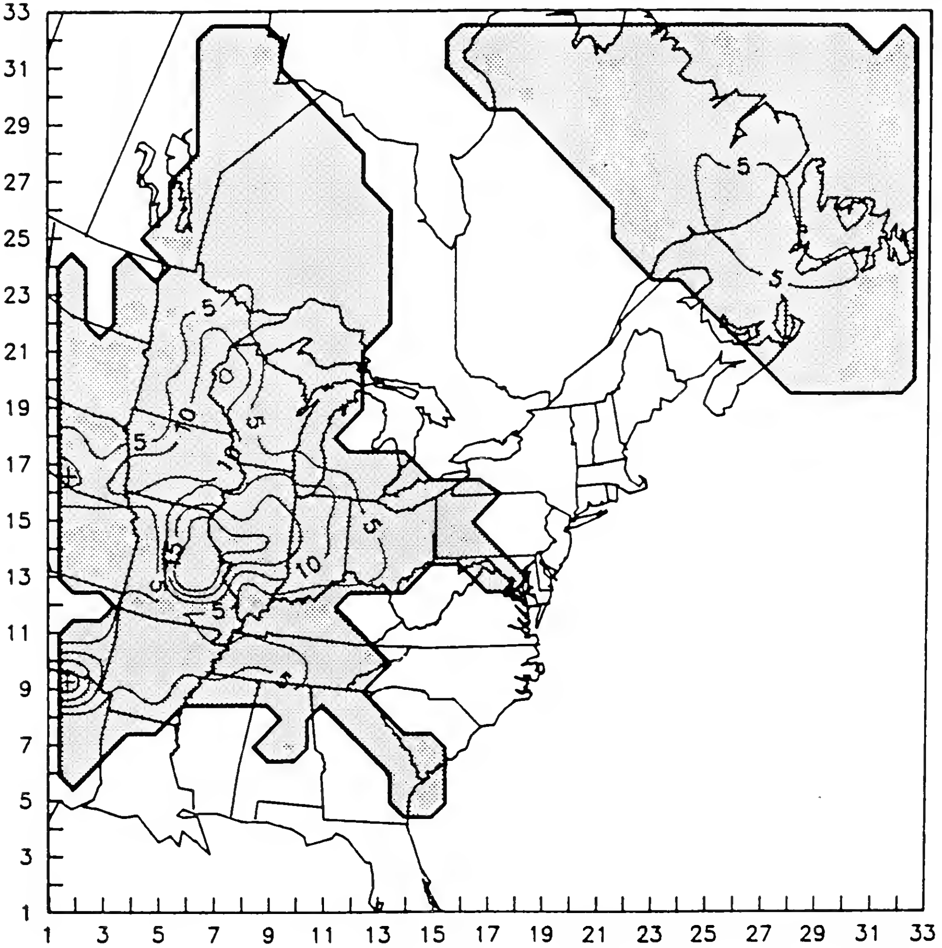

Figure 66a. Daily precipitation amount (mm) within the model domain for April 22-24(a-c), 1981. In Figures 66 - 70, 72 - 74, the hatched areas delineate the precipitation region. "+" and "-" at the centre of close contours indicate a local maximum and minimum, respectively. Thus, a "-" at the centre of a negative contour would indicate that the centre is more negative than the surrounding. All contour intervals are regular. The axes numbering are CMC grid numbers.

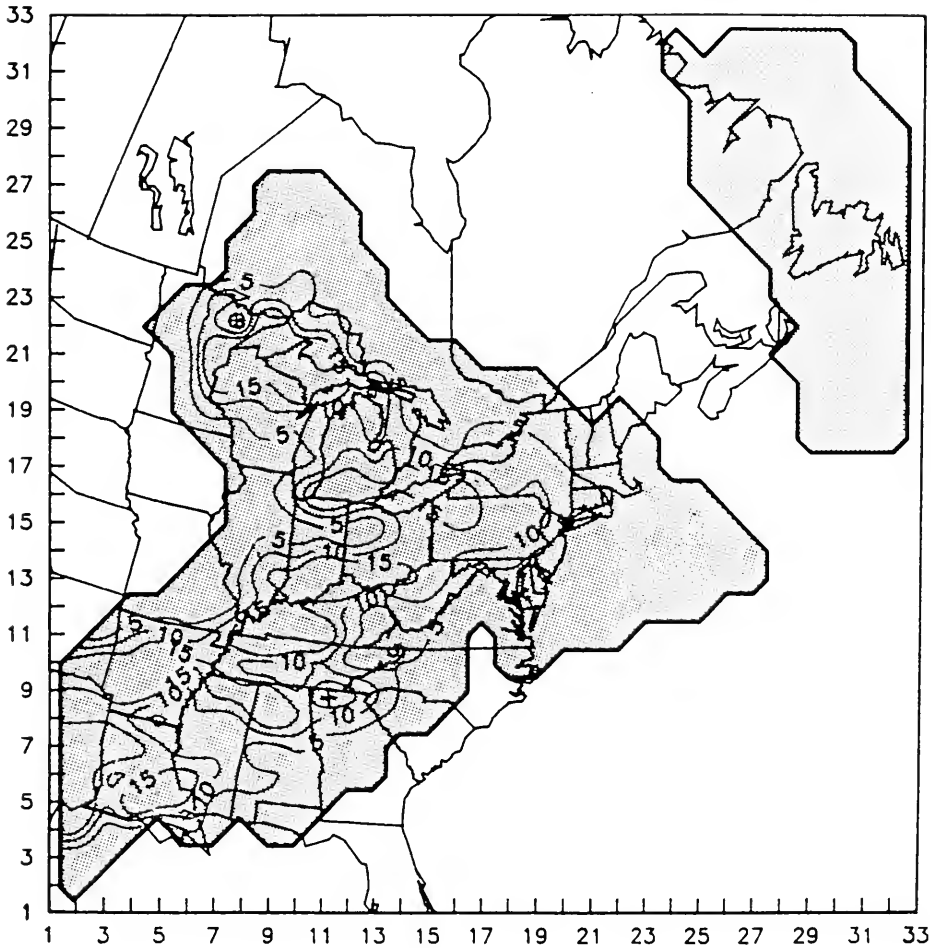

Figure 66b. See Figure 66a.

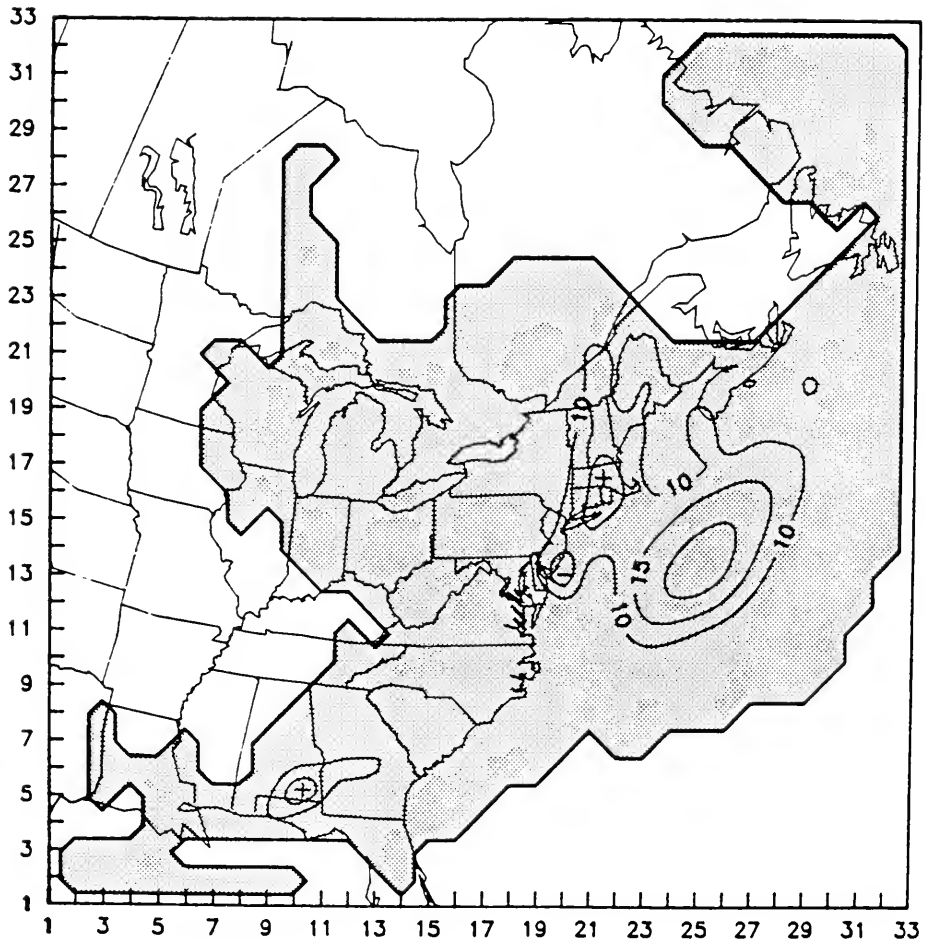

Figure 66c. See Figure 66a.

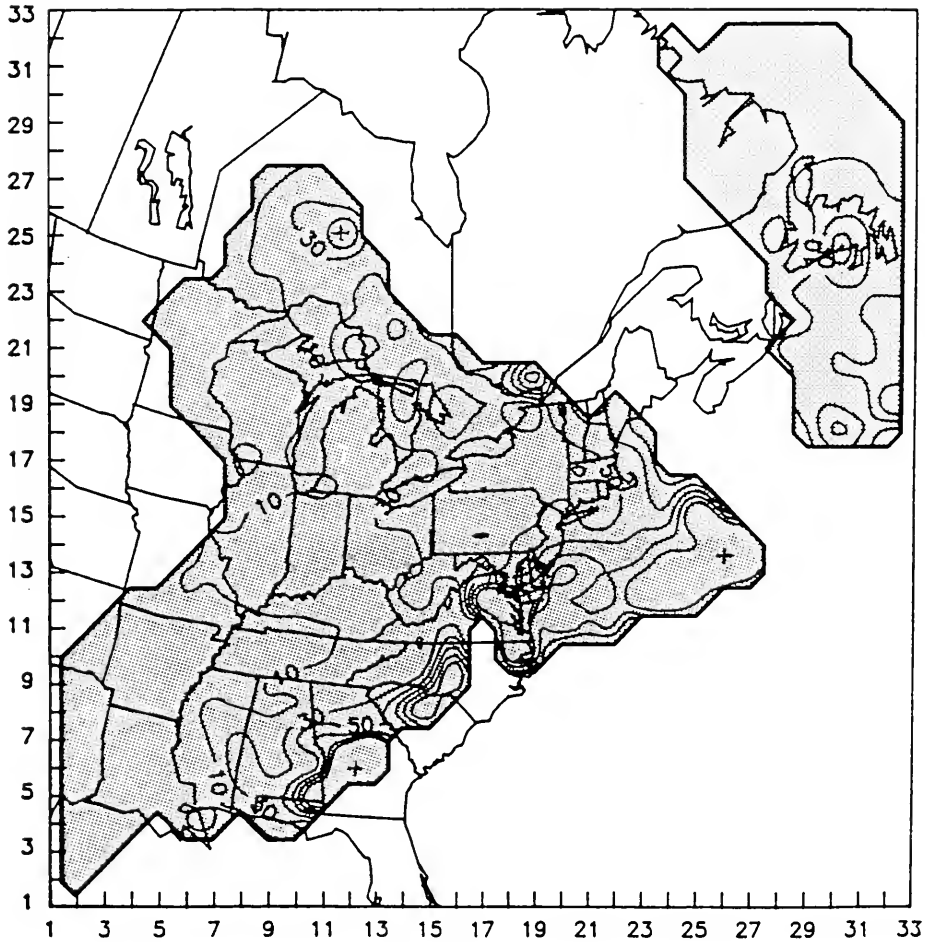

Figure 67a. Daily average SO_4^{2-} concentration ($\mu g/l$) in precipitation for April 23-24 (a-b), 1981 for the unperturbed case.

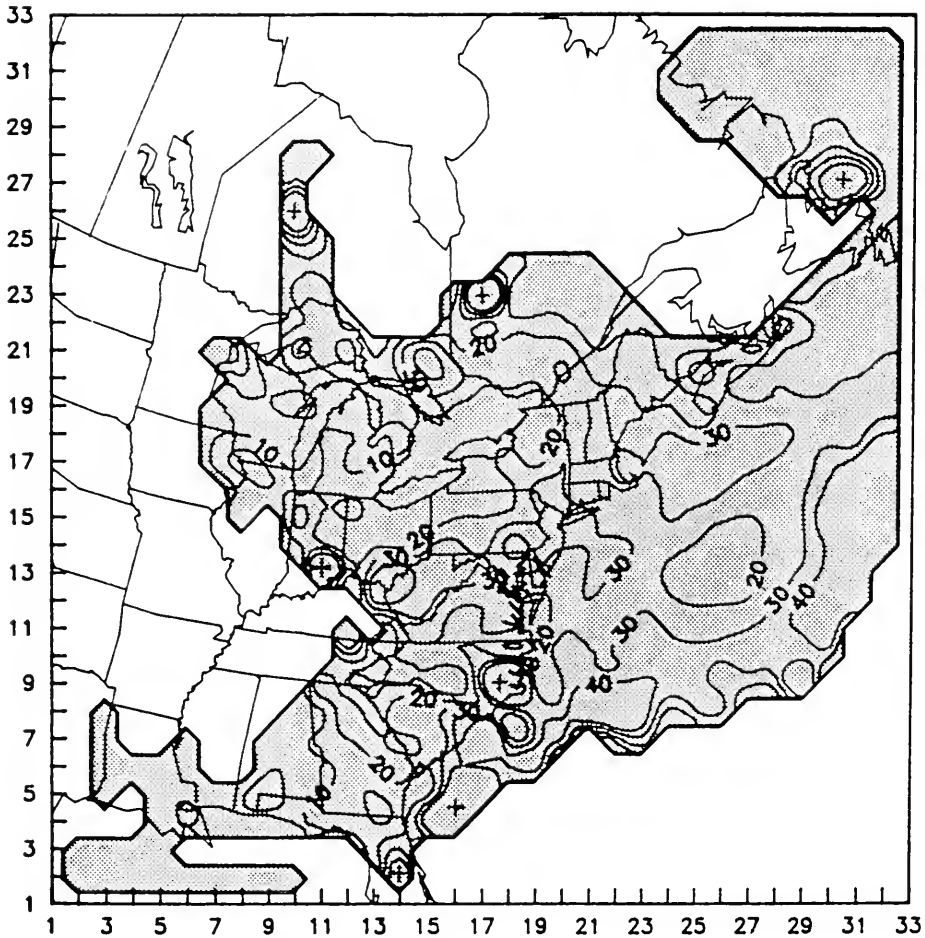

Figure 67b. See Figure 67a.

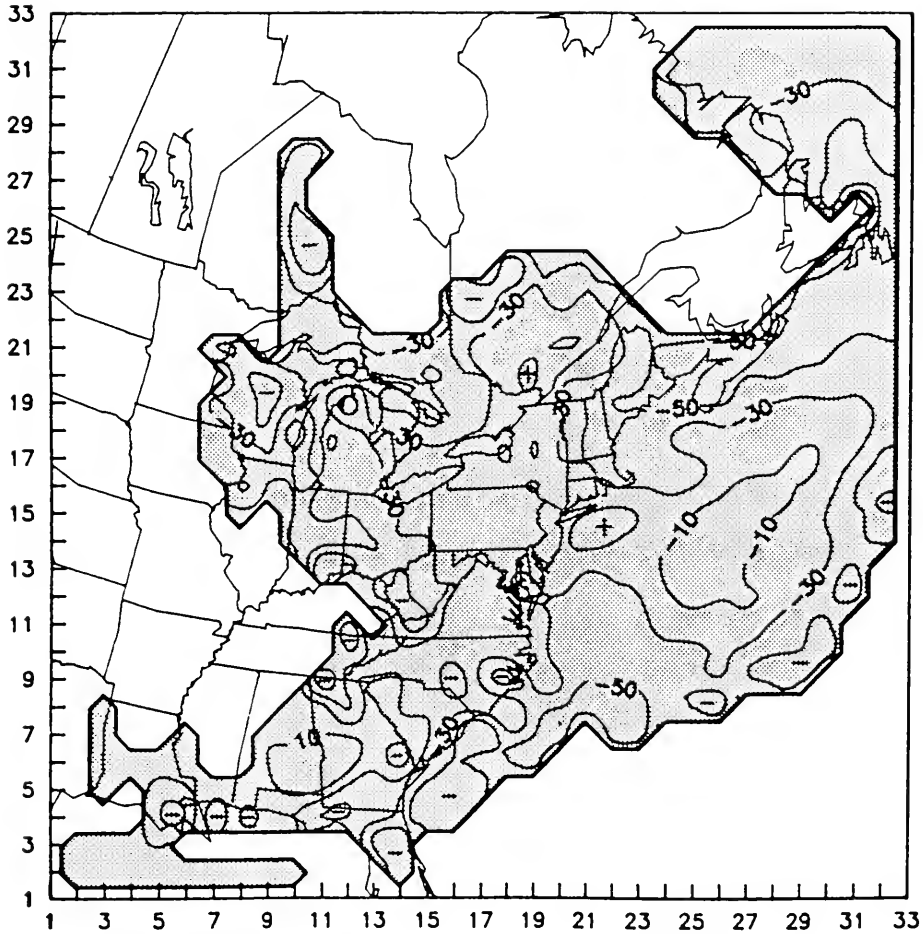

Figure 68. Average percentage change from base case of SO_4^{2-} concentrations in precipitation as a result of suppressing H_2O_2 oxidation for April 24, 1981.

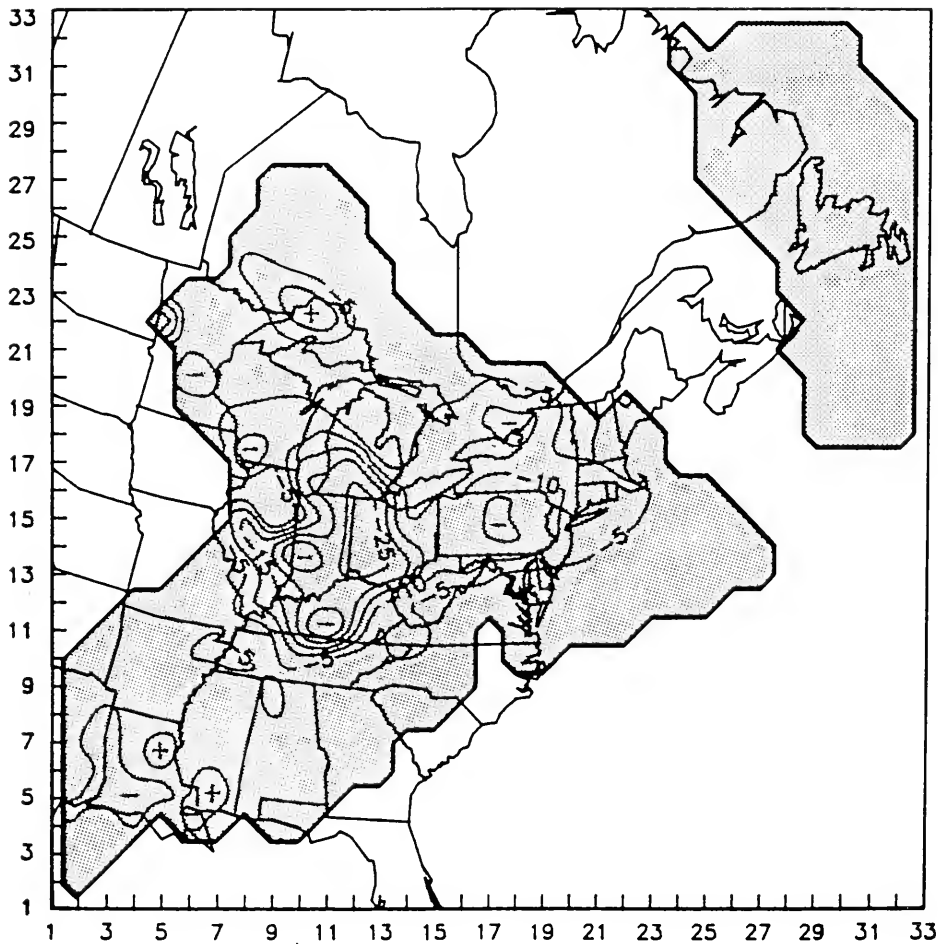

Figure 69a. Average percentage change from base case of SO_4^{2-} concentration in precipitation as a result of suppressing O_3 oxidation for April 23 (a) and 24 (b), 1981.

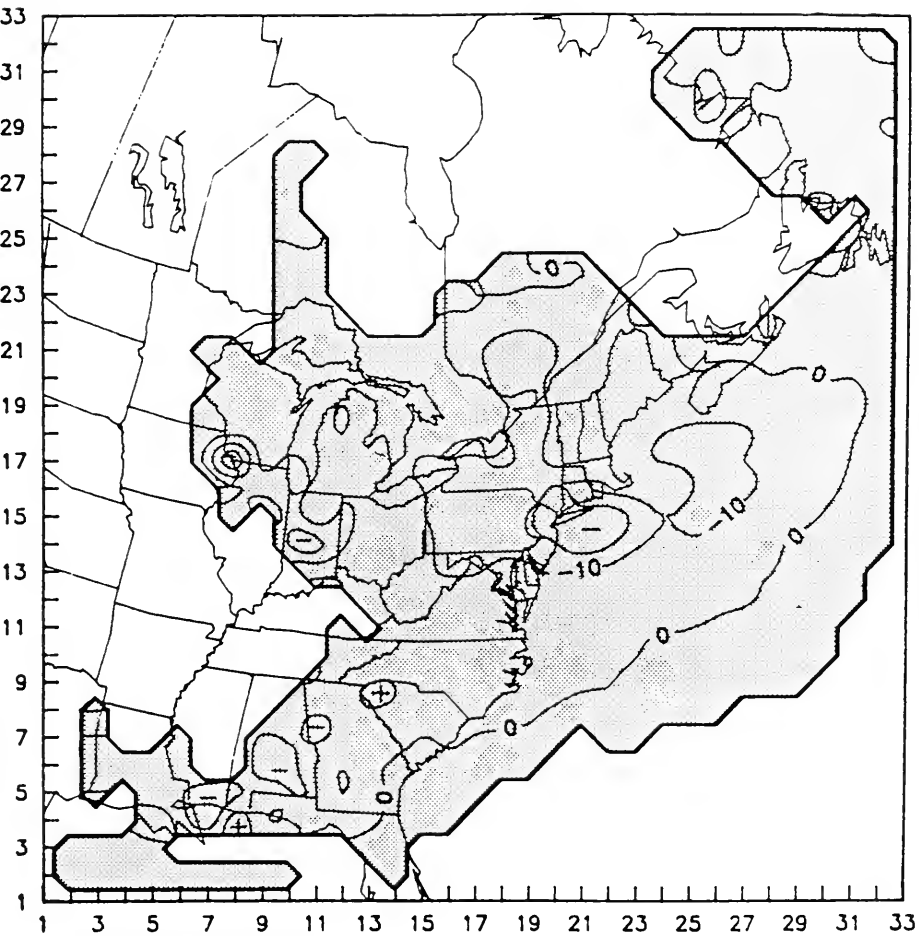

Figure 69b. See Figure 69a.

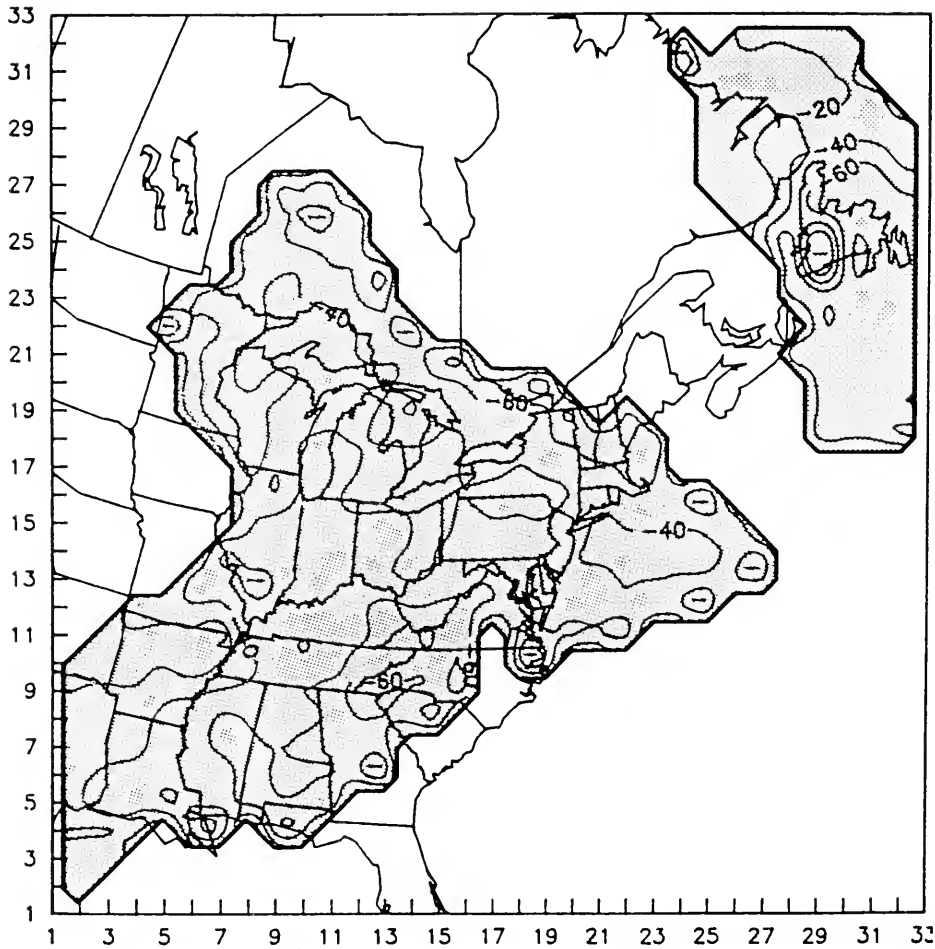

Figure 70. Average percentage change from base case of SO_4^{2-} concentration in precipitation as a result of suppressing all aqueous oxidations for April 23, 1981.

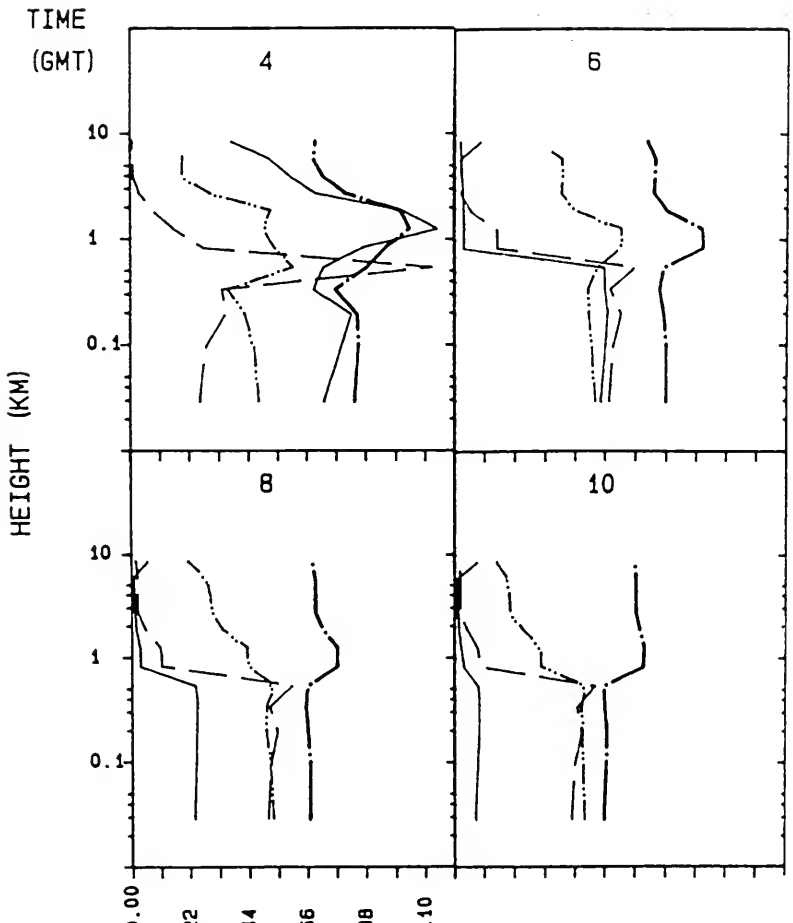

Figure 71. Time series of vertical ambient concentration profiles generated by ADOM on April 23 over grid (16, 19). The species shown are SO_2 (— — — — —), SO_4^{2-} (—··—··—··—), H_2O_2 (————) and O_3 (—·—·—·—). The stratiform cloud module is activated at time 0600 GMT. Concentrations are in $\mu g\ m^{-3}$.

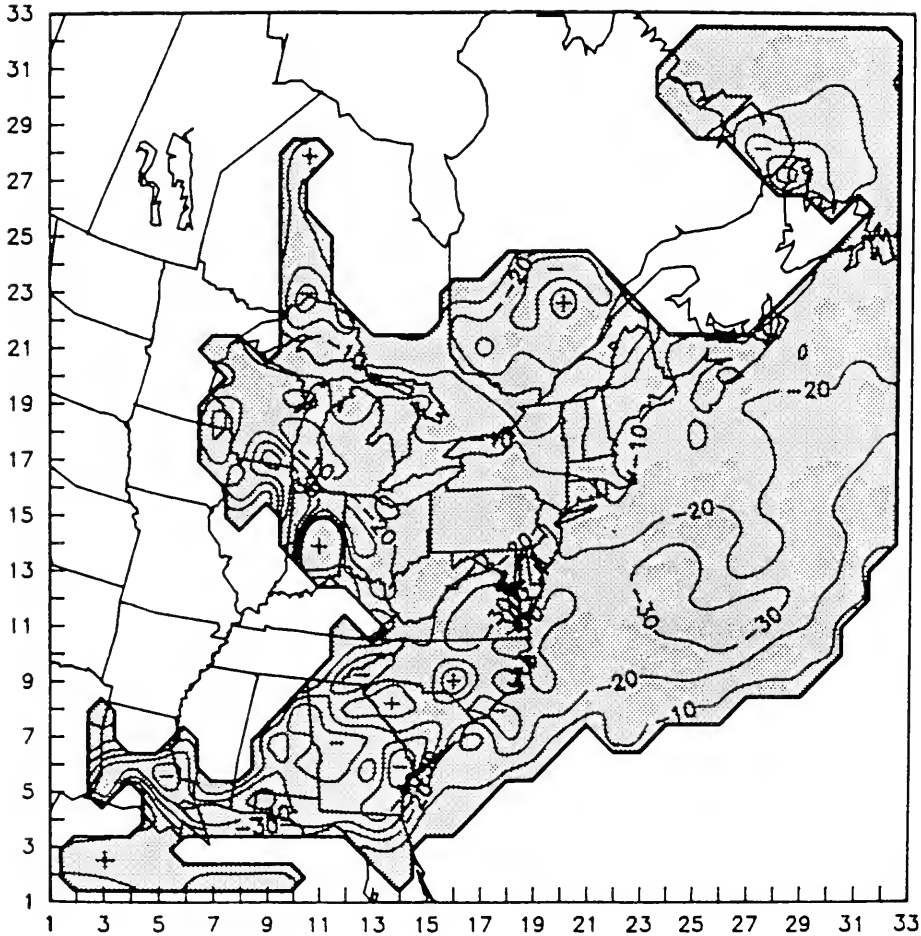

Figure 72. Percentage difference between the results of i) the sum of individual suppression of the three oxidations and ii) suppressing all three oxidations simultaneously for sulphate in precipitation for April 24, 1981. Displayed is i) minus ii).

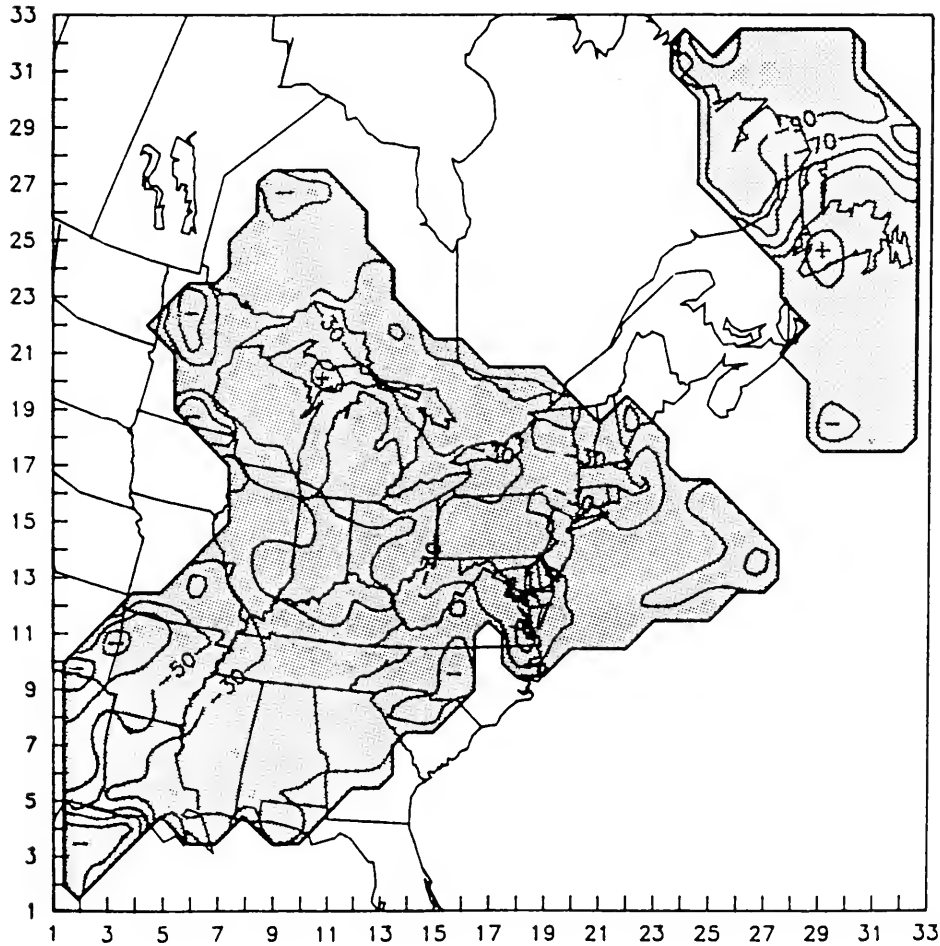

Figure 73a. Departure (%) from linearity of sulphate in precipitation: (Base case -2 x Perturbed Case)/Base case x 100. Base case: O_3 aqueous oxidation suppressed (Fig.69). Perturbed case: O_3 aqueous oxidation suppressed plus 50% SO_x emissions reduction. April 23 (a) and 24 (b), 1981.

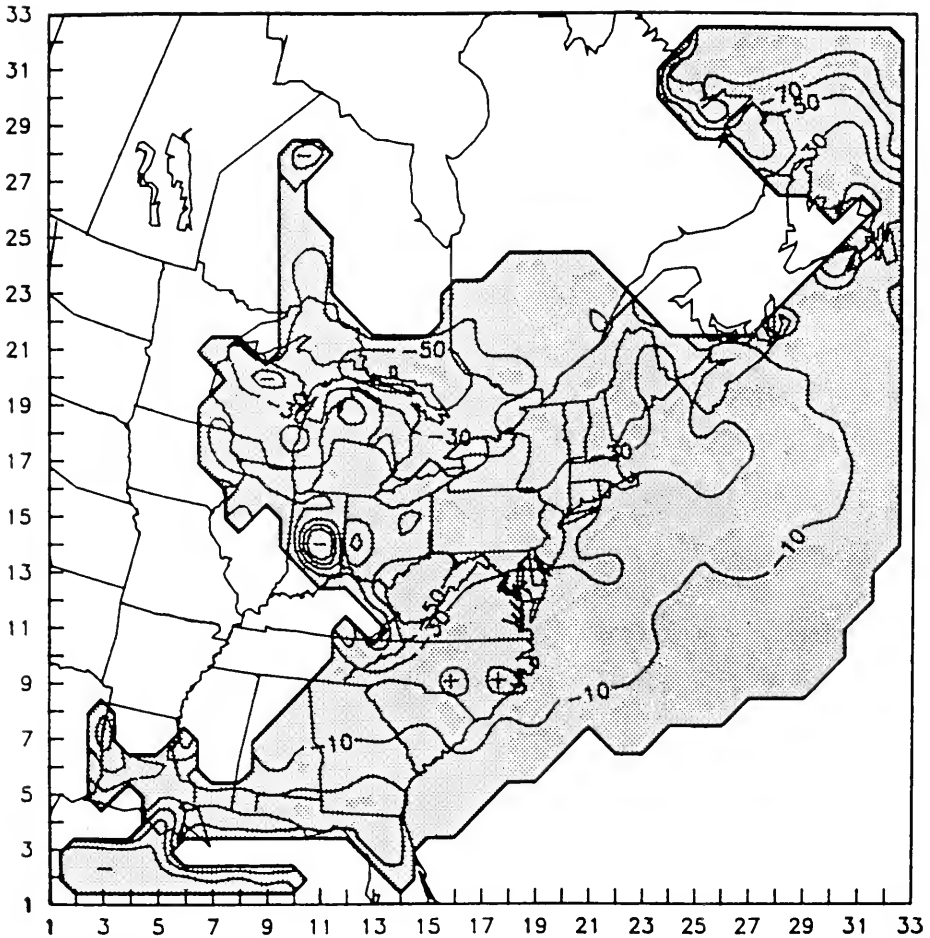

Figure 73b. See Figures 73a and 69b.

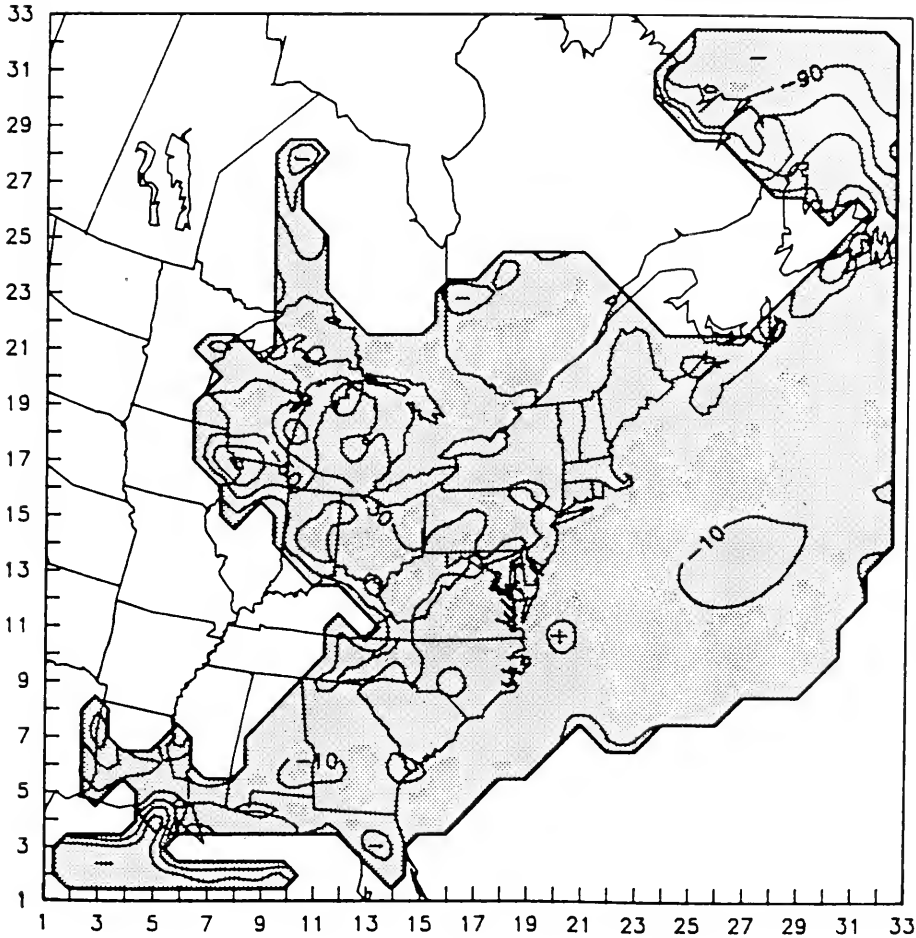

Figure 74. Same as Figure 73b except H_2O_2 oxidation suppressed. Base case is represented in Fig. 68.

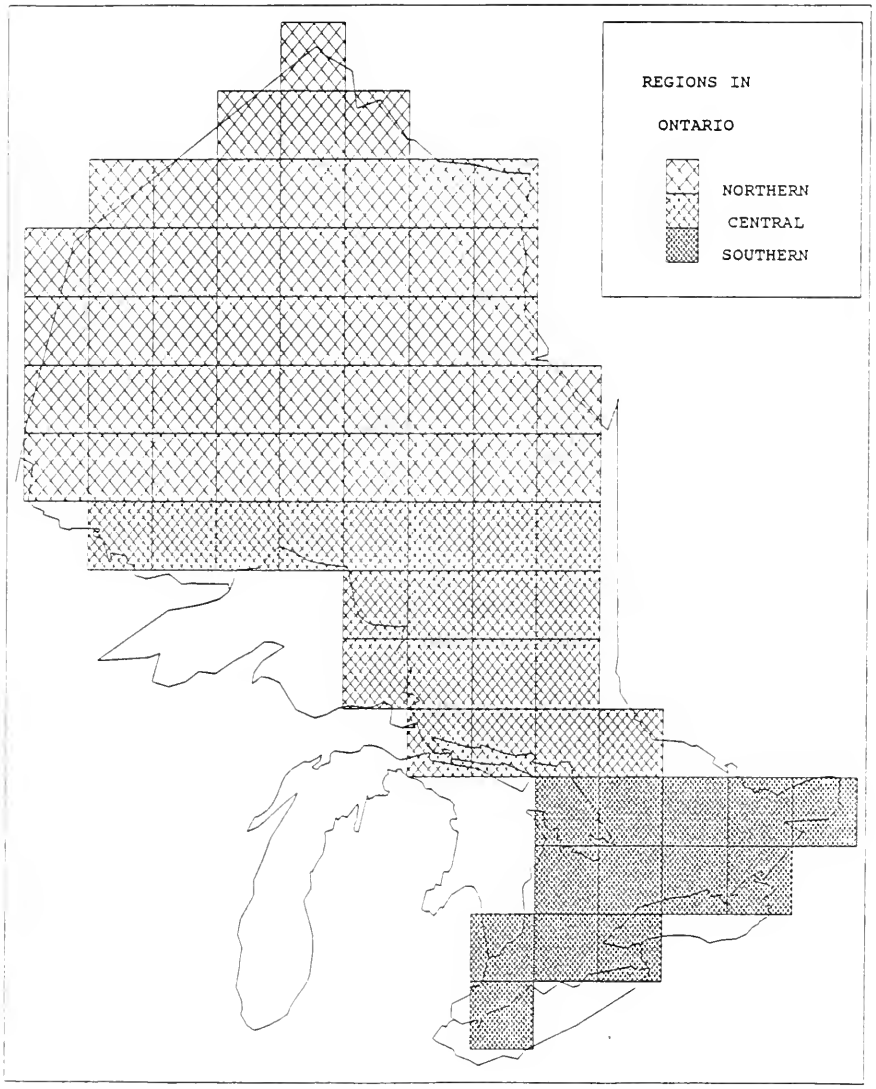

Figure 75. The division of Ontario into southern, central and northern Ontario for the purpose of delineating impact of emission scenarios on Ontario for the summer oxidant study.

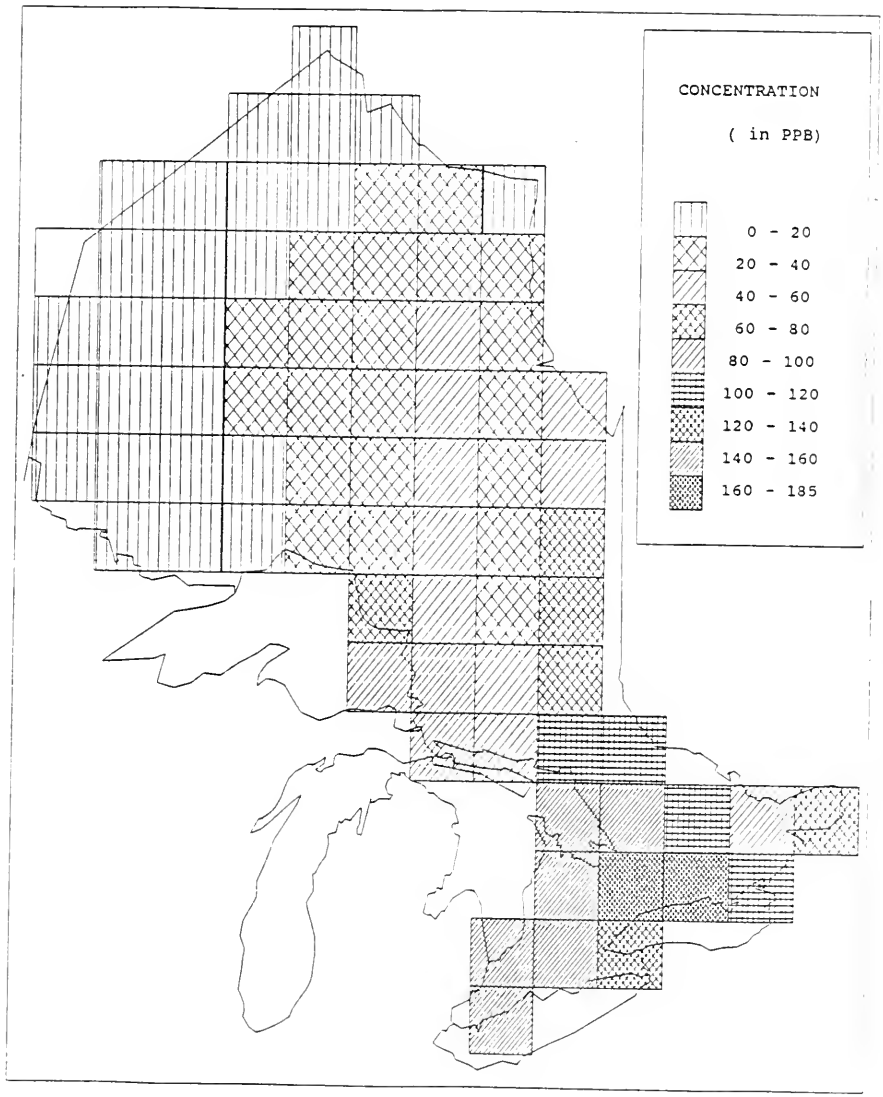

Figure 76. Predicted maximum base case surface ozone concentrations (ppb) in Ontario on June 14, 1983 for the summer oxidant study.

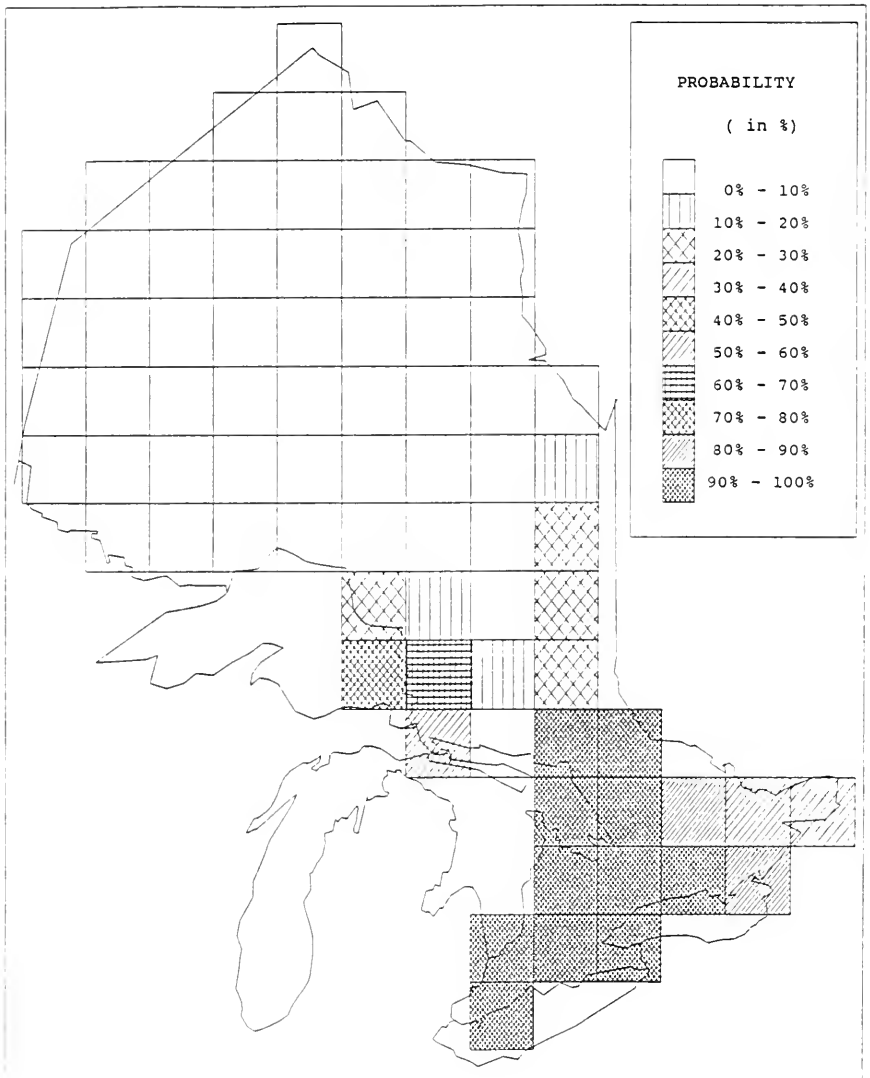

Figure 77. Probability of exceeding Ontario ozone criterion of 80 ppb on June 14, 1983 for the summer oxidant study.

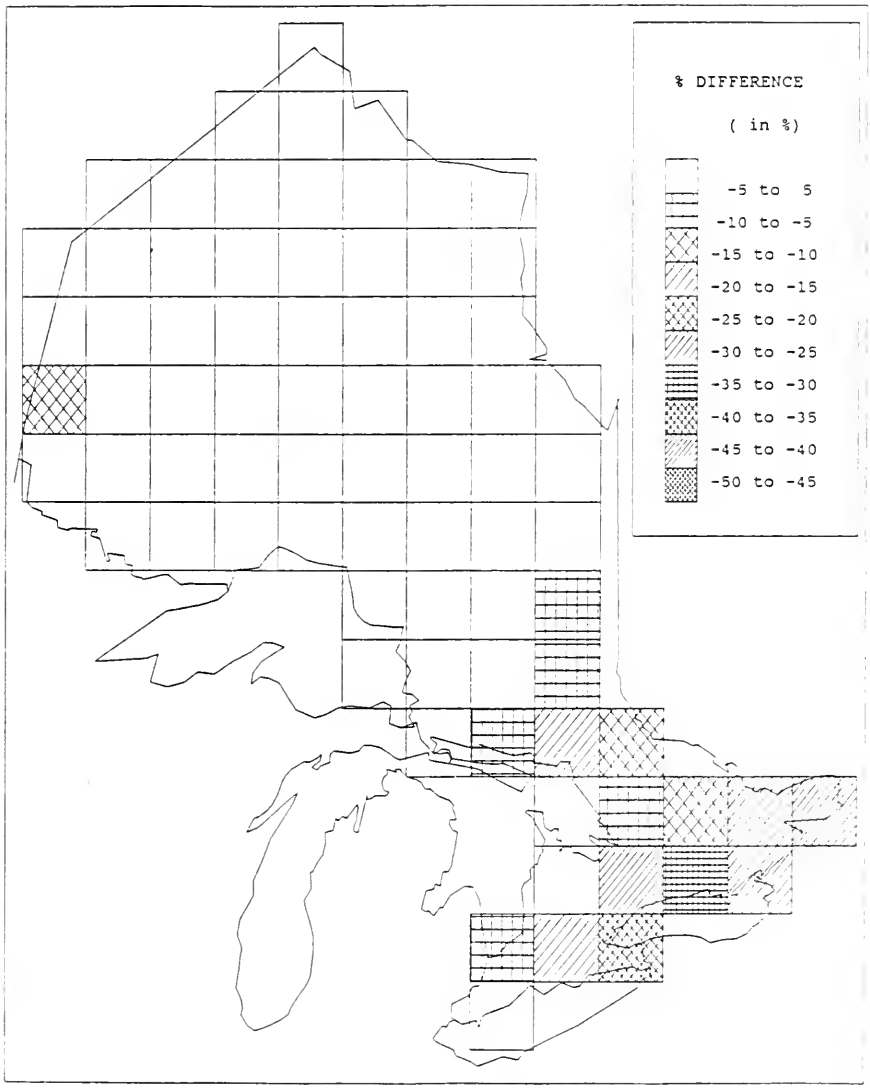

Figure 78. Relative change (%) in maximum surface ozone concentrations in Ontario as a result of reducing NO_x emissions in Ontario by 100% (June 14, 1983) for the summer oxidant study.

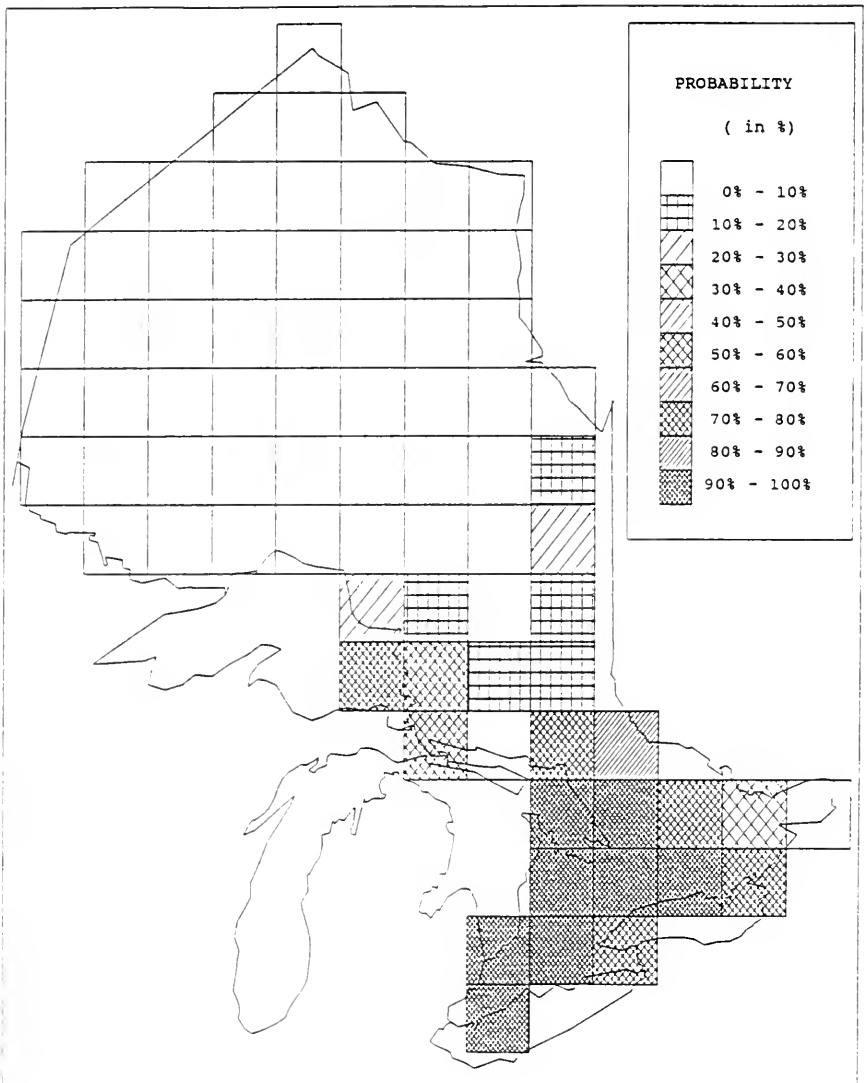

Figure 79. Probability of exceeding Ontario ozone criterion of 80 ppb when Ontario NO_x emissions are eliminated for the summer oxidant study.

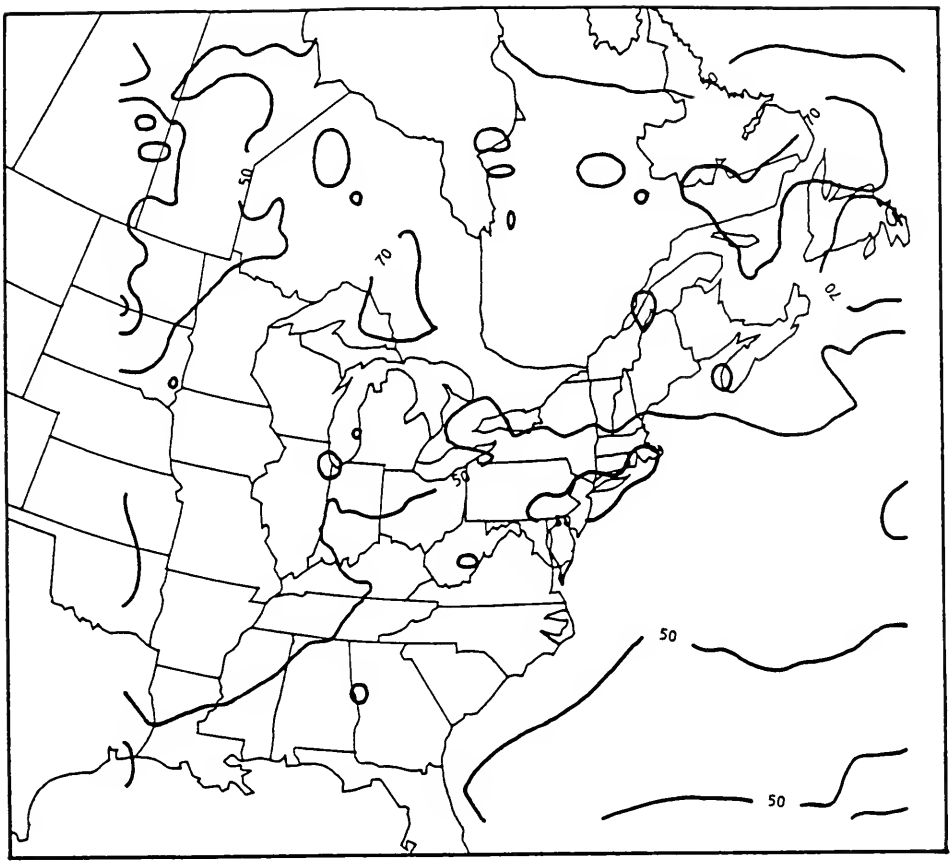

Figure 80. Change (%) in SO_4^{2-} wet deposition when all the aqueous pathways are suppressed during January 28 - February 8, 1985.

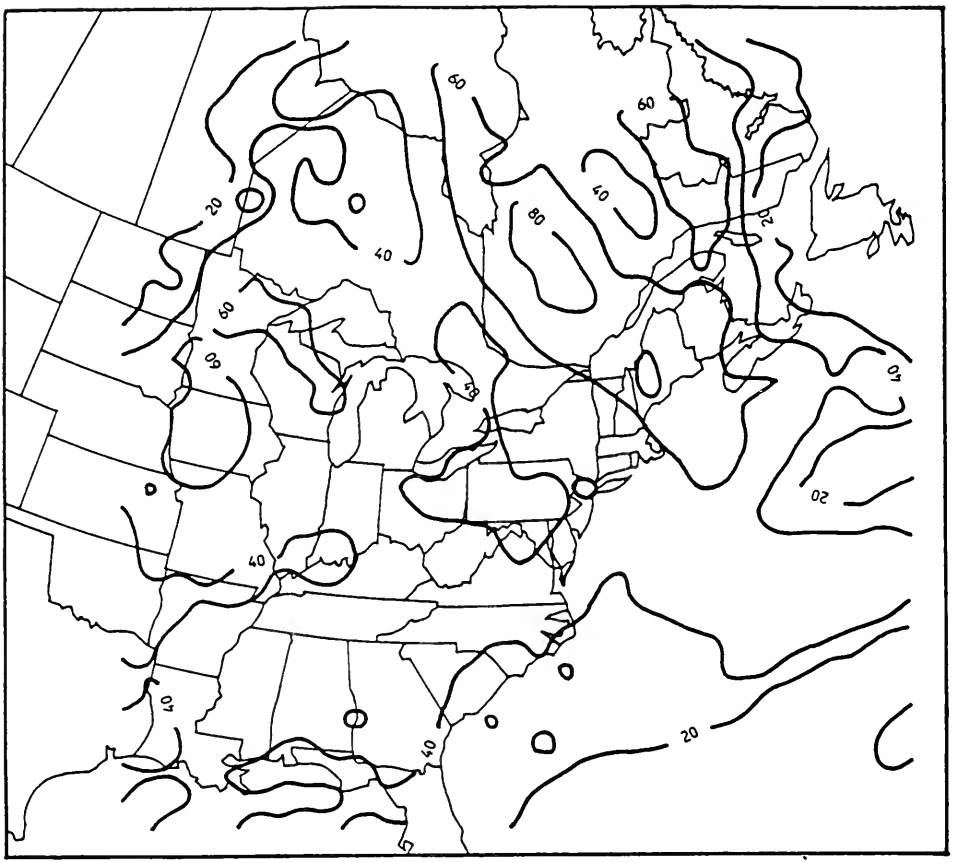

Figure 81. Change (%) in nitrate wet deposition when the NO_3/N_2O_5 pathway for the production of nitrate is shut off during January 28 -February 8, 1985.